



UNIL | Université de Lausanne

Unicentre

CH-1015 Lausanne

<http://serval.unil.ch>

---

Year : 2021

## 3D HUMAN iPSC-DERIVED BRAIN MODEL FOR NEUROTOXICOLOGY

Nunes Carolina Martins Resende Alves

Nunes Carolina Martins Resende Alves, 2021, 3D HUMAN iPSC-DERIVED BRAIN MODEL FOR NEUROTOXICOLOGY

Originally published at : Thesis, University of Lausanne

Posted at the University of Lausanne Open Archive <http://serval.unil.ch>

Document URN : urn:nbn:ch:serval-BIB\_DDA62CE75EC05

### **Droits d'auteur**

L'Université de Lausanne attire expressément l'attention des utilisateurs sur le fait que tous les documents publiés dans l'Archive SERVAL sont protégés par le droit d'auteur, conformément à la loi fédérale sur le droit d'auteur et les droits voisins (LDA). A ce titre, il est indispensable d'obtenir le consentement préalable de l'auteur et/ou de l'éditeur avant toute utilisation d'une oeuvre ou d'une partie d'une oeuvre ne relevant pas d'une utilisation à des fins personnelles au sens de la LDA (art. 19, al. 1 lettre a). A défaut, tout contrevenant s'expose aux sanctions prévues par cette loi. Nous déclinons toute responsabilité en la matière.

### **Copyright**

The University of Lausanne expressly draws the attention of users to the fact that all documents published in the SERVAL Archive are protected by copyright in accordance with federal law on copyright and similar rights (LDA). Accordingly it is indispensable to obtain prior consent from the author and/or publisher before any use of a work or part of a work for purposes other than personal use within the meaning of LDA (art. 19, para. 1 letter a). Failure to do so will expose offenders to the sanctions laid down by this law. We accept no liability in this respect.



UNIL | Université de Lausanne

Unicentre  
CH-1015 Lausanne  
<http://serval.unil.ch>

---

Year : 2021

## 3D HUMAN iPSC-DERIVED BRAIN MODEL FOR NEUROTOXICOLOGY

Carolina Martins Resende Alves Nunes

Carolina Martins Resende Alves Nunes, 2021, 3D human iPSC-derived brain model for neurotoxicology

Originally published at: Thesis, University of Lausanne

Posted at the University of Lausanne Open Archive <http://serval.unil.ch>  
Document URN :

### **Droits d'auteur**

L'Université de Lausanne attire expressément l'attention des utilisateurs sur le fait que tous les documents publiés dans l'Archive SERVAL sont protégés par le droit d'auteur, conformément à la loi fédérale sur le droit d'auteur et les droits voisins (LDA). A ce titre, il est indispensable d'obtenir le consentement préalable de l'auteur et/ou de l'éditeur avant toute utilisation d'une oeuvre ou d'une partie d'une oeuvre ne relevant pas d'une utilisation à des fins personnelles au sens de la LDA (art. 19, al. 1 lettre a). A défaut, tout contrevenant s'expose aux sanctions prévues par cette loi. Nous déclinons toute responsabilité en la matière.

### **Copyright**

The University of Lausanne expressly draws the attention of users to the fact that all documents published in the SERVAL Archive are protected by copyright in accordance with federal law on copyright and similar rights (LDA). Accordingly it is indispensable to obtain prior consent from the author and/or publisher before any use of a work or part of a work for purposes other than personal use within the meaning of LDA (art. 19, para. 1 letter a). Failure to do so will expose offenders to the sanctions laid down by this law. We accept no liability in this respect.



Département des Sciences Biomédicales

# 3D HUMAN iPSC-DERIVED BRAIN MODEL FOR NEUROTOXICOLOGY

Thèse de doctorat en Neurosciences

présentée à la

Faculté de biologie et de médecine  
de l'Université de Lausanne

par

**Carolina Martins Resende Alves NUNES**

Master in developmental and evolutionary biology, University of Lisbon, PT

**Jury**

Prof. Nicolas Toni, Président  
Prof. Aurélien Thomas, Directeur de thèse  
Dre Marie-Gabrielle Zurich, Co-directrice de thèse  
Prof. Ellen Fritsche, Experte  
Dre Anna Price, Experte

Thèse n° 322

Lausanne, 2021

*Programme doctoral interuniversitaire en Neurosciences  
des Universités de Lausanne et Genève*



Unil

UNIL | Université de Lausanne



UNIVERSITÉ  
DE GENÈVE

Programme doctoral interuniversitaire en Neurosciences  
des Universités de Lausanne et Genève

# Imprimatur

Vu le rapport présenté par le jury d'examen, composé de

<b>Président·e</b>	Monsieur	Prof.	Nicolas Toni
<b>Directeur·trice de thèse</b>	Monsieur	Prof.	Aurélien Thomas
<b>Co-directeur·trice de thèse</b>	Madame	Dre	Marie-Gabrielle Zurich
<b>Expert·e·s</b>	Madame	Prof.	Ellen Fritsche
	Madame	Dre	Anna Price

le Conseil de Faculté autorise l'impression de la thèse de

**Madame Carolina Martins Resende Alves Nunes**

Master in evolutionary and developmental biology,  
Universidade de Lisboa, PT

intitulée

**3D HUMAN iPSC-DERIVED BRAIN MODEL FOR NEUROTOXICOLOGY**

Lausanne, le 10 décembre 2021

pour Le Doyen  
de la Faculté de Biologie et de Médecine

Prof. Nicolas Toni

*Follow your heart but take your brain with you."*

**Alfred Adler**



---

# Acknowledgements

---

If I would go back and tell 2014-Carolina that she would ever start and be about to finish a PhD, she would think I was playing her. From finishing the master till today it feels like a lifetime has gone by. Along the way, I earned self-confidence and awareness, scientific maturity, critical thinking, good friends and memories thanks to mentorship, support, and friendship of several people.

I have to start with the boss. Marie-Gabrielle Zurich gave me the opportunity not only to join her lab, but also to join the immense MSCA-ITN in3 consortium. During the last 4 years, she enthusiastically guided me through this journey helping me develop my scientific, organizational, presenting and (hopefully) writing skills. I will be forever thankful for the long discussions that would start very scientific and sometimes end in a very personal note.

I would also like to thank the two very helpful and supportive supervisors I had along this PhD, Prof. Aurelien Thomas and Prof. Luc Pellerin, and committee members Anna Price and Prof. Ellen Fritsche for their scientific input and time.

I could not forget the members of Zurich's lab, from students to post-docs, thank you for helping me in this learning process. I've to specially thank Denise, Vanille and Cendrine for the help with experiments, the organization madness and the fun times!

I would also like to thank all the colleagues from de DBS for all the encouragement, lunch breaks, aperos, after-works and occasional scientific collaborations. It was a pleasure to share the last years and learn with you all. Special thanks to Sofia, Daniel, Valentina, Sylviane, Almar, Minie, Citla and Alessandro, you turned this process a joy.

To the in3 family, the warmest thank you. From PIs to ESRs, it was a pleasure to share this time with you and have the chance to learn from you. I will always remember with affection all the time, work, discussion, congresses, meetings, trips, hotels, food and drinks we shared. Special thanks to Prof. Paul Jennings for putting together all this people and for his dedication, Prof. Nynke Kramer and Susana Proença for kindly welcome me in their lab for two secondments and Gladys Ouedraogo and L'Oréal for the opportunity of visiting and learn with them. To my forever colleague Sara Wellens, thank you for always be there to share a room/house with me and kindly remind me of how short my legs are.

A special thanks to all the professors that fed my scientific curiosity and directly or indirectly were part of this journey, specially to Prof. Sylvie de Jesus, Prof. Sólveig Thorsteinsdóttir and Prof. Gabriela Rodrigues.

To all the people from Allinky and JRC that believed in me and in my skills, thank you.

And because friends are of extreme importance to keep the boat floating, I am lucky enough to have many to thank! Vee, Denys, Andreia, Ana, Fábio, Vera, Joana, Afonso, João, Bidarra, Cátia e Gui you are amazing and I am everyday thankful for having you to share life with and to be able to say that distance is not a thing.

Last but not least, I have to thank my very special, not so behaved, but very fun and supportive family that I love! To my parents that raised me like no one to take all the challenges with bravery but always spreading kindness, *é bom que estejam orgulhosos*. To madrinha Clara, Abilio, Fábio and Beatriz for the endless motivation, fun and care, *obrigadinha*. And Hugo, thank you for letting me freely compete with the french complaining mode, help manage my endless stress, for all the deep discussions and for always inspire me out of my comfort zone. But, most of all, thank you for being my home away from home.



---

# Abstract

---

Chemicals need to be tested for their potential to harm humans. Most of the guidelines for chemical risk assessment from the Organisation for Economic Co-operation and Development (OECD) include tests performed on animals, raising not only financial and ethical concerns but also scientific ones. Thus, the development and use of human-based models for toxicity testing is highly encouraged. Due to their few ethical constraints and ability to differentiate into all cell types, human induced pluripotent stem cells (hiPSC) have gained increasing scientific interest, and several hiPSC-derived neural and glial models have been proposed for neurotoxicity testing.

BrainSpheres (BS) is a hiPSC-derived 3D cell culture system containing various brain cell types, allowing cell-to-cell interactions and recapitulating the main neurodevelopmental processes. Here, the ability of BS to respond to chemical exposure has been characterized. Within the Marie Curie international training network in3, BS were exposed to various compounds, such as valproic acid, paraquat, amiodarone, cadmium, lead and doxorubicin. Cytotoxicity concentration-response curves were established to determine sub-lethal concentrations for further testing. The toxicogenomics tool TempO-Seq with a list of curated genes covering known stress pathways and cell-type specific markers showed to be a valuable tool to detect the biological processes disturbed by the tested chemicals. Data revealed that BS replicate the described mechanisms of action of the chemicals, such as oxidative stress and unfolded protein response for paraquat and metal response for cadmium, but also showed for the first time in brain cells, the perturbation of lipid metabolism after amiodarone exposure.

Since the nominal concentration of a chemical may not reflect its bioavailable concentration, distribution kinetics studies were performed. Results indicate a cellular accumulation of amiodarone with time, supporting the stronger adverse effects on neurons and astrocytes detected after repeated exposure, and an inefficient cellular uptake of Valproic acid, corroborating the few adverse effects observed.

Finally, to improve the ability of BS to mimic brain reactions to chemicals and therefore to better detect potential neurotoxicants, the possibility to reproduce the neuroinflammatory response was tested by adding hiPSC-derived microglia progenitors. In BS, the microglia progenitors gained microglia-like cells characteristics and, upon exposure to LPS and IFN $\gamma$ , became reactive and had deleterious effects on oligodendrocytes.

Overall, the work presented here emphasizes the interest of using BS for neurotoxicity testing and adds precious information on the way this system can be used for mechanistic neurotoxicity assessment. Furthermore, it shows the importance of associating toxicokinetics to toxicodynamics in order to make BS a useful tool for quantitative *in vitro* to *in vivo* extrapolations (QIVIVE).

---

# Résumé

---

Le potentiel toxique des produits chimiques présents dans l'environnement doit être évalué. Pour ce faire, la plupart des directives de l'Organisation de coopération et de développement économique (OCDE) incluent des tests à exécuter sur des animaux, ce qui soulève non seulement des questions financières et éthiques, mais aussi scientifiques. Le développement et l'utilisation de modèles basés sur des cellules humaines est donc fortement encouragé. Les cellules souches pluripotentes humaines induites (CSPHi) ont gagné un intérêt scientifique croissant étant donné le peu de contraintes éthiques qui leur sont liées, et leur capacité à se différencier dans tous les types de cellules de l'organisme. Ainsi, de nombreux modèles dérivés de CSPHis ont été proposés pour tester la neurotoxicité.

Le terme BrainSpheres (BS) désigne un modèle de cultures de cellules dérivées de CSPHis, contenant divers types cellulaires du cerveau, permettant de nombreuses interactions cellulaires et récapitulant les principaux processus du développement cérébral. Ici, la capacité des BS à répondre à une exposition aux produits chimiques a été caractérisée. Au sein du projet "in3" financé par le réseau international Marie Curie, les BS ont été exposées à différents composés, tels que paraquat, amiodarone, acide valproïque, cadmium, plomb et doxorubicine. Leur cytotoxicité a été établie pour sélectionner les concentrations à la limite de la toxicité. L'outil toxicogénomique Tempo-Seq, comprenant une liste de gènes recouvrant les voies de signalisation de stress et des marqueurs spécifiques pour les différents types cellulaires, s'est révélé être très bon pour détecter les processus biologiques modifiés par les composés chimiques. Les résultats montrent que les BS répliquent les mécanismes d'action des produits chimiques, comme le stress oxydatif et la réponse aux protéines non repliées pour le paraquat, et la réponse aux métaux pour le cadmium. Mais ils montrent aussi, pour la première fois dans les cellules cérébrales, la perturbation du métabolisme lipidique après exposition à l'amiodarone.

Puisque la concentration nominale d'un composé chimique ne représente pas forcément sa concentration bio-disponible, la cinétique de distribution des composés a été déterminée. Les résultats indiquent une accumulation intracellulaire d'amiodarone qui supporte les effets délétères plus marqués détectés sur les neurones et les astrocytes après une exposition répétée, et une capture inefficace de l'acide valproïque corroborant l'observation de peu d'effets toxiques.

Finalement, pour améliorer la capacité des BS à mimer les réactions des cellules cérébrales aux produits chimiques, et donc affiner sa détection des neurotoxines, la possibilité de reproduire la réponse neuro-inflammatoire a été testée en ajoutant des progéniteurs de microglies dérivés de CSPHi. Dans les BS, ces cellules ont développé des caractéristiques de microglies et, après activation, sont devenues délétères pour les oligodendrocytes.

Dans l'ensemble, ce travail montre l'importance des BS pour la neurotoxicologie et ajoute de précieuses informations sur la manière d'utiliser ce système pour l'évaluation des mécanismes de neurotoxicité. De plus, il montre l'importance d'associer la toxicocinétique à la toxicodynamique dans le but de faire des BS un outil utile pour l'extrapolation *in vitro-in vivo*.

---

# General public abstract

---

We are constantly exposed to chemicals in our daily life. Determining the harmful effects of chemicals is thus important for human safety. Safety assessment is currently performed mainly through expensive, time consuming, scientifically and ethically questionable tests in animals. Human induced pluripotent stem cells (hiPSC) have less ethical problems associated and can be differentiated into many different cell types. Thus, hiPSC-derived models have gained increasing interest for neurotoxicology testing.

BrainSpheres (BS) is a hiPSC-derived 3D cell culture system containing various brain cell types, allowing cell-to-cell interactions and recapitulating the main developmental processes occurring in the brain. To be use for neurotoxicity testing, the ability of BS to replicate expected effects of chemical exposure should be evaluated. Within the Marie Curie training network in3, BS were exposed to very well-known chemicals, such as the herbicide paraquat, the heavy metals lead and cadmium and the drugs doxorubicin, amiodarone and valproic acid. Gene and protein expression techniques showed that BS can reproduce the previously described effects of these 6 different chemicals, suggesting that they can be used to assess the potentially toxic effects of unknown chemicals. Furthermore, in order to link the toxic effects detected in BS to the effects these chemicals could trigger in humans, the concentration of chemical that is available to interact with its targets should be defined. Therefore, tests were made to understand how the chemicals distribute in the BS system, between the medium, the cell fraction and the binding to plastic ware.

Finally, to improve the ability of BS to mimic the reaction of brain cells to chemicals, and thus to refine its detection of neurotoxins, the possibility to reproduce the neuroinflammatory response was evaluated by adding microglia, the brain resident macrophages and key players of the neuroinflammatory process, lacking in BS. These cells proved to be able to reproduce neuroinflammation traits and to cause detrimental effects on oligodendrocytes upon activation.

Overall, BS showed the possibility of being used to detect potentially detrimental chemicals and to be modified to evaluate the activation of neuroinflammation, in order to make the system even more powerful. Information on the effects of a given chemical together with its distribution in BS can be used to better associate the exposure to chemicals and its effects on human.

---

# Résumé vulgarisé pour le grand public

---

Nous sommes constamment exposés à des produits chimiques dans notre vie de tous les jours. Il est donc très important d'en déterminer les effets nocifs pour notre santé. L'évaluation de la toxicité des produits chimiques est actuellement réalisée sur des animaux, ce qui soulève non seulement des questions financières et éthiques, mais aussi scientifiques. Les cellules souches pluripotentes humaines induites (CSPHi) présentent moins de contraintes éthiques, et sont capables de se différencier dans tous les types de cellules de l'organisme. Elles sont ainsi devenues très intéressantes pour tester la neurotoxicité.

Le terme BrainSpheres (BS) désigne un modèle de cultures de cellules dérivées de CSPHis, contenant divers types cellulaires du cerveau, permettant de nombreuses interactions cellulaires et récapitulant les principaux processus du développement cérébral. Ici, la capacité des BS à répondre à une exposition aux produits chimiques a été caractérisée. Au sein du projet «in3» financé par le réseau international Marie Curie, les BS ont été exposées à différents composés connus, tels que l'herbicide paraquat, les métaux lourds cadmium et plomb, ainsi que les médicaments doxorubicine et acide valproïque. Différentes techniques, telles que l'expression de gènes et de protéines, ont montré que les BS sont capables de reproduire les effets toxiques précédemment reportés pour ces 6 composés, suggérant que les BS pourraient être utilisées pour détecter le potentiel neurotoxique de produits encore non testés. De plus, afin de pouvoir relier les effets toxiques détectés dans les BS aux effets que pourraient déclencher ces composés chez l'homme, la concentration de composé ayant effectivement pénétré dans les cellules a été déterminée.

Finalement, pour améliorer la capacité des BS à mimer les réactions des cellules cérébrales aux produits chimiques, et donc affiner sa détection des neurotoxines, la possibilité de reproduire la réponse neuro-inflammatoire a été testée en ajoutant des microglies, les macrophages résidents du cerveau et cellules clés du processus neuro-inflammatoire, manquant dans les BS. Ces cellules se sont montrées capables de reproduire certaines caractéristiques de la neuro-inflammation et de causer des effets délétères sur les oligodendrocytes.

Dans l'ensemble, ce travail montre la possibilité d'utiliser les BS pour détecter des produits potentiellement neurotoxiques et décrit certaines améliorations qui pourraient être apportées à ce système afin de le rendre encore plus performant. De plus, il montre l'importance de combiner la distribution d'un produit chimique dans les BS aux effets toxiques qu'il y provoque, afin de rendre l'utilisation de ce système *in vitro* possible pour la prédiction des effets délétères des produits chimiques sur la santé humaine dans le futur.

---

# List of abbreviations

---

<b>3Rs</b> - Replacement, Reduction and Refinement of Animal Experiments	<b>MT1F</b> - metallothionein 1F
<b>7d</b> - 7 days repeated exposure	<b>MT1G</b> - metallothionein 1G
<b>7dW</b> - 7d followed by a week of wash-out	<b>MT1M</b> - metallothionein 1M
<b>AChE</b> - acetylcholinesterase	<b>MT1X</b> - metallothionein 1X
<b>AMI</b> - amiodarone	<b>MT2A</b> - metallothionein 2S
<b>AO</b> - adverse outcome	<b>NAM</b> - new approach methodology
<b>AOP</b> - adverse outcome pathway	<b>NANOG</b> - Nanog homeobox
<b>BBB</b> - Blood-brain barrier	<b>NEFL</b> - neurofilament light chain 68kDa
<b>BDNF</b> - brain derived neurotrophic factor	<b>NF200</b> - neurofilament heavy chain 200kDa
<b>BS</b> - BrainSphere	<b>NPC</b> - neural progenitor cells
<b>CdCl<sub>2</sub></b> - cadmium chloride	<b>NQO1</b> - NAD(P)H quinone dehydrogenase 1
<b>CRA</b> - chemical risk assessment	<b>NRC</b> - US National Research Council
<b>DEG</b> - differentially expressed probe	<b>NRF2</b> - nuclear factor, erythroid 2 Like 2
<b>DNT</b> - developmental neurotoxicity	<b>NT</b> - neurotoxicity testing
<b>DOXO</b> - doxorubicin hydrochloride	<b>O4</b> - oligodendrocyte marker 4
<b>ER</b> - endoplasmic Reticulum	<b>OECD</b> - organisation for economic co-operation and development
<b>ESCs</b> - embryonic stem cells	<b>Olig1</b> - oligodendrocyte transcription factor 1
<b>ESR</b> - estrogen response	<b>Olig2</b> - oligodendrocyte transcription factor 2
<b>GFAP</b> - glial fibrillary acidic protein	<b>Pb</b> - lead (ii) chloride
<b>GRIN1</b> - glutamate ionotropic receptor NMDA type subunit 1	<b>PBPK</b> - physiologically-based pharmacokinetic modelling
<b>hiPSC</b> - human induced pluripotent stem cell	<b>PCA</b> - principal component analysis
<b>HLC</b> - hepatocyte-like cell	<b>PQ</b> - paraquat dichloride hydrate
<b>HMOX</b> - heme oxygenase 1	<b>qAOP</b> - quantification of AOPs
<b>Iba1</b> - allograft inflammatory factor 1	<b>QSAR</b> - quantitative structure-activity relationship
<b>IFN<math>\gamma</math></b> - Interferon $\gamma$	<b>REACH</b> - Registration, Evaluation and Authorization of Chemicals
<b>in3</b> - <i>in vitro</i> , <i>in silico</i> and integration	<b>ROS</b> - reactive oxygen species
<b>iPSC</b> - induced pluripotent stem cells	<b>S100<math>\beta</math></b> - S100 calcium binding protein B
<b>KEs</b> - key events	<b>Sox2</b> - SRY-Box transcription factor 2
<b>Ki67</b> - marker of proliferation Ki-67	<b>SYP</b> - synaptophysin
<b>LD50</b> - median lethal dose	<b>TH</b> - tyrosine hydroxylase
<b>LFC</b> - log <sub>2</sub> fold change	<b>UPR</b> - unfolded protein responses
<b>LPS</b> - Lipopolysaccharide	<b>VPA</b> - valproic acid sodium salt
<b>MAP2</b> - microtubule associated protein 2	<b><math>\mu</math>BS</b> - BS with microglia-like cells
<b>MBP</b> - myelin basic protein	
<b>MIE</b> - molecular initiating event	
<b>MT1E</b> - metallothionein 1E	



---

# Table of Contents

---

IMPRIMATUR.....	I
ACKNOWLEDGEMENTS.....	IV
ABSTRACT.....	VI
RÉSUMÉ.....	VII
GENERAL PUBLIC ABSTRACT.....	VIII
RESUME VULGARISE POUR LE GRAND PUBLIC.....	IX
LIST OF ABBREVIATIONS.....	X
TABLE OF CONTENTS.....	II
<b>CHAPTER 1: INTRODUCTION.....</b>	<b>1</b>
1.1 HOMO SAPIENS AND CHEMICALS, AN OLD TOXIC FRIENDSHIP.....	2
1.2. ANIMAL TESTING AND THE DAWN OF TOXICOLOGY.....	5
1.3. THE WAY FORWARD: <i>IN VITRO</i> TESTING.....	6
1.4. NEUROTOXICOLOGY.....	8
1.5. BRAIN SPHERES.....	9
1.6. REGULATORY TOXICOLOGY AND CHEMICAL RISK ASSESSMENT, THE PERFECT SYMBIOSIS FOR A SAFER WORLD.....	10
1.7. MARIE CURIE TRAINING NETWORK: IN3.....	11
1.8. RESEARCH AIMS OF THIS THESIS AND ITS OUTLINE.....	14
<b>CHAPTER 2: AN <i>IN VITRO</i> STRATEGY USING MULTIPLE HUMAN INDUCED PLURIPOTENT STEM CELL-DERIVED MODELS TO ASSESS THE TOXICITY OF CHEMICALS.....</b>	<b>15</b>
2.1. INTRODUCTION.....	16
2.2. CONTRIBUTION.....	16
2.3. SUMMARY OF THE RESULTS.....	16
<b>CHAPTER 3: <i>IN VITRO</i> DISTRIBUTION KINETICS AND NEUROTOXICITY OF THE CARDIAC DRUG AMIODARONE IN THE IPSC-DERIVED HUMAN 3D MODEL BRAINSPHERES.....</b>	<b>33</b>
3.1. INTRODUCTION.....	34
3.2. CONTRIBUTION.....	34
3.3. SUMMARY OF THE RESULTS.....	34
1. INTRODUCTION.....	37
2. MATERIAL AND METHODS.....	39
3. RESULTS.....	44
4. DISCUSSION.....	57
5. REFERENCES.....	61
<b>CHAPTER 4: ABILITY OF BRAINSPHERES TO DETECT THE NEUROTOXICITY OF VARIOUS CLASSES OF CHEMICALS.....</b>	<b>65</b>
4.1. AIM.....	66
4.2. MATERIAL AND METHODS.....	66
4.3. RESULTS.....	68
4.4. RESULTS OUTLINE.....	75

<b>CHAPTER 5: FURTHER CHARACTERIZATION OF THE MODEL.....</b>	<b>77</b>
5.1. AIM.....	78
5.2 MATERIAL AND METHODS .....	78
5.3. RESULTS .....	79
5.4 RESULTS OUTLINE .....	81
<b>CHAPTER 6: ACTIVATION OF HUMAN MICROGLIA IS DELETERIOUS FOR OLIGODENDROCYTES IN A COMPLEX HUMAN IPSC-DERIVED 3D MODEL.....</b>	<b>83</b>
6.1. INTRODUCTION .....	84
6.2. CONTRIBUTION .....	84
6.3. SUMMARY OF THE RESULTS .....	84
1. INTRODUCTION .....	87
2. METHODS.....	89
3. RESULTS .....	93
4. DISCUSSION .....	99
5. CONCLUSIONS .....	101
6. REFERENCES.....	101
<b>CHAPTER 7: PARTICIPATION ON THE DEVELOPMENT OF AOP17 BINDING TO SH/SELEN-PROTEINS CAN TRIGGER NEUROINFLAMMATION LEADING TO NEURODEGENERATION .....</b>	<b>107</b>
7.1. ABSTRACT.....	108
7.2. CONTRIBUTION .....	108
<b>CHAPTER 8: DISCUSSION.....</b>	<b>109</b>
8.1. SUCCESSFUL ESTABLISHMENT OF BRAINSPHERES USING A NEW hiPSC LINE.....	111
8.2. ESTABLISHMENT OF AN EXPOSURE WINDOW TO ASSESS EFFECTS ON CELL TYPES AND THEIR INTERACTIONS.....	112
8.3. EXPOSURE CONCENTRATION AND THEIR EPIDEMIOLOGICAL RELEVANCE .....	113
8.4. BS CAN BE USED TO ASSESS CHEMICAL EFFECT ON DIFFERENT BIOLOGICAL PROCESSES.....	114
8.5. DISTRIBUTION KINETICS, AN IMPORTANT PLAYER IN NEUROTOXICITY ASSESSMENT .....	116
8.6. TEMPO-SEQ DATA ANALYSIS AS A SCREENING TOOL.....	117
8.7. MICROGLIA .....	118
8.8. CONCLUDING REMARKS AND PERSPECTIVES .....	119
<b>REFERENCES.....</b>	<b>122</b>
<b>SUPPLEMENTARY DATA .....</b>	<b>133</b>
<b>ANNEX 1.: CHAPTER 2 SUPPLEMENTARY DATA .....</b>	<b>138</b>
<b>ANNEX 2.: CHAPTER 3 SUPPLEMENTARY DATA .....</b>	<b>141</b>
<b>ANNEX 3.: AOP17 KER: OXIDATIVE STRESS LEADS TO CELL INJURY/DEATH .....</b>	<b>146</b>

---

# Chapter 1: Introduction

---

*Section 1.1 to 1.4 are heavily based on the book chapter “Neurotoxicology and disease modelling” (Nunes and Zurich, 2020).*

## 1.1 Homo sapiens and chemicals, an old toxic friendship

As a rather small and not so fast species, early Humans had to find creative ways to get food. When the other animal's hunting leftovers were not enough, early humans started to hunt with sharp objects, traps and venoms extracted from animals and plants. Later, sources indicate that Greeks, Scythians, and Nubians used poisoned dipped arrows, javelins, and other weapons in battle (Mayor, 2003). The extracted substances were also used to help overcome health issues.

The increasing knowledge of extracted substances and their effects on living organisms lead to a need to classify them. Although it is safe to assume that even pre-historic humans categorized some plants as harmful and other as safe, it is difficult to find evidence of such classification (Mayor, 2003). The Sumerians were the first making a written record of medicinal plants, they created a list of hundreds of plants in clay tablets (Sumner, 2000). Ancient Egyptians produced the Ebers Papyrus (1500 B.C.E.), a record containing mentions of over 700 substances and over 300 recipes detailing incantations and mixtures using poisonous or medicinal minerals and plants. Besides more medicinal records, it is possible to find references of venoms through several tales such as *The Odyssey and The Iliad* (850 B.C.E) where Homer describes the use of poisoned arrows.

As more substances were used, the classification got more complex and extended. In ancient Greek literature numerous poisons and their use are described (Gallo, 2013). Interestingly, Greeks defined all drugs or potions as "pharmaka" or "pharmakon" without making any distinction between harmful and safe compounds, or compounds used for the treatment of diseases (Bailey, 2007; Hayes and Gilbert, 2009). Dioscorides (40-90 C.E.), a Greek physician in the court of the Roman emperor Nero, published In *De Materia Medica* with the classification of about 600 substances. Dioscorides classification remained in use till 1600s and became the basis for the modern pharmacopoeia (Gallo, 2013; Hayes and Gilbert, 2009).

Quite early in society, murder became a way to escalate in the hierarchy, and venoms a clean way to reach this goal. Murder was so mainstream that around 81 B.C.E., Lucius Cornelius Sulla (138–78 B.C.E.) a Roman general, issued the law Lex Cornelia de Sicariis et Veneficiis. The law clearly stated that any person who makes, sells, possesses, or purchases a "venenum malum" (poisonous or noxious substance) with the intention of committing murder may be sent for trial (Hayes and Gilbert, 2009). However, despite these efforts, poisoning kept being common and socially accepted. In the Medieval and Renaissance periods there are several reports of influent people, like popes, being poisoned by their opponents. One could even learn the dark art of poisoning in specialized schools. Payment for poisoning people was quite common, as

testified by the price scale emitted for this type of services by the Venetian Council of Ten (1310-1797), the most important governing body in the state of Venice (Hayes and Gilbert, 2009).

Philippus Aureolus Theophrastus Bombastus von Hohenheim (1493–1541 C.E.), best known as Paracelsus, was a Swiss physician, alchemist, and astrologer. Paracelsus defined for the first time the importance of the dose by saying, ‘Alle Dinge sind Gift, und nichts ist ohne Gift; allein die Dosis macht, dass ein Ding kein Gift sei.’ interpreted as, the dose makes the poison. Paracelsus also believed that diseases were primarily associated with a specific organ in the body, giving rise to the idea of “target organ toxicity”. He questioned the long-standing ideas of his time and tried to rationalize the treatment of diseases (Hayes and Gilbert, 2009).

In the 19<sup>th</sup> century, following the birth of the synthetic chemical industry, the field of toxicology emerged in response to the need to understand how chemical substances might affect the health of workers and consumers. Bernardino Ramazzini (1633–1714), an Italian physician, published *De Morbis Artificum Diatriba (Diseases of Workers)* where he outlined the health hazards of chemicals in more than fifty occupations. Although he was not the first to correlate occupation and diseases, he gave rise to occupational medicine, advising physicians to relate their patients’ occupation to their symptoms. In 1775, Percival Potts (1714-1788), an English surgeon, became the first scientist to find an association between environmental chemicals and cancer. Potts established the occupational link between soot and scrotal cancer and can therefore be considered the founder of occupational toxicology (Pappas *et al.*, 1999). At the same time, there was very little, if any, legislation to govern the production or distribution of chemicals. Poisons such as arsenic were still easily accessible, being sold at drugstores, and medicines for children contained opium against hyperactivity, teething or cramps, heroin was sold as sedative for cough, and cocaine against toothache (Fig.: 1.1).

In 1906, one of the first laws regulating the marketing of drugs was released in the USA. From this date, manufacturers had to provide an accurate labelling of dosage and contents of their products. Prior to this, many drugs advertised benefits from secret ingredients. In 1937, more than 100 deaths by liver failure were linked to the consumption of a new formulation of the antibiotic Sulfanilamide produced in the USA, due to the toxicity of the diethylene glycol used as an excipient. This disaster emphasized the importance to regulate the commerce of chemicals and their safety. In consequence, in the USA the Federal Food, Drug and Cosmetic Act, which required Food and Drug Administration approval before the release of a new drug, was accepted in 1938. In Europe the conscience of the importance of this type of regulation only came after another tragic episode. Thalidomide was released as a sedative in 1957 and was prescribed to alleviate morning sickness in pregnant women. Malformations in more

than 10,000 children born in 46 different countries were linked to Thalidomide before it was withdrawn from the market in 1961. Nowadays, despite this tragedy, thalidomide is back for the treatment of skin lesions caused by leprosy and for multiple myeloma (Rehman *et al.*, 2011). In this case, excluding the pregnant women, the benefits of Thalidomide treatment are higher than the risks. Unfortunately, in many developing countries, drug control is deficient and babies continue to be born with birth defects due to Thalidomide.



**Figure 1.1** Now known dangerous chemicals were freely commercialized and publicized.

(A) A 19th century advertisement for arsenic wafers in the United States. (B) Cocaine Toothache drops from 1880's. (C) Sears, Roebuck and Co. where marketing laudanum (a tincture of opium containing approximately 10% powdered opium by weight) as a sleep remedy for infants. (D) Heroin was originally marketed in the end of the 19<sup>th</sup> century as a cough medicine.

## 1.2. Animal testing and the dawn of toxicology

The Society of Toxicology defines toxicology as the study of the adverse effects of chemical, physical or biological agents on living organisms and the ecosystem, including the prevention and amelioration of such adverse effects. After the start of toxicology studies in the 19<sup>th</sup> century, there was a rapid development of analytical methods in the late 19th century and then an acceleration of both method and scientific development in the latter half of the 20th century (Pappas *et al.*, 1999). The first scientific experimental determinations of the toxic effects of chemicals were performed on animals.

In 1927 the British pharmacologist J.W Trevan proposed to determine the median lethal dose (LD50) of chemicals to evaluate and compare their toxicity (Trevan, 1927). LD50 is the single dose of a given chemical required to kill half of the members of a tested population after a certain exposure time. This measurement appealed to governments and regulators since it provides one simple, generalized indicator of the toxicity of a chemical (Morris-Schaffer and McCoy, 2020).

Other animal tests were established during the 20th century. The standardized Draize test was developed by John Draize in 1944 to assess eye and skin irritation caused by chemicals. It consists in applying the test substance in the eye or skin of a restrained, conscious animal, usually albino rabbits, and to assess the effects until 14 days after exposure (Draize *et al.*, 1944). Animals that did not exhibit any permanent effects could be used for other tests. In the 1950s decade, a test was developed to identify carcinogenic chemicals through the daily dosing of rats and mice for 2 years (Parasuraman, 2011). After the Thalidomide incident, reproductive and developmental toxicity studies were introduced where the animals are exposed to chemicals at different steps of reproduction to assess the effects on the development of the offspring.

Animal experimentation allowed the establishment of dose-response relationships, the importance of the duration of the exposure and of the route of exposure. Soon it was recognized that industrial chemicals and even drugs could cause a wide range of diseases and/or disabilities, such as, birth defects, impairment of development, cancer, and impairment of learning and memory. As we stand today, regulatory toxicologists rely almost exclusively on animal *in vivo* experimentation for human safety assessment. In absence of other techniques and with very limited understanding of toxicological mechanism, animal *in vivo* studies were probably the only way to best ensure human safety (Jennings, 2015a). However, a deeper understanding of biology, species differences in xenobiotic handling and toxic mechanisms made clear the need for a paradigm shift in toxicology. Furthermore, the huge financial cost of animal testing and the burden on non-human mammals speak also in favour of a radical change in our way to assess

human safety. This shift was proposed by the US National Research Council (NRC) in 2007, in a report entitled “Toxicity Testing in the 21st Century: A Vision and a Strategy” (NRC, 2007). The basic proposal was to re-orient testing to the molecular level, rather than observing phenotypic responses at the level of whole organisms together with a strong encouragement for the development of human based models for toxicology.

### **1.3. The Way Forward: *In Vitro* Testing**

In the report Toxicity Testing in the 21st Century: A Vision and a Strategy, experts highlighted the concept of “toxicity pathways”, as the way forward to understand and interpret the toxicant-induced mode of action (NRC, 2007). Pathway responses are dose-dependent. At some low dose, a pathway may begin to be disrupted by a toxicant exposure, but, due to a homeostatic response, also called an “adaptive” behaviour, the pathway will continue to function. Increasing the dose, the adaptive and reparative response is eventually overcome, and an adverse effect takes place. Molecular pathways are better studied *in vitro* than *in vivo*, therefore, the implementation of this new strategy required the development of new *in vitro* tests. Due to metabolization differences between species, the new methods should preferably be based on human cells.

In 1959 Russell and Burch have delineated the “replace, reduce and refine” (3Rs) principle for animal testing in their book entitled, “The principles of humane experimental technique” (Russell and Burch, 1959). The 3Rs principle can be explained as follows: “Replace” the animal experimentation by methods which permit a given purpose to be achieved without conducting experiment or other scientific procedures on animals; “Reduce” by methods for obtaining comparable levels of information from the use of fewer animals in scientific procedures, or for obtaining more information from the same number of animals; and “Refine” by using methods which alleviate or minimise potential pain, suffering and distress, and which enhance animal well-being.

During his PhD, Björn Ekwall (1940-2000) proposed to predict human acute systemic toxicity of chemicals by using cell-culture tests instead of animal LD50 determinations. Ekwall also defined the “basal cytotoxicity concept” (Ekwall, 1983, 1980; Ekwall and Johansson, 1980) and classified the effect of chemicals into three categories: (i) basal cytotoxicity resulting from interference with structures and/or properties essential for cell survival, proliferation and/or functions; (ii) organ-specific toxicity, which affects organ-specific structures or functions; (iv) toxicity at the organizational level (Bernson *et al.*, 1986; Ekwall, 1983).

Since then, the field of *in vitro* toxicology progressed tremendously with the development of very performant organ-specific cell culture systems and of high throughput and high content analytical techniques. Yet, most of the cell cultures were derived from animals but, as already pointed out by Russel and Burch (1959), similar species do not necessarily represent good models for each other. They called this the “high fidelity fallacy”, which is well illustrated in the high rate of drug candidate failures during clinical testing, due to both a lack of efficacy in humans and the identification of unacceptable toxicities not previously identified in pre-clinical animal testing (Jennings, 2015a). Following the paradigm shift and the raised concerns about using animals-based studies for chemical safety assessment, there has been an effort to develop new tools based on human cell lines and primary cells. However, in order to keep their viability in culture, most of the established human cell lines exhibit cancerous phenotypes and thus have, by definition, an abnormal cell physiology. On the other hand, although primary cells tend to recapitulate largely normal cell physiology, it is difficult to keep them in culture for long periods maintaining the high-quality standards required to assure reproducible results. Furthermore, it is very difficult, technically and ethically, to obtain primary cells from certain organs, such as the brain.

The ultimate progress in the field of *in vitro* toxicology was made possible by the groundbreaking discovery by Takahashi and Yamanaka in 2007 of the technique allowing the derivation of induced pluripotent stem cells (iPSC) from human somatic cells (Takahashi *et al.*, 2007). At the time, they described how to derive iPSCs from human cultured fibroblasts by over-expressing the transcription factors Oct3/4, Klf4, Sox2 and c-Myc. While iPSCs share capacity for self-renewal and pluripotent potential of embryonic stem cells (ESCs), its generation from adult somatic cells come with a range of advantages while avoiding some controversies associated to ESCs (Liu *et al.*, 2017). The Nobel Prize in Physiology and Medicine 2012 was jointly awarded to John B. Gurdon and Shinya Yamanaka for this discovery highlighting the potential impact of this methodology. One of the biggest advantages of human iPSCs (hiPSC) is that they can be specifically differentiated in almost all human cell types which can be used, among other potential applications, for toxicity testing and disease modelling. Another advantage is the possibility of deriving hiPSCs from any living donor with a detailed health record and the possibility of being further followed. The methods to induce stemness have improved over the years using non-integrating techniques such as self-replicating RNA or Sendai virus. Also a lot of progress has been made in developing protocols to differentiate hiPSCs into specific cell types including neural, lung, liver, kidney, endothelial and vasculature lineages (Boon *et al.*, 2020; Stuart M Chambers *et al.*, 2009; Chandrasekaran *et al.*, 2021; Fransen and Leonard, 2021;

Gholami *et al.*, 2021; Lo Giudice *et al.*, 2019; Murphy *et al.*, 2019; Nunes and Zurich, 2020; Pamies *et al.*, 2017b; Wellens *et al.*, 2021). Due to the interest of hiPSCs for different fields, efforts have been made on the creation of cell banks for standardised, quality assured iPSCs (Morrison, 2018).

#### **1.4. Neurotoxicology**

Neurotoxicity or a neurotoxic effect is an adverse change in the structure or function of the nervous system following exposure to a chemical agent (Congress Office of Technology, 1990).

Nowadays guidelines for neurotoxicity (NT) testing and developmental neurotoxicity (DNT) testing are based exclusively on animal experimentation (OECD test guideline 418, 419, 424, 426) (Fritsche *et al.*, 2015; Masjosthusmann *et al.*, 2018). These guidelines are, in most cases, followed for chemicals that produced detectable adverse effects on the nervous system in the mandatory *in vivo* based standard single dose or repeated dose toxicity studies. The described *in vivo* tests are raising ethical, financial and scientific concerns. Indeed, while such guideline studies are currently necessary for consumer safety, it is already known that these animal tests might have limited prediction for human neurotoxicity due to inter-species variation (Leist and Hartung, 2013). Therefore, although decades of work on neuronal and glial cellular systems derived from several animal species has delivered a range of reliable *in vitro* assays highly valuable for neurotoxicity testing (Forsby *et al.*, 2009; Gabriel *et al.*, 2017; Schmidt *et al.*, 2017; Tiffany-Castiglioni, 1993; Veronesi, 1992; Zurich *et al.*, 2013, 2000), there is a growing need for human-based *in vitro* models.

Even with the constraints of getting neural human cells, there are various human neuronal-like immortalized cell lines available. However, as the expression of tumour growth-related genes expressed in these cell lines may affect the cellular responses to a chemical exposure, the use of human stem cells and their progeny is strongly advised (Bal-Price *et al.*, 2018, 2012). Due to their few ethical constraints, hiPSCs derived neuronal and glial models are currently gaining increasing scientific interest. Not surprisingly, it has been shown in the past that a given brain cell type reacts differently to a toxic substance when grown in a single cell-type culture than in a mixed-cell types culture (Eskes *et al.*, 2003, 2002; Zurich *et al.*, 1998). Therefore, complex 3D cell culture systems containing many brain cell types, allowing a maximum of cell-to-cell interactions and recapitulating the main neurodevelopmental processes are also of the utmost importance for the evaluation of the adverse effects of chemicals. Pamies

*et al.* (2017) recently described such a model derived from hiPSCs that was easily adapted for different studies related to toxicology, viral infection and cancer (see section 1.5 of this manuscript). A Human Cortical Organoids model derived from hiPSCs demonstrated the potential neurodevelopmental negative effects of methadone (Wu *et al.*, 2020). Another 3D model containing several brain cell types derived from human embryonic stem cells was also shown to be able to detect the toxicity of trimethyltin and paraquat, two known environmental neurotoxicants (Sandström *et al.*, 2017). Lancaster and colleagues (2014) reached an even higher level of biological complexity, by developing a hiPSC-derived 3D organoid culture system; however this model has not been yet used for neurotoxicity testing (Lancaster and Knoblich, 2014). In order to ensure the establishment of robust test systems, it is important to stress that growing stem cells and delivering reliable and well-characterized cultures for toxicity assessment require a high level of standardization of both undifferentiated and differentiated cell cultures. It is therefore of pivotal importance to define a set of quality control parameters suitable to properly characterize stem cell-derived models before using them for toxicity testing, especially those derived from hiPSCs (Coecke *et al.*, 2005; Pamies *et al.*, 2018a; Pistollato *et al.*, 2012).

Based on the current knowledge it can be stated that *in vitro* models of human brain cells, such as those derived from hiPSCs, can recapitulate a sequence of neurodevelopmental processes starting from neural progenitor cells (NPC) proliferation until an advanced stage of neuronal and glial differentiation and maturation. Quantitative evaluation of the impairment of these processes due to chemical exposure can serve as reliable readouts for *in vitro* neurotoxicology evaluation.

## **1.5. Brain Spheres**

In this thesis, the BrainSpheres (BS) model was used as a representative of the brain to test the neurotoxic potential of chemicals. The protocol was developed by Pamies *et al.* and published in 2017 (Pamies *et al.*, 2017b). The iPSC-derived human 3D brain microphysiological system was presented as a reproducible in terms of size, shape, and cell composition. Along 8 weeks in culture, NPCs differentiate into mature neurons and glial cells (astrocytes and oligodendrocytes). Indicating strong cell-to-cell interactions, BS show indication of the presence of active synapses (e.g., spontaneous electric field potentials) and neuronal-glial interactions (e.g., myelination).

Since its development, BS have been showed to be an interesting model to be used for different purposes. BS proven to be able to reproduce the developmental neurotoxicity of the pesticide rotenone and paroxetine (Pamies *et al.*, 2018b; Zhong *et al.*, 2020b) and the potential

neurotoxicity of the gold and poly-lactic acid nanoparticle (Leite *et al.*, 2019). Regarding disease modelling, BS were used to show that SARS-CoV-2 can infect neurons (Bullen *et al.*, 2020), test different treatment options for a given patient (Plummer *et al.*, 2019) and the synergy between an environmental exposure to the pesticide chlorpyrifos and autism specific mutations (Modafferi *et al.*, 2021).

Damage to the central nervous system (CNS) is associated with neuroinflammation, a pathophysiological process characterized by the activation of microglia cells and astrocytes, that constitutes a very sensitive indicator of neurotoxicity. To fully study the process of neuroinflammation in BS, besides neurons, astrocytes and oligodendrocytes, the model needs another cell type. Microglia cells, the immune resident cells of the brain, are missing in BS as their progenitors differentiate from another germ layer in the yolk sack and invade the brain during development (Sierra *et al.*, 2019). Abreu *et al.* have tried to add this cell type to the model by using a commercial available cell line (Abreu *et al.*, 2018). To improve the BS model, efforts are being made in the direction of adding hiPSC-derived microglia like cells to BS.

## **1.6. Regulatory Toxicology and chemical risk assessment, the perfect symbiosis for a safer world**

Humans may be exposed to chemicals, at the workplace (occupational exposure), from use of consumer products (consumer exposure) and indirectly via the environment. Regulatory toxicology aims to decrease the chance of human exposure to hazardous chemicals (Greim, 2020). To put in place regulatory actions, correct chemical risk assessment (CRA), with sufficient information on the hazardous properties of the chemical, relevance to human and environmental exposure, has to be assessed. The main CRA steps are: (1) problem formulation, (2) hazard assessment with identification and characterisation and (3) exposure assessment leading to risk characterisation (Greim, 2020; Wittwehr *et al.*, 2020). CRA process requires differentiation between reversible and irreversible effects. In case of irreversibility, the risk of the adverse effect should be estimated for each exposure scenario (Greim, 2020).

After the risk is well identified, characterised, assessed and estimated/quantified, risk management should be able to provide an answer as to how much risk is likely and which measures should be applied to reduce the chances of adverse effects on human health or the environment (Greim and Snyder, 2018; Leeuwen and Vermeire, 2007). Risk management has to take in account that effects on human health will depend on duration and route of exposure,

the toxicokinetics of the chemical, the dose–response relationship, and the susceptibility of the individual (Leeuwen and Vermeire, 2007).

As we stand today, strict testing guidelines are in place to understand the human and environmental effects of drugs, cosmetics and pesticides. For the new chemicals, that don't necessarily fit into these categories, several organizations developed programs to help collect and evaluate information about the ones that have high production rates (Greim and Snyder, 2018). In Europe, the implementation of the Registration, Evaluation and Authorization of Chemicals (REACH) regulation started in 2007. It was developed to identify potential hazardous substances and evaluate the risks associated with their exposure. Importantly, REACH places the burden of safety assessment of workers, users and environment on the producer or importer (Petry *et al.*, 2006; Williams *et al.*, 2009). Companies manufacturing or importing at least 1 tonne per year of a given compound, have to register all uses of chemical substances, either used on their own or in preparations. For quantities over 10 tonnes per year, the intrinsic properties and hazards of each substance have to be evaluated and a Chemical Safety Report has to be submitted for evaluation by the European Chemicals Agency and by the competent authorities from the member states. The tests to evaluate acute systemic toxicity, repeated dose toxicity and reproductive and developmental toxicity needed for the regulatory requirements keep relying mostly on animal studies (Pistollato *et al.*, 2021).

Since 2013 EU banned the marketing of cosmetics tested on animal for user safety (EC, 2013). This ban means that the consumers safety data of the commercialized formulation or individually used molecules cannot be acquired in animals. Even if a cosmetic proven to be safe for humans through non-animal methodologies, animal studies required for REACH continue to apply to assess risks for workers and environment (Pistollato *et al.*, 2021).

### **1.7. Marie Curie Training Network: in3**

Governmental agencies worldwide have been pushing towards the development of human-based assays for human safety assessment recognizing the need to develop new non-animal methodologies providing mechanistic understanding for toxicology testing (EUR-Lex, 2010; National Research Council, 2007; Oredsson *et al.*, 2019; Sewell *et al.*, 2017). The “in3” project (*in vitro*, *in silico* and *integration*) was funded by the EU's Marie Skłodowska-Curie Action - Innovative Training Network and aimed to drive the synergistic development and use of *in vitro* and *in silico* tools for human chemical and nanomaterial safety assessment by creating a multidisciplinary network with specific academic and industry expertise (Fig. x – in3 resume).

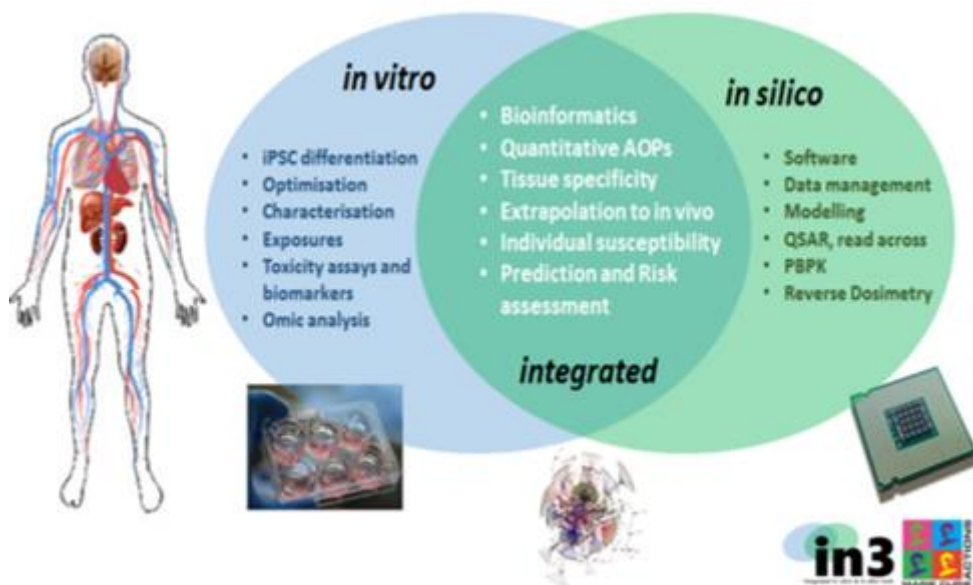


**Figure 1.2 – Graphical summary of the research carried by the in3 Project**

Adapted from the official website of the in3 Project (<https://www.estiv.org/in3/about.html>, accessed on September 07, 2021).

A number of selected 10 compounds (Doxorubicin hydrochloride, Pamidronate, Gentamicin sulphate, Paraquat dichloride, Cerium dioxide nanoparticles, Busulfan, Lead (II) chloride, Valproic acid, Amiodarone and Cyclosporine A) were tested in different tissue-representative models for the impact on cell viability, cell stress and inflammation. This data together with compound exposure kinetics was used to create tissue and organism-level models to predict adverse effects at human relevant doses. The approach required the integration of cell culture biology, mechanistic toxicology, cheminformatics, biokinetics, systems biology/toxicology and physiologically-based pharmacokinetic modelling (PBPK). The produced biological and mechanistic quality data for the 10 model compounds in different organ representatives meant to be used for the further development of read-across and quantitative structure-activity relationship (QSAR) already in place. Read-across is used to predict data gaps for chemical substances using a similar chemical with associated high quality toxicological data (Cronin, 2013; Gajewicz *et al.*, 2014). QSAR methods allow the identification of potential concern physicochemical properties.

One of the challenges shared by the *in silico* and *in vitro* side of the project was how to integrate all the new acquired information. From its establishment in 2010, the Adverse Outcome Pathway (AOP) framework allows the description of the evolution of an adverse event, from its molecular initiating event (MIE), to secondary, tertiary and downstream cascading key events (KEs) at the cellular, tissue or organism level leading eventually to a pathology or adverse outcome (AO). To the mechanism knowledge, a quantification of AOPs (qAOP) would make

possible to define the threshold underlining the transition of upstream KEs to downstream KEs describing the probability and severity of an AO for a given activation of a MIE (Conolly *et al.*, 2017; LaLone *et al.*, 2017). One of the goals of the in3 project was to develop and optimize qAOP models by exploit and integrating the existing and in house produced data and mechanistic knowledge.

In a world where multi-background teams are very valorised, the in3 consortium stays as an example of integration between *in silico* and *in vitro* towards a more animal free human risk assessment. Along the duration of the project and beyond, different teams in different countries and from different backgrounds worked daily to develop and improve new methodologies that will potentially allow a better hazard identification. The different final products created, from new human based *in vitro* models to read-across and PBK models, can be a valuable asset for regulation porpoises and be adapted for disease modelling and drug screening and pre-clinical testing.

## 1.8. Research aims of this thesis and its outline

At the current time, there is a raising interest of regulatory authorities and society for the development of human based models for toxicology. Due to its very complex developmental process and final intricate structure, the brain is a challenging organ to fully model *in vitro*. The hiPSC-derived 3D model BrainSpheres (BS) containing neurons, astrocytes and oligodendrocytes strongly interacting was used in this thesis. The work here presented aimed to characterize the ability of BS to be used for neurotoxicity testing by allowing to study chemical's effects on different biological processes and add microglia-like cells to assess activation of neuroinflammation. The specific objectives to achieve this aim were:

- I. Evaluate the ability of BrainSpheres to assess the mechanisms of action of a chemical:** In order to characterize the ability to reproduce known mechanism of action, BS were exposed to several model chemicals. The work developed on exposed BS is presented in chapter 3 with the study based on amiodarone, chapter 4 with the preliminary evaluation of effects produced by the acute and repeated exposure to valproic acid, doxorubicin, lead and paraquat. Additional characterization of the model is outlined in chapter 5 with TempO-Seq analysis of the developmental time course of BS and cadmium exposed samples.
  
- II. Demonstrate the importance of distribution kinetics studies to better assess neurotoxicity:** For efficient and reliable QIVIVE of the neurotoxic effects is of the utmost importance to define the *in vitro* distribution kinetics of a chemical. For the BS system this meant to define the concentration of chemical in the medium, on the cell and in the plastic fractions. Distribution kinetics data on BS for amiodarone are presented on chapter 3 and on chapter 4 for valproic acid.
  
- III. Investigate the application of toxicogenomics strategy as a technique to screen the mechanisms of action of chemicals:** To identify toxicity related pathways induced by chemical exposure, transcriptomic analysis was performed using the targeted gene expression TempO-Seq. Analysis of PQ exposed different organ/structure hiPSC-derived models acquired data can be found in chapter 1. Chapter 3 to 5 show other examples where TempO-Seq analysis was used as a chemical mechanism of action screening.
  
- IV. Improve BrainSpheres ability to reproduce neuroinflammation:** As one of the processes involved in neurotoxicity, it is important to characterize the potential chemical induced neuroinflammation. Astrocytes and microglia are the key players cells in neurotoxicity. Since microglia derive from a different germ layer of the NPC used to produce BS, we attempted to add hiPSC-derived microglia progenitors to the model.

---

## Chapter 2: An *in vitro* strategy using multiple human induced pluripotent stem cell-derived models to assess the toxicity of chemicals

---

*This manuscript has been published in Toxicology in Vitro.*

DOI.: 10.1016/j.tiv.2022.105333

*Supplementary data is in Annex 1.*

## **2.1. Introduction**

In this study, submitted to *In Vitro Toxicology* and currently under revision, we propose an *in vitro* multi-organ strategy to assess the toxicity of chemicals. Human induced pluripotent stem cells (hiPSCs)-derived models of the brain (2D and 3D mixed-cell cultures), blood-brain barrier (endothelial cells based), kidney (podocytes and proximal tubular cells), liver (hepatocyte-like cell) and vasculature (endothelial cells) were generated and exposed to paraquat (PQ), a widely used herbicide with known toxic effects in lungs, kidneys and brain. The main advantages of this strategy are to assess chemical toxicity on multiple organs in parallel, exclusively in human cells, and on cell-type- or organ-specific models derived from the same donors, eliminating the interspecies and genetic background biases, and allowing a better evaluation of the differential sensibility of the diverse organs, and increasing the chance to identify toxic compounds.

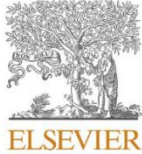
## **2.2. Contribution**

I participated in the study design and performed all the experiments concerning the BS (cell cultures, assessment of PQ-induced cytotoxicity and preparation of samples for TempO-Seq analysis). Regarding the *in silico* part, together with the other first authors, I collected the TempO-Seq raw data coming from all the models used, developed the analysis pipeline and performed the analyses. I participated in the writing of the first draft and was heavily involved in the construction of the final figures.

## **2.3. Summary of the results**

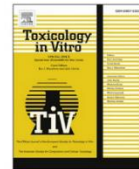
The models showed differential cytotoxic sensitivity to PQ after acute exposure. TempO-Seq analysis with a set of 3565 probes revealed the deregulation of oxidative stress, unfolded protein response and Estrogen Receptor-mediated signalling pathways, in line with the existing knowledge on PQ mechanisms of action. We focused on the mechanisms of action of PQ shared by the different models, but this strategy has also the potential to be used for evaluation of organ-specific response to chemical exposure.

*The published manuscript in Toxicology in Vitro can be found is the following pages.*



Contents lists available at ScienceDirect

Toxicology in Vitro

journal homepage: [www.elsevier.com/locate/toxinvit](http://www.elsevier.com/locate/toxinvit)

## An *in vitro* strategy using multiple human induced pluripotent stem cell-derived models to assess the toxicity of chemicals: A case study on paraquat

Carolina Nunes<sup>a,b,1</sup>, Pranika Singh<sup>c,d,1</sup>, Zahra Mazidi<sup>e,f,1</sup>, Cormac Murphy<sup>g,1</sup>,  
Aurore Bourguignon<sup>h,i</sup>, Sara Wellens<sup>j</sup>, Vidya Chandrasekaran<sup>g</sup>, Sreya Ghosh<sup>k</sup>, Melinda Zana<sup>h</sup>,  
David Pamies<sup>a,b</sup>, Aurélien Thomas<sup>l,m</sup>, Catherine Verfaillie<sup>k</sup>, Maxime Culot<sup>j</sup>,  
Andras Dinnyes<sup>h,i,n</sup>, Barry Hardy<sup>c</sup>, Anja Wilmes<sup>g</sup>, Paul Jennings<sup>g</sup>, Regina Grillari<sup>e</sup>,  
Johannes Grillari<sup>e,f,o</sup>, Marie-Gabrielle Zurich<sup>a,b,\*</sup>, Thomas Exner<sup>c,p,\*</sup>

<sup>a</sup> Department of Biomedical Sciences, University of Lausanne, Rue du Bugnon 7, 1005 Lausanne, Switzerland

<sup>b</sup> Swiss Centre for Applied Human Toxicology (SCAHT), University of Basel, Missionsstrasse 64, 4055 Basel, Switzerland

<sup>c</sup> Edelweiss Connect GmbH, Technology Park Basel, Hochbergerstrasse 60C, 4057 Basel, Switzerland

<sup>d</sup> Division of Molecular and Systems Toxicology, Department of Pharmaceutical Sciences, University of Basel, Klingelbergstrasse 50, 4056 Basel, Switzerland

<sup>e</sup> Evercyte GmbH, Vienna, Austria

<sup>f</sup> Institute of Molecular Biotechnology, Department of Biotechnology, BOKU - University of Natural Resource and Life science (BOKU), Vienna, Austria

<sup>g</sup> Division of Molecular and Computational Toxicology, Department of Chemistry and Pharmaceutical Sciences, AIMMS, Vrije Universiteit Amsterdam, De Boelelaan 1108, 1081 HZ Amsterdam, the Netherlands

<sup>h</sup> BioTalentum Ltd., Gödöllő, Hungary

<sup>i</sup> Department of Physiology and Animal Health, Institute of Physiology and Animal Nutrition, Hungarian University of Agriculture and Life Sciences, Gödöllő, Hungary

<sup>j</sup> University of Artois, UR 2465, Laboratoire de la Barrière Hémato-Encéphalique (LBHE), Faculté des sciences Jean Perrin, Rue Jean Souvraz SP18, F-62300 Lens, France

<sup>k</sup> Department of Development and Regeneration, Stem Cell Institute, KU Leuven, Leuven, Belgium

<sup>l</sup> Unit of Forensic Toxicology and Chemistry, CURML, Lausanne and Geneva University Hospitals, Geneva, Switzerland

<sup>m</sup> Faculty Unit of Toxicology, CURML, Faculty of Biology and Medicine, University of Lausanne, Lausanne, Switzerland

<sup>n</sup> Department of Cell Biology and Molecular Medicine, University of Szeged, Szeged, Hungary

<sup>o</sup> Ludwig Boltzmann Institute for Traumatology Research Center in cooperation with AUVA, Vienna, Austria

<sup>p</sup> Seven Past Nine d.o.o., Hribljane 10, 1380 Cerknica, Slovenia

### ARTICLE INFO

Editor: Dr. P. Jennings

#### Keywords:

Human induced pluripotent stem cells  
Paraquat  
New approach methodology  
Toxicology  
Acute toxicity

### ABSTRACT

Most OECD guidelines for chemical risk assessment include tests performed on animals, raising financial, ethical and scientific concerns. Thus, the development of human-based models for toxicity testing is highly encouraged. Here, we propose an *in vitro* multi-organ strategy to assess the toxicity of chemicals. Human induced pluripotent stem cells (hiPSCs)-derived models of the brain, blood-brain barrier, kidney, liver and vasculature were generated and exposed to paraquat (PQ), a widely employed herbicide with known toxic effects in kidneys and brain. The models showed differential cytotoxic sensitivity to PQ after acute exposure. TempO-Seq analysis with a set of 3565 probes revealed the deregulation of oxidative stress, unfolded protein response and estrogen receptor-mediated signaling pathways, in line with the existing knowledge on PQ mechanisms of action. The main advantages of this strategy are to assess chemical toxicity on multiple tissues/organs in parallel, exclusively in human cells, eliminating the interspecies bias, allowing a better evaluation of the differential sensitivity of the

**Abbreviations:** 3Rs, Replacement, Reduction and Refinement of Animal Experiments; BBB, Blood-brain barrier; BLECs, Brain-like endothelial cells; BS, Brain-Sphere; DEG, Differentially expressed gene; EC, Endothelial cell; ER, Endoplasmic Reticulum; ESC, Embryonic stem cell; ESCs, Embryonic stem cells; ESR, Estrogen Receptor; hiPSC, Human induced pluripotent stem cell; HLC, Hepatocyte-like cell; LFC, log<sub>2</sub> fold change; NAM, New approach methodology; NC, Neural cell; PODO, Podocyte; PTL, Proximal Tubular like cell; ROS, Reactive oxygen species; UPR, Unfolded protein response.

\* Corresponding authors.

E-mail addresses: [mzurich@unil.ch](mailto:mzurich@unil.ch) (M.-G. Zurich), [thomas.exner@sevenpastnine.com](mailto:thomas.exner@sevenpastnine.com) (T. Exner).

<sup>1</sup> Shared first authorship.

<sup>2</sup> Shared senior authorship.

<https://doi.org/10.1016/j.tiv.2022.105333>

Received 27 August 2021; Received in revised form 4 December 2021; Accepted 11 February 2022

Available online 16 February 2022

0887-2333/© 2022 The Authors. Published by Elsevier Ltd. This is an open access article under the CC BY-NC-ND license

(<http://creativecommons.org/licenses/by-nc-nd/4.0/>).

models representing the diverse organs, and increasing the chance to identify toxic compounds. Furthermore, although we focused on the mechanisms of action of PQ shared by the different models, this strategy would also allow for organ-specific toxicity testing, by including more cell type-specific probes for TempO-Seq analyses. In conclusion, we believe this strategy will participate in the further improvement of chemical risk assessment for human health.

## 1. Introduction

The need to develop new approach methodologies (NAMs) providing mechanistic understanding for toxicology testing is now well recognized, and governmental agencies worldwide have been pushing towards the development of human-based assays for human safety assessment (EUR-Lex, 2010; National Research Council, 2007; Oredsson et al., 2019; Sewell et al., 2017). For instance, the US Environmental Protection Agency plans to eliminate animal testing from regulatory requirements for pesticides and industrial chemicals by 2035 (EPA, 2019). However, the move from animal experimentation to NAMs highly depends on the ability of the NAMs to mirror human rather than animal physiology (Herrmann et al., 2019). Since their development, a little over a decade ago (Takahashi et al., 2007), human induced pluripotent stem cells (hiPSCs) have represented a potential paradigm shift across the biological sciences from developmental biology to regenerative medicine. For the field of toxicology, they have been seen as a valuable new tool to enable NAMs to achieve the ideals of the 3Rs through the production of *in vitro* models with human relevant phenotypes that can replace animal testing (Steimberg et al., 2020). While they share capacity for self-renewal and pluripotent potential of embryonic stem cells (ESCs), their generation from adult somatic cells come with a range of advantages while avoiding some of the controversies associated to ESCs (Liu et al., 2017). The relative ease by which hiPSCs can be generated from cells obtained with minimal discomfort on the part of the donor, from sources such as blood, skin and even urine (Zhou et al., 2011), has allowed for the establishment of large cell banks. StemBANCC is one such bank that generated hiPSCs lines from 500 healthy and diseased individuals, and most of these well described lines are now widely available for drug and chemical screening (Morrison et al., 2015) through the European Bank For Induced Pluripotent Stem Cells (EBiSC).

While traditionally, cancer or immortalised cell lines, and to a lesser extent, primary cells, have been the main cell sources for *in vitro* chemical safety assessment, each have their own drawbacks that hiPSCs can potentially overcome. Human primary cells, that would be the most adequate cells to use, can be difficult to obtain and are only available in a limited quantity for a limited time, while undifferentiated hiPSCs can, in theory, proliferate indefinitely. Immortalised cell lines, once made, can be continuously available; however, these models often lack some important biological aspects of their unaltered counterparts leading to concerns that they may be poor models for healthy human cells and lack the sensitivity for toxicity testing (Liu et al., 2017). While hiPSCs have their own challenges, chief among them being the establishment of robust and repeatable differentiation protocols that produce the desired cell type, once this is done, they are a renewable source of cells that can express many important intrinsic phenotypic features often lost in traditional cell lines. For example, a recently published hiPSC differentiation protocol produces kidney proximal tubular-like cells that, alongside other characteristic markers, expressed megalin (LRP2), an apical transporter that plays a key role in reabsorption and is absent in most available human immortalised cell lines (Chandrasekaran et al., 2021).

With the establishment of reliable differentiation protocols for more cell types, and with the emergence of complex culture systems, the possibility has emerged to use hiPSC-derived cells to model the impact of toxins on the different cell types/organs from the same human donor. In this study, we hypothesized that an *in vitro* multi-organ human iPSC-derived strategy will allow the reliable assessment of the toxicity of

chemicals. To test this, hiPSCs-derived models of the brain (2D and 3D mixed-cell cultures), blood-brain barrier (brain capillary endothelial cells), kidney (podocytes and proximal tubular cells), liver (hepatocyte) and vasculature (endothelial cells) were generated from two donors, using published or newly developed protocols, and were exposed to paraquat (PQ), a widely employed herbicide used as a reference compound chosen for its known toxic effects on a range of tissues across the body (Cicchetti et al., 2009; Dinis-Oliveira et al., 2008; Gao et al., 2020). TempO-Seq analysis showed the disruption of “Oxidative stress induced gene expression via Nrf2 markers”, as expected since oxidative stress is the well-known PQ mechanism of action, but also of two other pathways previously demonstrated to be involved in PQ toxicity, “Unfolded protein response” and “ESR-mediated signaling”, suggesting this strategy as a future tool for prioritization, screening of chemicals and risk assessment.

## 2. Materials and method

### 2.1. Cell cultures

Human iPSCs used in this study (SBAD3 clone 1 and SBAD2 clone 1) were generated in the IMI-funded StemBANCC project (<http://stembancc.org>) (Morrison et al., 2015) from purchased primary fibroblasts of non-diseased donors (Lonza). They were cultured on Matrigel® Growth Factor Reduced (GFR) (Corning) or Geltrex® (Gibco) in mTeSR™1 (StemCell Technology) feeder-free medium at 37 °C in a humidified 5% CO<sub>2</sub> incubator. Medium was replaced every day and cells were passaged every 4–5 days using Versene® according to the supplier's protocol (Thermo Fisher Scientific).

Human iPSCs were differentiated into different cell types to obtain *in vitro* models for several tissues/organs. Details on methodologies and characterization are found in the references given for each model, in Chandrasekaran et al. (in preparation – for this special issue), as well as in Table 1. BrainSpheres (BS), a 3D model containing neurons, astrocytes and oligodendrocytes, were prepared from neuroprogenitor cells (NPCs) derived from the SBAD3 clone 1 using a Gibco protocol (Nunes and Zurich, 2020; Pamies et al., 2017). Neural cells (NC), a 2D model containing neurons and astrocytes were generated from NPCs derived from the SBAD2 clone 1 using dual SMAD inhibition protocol (Chambers et al., 2009; Chandrasekaran et al., 2017; Lo Giudice et al., 2019; Ochalek et al., 2017). The brain-like endothelial cells (BLECs) transwell model was prepared from the SBAD3 clone 1 (Sevin et al., 2019; Wellens et al., 2021). The kidney cells, podocytes (PODO) (Murphy et al., 2019; Rauch et al., 2018) and proximal tubular like cells (PTL) (Chandrasekaran et al., 2021) were derived from the SBAD2 clone 1 containing a Green Fluorescent Protein (GFP) tag downstream of one allele of the HMOX-1 gene (SBAD2 clone 1 HMOX1-eGFP, prepared by Prof. Dinnyes's laboratory, Biotalentum, Hungary), although this fluorescent property was not utilised in this study. The endothelial cells (EC) (Gholami et al., 2021) representing the vascular system and the hepatocyte-like cells (HLC) (Boon et al., 2020) representing the liver were derived from SBAD2 clone 1.

### 2.2. Paraquat exposure

PQ (Sigma–Aldrich, catalogue No 36541, lot #BCBW5264, CAS #75365-73-0) was dissolved in ultrapure water. The different cell cultures were exposed to PQ for 24 h and BS was also exposed for 48 h, after

**Table 1**  
Characterization overview of the different models used.

Name	Organ	References	Time in culture before exposure	Characterization		Technique (Ref at protocol DOI)				Functional Assay		Observations			
				Cell Type	Marker	RT-qPCR	Immunocytochemistry	FACS	Western-blot	Tempo-Seq	Assay				
BS	Brain	<sup>1</sup> Pamiès et al., 2017	42d	Neurons	ACHE							Multi-Electrode Array/MEA (Pamiès et al., 2017)	Electrical activity		
					B3T										
					GABRA1		x <sup>1</sup>								
					GAD1		x <sup>1</sup>								
					GRIN1		x <sup>1</sup>								
					MAP2			x <sup>1</sup>							
					NFH		x <sup>1</sup>								
					SYN		x <sup>1</sup>								
					SYP		x <sup>1</sup>								
					TH		x <sup>1</sup>								
					TUJ1		x <sup>1</sup>								
					VGLUT1		x <sup>1</sup>								
					GFAP	Astrocytes	x <sup>1</sup>								
					S100		x <sup>1</sup>								
					VIM										
NC	Brain	<sup>1</sup> Ochalek et al., 2017, <sup>2</sup> Chandrasekaran et al., 2017	21d	Neurons	CNPase		x <sup>1</sup>					Calcium current measurements (Lo Giudice et al., 2019) and patch clamp (Chandrasekaran et al., 2017)	Electrical activity at later time-points		
					MBP		x <sup>1</sup>								
					NOGOA		x <sup>1</sup>								
					O1		-								
					O2		-								
					O4		-								
					OLIG2		x <sup>1</sup>								
					TUBB3		x <sup>1,2</sup>								
					MAP2		x <sup>2</sup>								
					NF200		x <sup>1</sup>								
					R67		x <sup>2</sup>								
					SOX1		x <sup>2</sup>								
					NESTIN		x <sup>2</sup>								
					PAX6		x <sup>2</sup>								
					BLECs	BBB	<sup>1</sup> Wellens et al., 2021	8d	Astrocytes	SOX9				x <sup>2</sup>	
GFAP		x <sup>2</sup>													
AQP4		x <sup>2</sup>													
ABC2		x <sup>2</sup>													
ABCB1															
CDH5		x <sup>1</sup>													
GLDN5		x <sup>1</sup>													
WVF															
GD81															
ABCC4															
ABCC5															
SLC25A46															
SLC26A2															
SLC27A2															
SLC27A3															
SLC2A1															
SLC35A3															
SLC7A5															
EC	Vasculature	<sup>1</sup> Ghodami et al., 2021	8d	Endothelial cells	TBXT		x <sup>1</sup>					Matrigel assay	Endothelial cells could form tubes at one of the beginning stages of angiogenesis (continued on next page)		
					CD31		x <sup>1</sup>								
					CDH5		x <sup>1</sup>								

Table 1 (Continued)

Name	Organ	References	Time in culture before exposure	Characterization		Technique (Ref at protocol DOI)				Functional Assay		Observations	
				Cell Type	Marker	RT-qPCR	Immunocytochemistry	FACS	Western-Blot	TempO-Seq	Assay		
PTL	Kidney	<sup>1</sup> Chandrasekaran et al., 2021	14d	Proximal tubule-like cells		VEGFR2							Increase levels of cAMP in response to PTH; Functional P-gp efflux; uptake of labelled albumin
						WVF	x <sup>1</sup>						
						LRP2	x <sup>1</sup>						
						TJPS	x <sup>1</sup>						
PODO	Kidney	<sup>1</sup> Rauch et al., 2016, <sup>2</sup> Murphy et al., 2019	12-14d	Podocytes		FBP1							Uptake of albumin by podocyte-like cells
						WT1	x <sup>1,2</sup>						
						SYNPO	x <sup>1</sup>						
						NPHS1	x <sup>1</sup>						
HLC	Liver	<sup>1</sup> Ghosh et al. (under revision for this special issue)	42d	Hepatocyte-like cells		NPHS2	x <sup>1</sup>						Albumin secretion was observed at about 40% of that of primary hepatocytes plated for 12 h. CYP3A4 activity was observed (about one-third that of primary hepatocytes).
						ALB	x <sup>1</sup>						
						AFP	x <sup>1</sup>						
						HNF4A	x <sup>1</sup>						
						CYP3A4	x <sup>1</sup>						
						CYP2C9	x <sup>1</sup>						
						G6PC	x <sup>1</sup>						
						PEPCK	x <sup>1</sup>						
						SLC10A1	x <sup>1</sup>						
						SERPINA1	x <sup>1</sup>						

NT: Not tested; x: detected; ND: not detected; NP: not present in the TempO-Seq panel; Superscript number: refers to publication listed under references column.

various duration in culture, corresponding to a maturation state defined by each lab. BS was exposed to PQ at day *in vitro* (DIV)42, NC at DIV21, BLECs at DIV8, PODO at DIV12-14, PTL at DIV14, EC at DIV8, and HLC at DIV40. Concentrations of paraquat are given in figure or figure captions (Figs. 2, 3 and Table 2). For cytotoxicity testing, 2–9 samples were run per group, and for TempO-Seq analysis 2–16 samples were run per group. Exposure of the cell models to PQ was conducted in 6 different labs, NC at BioTalentum Ltd. (Hungary), BS at University of Lausanne (Switzerland), PODO and PTL at Vrije Universiteit Amsterdam (Netherlands), EC at Evercyte GmbH (Austria), HLC at Katholieke Universiteit Leuven (Belgium) and BLECs at Université d'Artois (France).

### 2.3. Cytotoxicity assays

After exposure of the different iPSC-derived cell models to a large range of PQ concentrations, viability assays were run in order to establish cytotoxicity concentration-dependent curves.

#### 2.3.1. Resazurin assay

After treatment with PQ, the medium was removed and the cells were incubated with 44  $\mu$ M resazurin diluted in cell culture medium for a duration indicated in Table 2. The fluorescent product resorufin was measured at 530–560 nm excitation and 590 nm emission using a plate reader. After subtraction of the background (only resazurin solution), results of the treated cultures were expressed as percentage of the mean of the control cultures.

#### 2.3.2. ATP assay

ATP viability assay was performed using the CellTiter-Glo® 3D Cell Viability Assay, according to the manufacturer's protocol (Promega). NC were lysed with 100  $\mu$ L CellTiter-Glo® 3D Reagent for 90 min at RT. Luminescence signal was recorded with a Thermo VarioScan Flash plate reader (Thermo Fisher Scientific). Results of the treated cultures were expressed as percentage of the mean of the control cultures.

### 2.4. TempO-Seq sample collection

Samples of the different cell systems were treated with PQ at concentrations chosen on the basis of the previously established cytotoxicity curves (final concentrations and time points in Table 2 and indicated in figure captions). DMSO was added to all samples (final concentration 0.01%) due to the simultaneous testing of water-insoluble chemicals (results not presented in this manuscript). At the end of exposure, cells were collected and lysed with 1  $\times$  TempO-Seq Lysis Buffer in a ratio of 0.25 to 2 million cells/mL. Lysates were frozen at  $-80$  °C and shipped to BioClavis Technologies Ltd. (Glasgow) on dry ice where the TempO-Seq assay using the EU-ToxRisk v2.1 panel (3565 probes representing 3257 genes) was conducted with standard attenuators. The service also included primary processing to derive gene-annotated raw read counts and quality control, following a previously described procedure (Limonciel et al., 2018; Mav et al., 2018). Each sample FASTQ file was aligned against the TempO-Seq transcriptome using the Bowtie aligner (Li and Durbin, 2009). The output of this analysis generated a table of counts per gene per sample.

### 2.5. TempO-Seq data analysis and visualization

#### 2.5.1. Sample and probe filtering

The raw read count data of the samples provided by BioClavis was used for differential expression analysis. The raw data and corresponding metadata files were uploaded and maintained on an internal instance of the EdelweissData™ management system (SafeWorldbyDesign2020) for easier accessibility. All samples exposed to PQ and the respective controls from the different hiPSC-derived cell models were extracted using a python workflow as previously described (Singh et al., 2021).

**Table 2**

Description of all models used in the study and respective IC50/30/20/10 and PQ concentrations used for TempoSeq. BrainSpheres (BS), Neural Cells (NC), Blood-Brain Barrier (BBB), Endothelial cells (EC), renal proximal tubular epithelial-like cells (PTL) podocytes (PODO), hepatocytes-like cells (HLC).

Model	Organ	PQ exposure (h)	Cytotoxicity				TempOSeq			
			Assay for assessment	Incubation time (h)	Concentration ( $\mu\text{M}$ )					
					IC50	IC30	IC20	IC10	Concentrations ( $\mu\text{M}$ )	
BS	Brain	24	Resazurin	3	200	161	132	97	-	
		48			60	51	45	38	1–2.5–5	
NC	Brain	24	ATP	1 h30	49	31	24	16	0.05–0.1	
BLECs	BBB	24	Resazurin	2-2 h30	749	654	132	97	50–100–250	
EC	Vasculature	24	Resazurin	1 h30	114	55	35	17	1.25–2.5–5	
PTL	Kidney	24	Resazurin	1	561	405	327	237	25–100–300	
PODO	Kidney	24	Resazurin	2	373	164	97	45	5–50–100	
HLC	Liver	24	Resazurin	2	-	-	-	-	12.5–25–50–100	
		48			1093	797	590	376	-	

Before downstream analyses (Fig. 1), samples and probes were quality controlled. The samples were checked as described elsewhere (Singh et al., 2021) by investigating a) the total number of probe read counts per sample with a threshold of 50,000 under which samples were removed and b) the Pearson's correlation coefficient among replicates using Morpheus online tool with a threshold of 0.80 under which samples were removed. Concerning the probes, only the ones with median of raw read counts higher than 5 across all conditions for each model were used.

### 2.5.2. Differential expression analysis

The filtered raw data was analysed for differential expression using the R based library DESeq2 (Love et al., 2014). Samples underwent an r-log transformation and posterior unsupervised clustering using standard DESeq2 suggested settings to visualize the variance within and between

different cell models, as well as between treatment and control groups. Differential expression analysis was performed using DESeq2 library after normalization of read counts using its standard mean-median ratio method. An automatic script (Singh et al., 2021) was used to generate the statistical values log2fold changes, adjusted *p*-values and base means. To select the most significantly expressed probes in each cell model for further analyses, thresholds were set at: log2 fold changes > |0.58| and adjusted *p*-values < 0.05.

### 2.5.3. Gene-pathway association

ConsensusPathDB (v.34) (<http://cpdb.molgen.mpg.de>), a web-based meta-database integrating information from around 30 different publicly available databases including WikiPathway, Reactome and KEGG (Kamburov et al., 2013), was used to identify enriched pathways in each cell culture system. The analysis was done using the ConsensusPathDB's

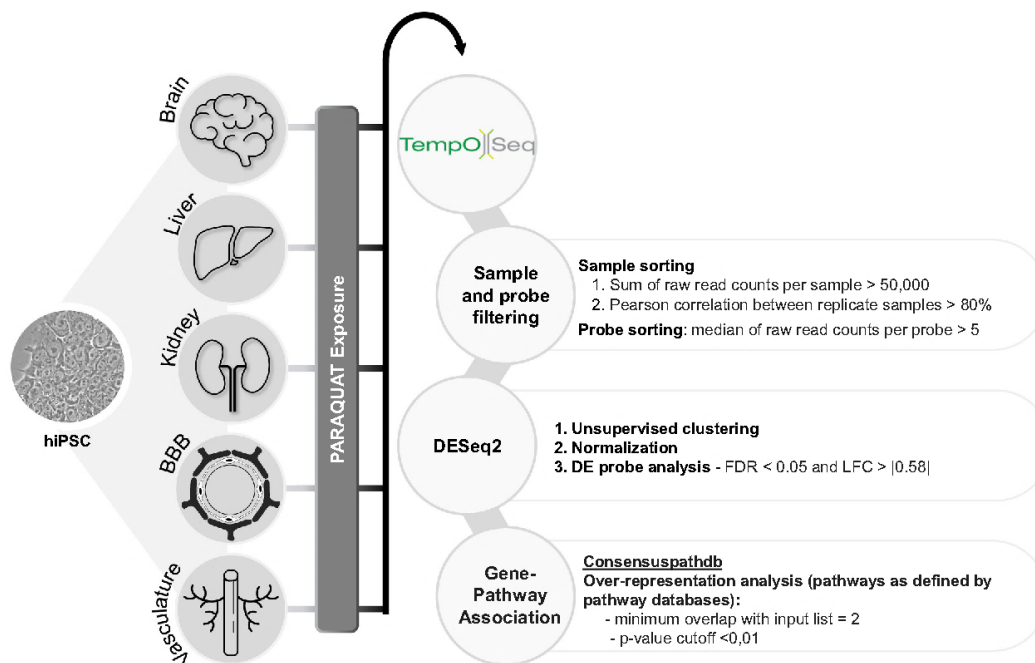


**Fig. 1.** *In vitro* strategy using multiple hiPSC-derived models to assess the toxicity of chemicals. Workflow used to compare the response of different hiPSC-derived cell models to PQ acute exposure based on TempoSeq data. The 7 models were differentiated from either SBAD2 or SBAD3 hiPSC lines to represent brain, liver, kidney, BBB and vasculature and exposed to different concentrations of PQ chosen on the basis of viability curves. Data from TempoSeq was analysed using R package DESeq2, after filtering and normalization of the raw data. The differentially expressed genes per model were analysed for pathway over-representation with ConsensusPathDB.

over-representation analysis (ORA) and the list of the most significantly differentially expressed genes of each system (taking all concentrations into account) as an input. HUGO gene nomenclature Committee (HGNC) symbols were employed as identifiers. ORA compares input gene list to all the genes associated to each pathway available in the databases. The default Consensus ORA settings require a minimum overlap of 2 genes between the input gene list and a given pathway associated gene list along with a *p*-value cutoff of 0.01 to define a pathway as over-represented. ORA *p*-value calculations are based on the hypergeometric distribution between the input list and existing pathway list (Kamburov et al., 2009).

#### 2.5.4. Gene and pathway intersection analysis

To find deregulated genes and pathways shared by the different cell systems, the lists of differentially expressed genes and enriched pathways from each cell model were compared using UpSetR package (Conway et al., 2017). UpSetR package helps in both visualization and extraction of the different intersections in a matrix format by assembling different set size combinations. Mode was set to “intersect” in the function “make\_comb\_mat()” and the function “extract\_comb()” was then used to obtain the intersections. Finally, intersection plots were created using UpSet() function in the UpSetR package (Conway et al., 2017).

### 3. Results

#### 3.1. Human iPSC-derived organ-specific models exhibit different sensitivity to paraquat

In order to assess the differential sensitivity of the iPSC-derived cell models to PQ, and to choose sub-cytotoxic concentrations for subsequent experiments to elucidate early pathways of toxicity, the different iPSC-derived cell culture models were exposed to a wide range of PQ concentrations for 24 h and/or 48 h, then concentration-dependent curves for cytotoxicity were established.

The most sensitive model was found to be 2D neural cell cultures (NC), with an IC<sub>50</sub> at 49 μM (Fig. 2 and Table 2). BS, the 3D brain cell model, was less sensitive to PQ (IC<sub>50</sub>: 200 μM after 24 h of exposure; 60 μM after 48 h). The toxicity of PQ to endothelial cells (EC) was found in the same range (IC<sub>50</sub>: 114 μM), whereas BLECs, used as a model for blood-brain barrier and later referred to as BBB, exhibited a much higher IC<sub>50</sub> (749 μM). Among the two cell culture models representing kidney, PTL was less sensitive to PQ than PODO (IC<sub>50</sub>: 561 μM and 373 μM, respectively). Finally, the hepatocyte cell-like model (HLC) seemed to be the least sensitive model out of the seven models tested; however, the IC<sub>50</sub> was determined only at 48 h (1093 μM, cytotoxicity data for HLC also used in Ghosh et al., submitted to Toxics) (Fig. 2 and Table 2).

The results reveal a differential response of the models to the

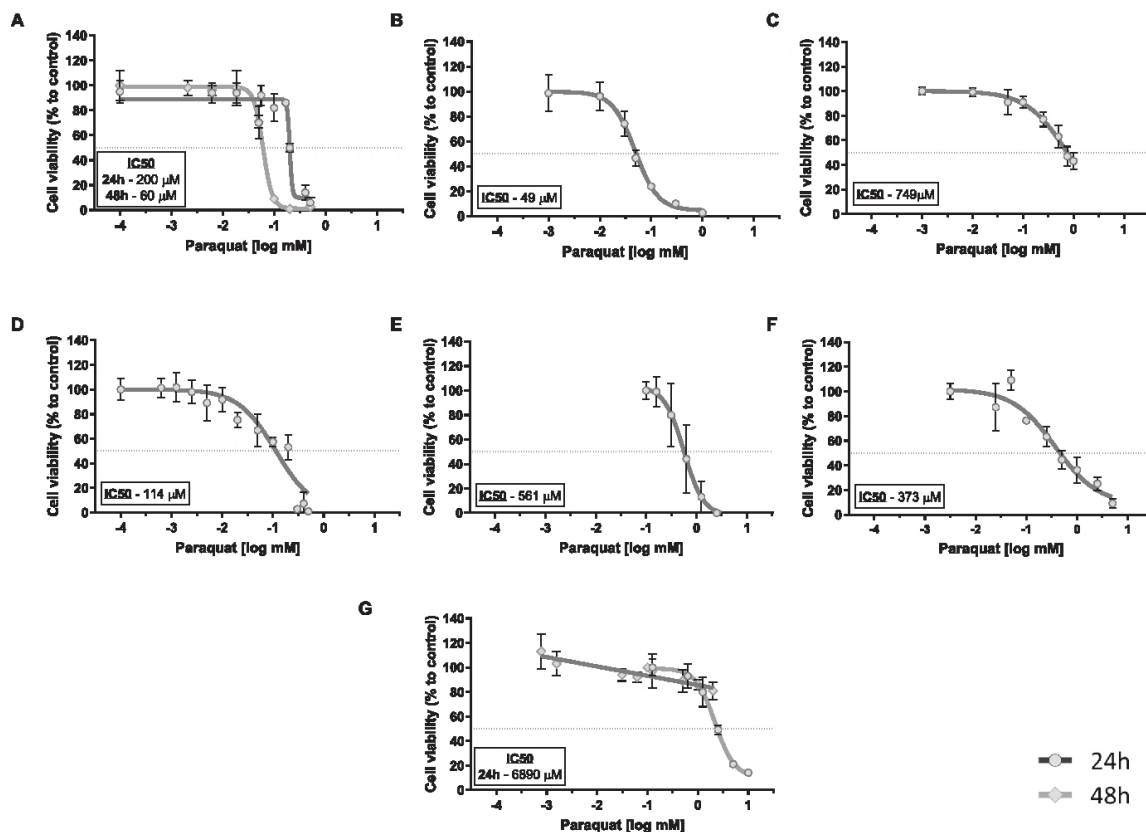


Fig. 2. Models present different sensitivity to PQ exposure. Concentration-dependent curves after 24 h and/or 48 h exposure to PQ: A) BS (0–0,5 mM), B) NC (0,001–1,5 mM), C) BLECs (0–1 mM), D) EC (0–0,5 mM), E) PTL (0–10 mM), F) PODO (0–5 mM), G) HLC (0–10 mM); data for 48 h also used in Ghosh et al., submitted to Toxics). Results are expressed as % of control cultures a non-linear regression (log (inhibitor) vs response - variable slope (four parameters)) was performed in order to calculate the inhibitory concentration (IC) using GraphPad Prism®. Means ±SD of 2–9 samples obtained in 1–3 independent experiments are shown. Black line: 24 h, grey line: 48 h.

cytotoxic effects of PQ, and show that the sensitivity to PQ depend not only on the organ but also on the specific cell type considered (NC vs BS, modelling the brain, and PTL vs PODO, modelling the kidney). To identify toxicity related pathways induced by PQ, transcriptomic analysis was performed using TempO-Seq as a cost-efficient tool. Each model was exposed to at least one concentration below cytotoxicity IC10 (Table 2).

3.2. hiPSC-derived models drive sample clustering of TempO-Seq data after paraquat exposure

All human iPSC-derived models, except EC, exhibited a sum of read counts per sample above 50,000 counts, and therefore passed our first sample quality filter. The second filter, namely the Pearson correlation, led us to the elimination of one replicate of the control group from NC; two control replicates and one replicate of the 25 μM group from PTL; one replicate of treated 250 μM group from BBB and one replicate sample from the 5 μM and from the 100 μM groups from PODO. For HLC (raw data for HLC also used in Ghosh et al., submitted to Toxics) and BS, the samples from all groups showed Pearson correlation ≥0.80 and therefore were all kept for further analyses. For EC model, very low sums of probe read counts (5000–12,000) were found for one replicate from each treatment group and therefore these samples were also extremely poorly correlated to their corresponding replicates (Pearson correlation coefficients between 0.09 and 0.22). After removing the low correlated samples from each cell model, probes with median read counts across all samples of the model considered <5 were filtered out. This caused the removal of 1456 probes from NC, 1208 from PTL, 1445 probes from HLC, 1175 probes from BBB, 1319 probes from PODO and 1517 probes from BS. For the EC model, 64% of the probes (2097) had to be

eliminated. Furthermore, although the controls of the EC model passed the 50'000 counts threshold, for undetermined reasons their read counts were much lower than in all the other models (Suppl. Fig. 1), causing a high variance potentially leading to biased normalization and distortion of the differential expression analysis. Based on these results, the data from the EC cell model were considered as unreliable, and the EC model was removed from further analyses.

After these steps of sample and probe filtering, unsupervised PCA of controls and treated samples for the 6 remaining models (Fig. 3A) showed four very distinct clusters. One cluster was formed by PODO and another cluster by HLC samples. A third cluster comprised samples from both brain models (NC and BS), whereas PTL and BBB samples were grouped together. On this PCA plot, BS was the only cell model to show clear separation between treated and control samples; however, the separation is visible when PCA is performed for each model individually, with the exception of PODO (Suppl. Fig. 2). It is remarkable that most of the variance was observed between cell models and less was due to paraquat treatment, even if the list of probes used did not comprise a lot of cell type-specific genes.

3.3. Paraquat deregulated several identical pathways in the different hiPSC-derived models

In total, we found 341 probes differentially expressed across the cell models and treatment groups upon PQ exposure. A heatmap of the 100 highest log2 FC probes (Fig. 3B), each one crossing the statistical thresholds in at least one treatment group, with values scaled for each model between the range -1 to 1 for better relative comparison among models, clearly shows concentration-dependent effects of paraquat in the different models.

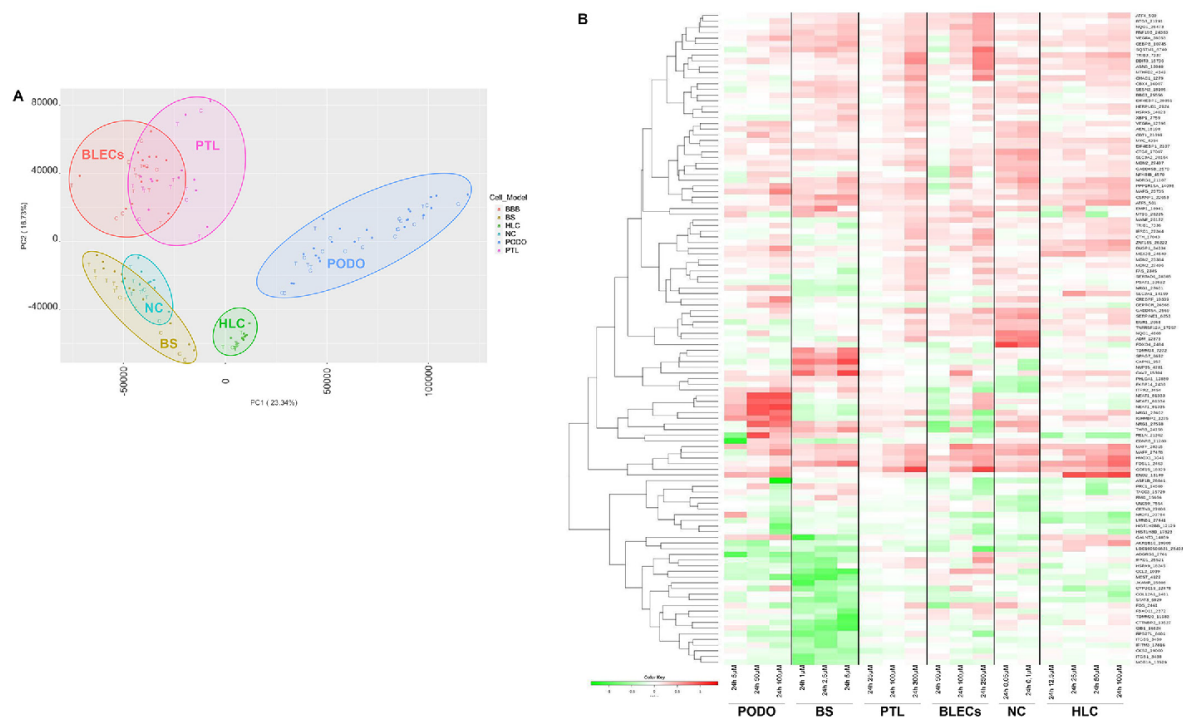


Fig. 3. Clustering of samples and the most deregulated genes after PQ exposure. A) PCA plot of all control and PQ treated samples Each dot represents a sample and each colour represents a cell model. Neuronal Cells (NC, turquoise, 2 samples), Brainsphere (BS, yellow), Podocytes (PODO, blue), Proximal tubule like cells (PTL, purple), Hepatocytes like cells (HLC, green) and Blood Brain Barrier (BLECs, pink). B) A heatmap of the 100 highest log2 FC probes (gene symbol\_probe ID), each one crossing the statistical thresholds in at least one treatment group. The relative expression values scaled between -1 (green) and 1 (red).

To investigate the mechanisms of PQ toxicity shared by the different models, pathway enrichment analysis using ConsensusPathDB was performed based on the list of differentially expressed genes (DEG) derived from each model. In total, 36 pathways were identified in HLC, 110 in PODO, 136 in NC, 134 in BBB, 164 in BS and 278 pathways in PTL. The number of pathways given here includes all similar pathways affected by different databases aggregated by ConsensusPathDB. Then, UpSetR package was used to find the intersections of these affected pathways in different combinations of 2, 3, 4 and 5 cell models. The pathway intersection graph (Fig. 4) shows that each cell model shared affected pathways with up to four other cell models (Fig. 4, intersections between 5 models). Furthermore, PODO and PTL that are both kidney related cell models shared 18 pathways, whereas BS and NC which are both brain-related cell models shared 17 pathways. No pathway shared by all 6 cell models was found with the criteria used in this study.

In the combinations of 5 cell models, “Oxidative stress induced gene expression via Nrf2” pathway was not found in BS (Table 3). However, read counts for Heme Oxygenase 1 (HMOX1), NAD(P)H Quinone Dehydrogenase (NQO1), MAF BZIP Transcription Factor F (MAFF) and G (MAFG) genes, all belonging to the oxidative stress pathway, show a concentration-dependent increase for the six models (Fig. 5), including BS. The other stress pathways found in the combination of 5 models are “Cellular responses to external stimuli” and “Cellular responses to stress” (Table 3). Among combinations of 4 cell models, many other stress pathways were identified, such as “Quercetin and Nf-kB- AP-1 Induced Cell Apoptosis”, “Photodynamic therapy-induced NFE2L2 (Nrf2) survival signalling” and “Photodynamic therapy-induced unfolded protein response”. Concentration-dependent increases were observed for Protein Phosphatase 1 Regulatory Subunit 15A (PPP1R15A), Activating Transcription Factor 4 (ATF4), DNA Damage Inducible Transcript 3 (DDIT3) and Asparagine Synthetase (ASNS) genes belonging to the latter pathway (UPR), even in BS, although this pathway was not identified in this model (Fig. 5). Only PODO did not show any regulation of these genes. Finally, more generic pathways such as “Cell cycle”, “Cellular

responses to external stimuli” and “Generic Transcription Pathway” (Table 3) were found in several combinations of four models, and “ESR-mediated signalling” pathway appeared in one of these combinations.

UpSetR package was also used to identify the genes differentially expressed in the combinations of 2, 3, 4 and 5 cell models in an unbiased way. The gene intersection graph shows that each cell model shared affected genes with up to four other cell models (Fig. 6, intersections between 5 models). No gene shared by all 6 cell models was found with the criteria used in this study. MAFF and PPP1R15A were found deregulated in 5 models (Table 4), but not in the same combination thereof, whereas Vascular Endothelial Growth Factor A (VEGFA), ATF4 and Growth Differentiation Factor 15 (GDF15) were found deregulated in 4 models. NC and BS, both CNS models, shared 6 deregulated genes (Table 4): Chromobox 4 (CBX4), Eukaryotic Translation Initiation Factor 1 (EIF1), PPP1R15A, Solute Carrier Family 3 member 2 (SLC3A2), and VEGFA, that were all upregulated in both models, as well as one downregulated gene, the tubulin alpha-1B chain (TUBA1B). Finally, PODO and PTL, models of two different kidney cell types, shared 9 upregulated genes: CD55 Molecule (CD55), Choline Kinase Alpha (CHKA), Dual Specificity Phosphatase 1 (DUSP1), Enolase 2 (ENO2), Heat Shock Protein Family A Member 1B (HSPA1B), MAFF, MAFG, PPP1R15A and VEGFA (Table 4), that were deregulated in the same direction, except for HSPA1B, downregulated in PODO but upregulated in PTL (Suppl. Fig. 3).

3.4. Specificity of hiPSC-derived models response to Paraquat

In addition to the cellular responses shared by the different models, we also interrogated the data for the genes that are specifically deregulated in each model. The number of deregulated probes (22–190) per model is given in Table 5. The number of down-regulated genes was very similar to the number of up-regulated genes in BS, NC and BBB models, whereas the proportion of up-regulated genes was much higher for PTL (73% of the deregulated genes), PODO (70%) and HLC (95%)

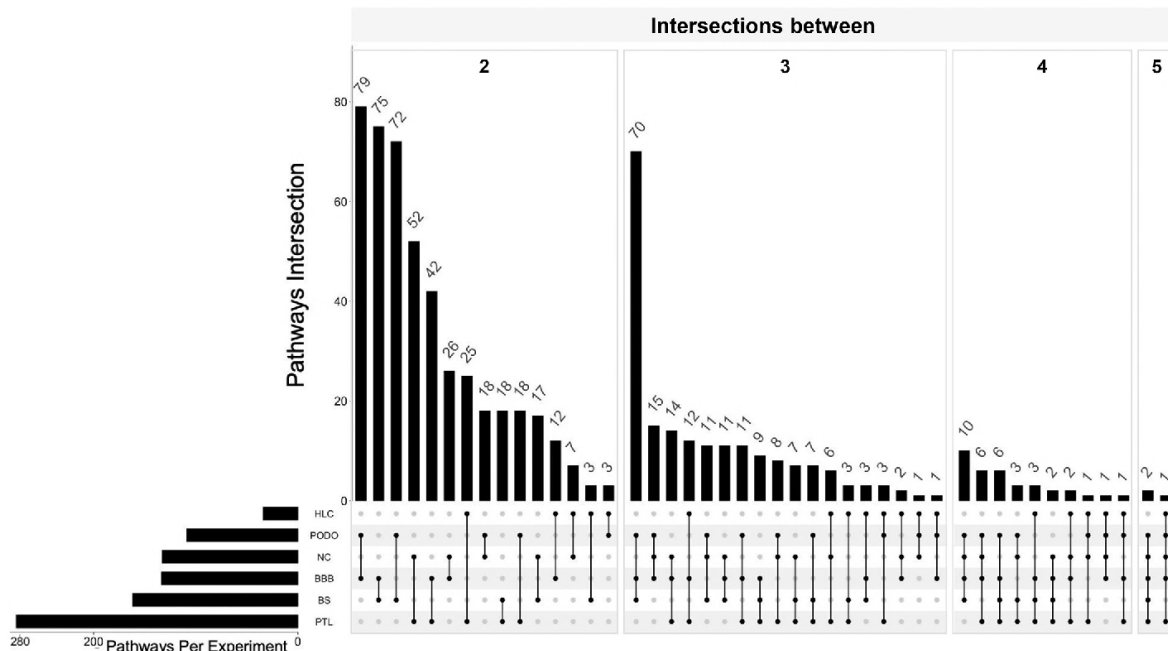


Fig. 4. All the models share perturbed pathways with at least 4 other systems. Intersection plot of the potentially affected pathways by PQ exposure shared by 2–5 models. For each model, the pathways were derived using the differentially expressed genes in the ConsensusPathDB for over-representation analysis (ORA).

**Table 3**  
List of pathways potentially disturbed by PQ exposure in at least 4 different models.

Models	Example
NC + PODO+PTL + HLC + BBB NC + BS + PODO+PTL + BBB	Oxidative stress induced gene expression via Nrf2 Cellular responses to external stimuli; Cellular responses to stress
NC + PODO+PTL + BBB	Oxidative stress induced gene expression via Nrf2; Cell cycle; Cellular responses to external stimuli; Cellular responses to stress; Direct p53 effectors; Generic transcription pathway
NC + BS + PODO+PTL	Cellular responses to external stimuli; Cellular responses to stress; Quercetin and NF- $\kappa$ B- AP-1 induced cell apoptosis
NC + PTL + HLC + BBB	Oxidative stress induced gene expression via Nrf2
NC + BS + PODO+BBB	Photodynamic therapy-induced unfolded protein response; ESR-mediated signaling; B-WICH complex positively regulates rRNA expression; Cell cycle checkpoints; Cellular responses to external stimuli; Cellular responses to stress; Epigenetic regulation of gene expression; Formation of the beta-catenin: TCF transactivating complex; Mitotic prophase; Signaling by nuclear receptors; TCF dependent signaling in response to WNT
NC + BS + PTL + BBB	Cellular responses to external stimuli; Cellular responses to stress
BS + PTL + HLC + BBB	NRF2-ARE regulation; Photodynamic therapy-induced NFE2L2 (Nrf2) survival signaling; Phytochemical activity on Nrf2 transcriptional activation
PODO+PTL + HLC + BBB	Oxidative stress induced gene expression via Nrf2

models (Table 5).

Among the top upregulated genes in BS (Table 5) genes involved in essential cellular functions were found, such as caveolin 2 (CAV2) and calpain 1 (CAPN1), but also genes involved in development such as SRY-BOX Transcription Factor 1 (SOX1), INSM transcriptional repressor 1 (INSM1) and Thyroid hormone receptor beta (THRB). On the other hand, the most down-regulated genes in BS were associated with cytoskeleton, such as Tubulin Alpha 1B chain (TUBA1B) and Cortactin Binding Protein 2 (CTTNBP2) and cell adhesion (Cadherin (CDH8)). In the other iPSC-derived model of brain cells, NC, the top 10 up-regulated genes included 4 genes involved in cellular stress responses, such as PPP1R15A, GDF15, Growth Arrest And DNA Damage Inducible Alpha (GADD45A) and MAFF, but also genes implicated in cell adhesion, such as Cellular Communication Network Factor 1 (CCN1 also called CYR61), Cellular Communication Network Factor 2 (CCN2 also called Connective Tissue Growth Factor (CTGF)) and Serpin Family E Member 1 (SERPINE1). In the down-regulated genes for this model, we found genes involved in mitosis (RecQ Mediated Genome Instability 1 (RMI1) and Centrin 3 (CETN3)), another one potentially mediating apoptosis during neuronal development (Pleckstrin Homology Like Domain Family A Member 1 (PHLDA1)) and an essential component of the nuclear pore complex, nucleoporin 85 (NUP85). In BBB model, most of the top ten up-regulated genes were associated with stress responses: Tribbles Pseudokinase 3 (TRIB3), DDIT3, CD55 Molecule (CD55), PPARGC1A, Sequestosome 1 (SQSTM1), and GDF15, whereas among the top ten down-regulated genes, five were histones, and one was a histone chaperone (Anti-Silencing Function 1B Histone Chaperone (ASF1B)).

For PTL, the up-regulated genes were all stress genes involved in oxidative stress and/or inflammation, except FOSL1 that is implicated in proliferation, differentiation and transformation; and among the down-regulated genes are 2 genes related to detoxification (Epoxide Hydrolase 2 (EPHX2) and Aldehyde Dehydrogenase 7 Family member A1 (ALDH7A1)), as well as pyruvate dehydrogenase kinase isoenzyme 4 (PDK4), that plays a crucial role in the control of metabolic flexibility under various physiological. For the other kidney cell type, PODO, 5 of the top upregulated genes were involved in stress pathways: Matrix

Metalloproteinase 2 (MMP2), Immunoglobulin Mu DNA Binding Protein 2 (IGHMBP2), CD55, MAFK and CREB3 regulatory Factor (CREBRF). Among the other upregulated genes we found Myelin Protein Zero Like 1 (MPZL1) and Ankyrin Repeat Domain 36 (ANKRD36B) involved in cell adhesion and cell membrane integrity. The down-regulated genes in PODO include five histones and one histone chaperone, ASF1B, just as observed for BBB.

The model for hepatocytes, HLC, showed 6 of its top ten upregulated genes associated with oxidative stress and/or inflammation, namely the rate limiting enzyme of glutathione synthesis, Glutamate-Cysteine Ligase Modifier Subunit (GCLM), HMOX1, C-X-C Motif Chemokine Ligand 8 (CXCL8), GDF15, TRIB3 and MAFF. Besides, Ras Association Domain Family Member 1 (RASSF) involved in cell cycle and Aldo-Keto Reductase Family 1 member 1 (AKR1B10) were also upregulated. The only down-regulated gene found with the criteria applied was a type of collagen (COL12A1).

Finally, basal expression of selected genes related to PQ transport, and enzymes involved in redox cycling and anti-oxidant defence were extracted from the Tempo-Seq data in order to investigate their potential contribution to the sensitivity of the various models to PQ. The basal expression of Solute Carrier Family 3 Member 2 (SLC3A2) and Solute Carrier Family 7 Member 11 (SLC7A11), two amino acid transporters, was higher in BS, NC and PODO than in the other models (Fig. 7). The expression of the NAD(P)H-cytochrome P450 oxidoreductase (POR), involved in the redox cycling of the PQ ion, was highest in HLC than in the other models, but also robustly expressed in BS, NC and PTL. Superoxide dismutases (SOD2 and SOD3) and glutathione S-transferases (GSTA2 and GSTM3), involved in anti-oxidant defence, showed a much higher basal expression in HLC than in all the other models, even being absent from some of them, whereas SOD 1 was more expressed in BS, NC and PTL than in HLC.

#### 4. Discussion

The development of new human-based assays for human safety assessment, highly encouraged by various authorities (EUR-Lex, 2010;

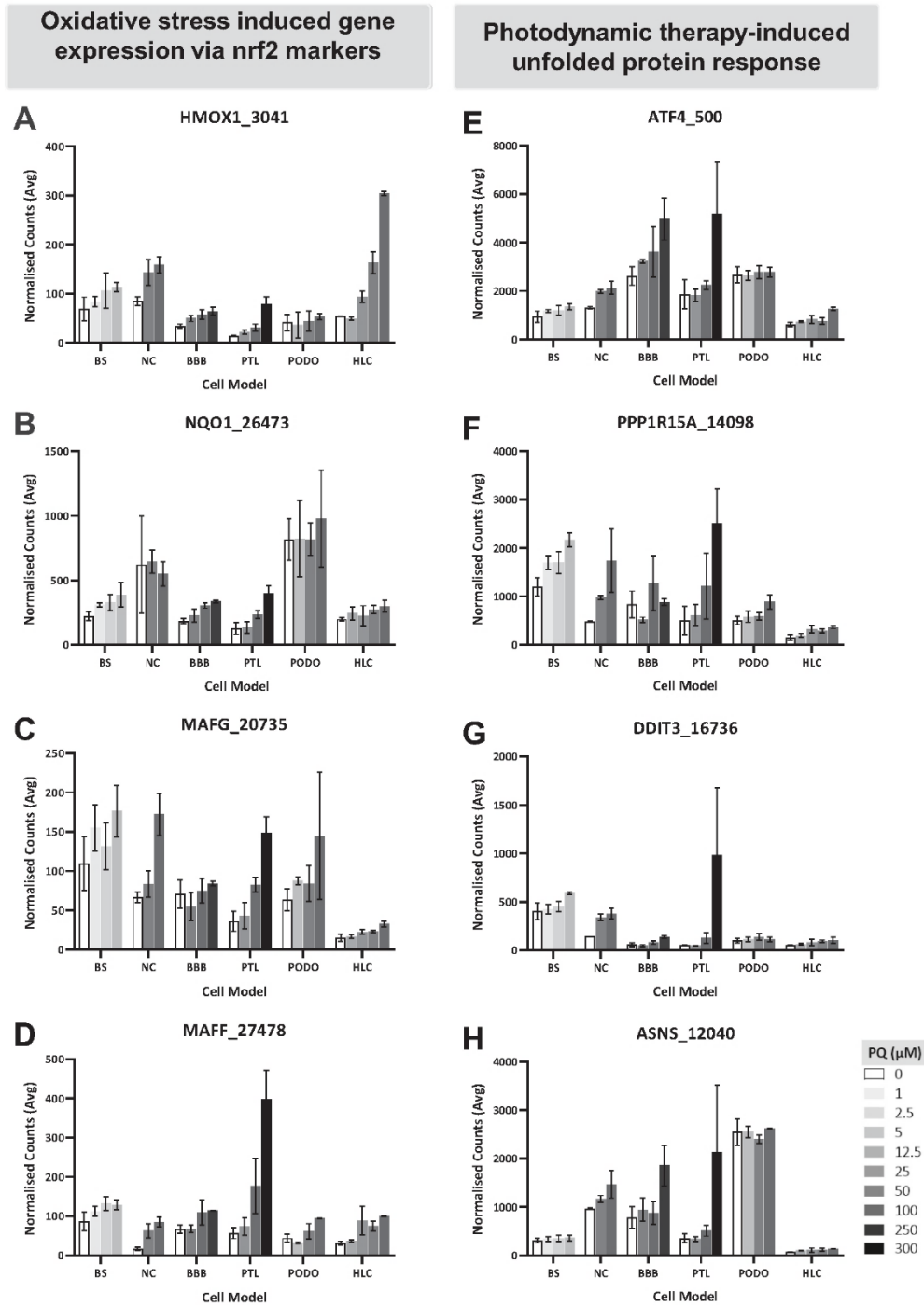


Fig. 5. PQ exposure induces upregulation of genes involved in the oxidative stress pathways Nrf2 and UPR (A-D) normalized read counts for HMOX1, NQO1, MAFG and MAFF probes (gene symbol\_probe ID) involved in the “oxidative stress induced gene expression via Nrf2” pathway from BioCarta database; (E-H) normalized read counts for ATF4, PPP1R15A, DDIT3 and ASNS probes (gene symbol\_probe ID) involved in “photodynamic therapy-induced unfolded protein response” pathway described in the Wikipathways database. Average normalized read counts ±SD are shown.

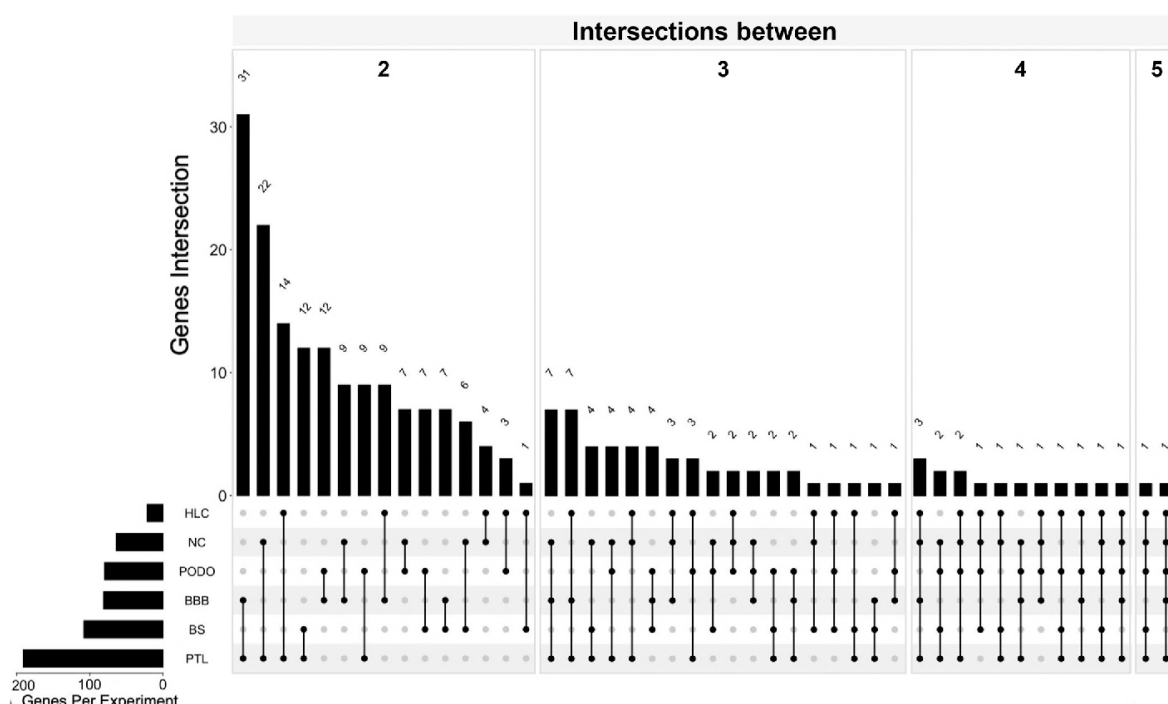


Fig. 6. All the models share differentially expressed genes with at least 4 other systems. Intersection plot of the PQ-induced DEG shared by 2–5 models using UpSetR pack. For each model, the DEG list was obtained with the DSeq2 Package.

Table 4

List of the DEGs shared by at least 4 models or by modeled organ (brain and kidney).

Organ	Intersections	Gene symbol_probe ID
	NC + PODO+PTL + HLC + BBB	MAFF.27478
	NC + BS + PODO+PTL + HLC	PPP1R15A.14098
	NC + BS + PODO+PTL	PPP1R15A.14098; VEGFA.28053
	NC + PODO+PTL + HLC	PPP1R15A.14098; MAFF.27478;
	NC + PTL + HLC + BBB	ATF4.500; GDF15.18329; MAFF.27478
Brain	NC + BS	CBX4.16907; EIF1.2074; PPP1R15A.14098; SLC3A2.20164; TUBA1B.7399; VEGFA.28053
Kidney	PODO+PTL	CD55.28297; CHKA.14315; DUSP1.24234; ENO2.13140; HSPA1B.3136; MAFF.27478; MAFG.20735; PPP1R15A.14098; VEGFA.28053

National Research Council, 2007; Oredsson et al., 2019; Sewell et al., 2017), has been made easier by the development of standardized ways to derive hiPSC from somatic cells and by the description of new methods for their differentiation into various cell types (Chandrasekaran et al., 2021; Murphy et al., 2019; Pamies et al., 2017). This raises the possibility to test for specific organ toxicity within the same genetic background to more fully assess the potential hazard of a chemical. Here we propose an *in vitro* multi-organ strategy with hiPSCs-derived models to assess the toxicity of chemicals through TempO-Seq analysis. We believe that a multi-organ approach associated with high throughput omics technology would improve the efficiency and reliability of chemical toxicity screening.

To test this approach, PQ, a herbicide widely employed with recognized toxic effects in many different organs, such as lung, kidney, central nervous system and liver (Delirrad et al., 2015; Gawarammana and Buckley, 2011; Saravu et al., 2013; Sittipunt, 2005), was used as a reference compound. The cytotoxic sensitivity to PQ we observed in this study was not the same for the different hiPSCs-derived models, with liver and kidney models being less sensitive than brain models. This is in line with a report showing that in rats, repeated, systemic low doses of

PQ are much better tolerated by peripheral organs than by brain, and suggesting this to be due to easier induction of adaptive mechanisms (Kuter et al., 2010). Furthermore, this observation suggests that the application of the diverse differentiation protocols was successful. The differential sensitivity observed might be explained by the higher basal expression of amino acid transporters, such as Solute Carrier Family 3 Member 2 (SLC3A2) and Solute Carrier Family 7 Member 11 (SLC7A11), shown by TempO-Seq analysis in the most sensitive models. Indeed, amino acid transporters have been suggested to be used by PQ to enter cells (for review, see Wang et al., 2021), their stronger expression might thus potentially lead to a higher cellular uptake of PQ. The highest level of genes coding for enzymes involved in anti-oxidant defence, such as SODs and GSTs, observed in HLC, might also explain the relatively highest resistance of this model to PQ, even so NAD(P)H-cytochrome P450 oxidoreductase (POR), engaged in ion redox cycling of PQ was a bit more expressed in HLC. However, other genes related to transport, redox cycling and anti-oxidant defence important for PQ mode of action and cellular response were unfortunately not available in the chosen TempO-Seq panel and more experiments are needed to fully characterize the causes of the differential sensitivity to PQ observed among the

**Table 5**

List of the 10 most upregulated and downregulated genes after exposure to the highest concentration of PQ for each model.

Model	Downregulated			Upregulated			Total DEG
	Gene symbol_probe ID	LCF	Number (% of total)	Gene symbol_probe ID	LCF	Number (% of total)	
BS	SPC25_6704	-3.0	55 (56)	CAV2_15304	2.5	43 (44)	98
	TOMM20_11983	-2.3		CAPN1_957	2.4		
	CIB1_16624	-2.3		SPAG7_6692	1.8		
	CTTNBP2_13527	-2.2		TOMM34_7272	1.7		
	FBXO11_2372	-1.8		THRB_24158	1.4		
	TRIM2_7343	-1.4		SOX1_27894	1.4		
	TUBA1B_7399	-1.4		CSRN1P_22653	1.3		
	NDUFA4_14125	-1.4		INSM1_21254	1.2		
	CDH8_19001	-1.3		TFAP2A_7039	1.2		
	HIST1H2BG_2953	-1.3		HIF1A_2945	1.2		
NC	SGK2_10628	-6.1	30 (47)	CYR61_24505	6.3	34 (53)	64
	EDNRA_25237	-5.1		PLK1_5203	3.6		
	IFI44L_19848	-3.0		EXOSC5_27191	3.4		
	TCF4_15698	-2.6		SERPINE1_6253	2.7		
	FKBP14_2430	-2.2		CTGF_17007	2.3		
	NUP85_4781	-2.1		MAFF_27478	2.3		
	MYBL1_22509	-2.0		SLC3A2_20164	2.2		
	RM11_15666	-2.0		GADD45A_2569	2.1		
	CETN3_27006	-1.8		GDF15_18329	1.9		
	PHLDA1_12880	-1.7		PPP1R15A_14098	1.9		
BBB	NTSDC2_4737	-2.6	43 (54)	GDF15_18329	1.9	36 (46)	79
	NCAM1_23834	-1.3		SPP1_6720	1.5		
	HMMR_3040	-1.2		SQSTM1_6740	1.5		
	HIST1H3H_2957	-1.0		PPARGCIA_12225	1.4		
	HIST1H2BG_2953	-1.0		CD55_1141	1.3		
	PSRC1_5548	-1.0		ASNS_12040	1.3		
	HIST2H2AA4_2963	-1.0		DDIT3_16736	1.2		
	HIST1H2BM_2956	-1.0		TRIB3_7337	1.2		
	HIST1H1E_14544	-1.0		CXCL2_28232	1.2		
	ASF1B_26041	-1.0		HSD17B11_3115	1.1		
PTL	CXCL14_22017	-2.2	51 (27)	GDF15_18329	6.8	139 (73)	190
	CSF3R_25969	-1.8		DDIT3_16736	4.2		
	PRR15L_5469	-1.7		NMRAL2P_81336	3.9		
	EPHX2_18456	-1.7		TRIB3_7337	3.8		
	CASP1_26966	-1.6		CHAC1_1279	3.4		
	GBP1_19263	-1.6		FOSL1_2463	3.2		
	DEPTOR_26568	-1.5		ATF3_499	3.1		
	ALDH7A1_227	-1.5		GADD45A_2569	2.9		
	CAPS_26136	-1.5		MAFF_27478	2.8		
	PDK4_28868	-1.4		IL1A_22714	2.8		
PODO	ASF1B_26041	-2.5	24 (30)	USP32P2_28186	2.2	55 (70)	79
	MYBL2_4391	-2.1		MPZL1_4249	2.1		
	HIST1H2BH_2954	-1.6		ANKRD36B_290	1.8		
	HIST1H2BB_12129	-1.4		MMP2_4213	1.8		
	HIST1H2BN_11971	-1.4		DMRTA1_14819	1.7		
	NFYB_16601	-1.3		NEAT1_81333	1.7		
	MEST_4122	-1.2		IGHMBP2_3275	1.5		
	HIST1H2B1_11969	-1.2		CD55_28297	1.5		
	IGFBP7_26667	-1.2		MAFG_20735	1.2		
	HIST2H2AA4_2963	-1.1		CREBRF_19339	1.1		
HLC	COL12A1_1461	-1.7	1 (5)	FOSL1_2463	2.7	21 (95)	22
				HMOX1_3041	2.5		
				AKR1B10_19908	1.8		
				MAFF_27478	1.7		
				GDF15_18329	1.7		
				CXCL8_14324	1.6		
				ZNF165_26222	1.6		
				TRIB3_7337	1.5		
				GCLM_25908	1.5		
				RASSF1_28369	1.5		

DEG: differentially expressed genes; LFC: log2 fold change.

various cell models. Both brain models also differ in their sensitivity to PQ. This may be explained by the cell composition and the type of cultures. The most sensitive model, NC, is a 2D model comprising neurons and a few astrocyte progenitors, whereas BS exhibit a higher astrocyte to neuron ratio, comprise oligodendrocytes and form 3D structures, possibly explaining its slightly highest resistance to paraquat.

PQ is known to produce high levels of reactive oxygen species (ROS) through mitochondrial redox cycling, and the induction of oxidative stress is one of its better described mechanisms of action in different

organs (Blanco-Ayala et al., 2014; Dinis-Oliveira et al., 2008; Gawarunnana and Buckley, 2011). In our study, one of the three pathways deregulated by PQ in five cell models, identified by enrichment analysis using ConsensusPathDB, was "Oxidative stress induced gene expression via Nrf2 markers". Keap1/Nrf2 activation functions mainly as an anti-oxidant mechanism helping cells to cope with oxidative stress and has been previously associated with PQ-induced injury (Dou et al., 2016; Kheiripour et al., 2021). Nrf2 transactivation induces the transcription of genes with upstream antioxidant response elements (ARE) to

1085.8	1825.3	1160.0	411.9	679.6	675.9	SLC3A2_20164
8.8	10.1	41.1	1.2	2.6	6.1	SLC7A11_14100
45.3	53.6	10.1	24.3	10.5	108.6	POR_23019
1762.8	1772.9	1126.4	1417.6	1312.9	1152.2	SOD1_24659
50.1	14.9	5.6	5.6	5.4	246.1	SOD2_22842
0.5	0.0	5.1	7.9	7.1	27.8	SOD3_17377
1.0	2.7	0.0	3.6	0.2	656.7	GSTA2_2817
0.0	0.0	0.0	0.5	0.1	4.5	GSTA2_17119
499.5	143.3	90.2	228.5	56.8	5509.7	GSTM3_17117
NC	BS	PODO	PTL	BLEC	HLC	

**Fig. 7.** Heatmap of Tempo-Seq normalized read counts data for selected genes involved in PQ transport, redox cycling and anti-oxidant defence. White to red intensity represents 0 (white) to highest normalized read counts (red) of the Tempo-Seq probe in the displayed data set. Annotations represent the gene symbol and Tempo-Seq probe ID. Non-normalized values are printed to allow for a quantitative comparison between genes.

counteract oxidative stress, including glutathione- reduction, –synthesis, and -recycling along with other reducing enzymes (Bugno et al., 2015; Wang et al., 2020). HMOX and NQO1 are such prototypical Nrf2 response genes (Hichor et al., 2017; Xu et al., 2017), and were induced in all the hiPSCs-derived cell systems exposed to PQ in this study. Indeed, although the thresholds were not reached to significantly activate this pathway for BS after acute exposure, we observed a concentration-dependent increase in the expression of the associated genes, and the pathway itself was impacted after 1 week of repeated exposure to PQ (Nunes et al., 2021, unpublished observation).

Endoplasmic reticulum (ER), the site of synthesis and folding of proteins, maintains a strict quality control targeting incorrectly folded proteins for proteasomal degradation (Smith et al., 2011). Upon accumulation of protein-folding alterations occurring during ER stress, cells activate a series of complementary adaptive mechanisms, the unfolded protein response (UPR), primarily serving to return normal ER function, and failure to adapt to ER stress may result in apoptosis triggered by UPR (Hetzel, 2012; Lin and LaVail, 2010). Perturbations in ER calcium, high ROS production, depletion of oxidised glutathione and proteotoxicity all have the potential to activate the UPR. Indeed, disturbance of ER and UPR have been described in human lung epithelial cells after PQ exposure (Chinta et al., 2008; Omura et al., 2013). Furthermore, recently UPR was reported after PQ treatment in primary cultures of human CD34+ derived dendritic cells, but not in macrophages (Fransen and Leonard, 2021). In the present study, the UPR pathway was highlighted in four out of the six models. As for the oxidative stress pathway, a repeated exposure to PQ was necessary to detect the UPR using ConsensusPathDB in BrainSpheres (Nunes et al., 2021, unpublished observation), although a clear concentration-dependent increase was observed in the expression of several genes involved in this pathway, such as ATF4, PPP1R15A and DDIT3, already after 24 h of exposure. The second model, for which ConsensusPathDB did not highlight UPR, the podocyte model (PODO), showed only a slight modification of PPP1R15A, suggesting no or only very weak activation of UPR-PERK branch, contrary to the observation made in the other kidney cell type, PTL. Further studies are needed to determine whether PQ activates

UPR through the induction of ER stress, as described in lung epithelial cells, or directly through the induction of ROS, since an interaction between UPR and oxidative stress has been described (Kupscio and Schlenk, 2015), involving the phosphorylated form of eIF2 $\alpha$ , ATF4, CHOP (transcription factor C/EBP homologous protein, also called DDIT3) and PPP1R15A (Harding et al., 2009; Hetzel, 2012; Pavitt and Ron, 2012; Tabara et al., 2018). Altogether, our results show that even though we used a minimum overlap of two genes between the input gene list and a given pathway associated gene list to define a pathway as overrepresented, our strategy using several hiPSC-derived models, with various cell type or organ specificities, allowed to detect the main mechanisms of action of PQ.

Another pathway revealed after PQ exposure in four cell culture systems, including both brain models (NC and BS), BLECs and HLC, was “ESR-mediated signaling”. This is interesting given that estrogenic dysfunction has recently been identified to be involved in toxicity induced by PQ on rat primary hippocampal neurons *in vitro* (Moyano et al., 2020a, 2020b) and that estradiol has been shown to protect a neuronal line from PQ toxicity (Gélinas et al., 2004). It is therefore remarkable to note that our strategy not only retrieved the main, known mechanisms of action of PQ, but also a recently proposed one that clearly deserves further studies.

Most of the top ten upregulated genes per model were involved in stress responses, in particular oxidative stress and inflammation for four hiPSC-derived models out of the six tested. The two brain models, NC and BS, however behaved differently, exhibiting genes involved in development, such as OX1 and INSM1 that promote generation and expansion of neuronal progenitor cells, and the thyroid receptor that is also important in the development and maintenance of brain structures. The lower proportion of genes involved in stress responses among the top upregulated genes in brain models suggest that brain cells have the weakest self-defence capacity against toxins or can less easily induce their adaptive mechanisms than peripheral organs (Kuter et al., 2010). These results show that although stress pathways shared by most of the models have been identified, each model seemed to also react in a specific way to paraquat. This is remarkable since in this study we used a

restricted number of probes, that were not specifically designed for cell type-specific discrimination.

Finally, VEGFA was induced by PQ in four of the models. VEGFA, a prototypical HIF1 alpha gene, primarily induced as a response to hypoxia, is mainly known for its activities related to angiogenesis, vascular permeability and vascular survival (Ferrara, 2004). There is a growing body of evidence, however, that VEGFA fulfils additional less 'traditional' functions in multiple organs during development, as well as homeostatic functions in fully developed organs (for review, see (Licht and Keshet, 2013)). Our results showing the upregulation of VEGFA shared by both brain models and both kidney models are perfectly in line with the current knowledge on the importance of VEGFA for these two organs. VEGFA, mainly expressed in astrocytes and neurons is upregulated in all brain cell types upon severe hypoxia (Jin et al., 2000). It is also expressed in glomerular podocytes, where it is critical for the establishment and maintenance of glomerular filtration (Eremina et al., 2003), and ample evidence supports important roles for this growth factor in the maintenance of tubulointerstitial integrity and the response to acute kidney injury (Doi et al., 2010; Schrijvers et al., 2004). The upregulation of VEGFA in brain and kidney models after exposure to PQ, again shows that the hiPSCs-derived models used in this study are reproducing the organ patho-physiology, and furthermore suggests this growth factor as marker of chemical injury.

Some limitations of the study should be stated. The cell models utilised here although from the same donors were cultured, differentiated and treated separately. Our systems and the majority of *in vitro* models in general represent a reductionist approach and does not fully reflect the physiology of a whole organism due to the lack of connections and communications between them through blood flow, endocrine and nervous systems. This could possibly be better recapitulated in the future by using organ-on-a-chip models and/or by the application of *in silico* modelling. Furthermore, the iPSCs-derived models used in this study, beside their great advantages, come also with some limitations. For example, although the BS model is multicellular and highly complex it does not (at this point in development) possess microglia, precluding the development of the full neuroinflammatory cascade. The HLC are not completely mature hepatocytes and lack cooperation with Kupfer cells, and the kidney model PODO lacks fenestrated endothelial cells and glomerular basement membrane to form a full glomerular model. These limitations can be overcome in the near future by co-culturing cells with their missing partners. Finally, in order to overcome the multiple differences linked to cell culture conditions that could impact the true comparisons of the effects of PQ in the different models, the distribution kinetics of PQ has to be established for each model, to correlate the observed toxic effects to the effective concentrations reaching the cells and not to the nominal concentrations used. This will allow a better comparison of the effects of chemicals on the various models.

## 5. Conclusions

Our strategy, taking advantage of the iPSC technology, allowed to determine the known and less known mechanisms of PQ toxicity with TempO-Seq analysis, using a cost-effective panel of probes specific for toxicity testing. The main advantages of this strategy are to assess chemical toxicity on cell types from multiple organs in parallel, exclusively in human cells, eliminating interspecies bias and allowing a better evaluation of the differential sensitivity of the models representing the diverse organs. To apply this approach to the general assessment of chemical toxicity, the strategy presented herein could be further improved by adding hiPSC-derived models for other organs, such as the heart and the lungs, and by standardization of procedures to reach a higher level of harmonization between the different laboratories. Furthermore, organ-specific toxicity testing could be reached by adding organ-specific genes to our set of TempO-Seq probes.

Given the present results showing the differential sensitivity of the various human models to PQ, we believe this strategy will contribute to

the further improvement of chemical risk assessment for human health, providing the above cited improvements combined with the evaluation of the distribution kinetics of the chemicals, as a key step for the *in vitro* to *in vivo* extrapolation (IVIVE) (Punt et al., 2020), absolutely required for regulatory decision-making.

Supplementary data to this article can be found online at <https://doi.org/10.1016/j.tiv.2022.105333>.

## Declaration of Competing Interest

The authors declare no competing interests.

## Acknowledgements

The work was funded by the European Union's Horizon 2020 Research and Innovation Programme MarieSkłodowska-Curie Action-Innovative Training Network project in3, under grant agreement no. 721975 (fellowships to Carolina Nunes, Pranika Singh, Zahra Mazidi, Connac Murphy, Aurore Bourguignon, Sara Wellens, Vidya Chandrasekaran and Sreya Ghosh).

## References

- Blanco-Ayala, T., Andérica-Romero, A.C., Pedraza-Chaverri, J., 2014. New insights into antioxidant strategies against paraquat toxicity. *Free Radic. Res.* **48**, 623–640. <https://doi.org/10.3109/10715762.2014.899694>.
- Boon, R., Kumar, M., Tricot, T., Bria, L., Ordovas, L., Jacobs, F., One, J., De Smedt, J., Eden, G., Bird, M., Roelandt, P., Doglioni, G., Vriens, K., Rossi, M., Vazquez, M.A., Vanwelden, T., Chesnais, F., El Taghdouini, A., Najimi, M., Sokal, E., Cassiman, D., Snoeys, J., Monshouwer, M., Hu, W.S., Lange, C., Carmeliet, P., Fendt, S.M., Verfaillie, C.M., 2020. Amino acid levels determine metabolism and CYP450 function of hepatocytes and hepatoma cell lines. *Nat. Commun.* **11**, 1–16. <https://doi.org/10.1038/s41467-020-15058-6>.
- Bugno, M., Danil, M., Chepel'ev, N.L., Willmore, W.G., 2015. Changing gears in Nrf1 research, from mechanisms of regulation to its role in disease and prevention. *Biochim. Biophys. Acta - Gene Regul. Mech.* **1849**, 1260–1276. <https://doi.org/10.1016/j.bbagr.2015.08.001>.
- Chambers, S.M., Fasano, C.A., Papapetrou, E.P., Tomishima, M., Sadelain, M., Studer, L., 2009. Highly efficient neural conversion of human ES and iPS cells by dual inhibition of SMAD signaling. *HHS Public Access Author manuscript. Nat. Biotechnol.* **27**, 275–280. <https://doi.org/10.1038/nbt.1529>.
- Chandrasekaran, A., Avcı, H.X., Ochalak, A., Rosingh, L.N., Molnár, K., László, L., Bellák, T., Téglási, A., Pesti, K., Mike, A., Phanthong, P., Bfiro, O., Hall, V., Kitiyanant, N., Krause, K.H., Kobláček, J., Dinnyés, A., 2017. Comparison of 2D and 3D neural induction methods for the generation of neural progenitor cells from human induced pluripotent stem cells. *Stem Cell Res.* **25**, 139–151. <https://doi.org/10.1016/j.scr.2017.10.010>.
- Chandrasekaran, V., Carta, G., Pereira, C., Gupta, R., Murphy, C., Feifel, E., Kern, G., Lechner, J., Cavallo, A.L., Gupta, S., Caiment, F., Kleinjans, J.C.S., Gstraunthaler, G., 2021. Generation and characterization of iPSC-derived renal proximal tubule-like cells with extended stability. *Sci. Rep.* **1–17**. <https://doi.org/10.1038/s41598-021-89550-4>.
- Chinta, S.J., Rane, A., Poksay, K.S., Bredesen, D.E., Andersen, J.K., Rao, R.V., 2008. Coupling endoplasmic reticulum stress to the cell death program in dopaminergic cells: effect of paraquat. *Neuro Mol. Med.* **10**, 333–342. <https://doi.org/10.1007/s12017-008-8047-9>.
- Cicchetti, F., Drouin-Ouellet, J., Gross, R.E., 2009. Environmental toxins and Parkinson's disease: what have we learned from pesticide-induced animal models? *Trends Pharmacol. Sci.* **30**, 475–483. <https://doi.org/10.1016/j.tips.2009.06.005>.
- Conway, J.R., Lex, A., Gehlenborg, N., 2017. UpSetR: an R package for the visualization of intersecting sets and their properties. *Bioinformatics* **33**, 2938–2940. <https://doi.org/10.1093/bioinformatics/btx364>.
- Delirrad, M., Majidi, M., Boushehri, B., 2015. Clinical features and prognosis of paraquat poisoning: a review of 41 cases. *J. Clin. Exp. Med* **8** (5), 8122–8128.
- Dinis-Oliveira, R.J., Duarte, J.A., Sánchez-Navarro, A., Remião, F., Bastos, M.L., Carvalho, F., 2008. Paraquat poisonings: mechanisms of lung toxicity, clinical features, and treatment. *Crit. Rev. Toxicol.* **38**, 13–71. <https://doi.org/10.1080/10408440701669959>.
- Doi, K., Noiri, E., Fujita, T., 2010. Role of vascular endothelial growth factor in kidney disease. *Curr. Vasc. Pharmacol.* **8**, 122–128. <https://doi.org/10.2174/157016110790226606>.
- Dou, T., Yan, M., Wang, X., Lu, W., Zhao, L., Lou, D., Wu, C., Chang, X., Zhou, Z., 2016. Nrf2/ARE pathway involved in oxidative stress induced by paraquat in human neural progenitor cells. *Oxidative Med. Cell. Longev.* **2016**. <https://doi.org/10.1155/2016/8923860>.
- EPA, 2019. Administrator Memo Prioritizing Efforts to Reduce Animal Testing. September 10, 2019. United States Environ. Prot. Agency.
- Eremina, V., Sood, M., Haigh, J., Nagy, A., Lajoie, G., Ferrara, N., Gerber, H.P., Kikkawa, Y., Miner, J.H., Quaggin, S.E., 2003. Glomerular-specific alterations of

- VEGF-A expression lead to distinct congenital and acquired renal diseases. *J. Clin. Invest.* 111, 707–716. <https://doi.org/10.1172/JCI17423>.
- EUR-Lex, 2010. Directive 2010/63/EU of the European parliament and of the Council of 22 September 2010 on the protection of animals used for scientific purposes. *Off. J. Eur. Union* 1–61.
- Ferrara, N., 2004. Vascular endothelial growth factor: basic science and clinical progress. *Endocr. Rev.* <https://doi.org/10.1210/er.2003-0027>.
- Fransen, L.F.H., Leonard, M.O., 2021. CD34+ derived macrophage and dendritic cells display differential responses to paraquat. *Toxicol. in Vitro* 75, 105198. <https://doi.org/10.1016/j.tiv.2021.105198>.
- Gao, L., Yuan, H., Xu, E., Liu, J., 2020. Toxicology of paraquat and pharmacology of the protective effect of 5-hydroxy-1-methylhydantoin on lung injury caused by paraquat based on metabolomics. *Sci. Rep.* 10, 4–8. <https://doi.org/10.1038/s41598-020-58599-y>.
- Gawaramma, I.B., Buckley, N.A., 2011. Medical management of paraquat ingestion. *Br. J. Clin. Pharmacol.* 72, 745–757. <https://doi.org/10.1111/j.1365-2125.2011.04026.x>.
- Gélinas, S., Bureau, G., Valastro, B., Massicotte, G., Cicchetti, F., Chiasson, K., Gagne, B., Blanchet, J., Martinioli, M.G., 2004. Alpha and beta estradiol protect neuronal but not native PC12 cells from paraquat-induced oxidative stress. *Neurotox. Res.* 6, 141–148. <https://doi.org/10.1007/BF03033216>.
- Gholami, S., Mazidi, Z., Pahlavan, S., Mostem, F., Hosseini, M., Taei, A., Hesarak, M., Barezkat, M., Aghdani, N., Baharvand, H., 2021. A novel insight into endothelial and cardiac cells phenotype in systemic sclerosis using patient-specific induced pluripotent stem cell. *Cell J.* 23 <https://doi.org/10.22074/cellj.2021.7244>.This.
- Harding, H.P., Zhang, Y., Scheuener, D., Chen, J.J., Kaufman, R.J., Ron, D., 2009. Ppp1r15 gene knockout reveals a essential role for translation initiation factor 2 alpha (eIF2 $\alpha$ ) dephosphorylation in mammalian development. *Proc. Natl. Acad. Sci. U. S. A.* 106, 1832–1837. <https://doi.org/10.1073/pnas.0809632106>.
- Herrmann, K., Pistollato, F., Stephens, M.L., 2019. Food for thought ... beyond the 3Rs: expanding the use of human-relevant replacement methods in biomedical research. *ALTEX* 36, 343–352. <https://doi.org/10.14573/altex.1907031>.
- Hetz, C., 2012. The unfolded protein response: controlling cell fate decisions under ER stress and beyond. *Nat. Rev. Mol. Cell Biol.* 13, 89–102. <https://doi.org/10.1038/nrm3270>.
- Hichor, M., Sampathkumar, N.K., Montanaro, J., Borderie, D., Petit, P.X., Gorgievski, V., Tzavara, E.T., Eid, A.A., Charbonnier, F., Genier, J., Massaad, C., 2017. Paraquat induces peripheral myelin disruption and locomotor defects: crosstalk with LXR and Wnt pathways. *Antioxid. Redox Signal.* 27, 168–183. <https://doi.org/10.1089/ars.2016.6711>.
- Jin, K.L., Mao, X.O., Nagayama, T., Gódsmit, P.C., Greenberg, D.A., 2000. Induction of vascular endothelial growth factor and hypoxia-inducible factor-1 $\alpha$  by global ischemia in rat brain. *Neuroscience* 99, 577–585. [https://doi.org/10.1016/S0306-4522\(00\)00207-4](https://doi.org/10.1016/S0306-4522(00)00207-4).
- Kamburov, A., Wierling, C., Lehrach, H., Herwig, R., 2009. ConsensusPathDB - a database for integrating human functional interaction networks. *Nucleic Acids Res.* 37, 623–628. <https://doi.org/10.1093/nar/gkn698>.
- Kamburov, A., Stelz, U., Lehrach, H., Herwig, R., 2013. The ConsensusPathDB interaction database: 2013 update. *Nucleic Acids Res.* 41, 793–800. <https://doi.org/10.1093/nar/gks1055>.
- Kheiripour, N., Plarak, A., Heshmati, A., Asl, S.S., Mehri, F., Ebadollahi-Natanzi, A., Ranjbar, A., Hosseini, A., 2021. Evaluation of the hepatoprotective effects of curcumin and nanocurcumin against paraquat-induced liver injury in rats: modulation of oxidative stress and Nrf2 pathway. *J. Biochem. Mol. Toxicol.* 1–9. <https://doi.org/10.1002/jbt.22739>.
- Kupsco, A., Schlenk, D., 2015. Oxidative Stress, Unfolded Protein Response, and Apoptosis in Developmental Toxicity, International Review of Cell and Molecular Biology. Elsevier Ltd. <https://doi.org/10.1016/bs.icmb.2015.02.002>.
- Kuter, K., Nowak, P., Gómbiowska, K., Ossowska, K., 2010. Increased reactive oxygen species production in the brain after repeated low-dose pesticide paraquat exposure in rats. A comparison with peripheral tissues. *Neurochem. Res.* 35, 1121–1130. <https://doi.org/10.1007/s11064-010-0163-x>.
- Li, H., Durbin, R., 2009. Fast and accurate short read alignment with burrows-wheeler transform. *Bioinformatics* 25, 1754–1760. <https://doi.org/10.1093/bioinformatics/btp324>.
- Licht, T., Keshet, E., 2013. Delineating multiple functions of VEGF-A in the adult brain. *Cell. Mol. Life Sci.* <https://doi.org/10.1007/s00018-013-1280-x>.
- Limonci, A., Ates, G., Carta, G., Wilmes, A., Watzel, M., Shepard, P.J., VanSteenhouse, H.C., Seigmann, B., Yealdy, J.M., van de Water, B., Vinken, M., Jennings, P., 2018. Comparison of base-line and chemical-induced transcriptomic responses in HepaRG and RPTEC/TERT1 cells using Tempo-Seq. *Arch. Toxicol.* 92, 2517–2531. <https://doi.org/10.1007/s00204-018-2256-2>.
- Lin, J.H., LaVail, M.M., 2010. Misfolded Proteins and Retinal Dystrophies, in: *Advances in Experimental Medicine and Biology*. Springer, New York, NY, pp. 115–121. [https://doi.org/10.1007/978-1-4419-1399-9\\_14](https://doi.org/10.1007/978-1-4419-1399-9_14).
- Liu, S., Yin, N., Faiola, F., 2017. Prospects and Frontiers of stem cell toxicology. *Stem Cells Dev.* 26, 1528–1539. <https://doi.org/10.1089/scd.2017.0150>.
- Lo Giudice, M., Mihalik, B., Turi, Z., Dinnyés, A., Kobolák, J., 2019. Calcilytic NPS 2143 reduces amyloid secretion and increases sA $\beta$ PP $\alpha$  release from PSEN1 mutant iPSC-derived neurons. *J. Alzheimers Dis.* 72, 885–899. <https://doi.org/10.3233/JAD-190602>.
- Love, M.I., Huber, W., Anders, S., 2014. Moderated estimation of fold change and dispersion for RNA-seq data with DESeq2. *Genome Biol.* 15, 550. <https://doi.org/10.1186/s13059-014-0550-8>.
- Mav, D., Shah, R.R., Howard, B.E., Auerbach, S.S., Bushel, P.R., Collins, J.B., Gethold, D. L., Judson, R.S., Karmaus, A.L., Maul, E.A., Mendrick, D.L., Merrick, B.A., Sipes, N. S., Svoboda, D., Paules, R.S., 2018. A hybrid gene selection approach to create the S1500+ targeted gene sets for use in high-throughput transcriptomics. *PLoS One* 13, e0191105. <https://doi.org/10.1371/JOURNAL.PONE.0191105>.
- Morrison, M., Klein, C., Clemann, N., Collier, D.A., Hardy, J., Hejzler, B., Cader, M.Z., Graf, M., Kaye, J., 2015. StemBANCO: governing access to material and data in a large stem cell research consortium. *Stem Cell Rev. Rep.* 11, 681–687. <https://doi.org/10.1007/s12015-015-9599-3>.
- Moyano, P., Sanjuan, J., García, J.M., Anadon, M.J., Lobo, M., Pelayo, A., García, J., Frejo, M.T., del Pino, J., 2020a. Primary hippocampal estrogenic dysfunction induces synaptic proteins alteration and neuronal cell death after single and repeated paraquat exposure. *Food Chem. Toxicol.* 136, 110961. <https://doi.org/10.1016/j.fct.2019.110961>.
- Moyano, P., Sanjuan, J., García, J.M., Anadon, M.J., Naval, M.V., Sola, E., García, J., Frejo, M.T., Pino, J. del, 2020b. Dysregulation of prostaglandin E2 and BDNF signaling mediated by estrogenic dysfunction induces primary hippocampal neuronal cell death after single and repeated paraquat treatment. *Food Chem. Toxicol.* 144. <https://doi.org/10.1016/j.fct.2020.111611>.
- Murphy, C., Feifel, E., Jennings, P., Gstraunthaler, G., Wilmes, A., 2019. A protocol for One-step differentiation of human induced pluripotent stem cells into mature podocytes. In: Mandenius, C.-F., Ross, J.A. (Eds.), *Cell-Based Assays Using iPSCs for Drug Development and Testing*. Springer, New York, New York, NY, pp. 93–99. [https://doi.org/10.1007/978-1-4939-9477-9\\_8](https://doi.org/10.1007/978-1-4939-9477-9_8).
- National Research Council, 2007. Toxicity Testing in the 21st Century: A Vision and a Strategy [WWW Document]. Natl. Acad. Press, Washington, DC. URL: [https://books.google.ch/books?hl=pt-PT&id=3AWfAwAAQBAJ&oi=fnd&pg=PT21&dq=Toxicity+Testing+in+the+21st+Century:+A+Vision+and+a+Strategy&ots=UwvqSFwazc&sig=KCxUqgElnoh\\_RuEZYHTTnNRMU&redir\\_esc=y#v=onepage&q=ToxicityTestinginthe21stCentury%3AAVIs](https://books.google.ch/books?hl=pt-PT&id=3AWfAwAAQBAJ&oi=fnd&pg=PT21&dq=Toxicity+Testing+in+the+21st+Century:+A+Vision+and+a+Strategy&ots=UwvqSFwazc&sig=KCxUqgElnoh_RuEZYHTTnNRMU&redir_esc=y#v=onepage&q=ToxicityTestinginthe21stCentury%3AAVIs) (accessed 4.30.21).
- Nunes, C., Zurich, M.-G., 2020. Neurotoxicology and Disease Modelling. Springer, Cham, pp. 229–246. [https://doi.org/10.1007/978-3-030-43939-2\\_12](https://doi.org/10.1007/978-3-030-43939-2_12).
- Ochalok, A., Mihalik, B., Avei, H.X., Chandrasekaran, A., Téglási, A., Bock, I., Giudice, M. Lo, Tancos, Z., Molnár, K., László, L., Nielsen, J.E., Holst, B., Freude, K., Hyytel, P., Kobolák, J., Dinnyés, A., 2017. Neurons derived from sporadic Alzheimer's disease iPSCs reveal elevated TAU hyperphosphorylation, increased amyloid levels, and GSK3B activation. *Alzheimers Res. Ther.* 9, 1–19. <https://doi.org/10.1186/s13195-017-0317-z>.
- Omura, T., Asari, M., Yamamoto, J., Oka, K., Hoshina, C., Maseda, C., Awaya, T., Tasaki, Y., Shiono, H., Yonezawa, A., Masuda, S., Matsubara, K., Shimizu, K., 2013. Sodium tauroursodeoxycholate prevents paraquat-induced cell death by suppressing endoplasmic reticulum stress responses in human lung epithelial A549 cells. *Biochem. Biophys. Res. Commun.* 432, 689–694. <https://doi.org/10.1016/j.bbrc.2013.01.131>.
- Oredsson, S., Coecke, S., van der Valk, J., Vinken, M., 2019. What is understood by "animal-free research"? *Toxicol. in Vitro* 57, 143–144. <https://doi.org/10.1016/j.tiv.2019.03.001>.
- Pamies, D., Barreras, P., Block, K., Makri, G., Kumar, A., Wiersma, D., Smirnova, L., Zhang, C., Bressler, J., Christian, K.M., Harris, G., Ming, G.L., Betlincke, C.J., Kyro, K., Song, H., Pardo, C.A., Hartung, T., Hogberg, H.T., 2017. A human brain microphysiological system derived from induced pluripotent stem cells to study neurological diseases and toxicity. *ALTEX* 34, 362–376. <https://doi.org/10.14573/altex.1609122>.
- Pavitt, G.D., Ron, D., 2012. New insights into translational regulation in the endoplasmic reticulum unfolded protein response. *Cold Spring Harb. Perspect. Biol.* 4, 1–13. <https://doi.org/10.1101/cshperspect.a012278>.
- Punt, A., Bouwmeester, H., Blaauw, B.J., Coecke, S., Hakker, B., Hendriks, D.F.G., Jennings, P., Kramer, N.I., Neuhoff, S., Masereeuw, R., Paini, A., Peijnenburg, A.A.C.M., Rooseboom, M., Shuler, M.L., Sorrell, I., Spee, B., Strikwold, M., Van der Meer, A. D., Van der Zande, M., Vinken, M., Yang, H., Bos, P.M.J., Heringa, M.B., 2020. New approach methodologies (NAMs) for human-relevant biokinetics predictions. Meeting the paradigm shift in toxicology towards an animal-free chemical risk assessment. *ALTEX* 37, 607–622. <https://doi.org/10.14573/altex.2003242>.
- Rauch, C., Feifel, E., Kern, G., Murphy, C., Meier, F., Parson, W., Beilmann, M., Jennings, P., Gstraunthaler, G., Wilmes, A., 2018. Differentiation of human iPSCs into functional podocytes. *PLoS One* 13. <https://doi.org/10.1371/journal.pone.0203869>.
- Saravu, K., Sekhar, S., Pai, A., Barkur, A.S., Rajesh, V., Eada, J.R., 2013. Paraquat – a deadly poison: report of a case and review. *Indian J. Crit. Care Med.* 17, 182–184. <https://doi.org/10.4103/0972-5229.117074>.
- Schrijvers, B.F., Flyvbjerg, A., De Vriese, A.S., 2004. The role of vascular endothelial growth factor (VEGF) in renal pathophysiology. *Kidney Int.* 65, 2003–2017. <https://doi.org/10.1111/j.1523-1755.2004.00621.x>.
- Sevin, E., Dehouck, L., Versèle, R., Calot, M., Gosselet, F., 2019. A miniaturized pump out method for characterizing molecule interaction with ABC transporters. *Int. J. Mol. Sci.* 20. <https://doi.org/10.3390/ijms20225529>.
- Sewell, F., Aggarwal, M., Bachler, G., Broadmeadow, A., Gellatly, N., Moore, E., Robinson, S., Rooseboom, M., Stevens, A., Terry, C., Burden, N., 2017. The current status of exposure-driven approaches for chemical safety assessment: a cross-sector perspective. *Toxicology* 389, 109–117. <https://doi.org/10.1016/j.tox.2017.07.018>.
- Singh, P., Chandrasekaran, V., Hardy, B., Wilmes, A., Jennings, P., Exner, T.E., 2021. Temporal transcriptomic alterations of cadmium exposed human iPSC-derived renal proximal tubule-like cells. *Toxicol. in Vitro* 73.
- Sittipunt, C., 2005. Paraquat Poisoning.
- Smith, M.H., Ploegh, H.L., Weissman, J.S., 2011. Road to ruin: targeting proteins for degradation in the endoplasmic reticulum. *Science* (80-). <https://doi.org/10.1126/science.1209235>.

- Steimberg, N., Bertero, A., Chiono, V., Dell'Era, P., Di Angelantonio, S., Hartung, T., Perego, S., Raimondi, M., Xinaris, C., Caloni, F., de Angelis, I., Aloisio, S., Baderna, D., 2020. iPSC, organoids and 3d models as advanced tools for in vitro toxicology. *ALTEX* 37, 136–140. <https://doi.org/10.14573/altex.1911071>.
- Tabara, K., Iwata, Y., Koizumi, N., 2018. The unfolded protein response. *Methods Mol. Biol.* 1691, 223–230. [https://doi.org/10.1007/978-1-4939-7389-7\\_17](https://doi.org/10.1007/978-1-4939-7389-7_17).
- Takahashi, K., Tanabe, K., Ohnuki, M., Narita, M., Ichisaka, T., Tomoda, K., 2007. Induction of Pluripotent Stem Cells from Adult Human Fibroblasts by Defined Factors, pp. 861–872. <https://doi.org/10.1016/j.cell.2007.11.019>.
- Wang, X., Zhang, Y., Wan, X., Guo, C., Cui, J., Sun, J., Li, L., 2020. Responsive expression of MafF to  $\beta$ -amyloid-induced oxidative stress. *Dis. Markers* 2020. <https://doi.org/10.1155/2020/8861358>.
- Wang, X., Wang, X., Zhu, Y., Chen, X., 2021. ADME/T-based strategies for paraquat detoxification: transporters and enzymes. *Environ. Pollut.* 291, 118137 <https://doi.org/10.1016/j.envpol.2021.118137>.
- Wellens, S., Dehouck, L., Chandrasekaran, V., Singh, P., Loida, R.A., Sevin, E., Exner, T., Jennings, P., Gosset, F., Culot, M., 2021. Evaluation of a human iPSC-derived BBB model for repeated dose toxicity testing with cyclosporine A as model compound. *Toxicol. in Vitro* 73, 105112. <https://doi.org/10.1016/j.tiv.2021.105112>.
- Xu, W., Li, F., Xu, Z., Sun, B., Cao, J., Liu, Y., 2017. Tert-butylhydroquinone protects PC12 cells against ferrous sulfate-induced oxidative and inflammatory injury via the Nrf2/ARE pathway. *Chem. Biol. Interact.* 273, 28–36. <https://doi.org/10.1016/j.cbi.2017.05.021>.
- Zhou, T., Benda, C., Duzinger, S., Huang, Y., Li, X., Li, Y., Guo, X., Cao, G., Chen, S., Hao, L., Chan, Y.C., Ng, K.M., Ho, J.C., Wieser, M., Wu, J., Redl, H., Tse, H.F., Grillari, J., Grillari-Voglauer, R., Pei, D., Esteban, M.A., 2011. Generation of induced pluripotent stem cells from urine. *J. Am. Soc. Nephrol.* 22, 1221–1228. <https://doi.org/10.1681/ASN.2011010106>.

---

## Chapter 3: *In vitro* distribution kinetics and neurotoxicity of the cardiac drug amiodarone in the iPSC-derived human 3D model BrainSpheres

---

*The following results are presented in the form of an article, that was submitted to ALTEX.*

*Supplementary data is in Annex 2.*

### 3.1. Introduction

Patients taking amiodarone (AMI), a broadly used class III antiarrhythmic drug, describe side effects such as headache, dizziness, tremor and ataxia, suggesting neurotoxicity. Clinical effects generally require serum concentration  $>0.5 \mu\text{M}$ , whereas increased risk of toxicity is associated with a serum concentration  $>3\mu\text{M}$ . Here, the neurotoxicity and distribution kinetics of AMI were evaluated, using the hiPSC-derived 3D model BrainSpheres. BS were exposed to AMI for 24h, 48h or repeatedly between week 6 and 7 *in vitro*. Samples were collected at the end of each exposure scenario and after one week of washout following the full week of exposure. This study will be submitted to ALTEX.

### 3.2. Contribution

For this study, I performed all the *in vitro* experiments (cell cultures including the derivation of NPCs from hiPSCs, and their characterization). I participated in the experimental design, and after assessing the cytotoxicity of AMI in BrainSpheres, I performed all RT-qPCR and immunohistochemical analyses (including confocal microscopy and ImageJ analyses). I also performed the HPLC analyses for distribution kinetics during my secondment in Prof. Nynke Kramer's lab, Utrecht, Netherlands. Finally, I analysed the raw data obtained from BioClavis for TempO-Seq analysis and I contributed to the first draft of the manuscript. I prepared all figures except the ones produced for the *in silico* prediction models.

### 3.3. Summary of the results

Cytotoxicity evaluated by MTT showed an  $\text{IC}_{50}$   $3.8\mu\text{M}$  after 24h of exposure,  $3.9 \mu\text{M}$  after 48h and  $1.8 \mu\text{M}$  after 7d of exposure and the same 7d of exposure plus a week of washout. At concentrations under  $\text{IC}_{50}$ , RT-qPCR analysis showed strong decrease of astrocytic markers after 48h of exposure and of neuronal markers after repeated exposure. TempO-Seq analysis revealed that AMI targets several Gene Ontology biological processes linked to lipid metabolism. These results were confirmed by RT-qPCR showing increase in the expression of markers for de novo lipogenesis and decrease in genes involved in the formation of lipid droplets. Evaluation of *in vitro* distribution kinetics of AMI by HPLC-UV/fluorescence show a dose- and time-dependent intracellular accumulation of AMI. *In silico* modelling of the acquired data proved to be able to predict the distribution kinetics profile.

*The submitted manuscript can be found in the following pages.*

## ***In vitro* distribution kinetics and neurotoxicity of the cardiac drug amiodarone in the iPSC-derived human 3D model BrainSpheres**

Carolina Nunes<sup>1,2</sup>, Susana Proença<sup>3</sup>, Giovanna Ambrosini<sup>4,5</sup>; David Pamies<sup>1,2</sup>; Aurélien Thomas<sup>6,7</sup>; Nynke I. Kramer<sup>3,8</sup>, Marie-Gabrielle Zurich<sup>1,2, #</sup>

<sup>1</sup>Department of Biomedical Sciences, University of Lausanne, Lausanne, Switzerland

<sup>2</sup>Swiss Centre for Applied Human Toxicology (SCAHT), Switzerland

<sup>3</sup>Institute for Risk Assessment Sciences, Utrecht University, Utrecht, The Netherlands

<sup>4</sup>The Swiss Institute for Experimental Cancer Research (ISREC), Swiss Federal Institute of Technology Lausanne (EPFL)

<sup>5</sup>Swiss Institute of Bioinformatics, Lausanne, Switzerland

<sup>6</sup>Unit of Forensic Toxicology and Chemistry, CURML, Lausanne and Geneva University Hospitals, Geneva, Switzerland.

<sup>7</sup>Faculty Unit of Toxicology, CURML, Faculty of Biology and Medicine, University of Lausanne, Lausanne, Switzerland.

<sup>8</sup>Toxicology Division, Wageningen University, Wageningen, The Netherlands

### **# Corresponding author**

**Keywords:** neurotoxicity, 3D cultures, *in vitro* distribution kinetics, organoid, iPSC, lipid metabolism

### **Abbreviations**

Amiodarone (AMI)

BrainSpheres (BS)

Developmental neurotoxicity (DNT)

Human induced Pluripotent Stem Cells (hiPSC)

Neurotoxicity (NT)

Organisation for Economic Co-operation and Development (OECD)

Test guidelines (TGL)

## Abstract

The importance to evaluate the potential neurotoxicity of chemicals before their release on the market is increasingly recognized. However, the current procedures based on animal experimentation need to be replaced by a combination of *in silico* and *in vitro* approaches, as evidenced by ethical, economic and scientific arguments. Here, we assessed the neurotoxicity of acute (48 h) and repeated exposure (7 days) to amiodarone, an antiarrhythmic drug, using the human induced pluripotent stem cells (hiPSCs)-derived 3D model BrainSpheres. The *in vitro* distribution kinetics, essential for the extrapolation of *in vitro* effect concentrations to human equivalent doses was quantified. We report a time- and concentration-dependent accumulation of amiodarone in brain cells coupled with increased neurotoxic effects, evidenced by immunostaining, TempO-Seq and qRT-PCR analyses. Astrocytes were highly sensitive to amiodarone. For the first time, lipid metabolism perturbation was found to occur in human brain cells, as previously reported in various other cell types. Furthermore, a compartmental model developed and parametrized in this study, allowed to predict the change in cell-associated concentrations in BrainSpheres, with time and for different exposure scenarios. Finally, our results suggest that human BrainSpheres are intrinsically slightly more sensitive to amiodarone exposure than *in vitro* rodent cells. In conclusion, we believe that determining the *in vitro* distribution kinetics, a key step for *in vitro-in vivo* extrapolation (IVIVE), together with the neurotoxicity of chemicals, in human-based complex models such as the human iPSC-derived BrainSpheres, will contribute to the refinement of chemical risk assessment for human health and help regulatory decision-making.

## 1. Introduction

The brain is a structurally and functionally very complex organ, particularly susceptible to toxic insults due to very low regeneration abilities after damage. However, in spite of this vulnerability, neurotoxicity is not systematically assessed in the safety evaluation of chemicals, potentially leading to the exposure of the general public to chemicals hazardous to the brain. If neurotoxicity is evaluated, it is generally on rodents. However, the structure and function of their brain is so notably different from ours that the relevance of these tests to assess chemical safety in humans is questioned (Bal-Price et al., 2010). In addition, the increasing onset of neuronal disorders and neurodegenerative diseases, linked to the aging of the population, represents a clear demand for drugs active on the nervous system for which safety has to be assessed in the early phases of drug development.

There is nowadays a large consensus that animal testing needs to be replaced by a combination of *in silico* and *in vitro* approaches, as evidenced by ethical and economic arguments, besides scientific ones (Bal-Price et al., 2010). The discovery of human induced Pluripotent Stem Cells (hiPSC) (Takahashi et al., 2007) allowed to produce promising test models for reducing, refining and replacing (3Rs) animal-based toxicity tests. These cells of human origin, can be differentiated into almost all cell types, and be obtained from specific patient populations, to assess interindividual sensitivities to toxic insults. Thus, the various models recently derived from hiPSCs fit well in the vision of the National Research Council, Toxicity Testing in the Twenty-first Century (NRC, 2007). Neurotoxic potencies of chemicals have already been assessed in human iPSC-differentiated neuroprogenitor cells (NPCs), neurons and glial cells (Pistollato et al., 2017; Pei et al., 2016; Ryan et al., 2016; Druwe et al., 2015). However, not surprisingly, it has been previously shown that a given brain cell type reacts differently to a toxic substance when grown in single cell type cultures than in mixed-cell type cultures (Eskes et al., 2003; Eskes et al., 2002). Therefore, complex 3D cell culture systems containing the main brain cell types, allowing for maximum cell-to-cell interactions and recapitulating relevant neurodevelopmental processes, are promising tools for the evaluation of the adverse effects of chemicals on the nervous system (NS). The BrainSphere (BS) model is one such complex 3D cell culture system meeting these requirement (Pamies et al., 2017). This model consists of electrophysiologically active neurons, astrocytes, and oligodendrocytes, which are able to form compact myelin sheaths around axons. BS already proved to be a reliable tool for *in vitro* neurotoxicity testing (Modafferi et al., 2021; Zhong et al., 2020; Pamies et al., 2018; Nunes et al., 2022; Chesnut et al., 2021). They were recently used to decipher the interactions between genes and environment in developmental neurotoxicity (Modafferi et al., 2021).

However, to compare BrainSphere model sensitivity to neurotoxic insults with other in vitro models, rank effect concentrations of different neurotoxicants, and extrapolate in vitro effect concentrations to human equivalent neurotoxic doses, the in vitro distribution kinetics of test chemicals should be determined (Groothuis et al., 2015; Kramer et al., 2015; Proenca et al., 2021; Honda et al., 2019). Traditionally, the nominal effect concentration (EC) has been used as a surrogate for biologically effective concentration and for quantitative in vitro to in vivo extrapolation (QIVIVE). However, the nominal concentration may not be a suitable proxy for the freely available concentration of chemicals, especially for lipophilic, volatile and unstable chemicals. Test chemicals differentially evaporate and bind to microtiter plate plastic and cells (Groothuis et al., 2019; Heringa et al., 2004; Gulden et al., 2001; Jager et al., 2011). The cell-associated dose will increase with every repeat dosing for chemicals that significantly accumulate in cells (Kramer et al., 2015; Wilmes et al., 2013). Uncertainties in dose extrapolation are exacerbated in repeat dose toxicity tests, since in it is difficult to determine if increased toxicity observed over time is due to the accumulation of the test chemical in the model system or “accumulation” of toxic effects (i.e., increase in damage accrual in time). The lack of regulatory acceptance of in vitro methods for repeated exposure scenarios may partially be explained by these uncertainties (Mahony et al., 2020).

Here we assessed the neurotoxicity and distribution kinetics of the very lipophilic drug, amiodarone (AMI), in BrainSphere cultures and used different in vitro dose metrics to calculate concentration-effect relationships. AMI is an effective antiarrhythmic drug frequently used in clinical practice (Marcus et al., 1981; Hamilton et al., 2020). It inhibits sodium and calcium L-type channels, modulates potassium outward current, and has antagonistic effects on adrenergic receptors in the heart (Varro et al., 1996; Polster and Broekhuysen, 1976). The long-term use of amiodarone has many unwanted side effects, including cardiac, pulmonary, hepatic, and neurological toxicities, the most common being tremor, ataxia and peripheral neuropathy (Jafari-Fesharaki and Scheinman, 1998; Hindle et al., 2008; Niimi et al., 2019). In addition, some cases of parkinsonism have also been reported (Ishida et al., 2010). However, the mechanisms of neurotoxicity remain obscure and research on this area is scarce. We report a time- and concentration-dependent accumulation of amiodarone in brain cells coupled to increased neurotoxic effects. Furthermore, we show that astrocytes are extremely sensitive to amiodarone, and that lipid metabolism perturbation occurs in brain cells, as previously reported in hepatocytes, alveolar epithelial cells, proximal tubule cells and macrophages (Antherieu et al., 2011; Pedro and Rudewicz, 2020; Kapatou et al., 2010).

## **2. Material and Methods**

### **2.1. Cell culture**

The hiPSC cell line SBAD3 was generated from fibroblasts purchased from Lonza using Sendai transfection in the IMI-funded StemBANCC project (<http://stembancc.org>) (Morrison et al., 2015), as previously described. Cells were cultured in serum-free mTeSR™1 medium (STEMCELL Technologies) in petri dishes coated with Corning® Matrigel® hESC-Qualified Matrix, LDEV-free ~18µg/cm<sup>2</sup> (Corning-), at 37°C in an atmosphere of 5% CO<sub>2</sub>. Medium was replaced every day. Cells were passaged every 4-5 days using Versene® (Life Technologies). All the experiments were made following good cell culture practice guidelines 2.0 (Pamies et al., 2022).

The Ad3G2 neuroprogenitor cells (NPC) were generated from the hiPSC SBAD3 clone 1 (Fig. 1A), following the protocol “Induction of Neural Stem Cells from Human Pluripotent Stem Cells Using Gibco PSC Neural Induction Medium”(Nunes and Zurich, 2020). Shortly, non-confluent cultures of hiPSCs in a 6well plate format were grown in PSC Neural Induction Medium (NIM, 10% Neural Induction Supplement in Neurobasal® Medium) (Gibco), leading to differentiation into NPCs in 7 days. For expansion, Ad3G2 were kept in Geltrex (Gibco) coated flasks in Neural Expansion Medium (NEM) containing 45% Neurobasal® Medium (Gibco), 45% Advanced™ DMEM/F-12 Medium (Gibco) and 10% Neural Induction Supplement (Gibco). They were passaged once per week with StemPro® Accutase® (Gibco) at 70-90% confluency. Medium was changed every other day. Cultures were maintained at 37°C in an atmosphere of 5% CO<sub>2</sub>.

BrainSpheres (BS) were prepared from the NPC line Ad3G2 (Fig. 1A) as previously described (Pamies et al., 2017). In short, NPCs were plated in non-coated 6-well plates (2x10<sup>6</sup> cells/well) in 2 mL of NEM. Over the following two days, the medium was gradually replaced with Neuronal Differentiation Medium (NDM, Neurobasal® Electro Medium (GIBCO) supplemented with 5% B-27® Electrophysiology (GIBCO), 1% glutamax (GIBCO), 1% Penincilin-Streptomycin (Gibco) 0.01 µg/mL human recombinant GDNF (PeproTech), 0.01 µg/mL Human/Murine/Rat recombinant BDNF (PeproTech). Medium was replaced three times a week. Cultures were maintained at 37°C in an atmosphere of 5% CO<sub>2</sub>, under constant gyratory shaking (86 rpm).

### **2.2. Amiodarone exposure**

Amiodarone (AMI) (purity ≥98%; Sigma–Aldrich, catalogue No A8423-1G, lot #SLBW3654V) was dissolved in dimethylsulfoxide (DMSO) (purity ≥99.9%; Sigma–Aldrich, catalogue No D2650). Stock solutions (1000 X) were freshly prepared for each experiment and were further diluted in NDM to reach the final concentration. Six-week-old BS were exposed acutely (1-48h), or

repeatedly (7 days, referred to as 7d) to AMI. The repeated exposure was also followed by a week in absence of amiodarone, called washout period (referred to as 7dW). Concentrations of AMI and time points are given in results section and in figure captions. Numbers of samples per group are indicated in figure captions.

### **2.3. Cytotoxicity Assay**

BS were exposed to a range of AMI concentrations (0-15  $\mu$ M), either one time and collected after 24h and 48h, or repeatedly (at each medium change) and collected immediately at the end of one-week treatment (7d) or after another week in absence of amiodarone (7dW) (Fig. 2A). After each exposure scenario, the medium was replaced by 1 mL of resazurin solution (44  $\mu$ M), and BS were incubated for 3h at 37°C. The fluorescent product resorufin was measured at 540 nm excitation and 590 nm emission using a Synergy plate reader (BioTek). After subtraction of the background (resazurin solution only), results were expressed as % of control (DMSO) cultures. A non-linear regression (log (inhibitor) vs response - variable slope (four parameters)) was performed in order to calculate the inhibitory concentration (IC) and derive exposure-dependent curves, using GraphPad Prism®.

### **2.4. Real-time RT-PCR analyses**

At collection, samples were washed twice with Dulbecco's phosphate-buffered saline (DPBS) and dry pellets were kept at -80°C. Total RNA was extracted automatically (QIAcube instrument from Qiagen) using QIAshredder (Qiagen) and RNeasy columns (Qiagen). RNA concentration was determined by spectrophotometry (Nanodrop ND-100). Reverse transcription was performed using 0.5-1  $\mu$ g total RNA with the high-capacity cDNA reverse transcription kit (Life Technologies) on a 2720 Thermo Cycler (Applied Biosystems). Semi-quantitative real-time PCR analyses were performed with SYBR Green® (ThermoFisher) or TaqMan® (ThermoFisher) technology in a total volume of 10  $\mu$ l. Sequences of primers, references for TaqMan® probes and cDNA input are given in Suppl. Table 1 and Suppl. Table 2. Each sample is analyzed in triplicates. The  $\Delta\Delta$ Ct method (Livak and Schmittgen, 2001) was used to calculate the relative mRNA expression. Data was accepted at < 40 cycles of amplification. Results are expressed as fold change to DMSO control cultures maintained under normal medium conditions, set at 1 baseline. RLP13A was used as reference gene, except for the developmental-dependent analyses where the  $\Delta$ Ct (Schmittgen and Livak, 2008) method was used since no satisfying internal control gene was found. Acquisition was performed using 7900HT Fast Real-Time PCR System (Applied Biosystems).

## 2.5. Immunohistochemistry

A At collection, BS were washed twice with DPBS, fixed for 1 h with 4% paraformaldehyde (PFA) and then kept in DPBS at 4°C until further processing. Fixed BS were incubated for 2 h in blocking solution (10% Normal Goat Serum (NGS) (ThermoFisher) in DPBS with 4% Triton-X100 at 4°C. BS were then incubated for 48h at 4°C with the primary antibodies (Suppl. Table 3) diluted 1:200 in DPBS containing 10% NGS and 1% Triton-X100. BS were then washed 3 times for 5 minutes in DPBS and incubated 1 hour at room temperature (RT) with the correspondent secondary antibody (Suppl. Table 3) diluted 1:200 in DPBS containing 10% NGS. BS were washed again 3 times for 5 minutes in DPBS, and the nuclei were stained with Hoechst 33342 (1:10,000 in PBS, ThermoFisher) for 5 min. Finally, BS were mounted on glass slides and coverslips with ProLong™ Gold antifade reagent (ThermoFisher). For BS characterization, one picture per sphere, at the plan with the highest fluorescence intensity was taken, using a Zeiss LSM 900. For the effects of AMI, Z stacks were acquired with a Leica Thunder Imaging System. Images were adjusted and quantified for “mean gray value” of a z-stack projection for “maximum intensity” using ImageJ® Fiji.

## 2.6. Statistical analyses

Prism (Version 9.01, GraphPad Software) was used for statistical analysis and graphical representation for gene expression, cell viability, distribution kinetics and immunocytochemistry quantifications. Statistical analysis was performed using the mixed-effects models with Geisser-Greenhouse correction followed by Dunnett’s multiple comparisons test. Statistically significant different comparisons are presented in figures as \*  $p < 0.05$ , \*\*  $p < 0.01$ , \*\*\*  $p < 0.001$  or \*\*\*\*  $p < 0.0001$ . Data are shown as mean  $\pm$  SD.

## 2.7. *In vitro* distribution Kinetics

### 2.7.1. Sample collection and HPLC analysis

AMI was extracted from medium, cells and well plate plastic and levels were analytically quantified. This allowed to determine how AMI distributed within the *in vitro* system in this study and follow levels of AMI associated with each *in vitro* compartment over time. AMI was extracted from medium, cells and well plate plastic at time-points 1, 3, 6, 24 and 48 h after a single exposure to 1, 2 and 3  $\mu$ M AMI. Medium was collected and centrifugated at 300 rpm for 5 min at 4°C, then supernatant was diluted 1:1 with methanol (purity  $\geq$  99.92%; Sigma–Aldrich, catalogue No 900688, EUA). For cell collection, BS were washed twice with DPBS and transferred

to Eppendorf tubes containing 250  $\mu$ L methanol. Cell extracts were stored at  $-80^{\circ}\text{C}$  before chemical analysis. On the day of the chemical analysis, BS were sonicated to homogenize the sample and centrifugated at 1200 g for 10 min. Supernatant was collected and analysed using HPLC-UV. To extract AMI from well plate plastic, wells were washed with DPBS after BS removal and then incubated with 1 mL of methanol (Sigma) for 2 h, at RT on an orbital shaker. AMI was also extracted from well plate plastic and medium from exposed *in vitro* systems without cells. All extracts were stored at  $-20^{\circ}\text{C}$  prior to chemical analysis. Before HPLC analysis, extracts were vortexed.

HPLC was used to quantify AMI concentration in each extract. The HPLC system consisted of several modules: two Shimazu LC-20AD XR liquid chromatograph pumps, a Shimazu SIL-20A XR autosampler, a Shimazu CTO-20A column oven, a Shimazu SPD-20AV UV-VIS detector, RF-20A XS fluorescence detector, and a Shimazu CBM-20A communication bus module. A Dr Maisch Great Smart RP column (18.5  $\mu\text{m}$  150 x 2 mm) was used as a stationary phase. MilliQ water (eluent A) and acetonitrile with 0.1 % formic acid (eluent B) were used as mobile phase with a flow rate of 0.2 mL/min. AMI was trapped in the stationary phase with 5 % eluent B. Then Eluent B rose to 95 % throughout 0.5 minutes, being kept constant till 7 minutes of run, after which it decreased back to 5 %. Amiodarone peaks were detected after 6.3 min at 242 nm UV wavelength. Mass of AMI was quantified using calibration standards prepared in the respective matrix (medium/methanol 1:1 or 100 % methanol).

### 2.8.2. *In silico* modelling of AMI *in vitro* distribution kinetics

#### *In silico* modelling of AMI *in vitro* distribution kinetics

To model the distribution of AMI in BS systems after repeat dosing, three model compartments were defined: medium, cells and plastic (Suppl. Fig. 1A). In the case of cell-free assays, the model compartments are plastic and medium. The change in AMI mass in each compartment was defined using rate constants in and out of each compartment. The ratio of AMI concentrations on plastic (amount AMI per exposed surface area of plastic) and in medium was not consistent across exposure levels, which suggests sorption to plastic is saturable. Therefore, besides the sorption and desorption rate constants ( $k_{\text{plastic}}$ ,  $k_{\text{dplastic}}$ ), the model included a maximum number of binding sites ( $N_{\text{max}}$ ) on plastic. The profile of AMI distribution in the *in vitro* system throughout time seems to indicate there is a slow irreversible loss of AMI from the system. This process was herein considered to be abiotic degradation ( $K_{\text{deg}}$ ) from medium.

The rate constants,  $N_{\text{max}}$  and  $K_{\text{deg}}$  were fit by minimizing the error between the predictions of AMI amount in the different compartments throughout the repeated exposure, and the

equivalent experimental data (Fig. 3). The error between prediction and experimental values were normalized to the respective experimental value, but also to the timepoint, to make sure the prediction errors for the different nominal concentrations, compartments and timepoints was balanced. Plots of the different residuals are presented in Suppl. Fig. 2. Minimization was obtained through Broyden–Fletcher–Goldfarb–Shanno (BFGS) algorithm implemented using optim function in R. The conceptual model and differential equations used to simulate the wells with cells are illustrated in Suppl. Fig.1 B. The model was then used to calculate different dose metrics for dose-response modelling. To calculate maximum concentration (C<sub>max</sub>) and (AUC) in cells, we assumed the cell number was the same after the exposure as at the time of seeding (two million cells/well). The model assumes that a dead cell has the same accumulation potential as a live cell (i.e., lipid and protein are still in the testing system) (Proenca et al., 2021). The model was written and simulated in R (version 3.63), using the RStudio interface.

## **2.9. TempO-Seq analysis**

### 2.9.1. TempO-Seq sample collection

At the end of exposure to AMI, cells were collected and lysed with 1X TempO-Seq Lysis Buffer (BioClavis) in a ratio of 0.25 to 2 million cells/mL. Lysates were frozen at –80 °C and shipped to BioClavis Technologies Ltd. (Glasgow) on dry ice where the TempO-Seq assay using the EU-ToxRisk v2.1 panel (3565 probes representing 3257 genes) was conducted with standard attenuators. The service also included primary processing to derive gene-annotated raw read counts and quality control, following a previously described procedure (Limonciel et al., 2018; Mav et al., 2018). Each sample FASTQ file was aligned against the TempO-Seq transcriptome using the Bowtie aligner (Li and Durbin, 2009). The output of this analysis generated a table of counts per gene per sample.

### 2.9.2. Differential Expression Analysis

Differential gene expression analyses were performed in R using DESeq2 v1.32.0 built-in functions (Love et al., 2014). Unsupervised clustering of the samples was performed after a r-log transformation using standard DESeq2 suggested settings to visualize the variance within and between treatment and control groups. To normalize for sequencing depth and RNA composition, DESeq2 uses the median of ratios method. To identify differentially expressed genes (DEGs) or probes, DESeq2 uses by default the Wald test. Differentially expressed probes were selected based on their multiple testing corrected adjusted P value (<0.05).

### 2.9.3. Gene Ontology analysis

Over-representation (or enrichment) analysis was performed on the differentially expressed probes using the enricher function in ClusterProfiler v4.0 (Yu et al., 2012) from Bioconductor v4.1.0 and the GO biological process gene sets from MSigDB at Broad Institute v7 (Liberzon et al., 2011; Subramanian et al., 2005). The lipid metabolism linked genes heatmap was generated using the heatmap package in R

## 3. Results

### 3.1. BrainSpheres (BS) reach a high level of cellular differentiation and maturation

Ad3G2 NPCs were differentiated from the hiPSC line SBAd3 and used to prepare BS (Fig. 1A). To characterize the 3D cultures, time-dependent expression of several markers for CNS cell populations was assessed using gene expression and immunohistochemistry. Quantitative real time RT-PCR (qRT-PCR) analysis showed a time-dependent decrease of proliferation- and stem cells-specific ((Marker Of Proliferation Ki-67 (Ki67), Nestin (NES), SRY-Box Transcription Factor 2 (SOX2), Nanog Homeobox (NANOG)) (Fig. 1B). In parallel, a time-dependent increase in the mRNA levels of neuronal- ((Microtubule-associated protein 2 (MAP2), Tyrosine Hydroxylase (TH), Synaptophysin (SYP), Acetylcholinesterase (ACHE and Glutamate Ionotropic Receptor NMDA Type Subunit 1 (GRIN1)), astrocyte- ((S100 Calcium Binding Protein B (S100B), Vimentin, and Glial fibrillary acidic protein (GFAP)) and oligodendrocyte-specific (Oligodendrocyte Transcription Factor 2 (Olig2)) markers (Fig. 1B) was observed. Whole mount immunohistochemistry at 2, 4, 6 and 8 weeks of differentiation confirmed the presence of neurons (neurofilament heavy chain (NF200) and SYP), astrocytes (S100B and GFAP), and oligodendrocytes (Oligodendrocyte Marker O4 (O4)) (Fig. 1C). NF200 immunostaining is already present at week 2 and shows an increased number of processes and a higher complexity of axonal network over time. In parallel, increased immunolabelling of the pre-synaptic protein SYP is observed from week 6. S100B staining is also stronger from week 6 and shows mostly cell bodies. On the other hand, GFAP immunostaining shows a network of processes, already at week 4, and becoming denser with time, particularly between week 4 and week 6. Oligodendrocyte 4 (O4) labelling follows a quite different pattern. It is stronger at week 2 and 4 than at later time-points.

Altogether, these data show that with time in culture cells are losing their stem cells properties while differentiating into neurons, astrocytes and oligodendrocytes. The presence of SYP suggests that neurons are forming synapses.

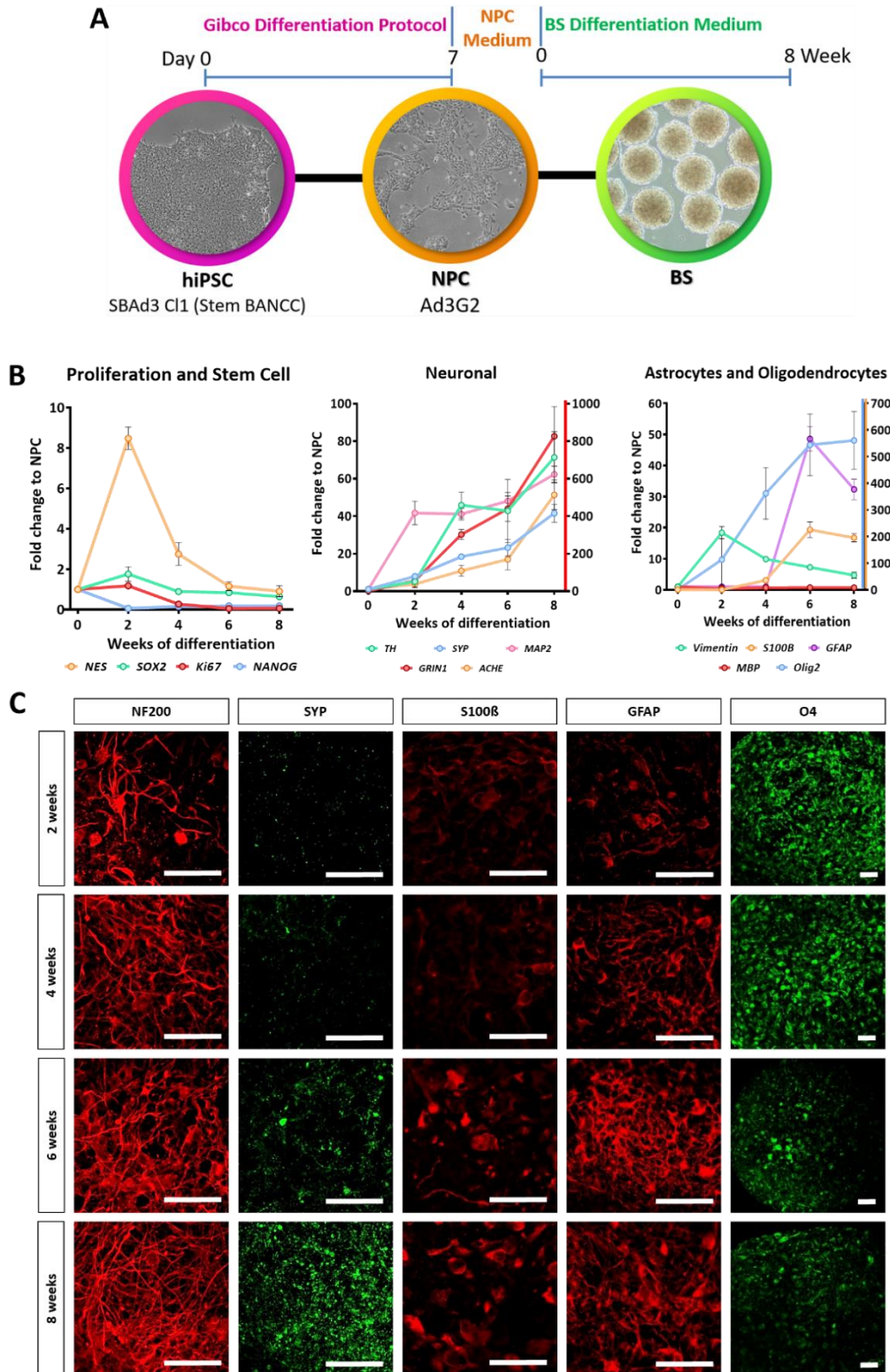


**Figure 1. BrainSpheres (BS) preparation and characterization** (A) Schematic description of the 3D culturing process. (B) Developmental-dependent gene expression of various markers (Neuronal: right y-axis relative quantification of GRIN1; astrocytes and oligodendrocytes: right y-axis relative quantification of S100B and Olig2). Each point represents the mean ( $\pm$ SD) of 6 samples obtained in 2 independent experiments. (C) Representative immunostaining images of different markers for neurons (high molecular weight neurofilament (NF200), synaptophysin (SYP)), Astrocytes (S100 calcium binding protein (S100B), glial fibrillary acidic protein (GFAP)) and oligodendrocytes (O4), at 2, 4, 6 and 8 weeks of differentiation. Scale bar = 50 $\mu$ m.

### 3.2. Bioaccumulation of amiodarone leads to increased neurotoxicity

BS were exposed to AMI after 6 weeks of differentiation, when neurons, astrocytes and oligodendrocytes clearly express specific cell-type markers. Fig. 2A describes the different exposure scenarios.

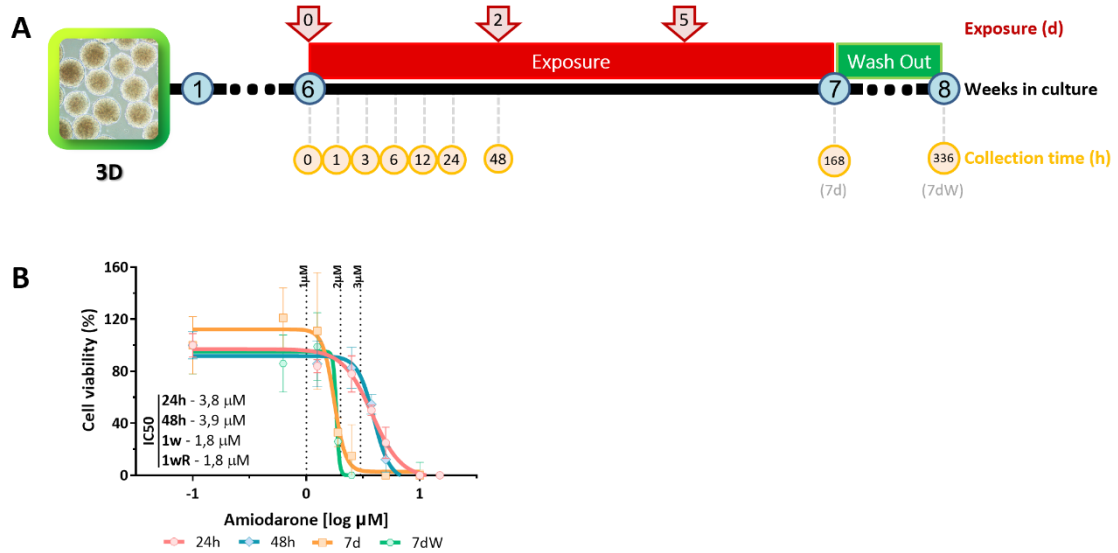


**Figure 2. AMI-induced cytotoxicity in BS** (A) Schematic description of the exposure and sample collection scenario. Spheres were exposed to AMI after 6 weeks of differentiation. Samples were collected (yellow circles) 1, 3, 6, 24 and 48 h after the first exposure (red arrows), after 1 week of repeated exposure (168h = 7d) and after a washout period (336h = 7dW). (B) Cytotoxicity concentration-dependent curves established after 1 single (24 h, 48 h) or repeated (7d and 7dW) exposure to AMI (0 - 15  $\mu\text{M}$ ). Results are expressed as % of control cultures (DMSO). Each point is the mean  $\pm$  SD of 3-9 samples obtained in 3 independent experiments. A non-linear regression (log (inhibitor) vs response - variable slope (four parameters)) was performed in order to calculate the inhibitory concentration (IC) using GraphPad Prism®.

Time-dependent cytotoxicity was first evaluated. BS were exposed to AMI concentrations ranging from 1 to 15  $\mu\text{M}$ , and samples were collected after a single treatment (24 h or 48 h), repeated treatments (7d), and repeated treatments followed by a wash-out period (7dW). Resazurin assay showed (Fig. 2 B) higher cytotoxicity after 1 week of repeated exposure, with an IC<sub>50</sub> of 1.8  $\mu\text{M}$  at 7d, than after acute exposure (IC<sub>50</sub> at 24h = 3.8  $\mu\text{M}$ ). No difference was observed between 24 h and 48 h of exposure (IC<sub>50</sub> 3.8 vs 3.9  $\mu\text{M}$ , respectively) nor between repeated exposure and repeated exposure followed by a wash out period (1.8  $\mu\text{M}$  in both cases). The slopes of the curves are steep, particularly after 7d of treatment (Fig. 2B, 7d and 7dW).

The kinetic behaviour of AMI in our *in vitro* system was then assessed to help explain the changes in cytotoxic potency in time. AMI was quantified in cell lysates, in medium, and in methanol extract of plastic plates, after a single exposure to 1, 2 or 3  $\mu\text{M}$  for 1 to 48h, or after a repeated exposure to 1 or 2  $\mu\text{M}$  for 7days (7d), and repeated treatments followed by a wash-out period (7dW).

Overall full mass balance (90-110% recovery) was recovered after the first timepoints (1-24 hours) (Fig. 3 A). A quick and continuous loss of AMI from medium was observed (12, 28 and 31 % of the nominal amount after 24 hours exposure to AMI 1, 2 and 3  $\mu\text{M}$ , respectively; Fig. 3 A and B orange line), that was compensated by uptake into cells and binding to plastic till 24 h. However, after 48 h of exposure, a consistently lower total recovery of AMI (losses up to 23% of mass balance) in presence (Fig. 3 A) or absence of cells (Suppl. Fig. 3) was observed. On the other hand, due to the retention of AMI in cells and on plastic when refreshing medium, the mass balance after 7d showed a higher amount of AMI in the system than dosed (Fig. 3 A 168 h, 1 and 2  $\mu\text{M}$ ). After 7dW the total mass of AMI was decreased, but it could still be detected in the cell lysates. Finally, the main oxidative AMI metabolite, mono-N-desethylamiodarone (MDEA) was not found in the cell lysates, nor in medium (not shown).

AMI showed slow cell uptake kinetics, with 12, 16 and 17% of the mass accumulated in cells after one 1 h-exposure to 1, 2 and 3  $\mu\text{M}$  (Fig. 3 and Suppl. Fig. 4; Suppl. Fig. 5 is added to better appreciate the experimental values at short time-points). This uptake led to a continuous increase to 45, 44 and 32% after 24 hours of exposure to 1, 2 and 3  $\mu\text{M}$ , followed by a slight decrease at 48 h, possibly related to the decrease found in medium in conditions with and without cells (Fig. 3A and Suppl. Fig. 3). A peak of AMI in cells was reached after 7d (168h), decreasing with the washout period to 48 and 30 % of the maximum mass reached in cells, after 1 and 2  $\mu\text{M}$ , respectively (Fig. 3A, 3B, red circles, and Suppl. Fig. 4A, red circles). Binding to plastic was quicker than sorption to cells with 35, 27 and 23 % of total mass found in plastic already after 1 h of exposure to 1, 2 and 3  $\mu\text{M}$ , respectively. The amount of chemical in plastic increased up until 48 hours of exposure, reaching 29-40 % of total mass (Fig. 3A, 3B, blue circles and Suppl. Fig. 4, blue circles). Similar to cells, the amount of AMI sorbed into plastic also reached its maximum after 7d, followed by very slow desorption during the wash-out phase. The mass of chemical decreased to 60 and 68 % of the peaked mass after exposure to 1 and 2  $\mu\text{M}$  AMI (Fig. 3A, 3B blue circles and Suppl. Fig. 4, blue circles). Plastic binding was still observed at the end of the washout period (7dW). Finally, AMI levels decreased in time in medium (Fig. 3A and B, orange circles and Suppl. Fig. 4, orange circles) up to 48h. Levels of AMI in medium after the washout period were undetectable.

Rate constants of AMI from exposure medium into and from cells as well as onto and off plastic were fit using a three compartmental model for each nominal concentration tested (1, 2 and 3  $\mu\text{M}$ ). Concentration-time profiles in medium and plastic of systems free of cells were used to correct for abiotic degradation of AMI. The best fit values for sorption and desorption rate constants into cells and plastic are given in Suppl. Fig. 1C.

The concentration of AMI in medium was well predicted for acute exposure to 2 and 3  $\mu\text{M}$  (80-120% of experimental value (Fig. 3B and Suppl. Fig. 4B), whereas the medium concentration-time profile in systems dosed with 1  $\mu\text{M}$  AMI in medium was overpredicted (Suppl. Fig. 4A). On the other hand, predicted concentration-time profiles for AMI in cells were between 70-160 % of the experimental values, with an average of 106 % and without an obvious bias in predictions (Fig. 3B and Suppl. Fig. 4). Similar observations are true for binding to plastic (71-141% of the experimental values) with an average 100% of the experimental value (Fig. 3B and Suppl. Fig. 4).

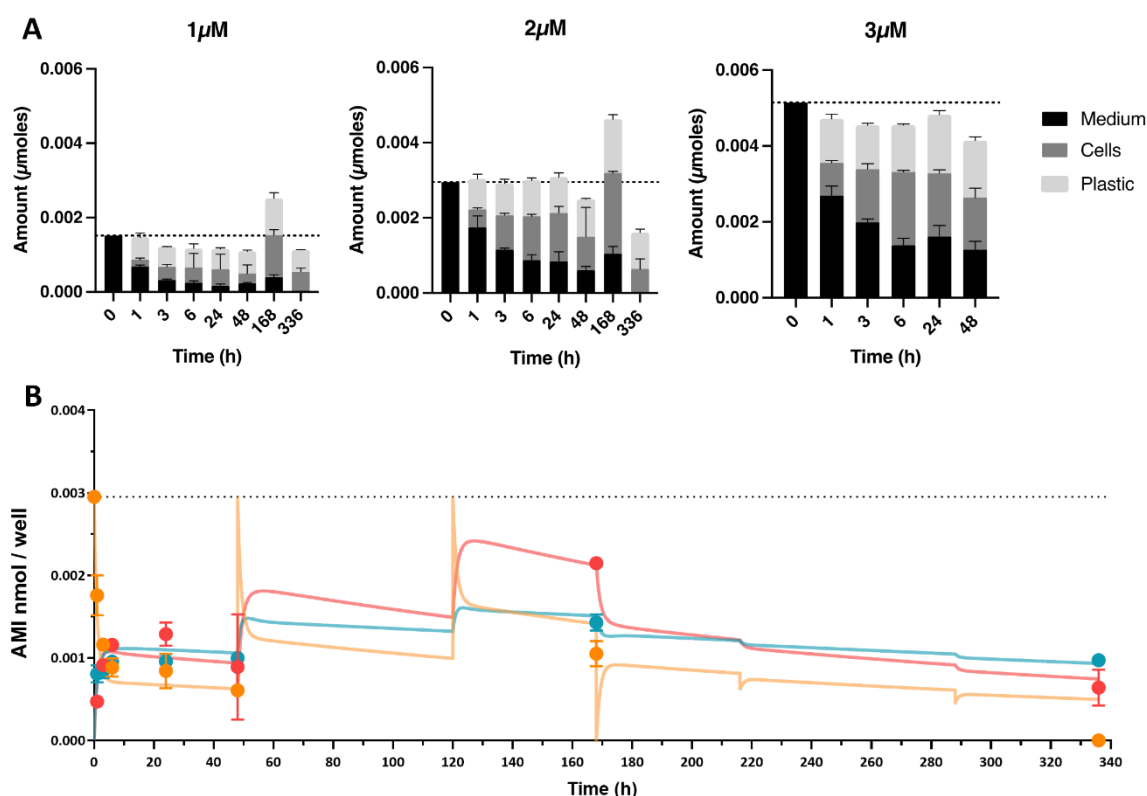


**Figure 3. AMI distribution kinetic: in vitro experimental values and in silico prediction.** (A) Relative distribution of AMI quantified in the different compartments of the model: medium (black bars), cell lysates (grey bars) and plastic binding (light grey bars) after acute (1 - 48 h) and repeated treatment (168 h = 7d and 336 h = 7dW). Results are reported as mean  $\pm$  SD of three replicates. (B) Kinetic profiles of AMI experimentally measured in cell lysates (red circles), in medium (orange circles) and in plastic bound fraction (blue circles) of BS exposed to AMI 2  $\mu\text{M}$ . Each value is the mean ( $\pm$ SD) of 3 replicates. Predicted curves are superimposed on experimentally measured values, cells (red line), medium (orange line), plastic binding (blue line). Dotted line represents the quantification of AMI in the medium at time = 0.

Altogether, these data show an increased cytotoxicity of AMI with repeated exposure and suggest it to be due to its bioaccumulation in cells.

### 3.3. Cmax in cells is a setup-independent dose metric for dose response modeling

The compartmental model was applied to simulate the distribution and accumulation of amiodarone in the different in vitro compartments for all nominal test concentrations and exposure scenarios. This simulation allowed us to calculate the Cmax in medium and cells and the AUC of the amount in medium and cells. Fig. 4 (A to D) shows how plotting the Cmax in cells against viability causes concentration-effect curves for each exposure scenario to cluster together. EC50s as Cmax in cells ranged from 0.1559 (7d) to 0.1626 (7dW) nmol per 100,000 cells. The concentration-effect curves using AUC medium and AUC cells as dose metric clustered less closely together than the curves using Cmax in medium as dose metric. When using AUC in medium as a dose metric, 24 h single exposure gave the lowest EC50 (58.0 nmol·h) and 7dW the highest EC50 (410.2 nmol·h) (Table 1). When using AUC in cells as dose metric, 24 h single exposure resulted in the lowest EC50 (73.9 nmol·h) and 7dW-exposures gave the highest EC50 (604.1 nmol·h) (Table 1).

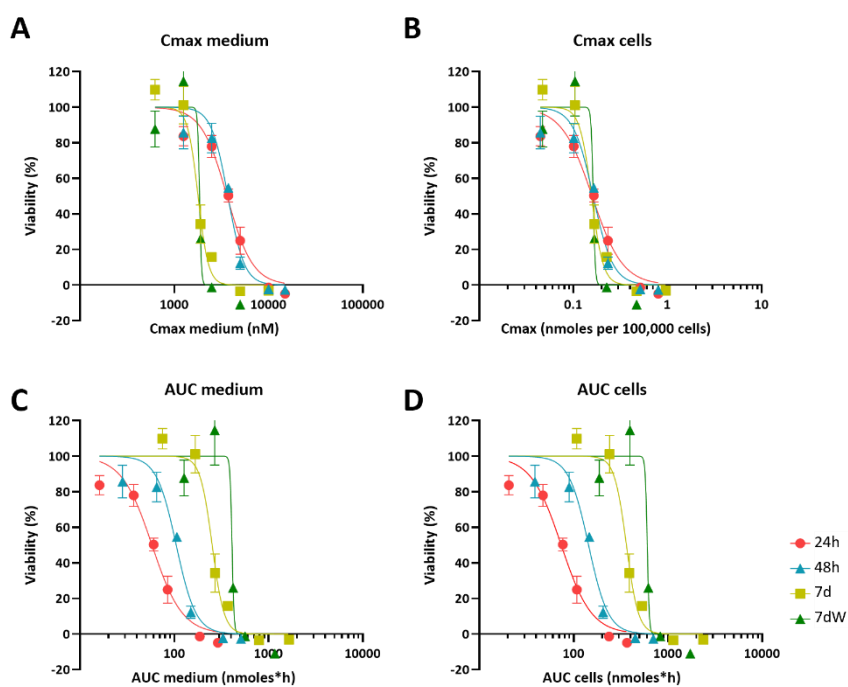


**Figure 4. Dose metrics representing concentration-dependent cytotoxicity curves for AMI.** The dose-responses after 1 single (24 h, 48 h) or repeated (7d and 7dW) exposure to AMI (0 - 15  $\mu$ M) are illustrated for the different calculated dose metrics: (A) Cmax in medium, (B) Cmax in cells, (C) AUC of the amount in medium and (D) AUC of the amount in cells. All results are expressed as % of control cultures (DMSO). Each point is the mean  $\pm$  SD of 3-9 samples obtained in 3 independent experiments.

**Table 1. EC50s for the different dose metrics calculated through [Inhibitor] vs. normalized response -- Variable slope Least squares fit regression using GraphPad Prism®.**

	<b>Cmax medium (<math>\mu</math>M)</b>	<b>Cmax cells (nmoles/100,000 cells)</b>	<b>AUC medium (nmoles·h)</b>	<b>AUC cells (nmoles·h)</b>
	<b>EC50</b>	<b>EC50</b>	<b>EC50</b>	<b>EC50</b>
<b>24h</b>	3.63	0.1583	58.02	73.87
<b>48h</b>	3.70	0.1624	104.9	144
<b>7d</b>	1.79	0.1559	252.4	363.1
<b>7dW</b>	1.8	0.1626	410.2	604.1

### **3.4. Amiodarone has a deleterious effect on neurons and astrocytes**

To assess neurotoxicity, BS were treated with various concentrations of AMI (1, 1.5 and 2  $\mu$ M) and were collected after an acute (48h; all concentrations tested were < IC10 for cytotoxicity) or a repeated (1 week; 1  $\mu$ M < IC10; 1.5  $\mu$ M < IC20; 2  $\mu$ M > IC50) exposure. mRNA levels of cell-specific markers were determined by real-time RT-PCR.

After 1 week of exposure, AMI induced a concentration-dependent significant decrease in the mRNA levels of the neuronal markers Tubulin Beta-3 chain (TBB3), MAP2 and SYP (Fig. 5A). Markers of neuronal subtypes showed that AMI also significantly decreased the expression of ACHE, GRIN1 and GABBR1, after 7 days of exposure. ACHE expression was already reduced after 48h of treatment, whereas the level of TH mRNA was not modified at any time-point. Results after the washout period (7dW) were very similar to those observed at the end of the 7d-treatment, with only a slightly stronger decrease observed after the highest concentration (2  $\mu$ M). Immunostaining (Fig. 5B) showed a decreased network of fibers stained for TBB3 after one week of exposure to AMI and after the washout period. Image quantification confirmed this decrease, although it was statistically significant only after the washout period (Fig. 5C).

AMI significantly decreased the mRNA levels of S100B and GFAP in a concentration-dependent way, already after 48 h of exposure (Fig. 6A), with a slightly stronger effect on GFAP. Results were very similar after the repeated exposure (7d) and the washout period (7dW). On the opposite, an increased immunostaining for S100B was observed after AMI repeated exposure (7d) (Fig. 6B and D). At that time point, astrocytic processes appeared thicker than in the control cultures (Fig. 6B, 7d), and quantification showed a significant increase (Fig. 6D). These changes in immunolabelling were not present anymore after the washout period (7dW), and a significant decrease was quantified. Ki67, a marker of proliferation, was slightly but significantly downregulated 48h after the first treatment, more strongly after 1 week, and a

slight recovery of the mRNA level was observed after the washout period (Fig. 6A). Finally, AMI did not produce any change in the expression of Oligodendrocyte transcription factor 2 (Olig2) and Myelin Basic Protein (MBP) gene (Fig. 7A), nor in the immunostaining for O4 protein (Fig. 7B and C).

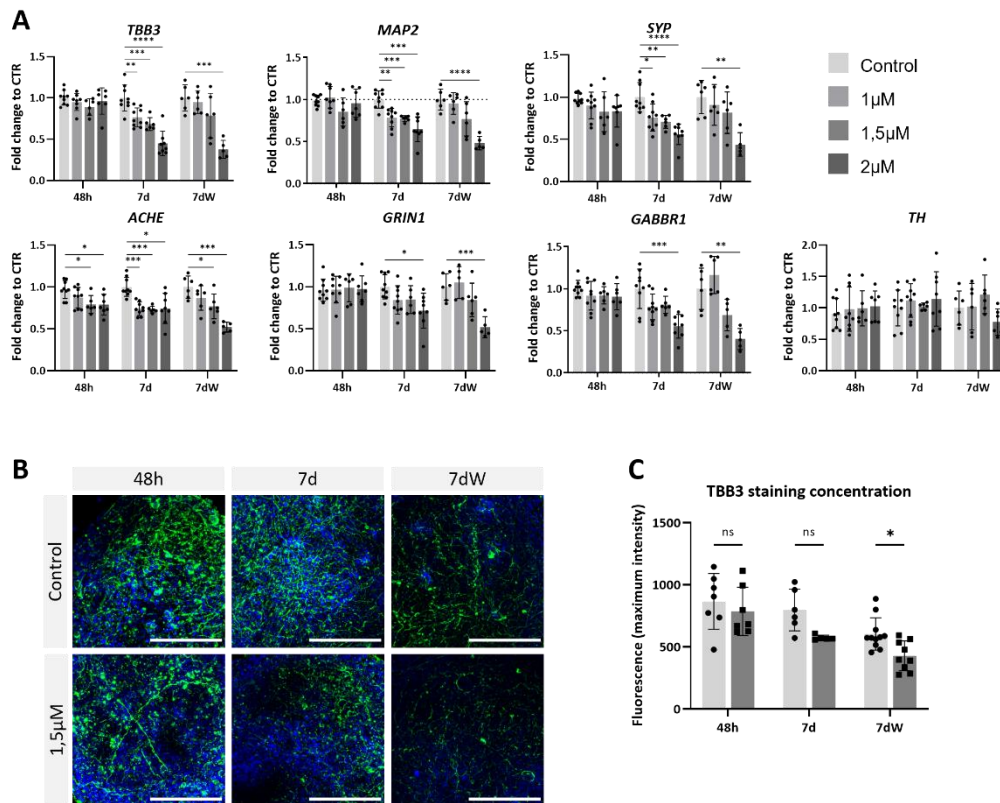


**Figure 5. Neurons are affected by amiodarone** (A) Relative gene expression of neuronal- (TBB3 and MAP2), pre-synaptic- (SYP) markers, cholinergic- (ACHE), glutamatergic- (GRIN1), GABAergic- (GABBR1), and dopaminergic- (TH) markers. Data are expressed as fold change to control. Each value is the mean ( $\pm$  SD) of = 3-9 samples coming from 3 independent experiments. (B) Immunostaining for TBB3 (green) in BS control and treated with 1.5  $\mu$ M AMI at 48h, 7d, and 7dW; nuclei are stained with Hoechst (blue). Scale bars indicate 50  $\mu$ m. (C) Quantification of maximum intensity of TBB3 immunostaining. Each value is the mean ( $\pm$  SD) of 3-5 spheres. \*  $p < 0.05$ , \*\*  $p < 0.01$ , \*\*\*  $p < 0.001$ , \*\*\*\*  $p < 0.0001$ .

These results suggest that brain cells are susceptible to AMI, with astrocytes affected earlier and in a stronger way than neurons.

### 3.5. TempO-Seq analysis highlights lipid metabolism as an important target of AMI action

To understand how the cellular program is altered in response to AMI exposure, we collected and analyzed exposed and control samples with the new, cost-effective technique, TempO-Seq for the expression of a set of genes (3257) selected for their representation in pathways involved in toxicity.

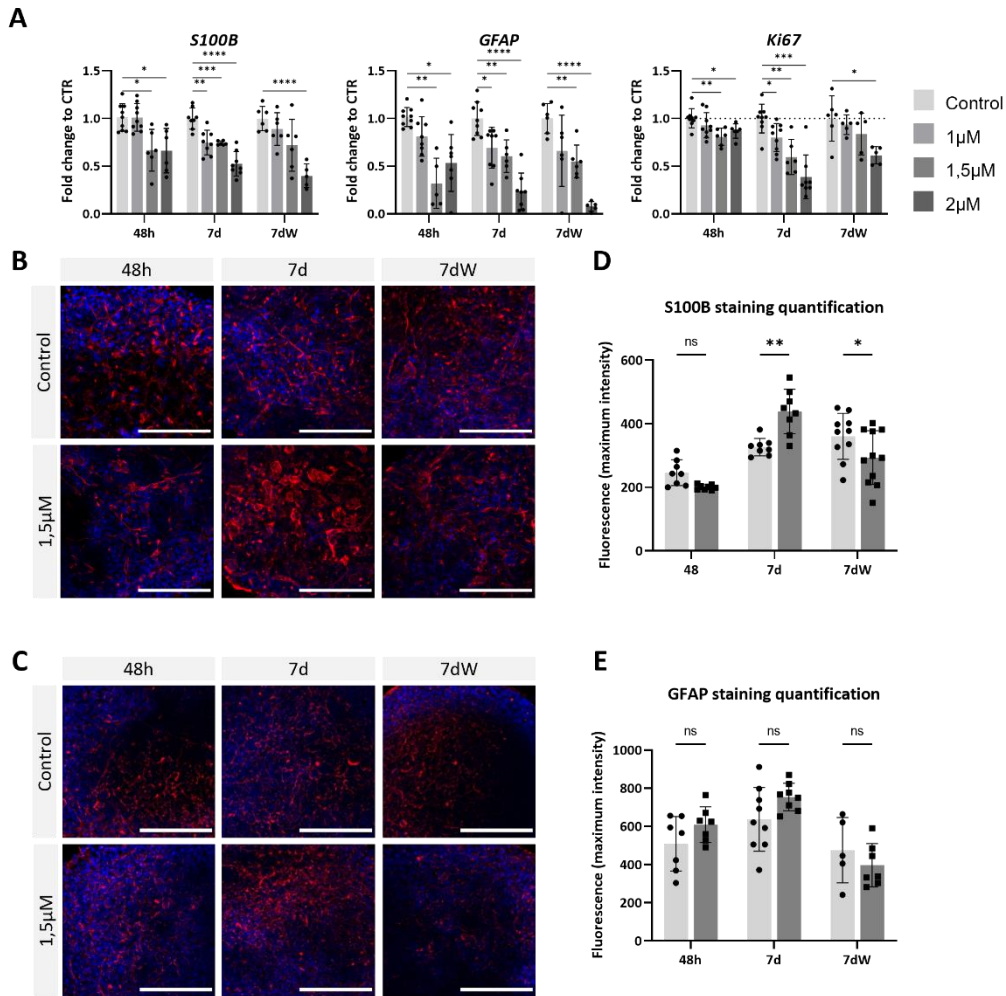


**Figure 6. Astrocytes are strongly affected by amiodarone** (A) Relative gene expression of astrocytic markers (GFAP, S100B) and PSM8. Data are expressed as fold change to control. Each value is the mean ( $\pm$  SD) of 3 to 9 samples coming from 3 independent experiments. (B) Immunostaining for S100B (red) and (C) GFAP (red) in BS control and treated with AMI; nuclei are stained with Hoechst (blue). Scale bars indicate 50  $\mu$ m. (D) Quantification of maximum intensity of S100B immunostaining and (E) GFAP. Each value is the mean ( $\pm$  SD) of 3 to 5 spheres. \*  $p < 0.05$ , \*\*  $p < 0.01$ , \*\*\*  $p < 0.001$ , \*\*\*\*  $p < 0.0001$ .

The unsupervised PCA of the samples exposed to AMI (1, 2 and 3  $\mu$ M) for 48h or one week of repeated exposure showed that samples cluster along the x axis (PC1) in accordance with the concentration of AMI they were exposed to (Fig. 8A). After differential expression analysis (usingDSeq2), we detected 24 differentially expressed genes (DEGs) after 48h of acute exposure to AMI 1  $\mu$ M, 46 DEGs for 2  $\mu$ M and 116 for 3  $\mu$ M (Fig. 8B). Repeated exposure showed 1 and 20 DEGs after exposure to AMI 1  $\mu$ M and 2  $\mu$ M, respectively, that is less than after acute exposure. The highest concentration (3  $\mu$ M) was not used for repeated exposure, due to its very high cytotoxicity.

Gene set overrepresentation analysis was performed based on hallmark gene sets from MsigDB at Broad Institute using the enricher function from the clusterProfiler R package. Biological processes (BPs) were distributed in 3 categories: lipid metabolism, neural function,

differentiation and development (Table 2). BPs associated to neural function were only detected after 48h exposure to 3  $\mu$ M, whereas BPs associated to differentiation and development were also detected after 2  $\mu$ M (48h and 168h), and BPs associated to lipid metabolism were found in all conditions, except after the repeated exposure (168h) to 1  $\mu$ M (Table 2).

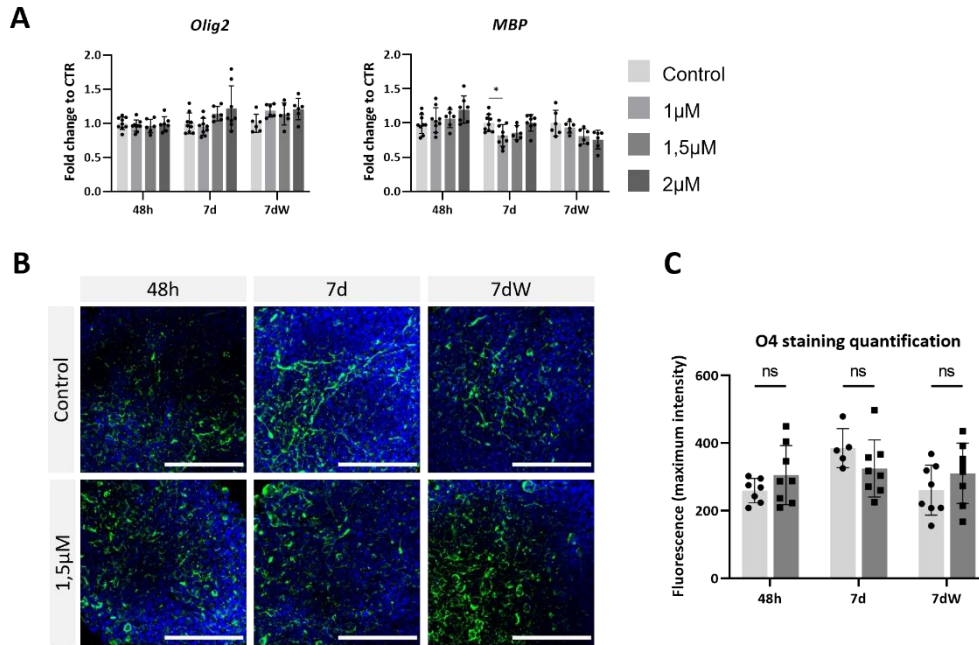


**Figure 7. Amiodarone does not seem to affect oligodendrocytes** (A) Relative gene expression of oligodendrocyte- (*Olig2*) and myelin- (*MBP*) markers. Data are expressed as fold change to control. Each value is the mean ( $\pm$  SD) of 3 to 9 samples coming from 3 independent experiments. (B) Immunostaining for O4 in BS control and treated with AMI, at 48h, 7d, and 7dW; nuclei are stained with Hoechst (blue). Scale bars indicate 50 $\mu$ m. (C) Quantification of maximum intensity of O4 immunostaining images. Each value is the mean ( $\pm$  SD) of 3 to 5 spheres. \*  $p < 0.05$ .

**Table 2. List of the number of Biological Processes (BP) from Gene Ontology ( $p_{adj} < 0.05$ ) potentially affected by AMI, for all exposure.**

$\mu$ M	h	Total BP	Neural	Diff/Dev	Lipids
1	48	31	-	-	8
	168	13	-	-	-
2	48	57	-	18	12
	168	33	-	1	13
3	48	292	38	91	15

### 3.6. Amiodarone disrupts lipid metabolism

A total of 20 different BPs associated to lipid metabolism were affected by AMI (Table 3). A rapid and transient deregulation of the genes associated to these BPs was observed. Indeed,

more DEGs are detected at 48h than after 1 week of repeated exposure (Fig. 8B). Some of these BPs present a concentration-dependent increase of the number of DEGs after 48h of exposure. Among them, “regulation of lipid metabolic process”, “regulation of steroid metabolic process”, “steroid metabolic process”, and “sterol metabolic process”. These two last BPs were associated with the highest number of DEGs after 168 h. At that time-point, no DEGs were observed at 1  $\mu$ M.

A heatmap shows the list of DEGs associated with lipid metabolism BPs extracted from the different conditions (Fig. 8C). The expression of 2 genes is modified only at 48h, carboxyl ester lipase (CEL) is strongly up-regulated (LFC > 4), whereas nuclear receptor subfamily 2 group F member 1 (NR2F1) is downregulated (LFC < -0.4). The differential expression of some genes was clearly more affected after 1 week of repeated exposure than after 48h, such as DNA damage inducible transcript 3 (DDIT3), methylsterol monooxygenase 1 (MSMO1), transmembrane protein 97 (TMEM97), CCAAT enhancer binding protein alpha (CEBPA), thyroid hormone receptor beta (THRB), isopentenyl-diphosphate delta isomerase 1 (IDI1), lanosterol synthase (LSS) and Niemann-Pick type C disease intracellular cholesterol transporter 1 (NPC1).

The quantification by real-time RT-PCR showed a concentration-dependent increase in fatty acid synthase (FASN) expression after 48h and 1 week (Fig. 8D), whereas after the washout period FASN expression went back to control levels, except for a significant decrease at 2  $\mu$ M, a concentration above IC50 for cytotoxicity (Fig. 2B). The mRNA levels of peroxisome proliferator activated receptor gamma coactivator 1 alpha (PPARGC1) and glycerophosphodiester phosphodiesterase domain containing 3 (GDPD3) were significantly reduced at 2  $\mu$ M after the washout period, whereas solute carrier family 27 member 4 (SLC27A4) was also decreased at the end of the 7-days repeated exposure. Lipoprotein lipase (LPL) expression was not statistically significant changed after AMI exposure. Finally, the expression of perilipin (PLINs) 2-5 was more strongly and significantly diminished after one week of exposure and after the wash-out period, whereas PLIN1 showed only slight changes after the washout period.

All together these data indicate that profound changes in different lipid metabolism-related processes occur in BS exposed to AMI.

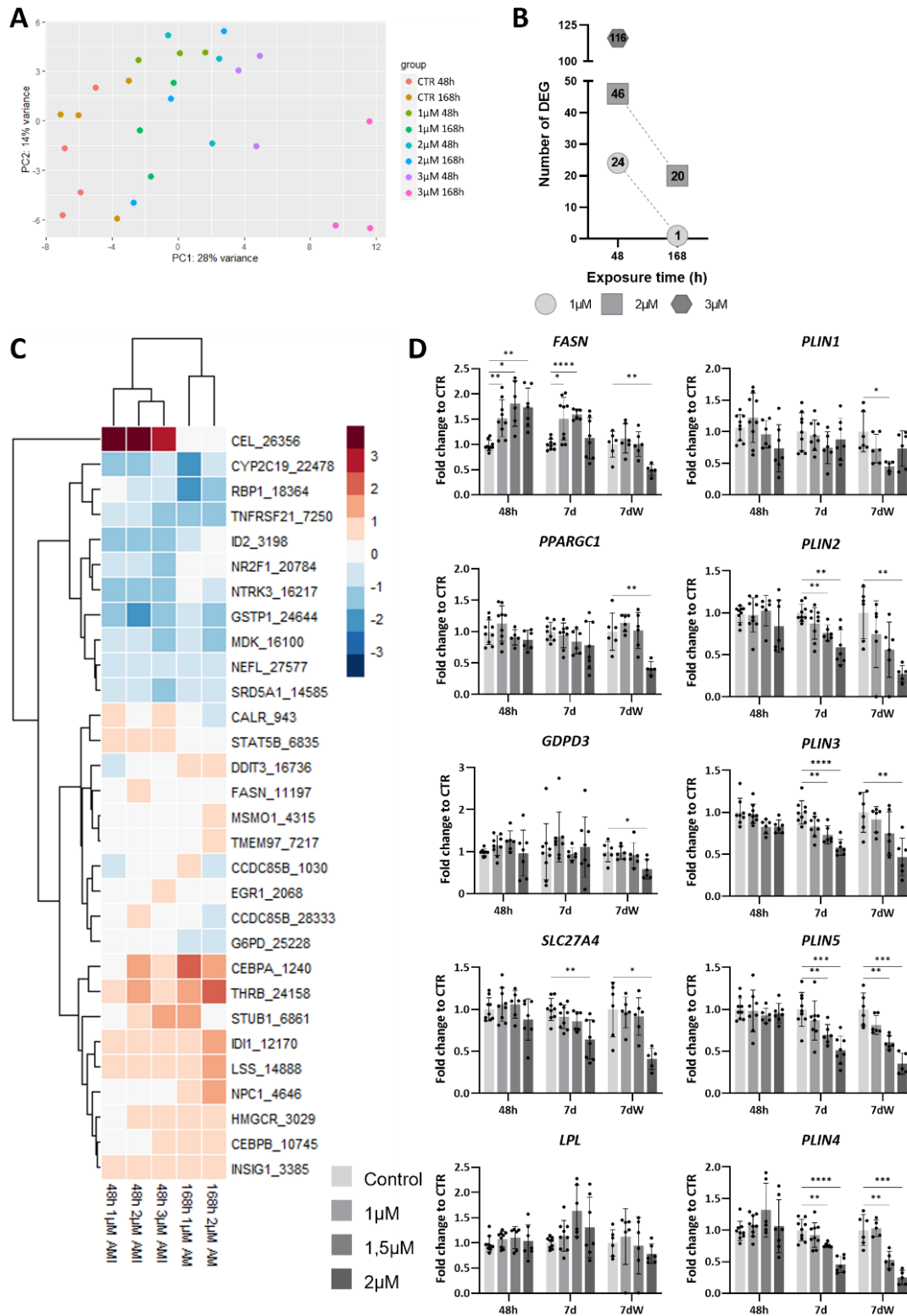


**Figure 8. TempO-Seq analysis of BS exposed to AMI.** (A) PCA of all control and AMI treated samples. Each dot represents a sample and each colour represents a group (control or treated). (B) Number of DEGs per condition. (C) Heatmap of the log<sub>2</sub> fold changes compared to control of genes linked to lipid biological processes, in all treated groups. Red: upregulation, blue: downregulation; (D) Relative gene expression of markers of fatty acid transport (SLC27A4), mitochondrial biogenesis (PPARGC1), de novo lipogenesis (FASN), degradation of phospholipids (GDPD3), lipid hydrolysis (LPL) and formation of lipid droplets (PLIN1-5). Data are reported as fold change to control and each value is the mean (± SD) of 3-9 samples coming from 3 independent experiments. \* p < 0.05, \*\* p < 0.01, \*\*\* p < 0.001, \*\*\*\* p < 0.0001.

**Table 3. List of genes involved in the Biological Processes from Gene Ontology (p.adj < 0.05) potentially affected by AMI, for all exposures.**

Biological Processes	Number of DEGs per exposure time and concentration (µM)					Genes
	48h			7d		
	1	2	3	1	2	
C21 steroid hormone metabolic process			3			<i>STAT5B/EGR1/SRD5A1</i>
Cellular response to steroid hormone stimulus			6			<i>THRB/NPC1/CALR/SRD5A1/NR2F1/GSTP1</i>
Fat cell differentiation		4				<i>INSIG1/CEBPA/CCDC85B/ID2</i>
sterol biosynthetic process				4		<i>IDI1/HMGCR/MSMO1/INSIG1</i>
Lipid homeostasis				4		<i>NPC1/INSIG1/TMEM97/RBP1</i>
Negative regulation of fat cell differentiation				2		<i>INSIG1/DDIT3</i>
Regulation of cholesterol biosynthetic process	2	4	4		2	<i>IDI1/FASN/LSS/HMGCR</i>
Regulation of cholesterol metabolic process		4	4		2	<i>IDI1/FASN/LSS/HMGCR</i>
Regulation of fat cell differentiation		4	5			<i>INSIG1/CEBPA/CCDC85B/ID2/CEBPB/DDIT3</i>
Regulation of lipid biosynthetic process	3	5	6		3	<i>IDI1/INSIG1/FASN/LSS/HMGCR/EGR1</i>
Regulation of lipid metabolic process		6	10		4	<i>INSIG1/IDI1/STAT5B/HMGCR/LSS/STUB1/EGR1/FASN/TNFRSF21/ID2</i>
Regulation of steroid biosynthetic process	3	5	6		3	<i>INSIG1/IDI1/HMGCR/LSS/EGR1/FASN</i>
Regulation of steroid metabolic process	3	5	8		3	<i>INSIG1/IDI1/STAT5B/HMGCR/LSS/STUB1/EGR1/FASN</i>
Response to corticosteroid			5			<i>SRD5A1/NEFL/MDK/GSTP1/NTRK3</i>
Response to steroid hormone			9			<i>THRB/NPC1/CALR/SRD5A1/NR2F1/NEFL/MDK/GSTP1/NTRK3</i>
Steroid biosynthetic process	3	6	9		4	<i>INSIG1/IDI1/HMGCR/LSS/EGR1/FASN/MSMO1/G6PD/SRD5A1</i>
Steroid metabolic process	4	8	14		5	<i>INSIG1/IDI1/CEL/STAT5B/HMGCR/CEBPA/LSS/STUB1/NPC1/EGR1/FASN/MSMO1/G6PD/SRD5A1/CYP2C19</i>
Sterol biosynthetic process	3	6	7			<i>INSIG1/IDI1/HMGCR/LSS/FASN/MSMO1/G6PD</i>
Sterol homeostasis				3		<i>NPC1/INSIG1/TMEM97</i>
Sterol metabolic process	3	8	10		5	<i>INSIG1/IDI1/CEL/HMGCR/CEBPA/LSS/NPC1/FASN/MSMO1/G6PD</i>

#### 4. Discussion

The characterization of BrainSpheres (BS) generated from the iPSC line SBAD3 showing the decrease of stem cells properties paralleled by the differentiation and maturation of the various brain cell types, is very similar to what was observed in the original publication (Pamies et al., 2017), although here we used an alternative way to derive the NPCs (Nunes and Zurich, 2020), skipping the formation of rosettes (Wen et al., 2014). After two weeks in cultures, neuron- and oligodendrocyte-markers were already clearly present, whereas at that time the markers for astrocytes were very low. Then, the evolution in time of the various brain cell populations differed. Indeed, we observed a strong development of neuronal and astrocytic processes, as well as the appearance of synaptophysin, suggesting the formation of synapses from 6 weeks onwards, whereas the number of oligodendrocytes seem to reduce between the fourth and the sixth week of culture. The latter result is in line with the decrease in the number of oligodendrocytes observed during brain development (for review, Casaccia-Bonnel, 2000).

Nominal median effect concentrations after seven days of exposure to AMI and after the washout period were similar, indicating that no further progression of cell death or proliferation occurred after removal of AMI. The absence of proliferation was confirmed by the observation of a decreased gene expression of the proliferation marker Ki67 after the washout period. The nominal effect concentration also did not change between 24 hour and 48 hours single exposure. These results point to AMI accumulation in cells after repeat dosing driving the difference in effect concentrations after single and repeat dosing, rather than longer exposures to AMI. This explains why concentration-effect relationships based on the C<sub>max</sub> in cells, a threshold concentration rather than cumulative concentration (AUC), cluster. The EC<sub>50</sub> based on C<sub>max</sub> in cells suggests that amiodarone is a baseline toxicant in this assay and that the mechanism of toxicity is reversible (Escher et al., 2011). Prediction of the dose range for adverse neurological effects of AMI in humans was previously performed by quantitative in vitro-in vivo extrapolation (QIVIVE) (Algharably et al., 2021), from results of choline acetyltransferase inhibition, used as a marker of neurotoxicity, obtained with a 3D rat brain cell model (Pomponio et al., 2015b). To this end, the authors used the AUC in cells measured on the last day of 14 days of repeated exposure to 1.25 µM of AMI. However, in light of the results obtained in the present study using 3D human BS, C<sub>max</sub> in cells appeared to be the dose metric most independent to the exposure scenario for AMI, when considering the cytotoxicity. For this reason, the C<sub>max</sub> in cells, as opposed to the AUC in cells, may be a more robust dose metric to use in concentration-response modelling and as a point of departure for quantitative in vitro to in vivo extrapolation (QIVIVE), when using the human BS model.

In the present study, two brain cell populations were clearly affected by AMI. The network of neuronal processes was reduced after 1 week of exposure as seen not only at the gene expression level for TBB3 and MAP2, but also at the protein level for TBB3. The absence of AMI during one week did not allow these neuronal processes to recover, suggesting a loss of neurons. Among them, cholinergic, glutamatergic and GABAergic neurons seemed to be more sensitive to AMI than dopaminergic ones. These deleterious effects on neurons are in line with studies showing modifications of the release of neurotransmitters after injection of AMI in the rat medulla oblongata (Turovaya et al., 2005) and reduction of the depolarization-evoked glutamate release from rat synaptosomes (Chang et al., 2017). On the other hand, astrocytes seemed to be more affected than neurons, and also at an earlier time-point. Gene expression for S100B and GFAP were strongly and rapidly reduced after exposure to AMI and mRNA levels did not recover after one week of washout, suggesting a loss of astrocytes. However, a modification of S100B immunolabelling was observed after one week of repeated exposure, suggesting a reactivity of the remaining astrocytes, that was transient, since the modification in S100B labelling disappeared after the washout period. These results differ from a previous report on the effects of AMI on rat mixed brain cell cultures showing a slightly higher sensitivity of neurons (Pomponio et al., 2015b). Also, in rat brain cell cultures, the astrocytes increased their level of GFAP mRNA after 10 days of exposure to AMI, suggesting astrocyte reaction, whereas in the human model used in this study, GFAP was strongly diminished, already after 48 hours. In human BS, the modifications observed in S100B immunostaining also suggest astrocyte reaction of the remaining astrocytes, however, the strong decrease of mRNA and protein content, together with a decrease of the proliferation marker Ki67, suggest a loss of astrocytes. It has to be noted that human BS were more sensitive to AMI, with 70% cell death observed after 7 days of exposure to 2  $\mu$ M, than the rat 3D model that showed 25% of cell death after 14 days of exposure to 2.5  $\mu$ M (Pomponio et al., 2015b). The differences observed in these two studies may be explained by the species, and/or by differences in the proportion of the diverse cell types, the rat model comprising an estimated higher proportion of glial cells (50 %) vs 30 % in BS (Zurich et al., 1998; Pamies et al., 2017). Alternatively, the higher sensitivity of human astrocytes vs rat ones, may also be due to the state of maturation, human BS being probably less mature than rat 3D cultures, given the differences in the duration of the developmental processes between the two species. Finally, due to the intense relationship between the various glial cell types, we may hypothesize that the absence of microglial cells in the human BS render the astrocytes more vulnerable to AMI.

To quantitatively assess differences in sensitivity to AMI between the BS herein used and other cell models, variations in the in vitro setup has to be accounted for (Proenca et al., 2021). AMI, a highly lipophilic chemical, will differentially bind to various cell culture containers, causing concentration-time profiles at the cellular targets to vary despite similar nominal concentrations added. As already mentioned here, AMI concentration-effect relationships and mode of action were already examined before in single and repeated-dose assays in the EU project Predict-IV. One study focused on 2 models of human hepatic cells, the sandwich cultures of primary human hepatocytes and monolayers of HepaRG cells (Pomponio et al., 2015a). The other study focused on two models of brain cells, 2D mouse brain cultures and 3D rat brain cultures (Pomponio et al., 2015b). Both studies also determined the distribution kinetics. In these studies, the mass of AMI in the systems decreased after a single exposure, similarly to the depletion observed in the present study in human BS after 24 and especially after 48 hours. In the Predict-IV study, the depletion of AMI from both 2D mouse and 3D rat brain in vitro systems was partly attributed to the biotransformation of AMI into desethylamiodarone (DEA). This is not possible in the present study, since no DEA was found and the same degradation rate constants were estimated in systems with and without BS. The ratio of exposed plastic surface area to exposure medium in the mouse 2D model and liver Predict-IV studies and this study are the same, yet the amount of AMI found in plastic after 24h exposure was higher in this study. This suggests that higher nominal concentrations, higher cell densities, as well as the presence of extracellular matrix and 2% serum in the exposure medium in the Predict-IV studies limited the extent to which AMI bound to plastic.

AMI differentially accumulated in cells (as a fraction of total AMI added to the system) of the various culture systems. Whereas cellular accumulation in BS reached 32 - 44 % of the total added AMI dose after 24 hours, 2D mouse brain cells accumulated 60 % and the 3D rat aggregating brain cell model accumulated the totality (100 %). Since AMI has not yet been described as substrate of any specific membrane transporter, differences in cell accumulation may be attributed to variations in lipid content and lysosome numbers between the cell systems. These results suggest that small variations in cell density, ratio of exposed surface plastic area to exposure medium, and frequency of exposure medium replacement may significantly affect the maximum concentration of AMI at the cellular target. The compartmental model developed and parametrized in this study allowed us to predict the change in cell-associated concentrations in BS in time for different exposures scenarios. Ideally the model can be used to simulate the C<sub>max</sub> in cells for different assays set ups (e.g. volume of medium and surface of plastic exposed) and different number of cells, allowing a more direct comparison. The EC<sub>50</sub> based on the C<sub>max</sub>

in cells is lower in this study with BS than in the *in vitro* toxicity assay with rodent cells in the study by Pomponio et al. (2015b). This suggests that human BS are intrinsically slightly more sensitive to AMI exposure. However, this species difference needs to be confirmed with BS prepared from other human donors.

Numerous biological processes related to lipid and cholesterol metabolism were found in this study after gene set overrepresentation analysis of TempO-Seq data. In particular, the upregulation of the genes *MSMO1*, *IDI1*, *LSS* and *HMGCR* suggested enhanced synthesis of cholesterol, and the upregulation of *FASN* an increased synthesis of fatty acids, that may in turn induce phospholipidosis (Sawada et al., 2005; Antherieu et al., 2011). This would be in agreement with the reported induction of phospholipidosis by AMI, in various cell types, such as macrophages, alveolar epithelial cells and hepatocytes (Lewis et al., 1990; Nonoyama and Fukuda, 2008; Ohlinger et al., 2020; Kapatou et al., 2010). However, this upregulation of lipogenic genes was not accompanied by the upregulation of *PLINs*, that are essential for lipid droplets building and therefore lipid storage. Therefore, these results suggest that the newly produced lipids could not be stored in droplets, but in another cellular structure or immediately consumed. Astrocytes produce lipids more efficiently than neurons, and it has recently been shown that astrocyte lipid metabolism is critical for the development and function of synapses in mice (van Deijk et al., 2017). The highest toxicity observed in astrocytes may derive from their higher ability to oxidize fatty acids, as compared to neurons, that may generate harmful products, for review (Schonfeld and Reiser, 2021). Contrarily to the other cell types present in the BrainSpheres, oligodendrocytes did not seem to be affected by AMI, although this drug has been shown to induce demyelination in the peripheral nervous system (Niimi et al., 2016; Niimi et al., 2019; Pulipaka et al., 2002). Further investigations are needed to determine the exact status of the oligodendrocytes and of the myelin sheath after exposure of BS to AMI.

In conclusion, our study provides for the first time *in vitro* the evidence that AMI induces lipid metabolism perturbation in human brain cells, that seems associated to a strong deleterious effect on astrocytes. When correcting for differences in *in vitro* distribution kinetics, our study indicates that human brain cells are intrinsically more sensitive to AMI exposure than rodent brain cultures. This study illustrates the benefit of assessing the accumulation of test chemicals in cells of *in vitro* toxicity tests to explain variation in effect concentrations between *in vitro* assays differing in setup. We believe that *in vitro* determination of neurotoxicity using human-based complex models, such as the human iPSC-derived BrainSpheres, coupled to *in vitro* distribution kinetics, as a key step for IVIVE, will contribute to the refinement of chemical risk assessment for human health.

**Conflict of interest statement:** The authors declare no competing interests.

**Data Availability Statement:** The data that support the findings of this study are available from the corresponding author upon request.

**Authors' contributions:** Conceptualization, C.N and M.-G.Z.; Formal analysis, C.N. and S.P.; Investigation, C.N.; Data curation, C.N and G.A.; Writing – original draft, C.N.; Writing – review and editing, C.N., S.P., G.A., D.P., A.T., N.I.K., and M.-G.Z.; Visualization, C.N and S.P.; Project administration, N.I.K. and M.-G.Z.; Funding acquisition, N.I.K. and M.-G.Z.

**Acknowledgements:** The work was funded by the European Union's Horizon 2020 Research and Innovation Programme MarieSkłodowska-Curie Action-Innovative Training Network project in3, under grant agreement no. 721975 (fellowships to Carolina Nunes and Susana Proença).

## 5. References

- Algharably, E. A. E., Di Consiglio, E., Testai, E. et al. (2021). Prediction of the dose range for adverse neurological effects of amiodarone in patients from an in vitro toxicity test by in vitro-in vivo extrapolation. *Arch Toxicol* 95, 1433-1442. doi:10.1007/s00204-021-02989-2
- Antherieu, S., Rogue, A., Fromenty, B. et al. (2011). Induction of vesicular steatosis by amiodarone and tetracycline is associated with up-regulation of lipogenic genes in heparg cells. *Hepatology* 53, 1895-1905. doi:10.1002/hep.24290
- Bal-Price, A. K., Hogberg, H. T., Buzanska, L. et al. (2010). Relevance of in vitro neurotoxicity testing for regulatory requirements: Challenges to be considered. *Neurotoxicol Teratol* 32, 36-41. doi:10.1016/j.ntt.2008.12.003
- Casaccia-Bonnel, P. (2000). Cell death in the oligodendrocyte lineage: A molecular perspective of life/death decisions in development and disease. *Glia* 29, 124-135. doi:10.1002/(sici)1098-1136(20000115)29:2<124::aid-glia5>3.0.co;2-o
- Chang, C. Y., Hung, C. F., Huang, S. K. et al. (2017). Amiodarone reduces depolarization-evoked glutamate release from hippocampal synaptosomes. *J Pharmacol Sci* 133, 168-175. doi:10.1016/j.jphs.2017.02.014
- Chesnut, M., Paschoud, H., Repond, C. et al. (2021). Human ipsc-derived model to study myelin disruption. *Int J Mol Sci* 22, doi:10.3390/ijms22179473
- Druwe, I., Freudenrich, T. M., Wallace, K. et al. (2015). Sensitivity of neuroprogenitor cells to chemical-induced apoptosis using a multiplexed assay suitable for high-throughput screening. *Toxicology* 333, 14-24. doi:10.1016/j.tox.2015.03.011
- Escher, B. I., Ashauer, R., Dyer, S. et al. (2011). Crucial role of mechanisms and modes of toxic action for understanding tissue residue toxicity and internal effect concentrations of organic chemicals. *Integr Environ Assess Manag* 7, 28-49. doi:10.1002/ieam.100
- Eskes, C., Honegger, P., Juillerat-Jeanneret, L. et al. (2002). Microglial reaction induced by noncytotoxic methylmercury treatment leads to neuroprotection via interactions with astrocytes and il-6 release. *Glia* 37, 43-52. doi:10.1002/glia.10019
- Eskes, C., Juillerat-Jeanneret, L., Leuba, G. et al. (2003). Involvement of microglia-neuron interactions in the tumor necrosis factor- $\alpha$  release, microglial activation, and neurodegeneration induced by trimethyltin. *J Neurosci Res* 71, 583-590. doi:10.1002/jnr.10508
- Groothuis, F. A., Heringa, M. B., Nicol, B. et al. (2015). Dose metric considerations in in vitro assays to improve quantitative in vitro-in vivo dose extrapolations. *Toxicology* 332, 30-40. doi:10.1016/j.tox.2013.08.012
- Groothuis, F. A., Timmer, N., Opsahl, E. et al. (2019). Influence of in vitro assay setup on the

- apparent cytotoxic potency of benzalkonium chlorides. *Chem Res Toxicol* 32, 1103-1114. doi:10.1021/acs.chemrestox.8b00412
- Gulden, M., Morchel, S. and Seibert, H. (2001). Factors influencing nominal effective concentrations of chemical compounds in vitro: Cell concentration. *Toxicol In Vitro* 15, 233-243. doi:10.1016/s0887-2333(01)00008-x
- Hamilton, D., Sr., Nandkeolyar, S., Lan, H. et al. (2020). Amiodarone: A comprehensive guide for clinicians. *Am J Cardiovasc Drugs* 20, 549-558. doi:10.1007/s40256-020-00401-5
- Heringa, M. B., Schreurs, R. H., Busser, F. et al. (2004). Toward more useful in vitro toxicity data with measured free concentrations. *Environ Sci Technol* 38, 6263-6270. doi:10.1021/es049285w
- Hindle, J. V., Ibrahim, A. and Ramaraj, R. (2008). Ataxia caused by amiodarone in older people. *Age Ageing* 37, 347-348. doi:10.1093/ageing/afn063
- Honda, G. S., Pearce, R. G., Pham, L. L. et al. (2019). Using the concordance of in vitro and in vivo data to evaluate extrapolation assumptions. *PLoS One* 14, e0217564. doi:10.1371/journal.pone.0217564
- Ishida, S., Sugino, M., Hosokawa, T. et al. (2010). Amiodarone-induced liver cirrhosis and parkinsonism: A case report. *Clin Neuropathol* 29, 84-88. doi:10.5414/npp29084
- Jafari-Fesharaki, M. and Scheinman, M. M. (1998). Adverse effects of amiodarone. *Pacing Clin Electrophysiol* 21, 108-120. doi:10.1111/j.1540-8159.1998.tb01068.x
- Jager, T., Albert, C., Preuss, T. G. et al. (2011). General unified threshold model of survival--a toxicokinetic-toxicodynamic framework for ecotoxicology. *Environ Sci Technol* 45, 2529-2540. doi:10.1021/es103092a
- Kapatou, E., Skyrilas, A., Agelaki, M. G. et al. (2010). Amiodarone attenuates apoptosis, but induces phospholipidosis in rat alveolar epithelial cells. *J Physiol Pharmacol* 61, 671-677.
- Kramer, N. I., Di Consiglio, E., Blaauboer, B. J. et al. (2015). Biokinetics in repeated-dosing in vitro drug toxicity studies. *Toxicol In Vitro* 30, 217-224. doi:10.1016/j.tiv.2015.09.005
- Lewis, J. H., Mullick, F., Ishak, K. G. et al. (1990). Histopathologic analysis of suspected amiodarone hepatotoxicity. *Hum Pathol* 21, 59-67. doi:10.1016/0046-8177(90)90076-h
- Li, H. and Durbin, R. (2009). Fast and accurate short read alignment with burrows-wheeler transform. *Bioinformatics* 25, 1754-1760. doi:10.1093/bioinformatics/btp324
- Liberzon, A., Subramanian, A., Pinchback, R. et al. (2011). Molecular signatures database (msigdb) 3.0. *Bioinformatics* 27, 1739-1740. doi:10.1093/bioinformatics/btr260
- Limonciel, A., Ates, G., Carta, G. et al. (2018). Comparison of base-line and chemical-induced transcriptomic responses in heparg and rptec/tert1 cells using tempo-seq. *Arch Toxicol* 92, 2517-2531. doi:10.1007/s00204-018-2256-2
- Livak, K. J. and Schmittgen, T. D. (2001). Analysis of relative gene expression data using real-time quantitative pcr and the 2(-delta delta c(t)) method. *Methods* 25, 402-408. doi:10.1006/meth.2001.1262
- Love, M. I., Huber, W. and Anders, S. (2014). Moderated estimation of fold change and dispersion for rna-seq data with deseq2. *Genome Biol* 15, 550. doi:10.1186/s13059-014-0550-8
- Mahony, C., Ashton, R. S., Birk, B. et al. (2020). New ideas for non-animal approaches to predict repeated-dose systemic toxicity: Report from an epaa blue sky workshop. *Regul Toxicol Pharmacol* 114, 104668. doi:10.1016/j.yrtph.2020.104668
- Marcus, F. I., Fontaine, G. H., Frank, R. et al. (1981). Clinical pharmacology and therapeutic applications of the antiarrhythmic agent amiodarone. *Am Heart J* 101, 480-493. doi:10.1016/0002-8703(81)90140-x
- Mav, D., Shah, R. R., Howard, B. E. et al. (2018). A hybrid gene selection approach to create the s1500+ targeted gene sets for use in high-throughput transcriptomics. *PLoS One* 13, e0191105. doi:10.1371/journal.pone.0191105

- Modafferi, S., Zhong, X., Kleensang, A. et al. (2021). Gene-environment interactions in developmental neurotoxicity: A case study of synergy between chlorpyrifos and chd8 knockout in human brainspheres. *Environ Health Perspect* 129, 77001. doi:10.1289/EHP8580
- Morrison, M., Klein, C., Clemann, N. et al. (2015). Stembancc: Governing access to material and data in a large stem cell research consortium. *Stem Cell Rev Rep* 11, 681-687. doi:10.1007/s12015-015-9599-3
- Niimi, N., Yako, H., Tsukamoto, M. et al. (2016). Involvement of oxidative stress and impaired lysosomal degradation in amiodarone-induced schwannopathy. *European Journal of Neuroscience* 44, 1723-1733. doi:https://doi.org/10.1111/ejn.13268
- Niimi, N., Takaku, S., Yako, H. et al. (2019). Drug-induced demyelinating neuropathies. In K. Sango, J. Yamauchi, T. Ogata and K. Susuki (eds.), *Myelin: Basic and clinical advances*. Singapore: Springer Singapore. https://doi.org/10.1007/978-981-32-9636-7\_23 doi:10.1007/978-981-32-9636-7\_23
- Nonoyama, T. and Fukuda, R. (2008). Drug-induced phospholipidosis -pathological aspects and its prediction. *J Toxicol Pathol* 21, 9-24. doi:10.1293/tox.21.9
- NRC (2007). National research council, toxicity testing in the 21st century: A vision and strategy. In (eds.), Washington, D.C.: National Academy Press.
- Nunes, C. and Zurich, M.-G. (2020). Neurotoxicology and disease modelling. In G. Rodrigues and B. A. J. Roelen (eds.), *Concepts and applications of stem cell biology: A guide for students*. Cham: Springer International Publishing. https://doi.org/10.1007/978-3-030-43939-2\_12 doi:10.1007/978-3-030-43939-2\_12
- Nunes, C., Singh, P., Mazidi, Z. et al. (2022). An in vitro strategy using multiple human induced pluripotent stem cell-derived models to assess the toxicity of chemicals: A case study on paraquat. *Toxicol In Vitro* 81, 105333. doi:10.1016/j.tiv.2022.105333
- Ohlinger, K., Absenger-Novak, M., Meindl, C. et al. (2020). Different sensitivity of macrophages to phospholipidosis induction by amphiphilic cationic drugs. *Int J Mol Sci* 21, doi:10.3390/ijms21218391
- Pamies, D., Barreras, P., Block, K. et al. (2017). A human brain microphysiological system derived from induced pluripotent stem cells to study neurological diseases and toxicity. *ALTEX* 34, 362-376. doi:10.14573/altex.1609122
- Pamies, D., Block, K., Lau, P. et al. (2018). Rotenone exerts developmental neurotoxicity in a human brain spheroid model. *Toxicol Appl Pharmacol* doi:10.1016/j.taap.2018.02.003
- Pamies, D., Leist, M., Coecke, S. et al. (2022). Guidance document on good cell and tissue culture practice 2.0 (gccp 2.0). *ALTEX* 39, 30-70. doi:10.14573/altex.2111011
- Pedro, L. and Rudewicz, P. J. (2020). Analysis of live single cells by confocal microscopy and high-resolution mass spectrometry to study drug uptake, metabolism, and drug-induced phospholipidosis. *Anal Chem* 92, 16005-16015. doi:10.1021/acs.analchem.0c03534
- Pei, Y., Peng, J., Behl, M. et al. (2016). Comparative neurotoxicity screening in human ipsc-derived neural stem cells, neurons and astrocytes. *Brain Res* 1638, 57-73. doi:10.1016/j.brainres.2015.07.048
- Pistollato, F., Canovas-Jorda, D., Zagoura, D. et al. (2017). Nrf2 pathway activation upon rotenone treatment in human ipsc-derived neural stem cells undergoing differentiation towards neurons and astrocytes. *Neurochem Int* 108, 457-471. doi:10.1016/j.neuint.2017.06.006
- Polster, P. and Broekhuysen, J. (1976). The adrenergic antagonism of amiodarone. *Biochem Pharmacol* 25, 131-134. doi:10.1016/0006-2952(76)90279-3
- Pomponio, G., Savary, C. C., Parmentier, C. et al. (2015a). In vitro kinetics of amiodarone and its major metabolite in two human liver cell models after acute and repeated treatments. *Toxicol In Vitro* 30, 36-51. doi:10.1016/j.tiv.2014.12.012

- Pomponio, G., Zurich, M. G., Schultz, L. et al. (2015b). Amiodarone biokinetics, the formation of its major oxidative metabolite and neurotoxicity after acute and repeated exposure of brain cell cultures. *Toxicol In Vitro* 30, 192-202. doi:10.1016/j.tiv.2015.01.012
- Proenca, S., Escher, B. I., Fischer, F. C. et al. (2021). Effective exposure of chemicals in in vitro cell systems: A review of chemical distribution models. *Toxicol In Vitro* 73, 105133. doi:10.1016/j.tiv.2021.105133
- Pulipaka, U., Lacomis, D. and Omalu, B. (2002). Amiodarone-induced neuromyopathy: Three cases and a review of the literature. *J Clin Neuromuscul Dis* 3, 97-105. doi:10.1097/00131402-200203000-00001
- Ryan, K. R., Sirenko, O., Parham, F. et al. (2016). Neurite outgrowth in human induced pluripotent stem cell-derived neurons as a high-throughput screen for developmental neurotoxicity or neurotoxicity. *Neurotoxicology* 53, 271-281. doi:10.1016/j.neuro.2016.02.003
- Sawada, H., Takami, K. and Asahi, S. (2005). A toxicogenomic approach to drug-induced phospholipidosis: Analysis of its induction mechanism and establishment of a novel in vitro screening system. *Toxicol Sci* 83, 282-292. doi:10.1093/toxsci/kfh264
- Schmittgen, T. D. and Livak, K. J. (2008). Analyzing real-time pcr data by the comparative c(t) method. *Nat Protoc* 3, 1101-1108. doi:10.1038/nprot.2008.73
- Schonfeld, P. and Reiser, G. (2021). How the brain fights fatty acids' toxicity. *Neurochem Int* 148, 105050. doi:10.1016/j.neuint.2021.105050
- Subramanian, A., Tamayo, P., Mootha, V. K. et al. (2005). Gene set enrichment analysis: A knowledge-based approach for interpreting genome-wide expression profiles. *Proceedings of the National Academy of Sciences* 102, 15545-15550. doi:10.1073/pnas.0506580102
- Takahashi, K., Tanabe, K., Ohnuki, M. et al. (2007). Induction of pluripotent stem cells from adult human fibroblasts by defined factors. *Cell* 131, 861-872. doi:10.1016/j.cell.2007.11.019
- Turovaya, A. Y., Galenko-Yaroshevskii, P. A., Kade, A. K. et al. (2005). Effects of verapamil and amiodarone on sympathoadrenal system and balance of excitatory and inhibitory amino acids in rat medulla oblongata. *Bulletin of Experimental Biology and Medicine* 139, 665-667. doi:10.1007/s10517-005-0372-5
- van Deijk, A. F., Camargo, N., Timmerman, J. et al. (2017). Astrocyte lipid metabolism is critical for synapse development and function in vivo. *Glia* 65, 670-682. doi:10.1002/glia.23120
- Varro, A., Virag, L. and Papp, J. G. (1996). Comparison of the chronic and acute effects of amiodarone on the calcium and potassium currents in rabbit isolated cardiac myocytes. *Br J Pharmacol* 117, 1181-1186. doi:10.1111/j.1476-5381.1996.tb16713.x
- Wen, Z., Nguyen, H. N., Guo, Z. et al. (2014). Synaptic dysregulation in a human ipsc cell model of mental disorders. *Nature* 515, 414-418. doi:10.1038/nature13716
- Wilmes, A., Limonciel, A., Aschauer, L. et al. (2013). Application of integrated transcriptomic, proteomic and metabolomic profiling for the delineation of mechanisms of drug induced cell stress. *J Proteomics* 79, 180-194. doi:10.1016/j.jprot.2012.11.022
- Yu, G., Wang, L. G., Han, Y. et al. (2012). Clusterprofiler: An r package for comparing biological themes among gene clusters. *OMICS* 16, 284-287. doi:10.1089/omi.2011.0118
- Zhong, X., Harris, G., Smirnova, L. et al. (2020). Antidepressant paroxetine exerts developmental neurotoxicity in an ipsc-derived 3d human brain model. *Front Cell Neurosci* 14, 25. doi:10.3389/fncel.2020.00025
- Zurich, M. G., Monnet-Tschudi, F., Berode, M. et al. (1998). Lead acetate toxicity in vitro: Dependence on the cell composition of the cultures. *Toxicol In Vitro* 12, 191-196. doi:10.1016/s0887-2333(97)00089-1

---

## Chapter 4: Ability of BrainSpheres to detect the neurotoxicity of various classes of chemicals

---

#### **4.1. Aim**

Within the in3 consortium, 10 chemicals, chosen based on their known specific toxicity for the various organs or cell types represented in this project, were used as reference chemicals. They were tested in the models used in the different labs for their impact on cell viability and cell stress responses, as well as to determine their distribution kinetics. The testing of the 10 chemicals should allow defining if the model present the expected biological responses. This will ultimately help to establish the limits of human response extrapolation abilities of the models.

In this chapter the preliminary analysis performed on acute and repeated exposure of BS to lead, doxorubicin, valproic acid and paraquat is presented.

#### **4.2. Material and Methods**

All procedures not described here (cell cultures, cytotoxicity assay, statistical analysis and TempO-Seq sample collection) can be found in chapter 2 and 3.

##### **4.2.1 Exposure to chemicals**

Lead (II) chloride (Pb - Sigma-Aldrich, catalogue No 268690-5G, lot # BCBT2452), doxorubicin hydrochloride (DOXO - jk-scientific, catalogue No 113424-50MG), valproic acid sodium salt (VPA- Sigma-Aldrich, catalogue No P4543-10G, lot #MKCF4674) and paraquat dichloride hydrate (PQ - Sigma-Aldrich, catalogue No 36541-100MG, lot #BCBW5264) were dissolved in ultrapure water. Stock solutions of 100x of final concentration were prepared for each experiment and further diluted to final concentration in neural differentiation medium. For the different experiments, BS were exposed to each chemical after 6 weeks in culture for 1-48h (acute exposure), one week (repeated exposure- 7d) and one week plus a further week of washout period (7dW). Concentrations and time points used in each experiment are described in the technique description. Samples per group are indicated in figure captions.

##### **4.2.2. TempO-Seq analysis**

Analysis of samples exposed to VPA, Pb and DOXO and their controls was performed as described in chapter 3.

To allow comparison with the results obtained in the PQ study presented in chapter 2, PQ exposed samples were analysed as described in chapter 2.

#### 4.2.3. Real-time RT-PCR analyses

As previously described. Sequences of RT-qPCR SYBR Green® primers and references for RT-qPCR TaqMan® probes are listed in Table 4.1 together with the needed cDNA amount.

**Table 4.1.: Sequences of semi-quantitative real time PCR SYBR Green® primer, reference of semi-quantitative real time PCR TaqMan® probes and the needed cDNA concentration per analysed well.**

Technology	Gene name	Sequence (3'-5') / Reference	cDNA (ng/well)
SYBR Green®	HMOX	F' GAGTGTAAGGACCCATCGGA R' GCCAGCAACAAAGTGCAAG	1
	TH	F' GGTGGATTTTGGCTTCAAAC R' CTGTGGCCTTTGAGGAGAAG	1
	MAP2	F' GGGTCTACTGCCATCACTCC R' GATGGCGACCTTCTCTCAC	1
	S100b	F' ATGTCTGAGCTGGAGAAGGC R' TTCAAAGAAGCTCGTGGCAGG	1
	OLIG2	F' TGGCTTCAAGTCATCCTCGTC R' ATGGCGATGTTGAGGTCGTG	1
TaqMan®	GFAP	Thermo Fischer Hs00909233_m1	20

#### 4.2.4. VPA Distribution Biokinetics

Samples of medium, cells and fraction bound to plastic were collected after exposure to VPA for 0-336h to 250, 500 and 1000 µM. Medium was collected and centrifugated at 300rpm for 5 min at 4 °C. Supernatant was diluted in 1:1 methanol (Sigma). BS were collected, washed two times with DPBS and kept with 250 µL of methanol. Before HPLC analyses, BS were sonicated in a Soniprep 150 (MSE) ultrasonic desitegrator, maximum 25 microns amplitude, three 10 secs cycles and supernatant was collected after centrifugation at 1200 G for 10 min for reading. Plastic fraction (in methanol) of each well was collected after washing with DPBS and incubation with 1mL of methanol (Sigma) for 2h at RT in constant see-saw rocking. Plastic and medium samples were collected from wells without the presence of cells in the same conditions. All samples in methanol were kept at -20 °C till analysis and vortexed prior to performing HPLC analyses

To quantify chemical mass in each sample, Liquid Chromatograph-Mass Spectrometry was used. The MS system was configured for negative mode (143.1-143.1 (m/z)), Q1 pre bias (17 V), CE prebias (12 V) and Q3 Bias (15 V). A Reverse phase Grace smart column (150 mm x 2.1 mm) was used as a stationary phase. MilliQ water with 5 mM ammonium acetate and methanol with 5 mM ammonium acetate were used as mobile phase with a flow rate of 0.2 ml/min (Table 4.2).

**Table 4.2.: Mobile phase gradient used for liquid chromatography separation of VPA**

Time (min)	Action	Values (%)
1	Pump B	5
2.5	Controller change valve to MS	
3	Pump B	95
6	Pump B	95
6.5	Pump B	5
7.5	Controller change valve to waste	
8	Controller stop	

### 4.3. Results

#### 4.3.1. Lead (II) chloride

The heavy metal lead (Pb) is used in fuel, chemical industries, batteries, paint, drinking water infrastructure and roadways (JJ *et al.*, 2019). Regulatory interventions have resulted in a significant decreased Pb exposure by paint, gasoline and in occupational Pb usage. Depending on the amount and route of exposure, Pb can affect the nervous system, kidneys, the immune, reproductive and the cardiovascular system (Gillis *et al.*, 2012). Its toxic effects vary from subtle changes in neurocognitive function in low-level exposures to a potentially fatal encephalopathy in acute Pb poisoning (Needleman, 2004). From all the different studies done to date, oxidative stress seems to be the most unifying factor in pathogenesis of various harmful manifestations of Pb exposure (Mitra *et al.*, 2017).

To assess the sensitivity of BS to Pb and to define concentrations for additional testing, BS were exposed to a wide range of Pb concentrations (1-500 $\mu$ M) for one week (7d) and one week followed by a wash-out period of one more week (7dW). The concentration-dependent curves for cytotoxicity showed that the IC<sub>50</sub> for the two exposure scenarios are similar (7d = 11.4  $\mu$ M; 7dW = 12.1  $\mu$ M) (Fig. 4.1 A).

Analysis performed with RT-qPCR showed an increased expression of the neuron-specific marker Microtubule Associated Protein 2 (MAP2) after 7d that goes back to control levels after the wash-out period (Fig 3.1B). The oxidative stress marker Heme Oxygenase 1 (HMOX1) expression was also increased by repeated exposure to Pb. HMOX1 levels decreased after wash-out period. No effects were detected on the astrocytes (Glial Fibrillary Acidic Protein (GFAP)) and oligodendrocytes (Oligodendrocyte Transcription Factor 2 (OLIG2)) markers.

With TempO-Seq analysis, it was possible to detect more differentially expressed genes (DEG) and associated biological processes after the acute exposure of 48h than after the 7d to 10 and 15  $\mu$ M of Pb (Fig 4.1 C and D). Confirming effects on neurons, decreased expression was detected for the probes Neurotrophic Receptor Tyrosine Kinase 3 (NTRK3\_13217) after 48h and after 7d Neurofilament Light Chain (NEFL\_27577) and Glutamate-Ammonia Ligase

(GLUL\_19900) with 10  $\mu\text{M}$  of Pb (Table 4.3). Two oxidative stress markers appeared upregulated. The NAD(P)H Quinone Dehydrogenase 1 (NQO1\_26473) was upregulated after 48h and 7d, while the HMOX1\_3041 probe was upregulated only after the repeated exposure of one week (7d).

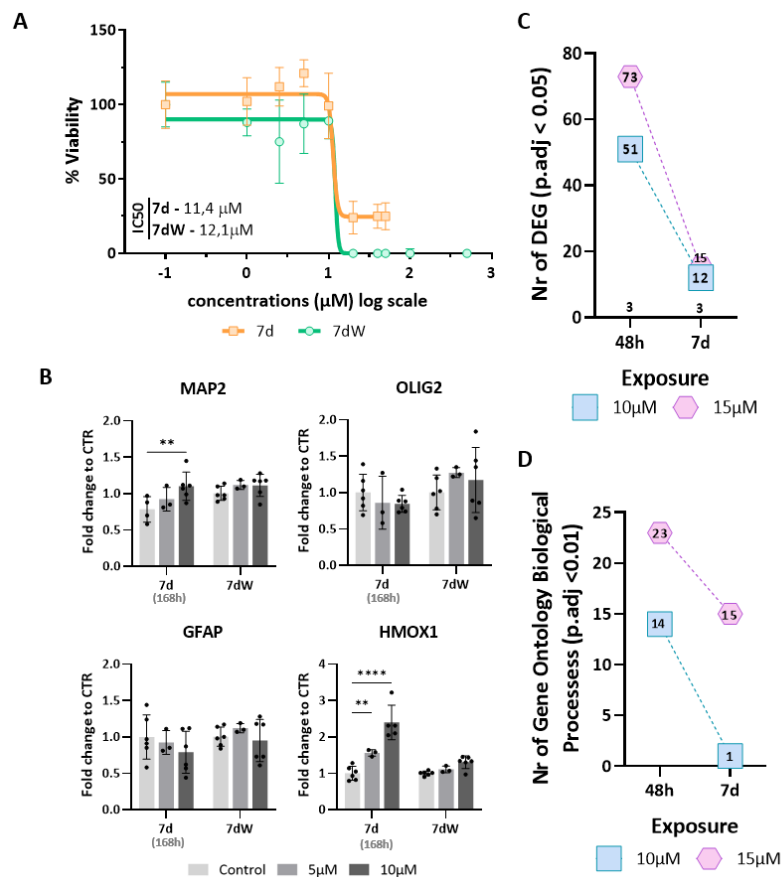


**Figure 4.1.: Pb induces cytotoxicity and differential gene expression on BS**

(A) Cytotoxicity concentration-dependent curves established after repeated (7d and 7dW) exposure to Pb (0 - 500  $\mu\text{M}$ ). Results are expressed as % of control cultures. Each point is the mean  $\pm$  SD of 3-6 samples obtained in 2 independent experiments. A non-linear regression (log (inhibitor) vs response - variable slope (four parameters)) was performed in order to calculate the inhibitory concentration (IC) using GraphPad Prism<sup>®</sup>. (B) Relative gene expression of neuronal- (MAP2), oligodendrocyte- (OLIG2), astrocytic (GFAP) and oxidative stress (HMOX1) markers. Data are expressed as fold change to control. Each value is the mean ( $\pm$  SD) of 3-6 samples coming from 2 independent experiments. (C) Number of DEG (p.adj < 0.05) per condition after DSeq2 analysis. (D) Number of gene ontology biological processes (p.adj < 0.01) per condition.

TempO-Seq analysis of samples exposed to 10  $\mu\text{M}$  of Pb shows the increased expression of Protein Phosphatase 1 Regulatory Subunit 15A gene (PPP1R15A\_14098) after 48h exposure. Together with the number of biological processes linked to protein location in ER, the results

indicate a potential activation of ER stress by acute exposure to Pb (Table 4.3 and Supplementary Table 1).

**Table 4.3.: Differential expressed probes involved in oxidative stress and neuronal function (p.adj value <0.05) after treatment with 10  $\mu$ M Pb.**

Time Point (h)	Gene	log2Fold Change	p.adj	Time Point (h)	Gene	log2Fold Change	p.adj
48	NQO1_26473	1.0	3.9E-05	7d	NQO1_26473	1.2	9.3E-08
	NTRK3_16217	-1.1	4.6E-02		NEFL_27577	-0.6	1.4E-02
	PPP1R15A_14098	0.6	3.0E-02		HMOX1_3041	1.2	4.5E-02
					GLUL_19900	-0.7	4.8E-02

#### 4.3.2. Doxorubicin (DOXO)

Commonly used in the adjuvant chemotherapy regimens for breast cancer, the anthracycline class drug DOXO has an antineoplastic effect through DNA insertion and inhibition of topoisomerase II which induces a subsequent blockage of DNA resealing during cell replication (Du *et al.*, 2021; Hernandez-Aya and Gonzalez-Angulo, 2013). Mitochondrial toxicity and mitochondrial derived ROS are thought to be involved in DOXO's toxicity (Green and Leeuwenburgh, 2002). Even though DOXO is known to have limited passage through the BBB, chemotherapy-induced cognitive impairments have been reported in treated patients of all ages (Andryszak *et al.*, 2018; Aotani *et al.*, 2016; Eskes *et al.*, 2002; John *et al.*, 2017; Ramalho *et al.*, 2017).

The concentration-dependent curves for cytotoxicity of DOXO (0.0375-10nM) in BS after 7d exposure showed a IC50 = 0,113  $\mu$ M (Fig. 4.2 A). Unsupervised clustering of all control and treated samples showed that the samples plot together according to exposure time and concentration (Fig. 4.2 B). Differential expression analysis showed an increased level of DEG with time and concentration of DOXO (Fig. 4.2 C). Except when BS are exposed to 50 nM, biological processes reflect the same tendency (Fig.4.2 D). After the 7d exposure to 25nM, out of the 419 total biological processes can be related to oxidative stress (e.g., "response to oxidative stress"), DNA damage (e.g., "G1 DNA damage checkpoint") and neural function and development (Supp. table 2). In particular, it is possible to detect several biological processes involved in neurogenesis (e.g., "positive regulation of neuron differentiation"), axonogenesis (e.g., "axon extension"), synapses (e.g., "regulation of trans synaptic signalling") and glial cells (e.g., "glial cell differentiation").

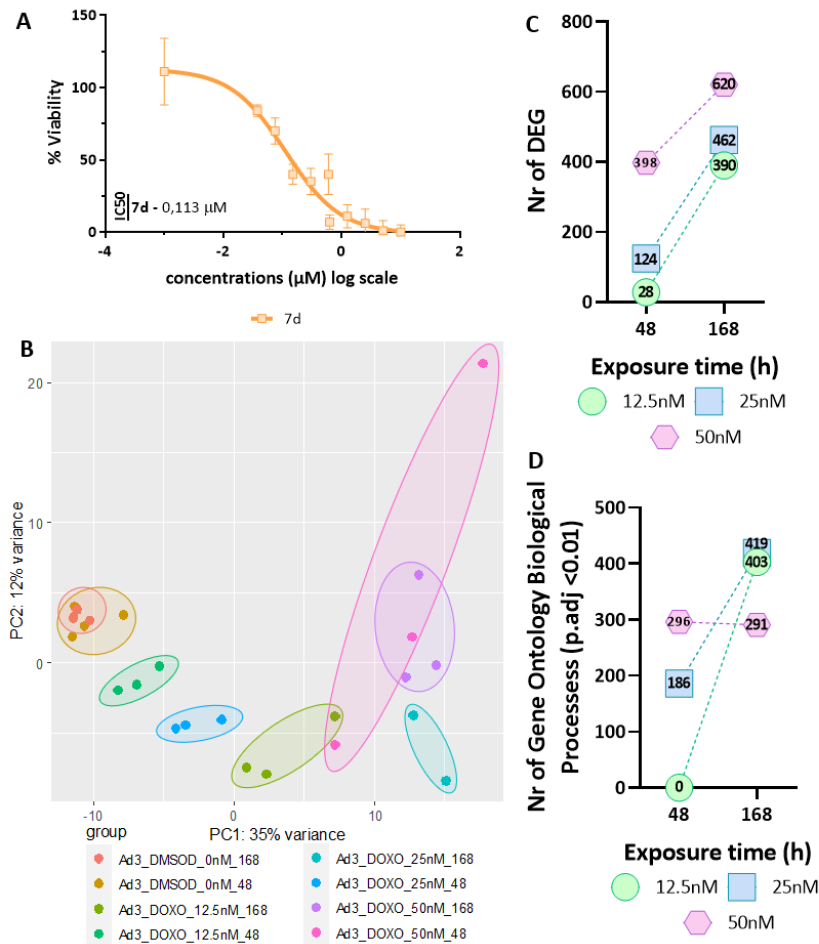


**Figure 4.2.: DOXO induces cytotoxicity and differential gene expression on BS**

(A) Cytotoxicity concentration-dependent curves established after one week (7d) repeated exposure to DOXO (0 - 10 μM). Results are expressed as % of control cultures. Each point is the mean ± SD of 3-6 samples obtained in 2 independent experiments. A non-linear regression (log (inhibitor) vs response - variable slope (four parameters)) was performed in order to calculate the inhibitory concentration (IC) using GraphPad Prism®. (B) PCA plot of all control and DOXO treated samples. Each dot represents a sample and each colour represents a control or treated group. All groups are represented by 3 independent biological replicates except 25nM for 48h which has 2 replicates. (C) Number of DEG (p.adj < 0.05) per condition after DSeq2 analysis. (D) Number of gene ontology biological processes (p.adj < 0.01) per condition.

#### 4.3.3. Valproic acid (VPA)

The drug VPA is used as a treatment for different pathologies such as epilepsy, migraine, personality and anxiety disorders (Tunali *et al.*, 2020). VPA appears to function through regional changes in concentration of γ-aminobutyric acid (GABA), the principal inhibitory brain neurotransmitter, by an indirect mechanism involving inhibition of the enzyme succinate semialdehyde dehydrogenase (Sztajnkrzyca, 2002). A recent study related VPA prenatal exposure to development of autism-related behaviour in the offspring of rats (Gąssowska-

Dobrowolska *et al.*, 2020). Recently, VPA has been described as an HDAC inhibitor, resulting in an increased interest for its use in cancer therapy (Diederich *et al.*, 2010).

Concentration ranging from 62.5 - 1000  $\mu\text{M}$  were used to assess the cytotoxicity of VPA on BS. Even the maximum concentration (1000  $\mu\text{M}$ ) tested did not induce 100% of cell death, making the calculation of a reliable IC50 impossible (Fig. 4.3 A). A slightly higher sensitivity of BS was observed after 7dW.

Gene expression analysis with RT-qPCR showed effects on neurons with decreased expression of MAP2 after 7d and 7dW. The expression of the oxidative stress marker HMOX1 was significantly increased after 7d exposure to 1000  $\mu\text{M}$  of VPA (Fig. 4.3.B)

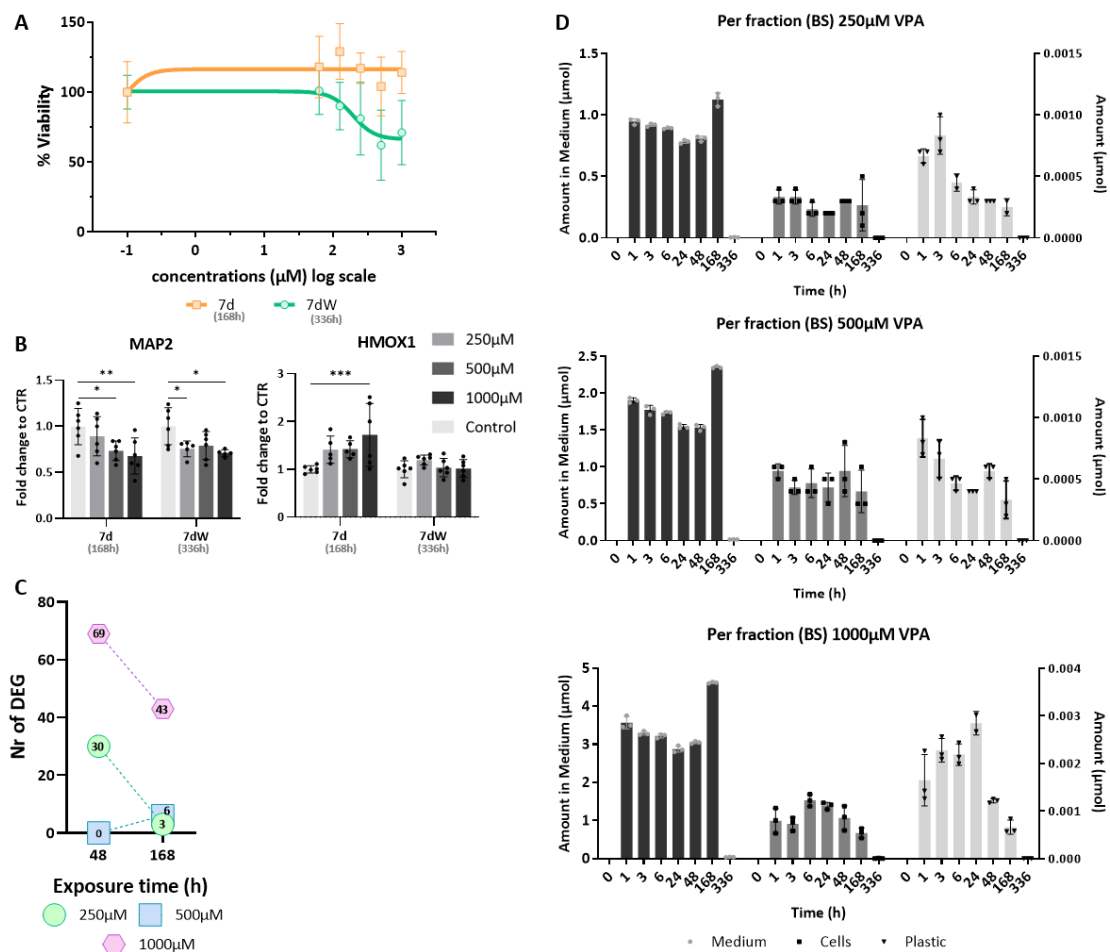


**Figure 4.3.: VPA induces cytotoxicity and differential gene expression in BS**

(A) Cytotoxicity concentration-dependent curves established after repeated (7d and 7dW) exposure to VPA (0 - 1000  $\mu\text{M}$ ). Results are expressed as % of control cultures. Each point is the mean  $\pm$  SD of 6 samples obtained in 2 independent experiments. A non-linear regression (log (inhibitor) vs response - variable slope (four parameters)) was performed in order to calculate the inhibitory concentration (IC) using GraphPad Prism<sup>®</sup>. (B) Relative gene expression of neuronal- (MAP2) and oxidative stress (HMOX1) markers. Data are expressed as fold change to control. Each value is the mean ( $\pm$  SD) of 3-6 samples coming from 2 independent experiments. (C) Number of DEG ( $p_{\text{adj}} < 0.05$ ) per condition after DSeq2 analysis. (D) Relative distribution of VPA in the different compartments of the model: medium (black bars, circles), cell lysates (dark grey bars) and plastic binding (light grey bars) after acute (1 - 48 h) and repeated treatment (168 h = 7d and 336 h = 7dW). Results are reported as mean  $\pm$  SD of three replicates. Right y-axis represents cell and plastic fraction and left y-axis the medium fraction.

Differential expression analysis of the Tempo-Seq data detected more DEGs after 48h than after 7d when BS were exposed to 250  $\mu$ M and 1000  $\mu$ M of VPA (Table 4.7). After exposure to 1000  $\mu$ M of VPA numerous DEGs are histones, with most of the detected histone downregulated (HIST1H2AE\_2951, HIST1H2BC\_28172, HIST1H2BD\_18171 and HIST1H2BF\_11973) and only one upregulated (HIST1H3H\_2957). The ER stress marker probe PPP1R15A\_18156 was downregulated after 48h exposure and the PPP1R15A\_14098 and GDF15\_18329 upregulated after 1w. Even if HMOX was not detected as differentially expressed, contrarily to what was observed by RT-qPCR, other oxidative stress markers, such as MAFG\_20735 and NQO1\_26473 were upregulated after the repeated exposure to 1000  $\mu$ M of VPA. Furthermore, VPA repeated exposure led to the upregulation of the probe NEFH\_18808 and downregulation of NEFL\_27577, both neuronal markers.

**Table 4.4.: Differential expressed probes of histones and related to ER stress, oxidative stress and neuronal function (p.adj value <0.05) after treatment with 1000  $\mu$ M VPA.**

Time Point	Gene	log2Fold Change	p.adj		Time Point	Gene	log2Fold Change	p.adj
48h	HIST1H2AE_2951	-1.6	4.90E-02		7d	GDF15_18329	1.3	2.70E-05
	HIST1H2BC_28172	-1	2.80E-02			HIST1H2BD_18171	-0.6	7.20E-04
	HIST1H2BD_18171	-0.9	3.40E-04			MAFG_20735	1.1	1.00E-04
	HIST1H2BF_11973	-1.4	2.00E-03			NEFH_18808	1.5	4.40E-04
	HIST1H3H_2957	0.7	1.60E-02			NEFL_27577	-0.6	1.70E-04
	PPP2R1A_18156	-1.4	3.40E-02			NQO1_26473	1	4.90E-04
				PPP1R15A_14098		1	1.60E-04	

Samples of medium, cells and plastic fractions of the control and treated BS were collected for VPA distribution kinetics assessment (Fig. 4.3 D). The amount of VPA in the medium decreased over the first 48h of exposure, increased after the full week of exposure and was not detectable anymore after the wash-out period. In the cell fraction VPA amount stayed quite stable from 1h after the beginning of the exposure till the end of the 168h exposure. After the wash-out period VPA was not detected anymore in the cell fraction. VPA intracellular amount did not increase in a concentration-dependent way. It was very similar after exposure to 250 and 500  $\mu$ M, and increased after exposure to 1000 M. The amount of VPA bound to plastic varied depending on the concentration used for the exposure. For the two lowest concentrations VPA bound to plastic decreased along the exposure time (1-168h), however for the highest concentration tested (1000  $\mu$ M), the bound fraction increased between 1-24h, then decreased at 168h. After the wash-out period VPA was not measurable anymore in the plastic fraction for all concentrations used.

#### 4.3.4. PQ

The herbicide PQ is known to increase oxidative stress, mitochondrial dysfunction,  $\alpha$ -synuclein aggregation, excitotoxicity and autophagy (Chinta *et al.*, 2018; Dinis-Oliveira *et al.*, 2008). The impact of paraquat toxicity on the dopaminergic neurons and induced senescence in astrocytes have been suggested as reasons of the epidemiological link between exposure to PQ and the development of Parkinson's diseases (Chinta *et al.*, 2018; Shimizu *et al.*, 2003).

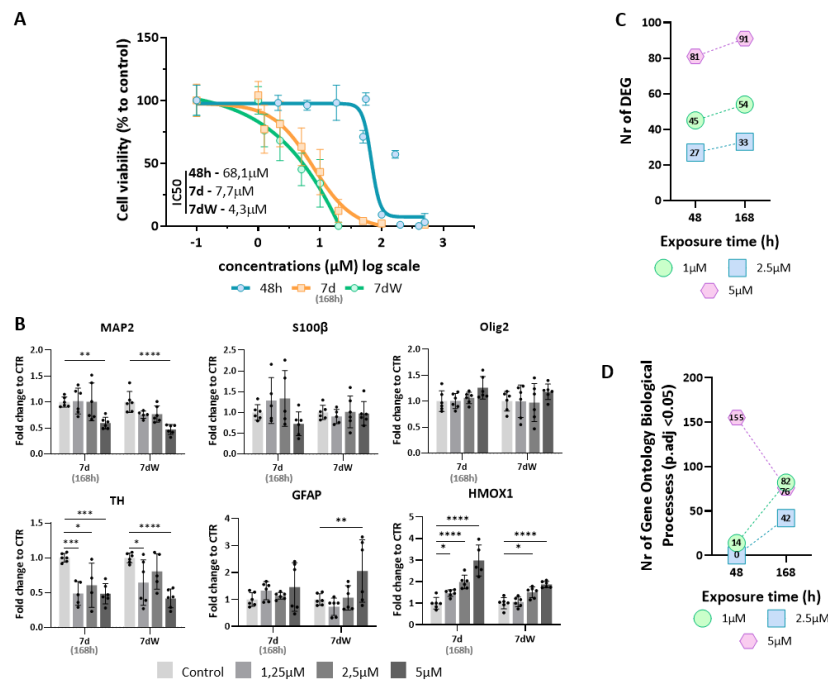


**Figure 4.4.: PQ induces cytotoxicity and differential gene expression on BS**

(A) Cytotoxicity concentration-dependent curves established after repeated (48h, 7d and 7dW) exposure to PQ (0 - 1000 μM). Results are expressed as % of control cultures. Each point is the mean  $\pm$  SD of 3-9 samples obtained in 3 independent experiments. A non-linear regression (log (inhibitor) vs response - variable slope (four parameters)) was performed in order to calculate the inhibitory concentration (IC) using GraphPad Prism®. (B) Relative gene expression of neuronal- (MAP2 and TH), oligodentocyte- (OLIG2), astrocytic (GFAP, S100b) and oxidative stress (HMOX1) markers. Data are expressed as fold change to control. Each value is the mean ( $\pm$  SD) of = 3-6 samples coming from 2 independent experiments. (C) Number of DEG (p.adj < 0.05) per condition after DSeq2 analysis. (D) Number of gene ontology biological processes (p.adj < 0.01) per condition.

Some of the TempO-Seq samples in this section were used for the study described in chapter 2. To be able to later compare the two analyses, the samples here were sorted and analysed with DSeq2 R package having the same thresholds in consideration. The cytotoxicity curves showed a much higher cytotoxicity after repeated than after acute exposure (IC50 values: 7.7 μM at 7d, 4.3 μM at 7dW, and 68.1 μM at 48 h) (Fig. 4.4 A).

PQ induced the downregulation of MAP2 gene, that was more marked after the washout period (Fig 4.4 B). Analysis of the TempO-Seq data also showed the impact of acute and repeated exposure to PQ on neurons and other neural cells in all the conditions (Suppl. table 3). The effect of PQ in dopaminergic neurons is demonstrated by the significant downregulation of the specific

marker tyrosine hydroxylase (TH) after repeated exposure (7d). The washout period did not allow any recovery of this marker (7dW) (Fig 4.4 B). mRNA levels for the oxidative stress marker HMOX1 increased in a concentration-dependent way after 7d and 7dW, although at that point a tendency to return to control level was observed (Fig 4.4 B). As in the results obtained with ConsensusPathDB in chapter 2, gene ontology shows oxidative stress affected after the acute exposure while repeated exposure to PQ seems to have a higher impact on endoplasmic reticulum stress (Suppl. Table 3).

Quantification of GFAP mRNA levels showed a significant increase at 5  $\mu$ M after the washout period (7dW), however no significant change was observed for S100b. The oligodendrocytic marker OLIG2 stayed unchanged (Fig. 4.4 B)

#### **4.4. Results Outline**

Even with a very preliminary analysis, the results presented in this chapter demonstrated that BS respond to exposure to Pb, DOXO, VPA and PQ according to what has already been described. Further analysis must be performed for quality control of TempO-Seq data, and to determine if other mechanisms of action could be found. The data presented here also underlined the importance of the choice of the exposure scenarios to be used. Finally, the weak toxicity of VPA was explained by distribution kinetics, emphasizing the importance of its determination for the understanding of *in vitro* toxicity data.



---

## Chapter 5: Further characterization of the model

---

## 5.1. Aim

George Edward Pelham Box was a British statistician that in 1987 clearly stated that “essentially, all models are wrong, but some are useful” (Box and Draper, 1987). If we consider this to be true, then the question is not if a model is the best described representative of an organ/structure, but actually what characteristics does the model replicate and is able to simulate. Extensive characterization was already performed on BS, but if we aim to understand which parameters/characteristics/responses to chemical BS can replicate, the more information about the model we have the merrier.

Taking advantage of the opportunity to perform TempO-Seq analysis, samples from NPCs to BS after 56 days in culture. For further characterization of which pathways could be activated in the BS, different chemicals that activate very specific pathways were used. Rotenone was used to study mitochondria complex I, the mitochondria complex III using Antimycin A, Tunicamycin the UPR, Arsenic for the Nrf2 and Cadmium the metal response. As an example of the developed work, cadmium will be presented. In order to access the expression dynamic of the genes involved in the different pathways, samples were collected after 6, 12, 24 and 48 h after acute exposure. As an example of the developed work, the analysis performed in cadmium-exposed BS is presented.

## 5.2 Material and Methods

All procedures not described here (cell cultures and gene ontology analysis) can be found in chapter 3.

### 5.2.1. Exposure to chemicals

Cadmium chloride ( $\text{CdCl}_2$  – Sigma-Aldrich, catalogue No 202908-10G) was dissolved in ultrapure water. The stock solutions of 100x of final concentration ( $5 \mu\text{M}$ ) was prepared for each experiment and further diluted to final concentration in NDM. BS were exposed to  $\text{CdCl}_2$  after 6 weeks in culture for 6-48h (acute exposure).

### 5.2.2. TempO-Seq sample collection

DMSO was added to all samples (final concentration 0.01%) due to the simultaneous testing of water-insoluble chemicals. Collected samples of NPC, BS after every week in culture and BS exposed to  $\text{CdCl}_2$  for 6-48h plus control of each time point were processed as described in the previous chapters.

## 5.3. Results

### 5.3.1. Developmental time course

To study the development-dependent expression of genes in the BS model, NPCs and BS samples collected after every week in culture were sent for TempO-Seq analysis. Unsupervised clustering of the different samples showed a clear separation between the groups (Fig. 5.1 A). The distance between consecutive clusters decreased with time in culture, the biggest difference being detected between 7d and 14d. Differential expression analysis showed a development-dependent increase in the number of DEGs (Fig. 5.1 B). As in the PCA plot, the highest difference in number of DEGs between two consecutive collection of samples was observed between 7d and 14d. At the latest assessed time (56d), gene ontology analysis detected different biological processes associated with axonogenesis, dendrite development, glial cells, neuron function and synapses (Supp. Table 4). Deeper analyses have to be performed to study the dynamic of these biological processes related to brain development, but also to define the development-dependent appearance of the genes associated to the biological pathways associated to toxicity, also called toxicity pathways.

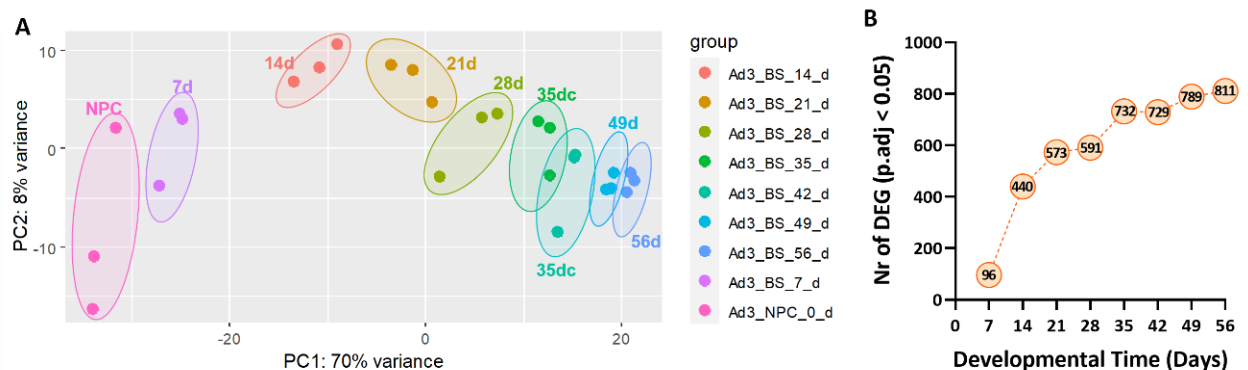


**Figure 5.1.: Development-dependent gene expression in BS**

(A) PCA of all NPCs and BS along differentiation weeks in culture. Each dot represents a sample and each colour represents a differentiation time point. (D) Number of DEGs (p.adj < 0.05) per condition after DSeq2 analysis.

### 5.3.2. Characterization of the presence of the metal response pathway

Cadmium ( $\text{CdCl}_2$ ) is an environmental pollutant and exposure happens through food, via plant uptake of cadmium in soil, and via smoking (Ismael *et al.*, 2019). One of the defence mechanisms of the cells against oxidative stress caused by exposure to  $\text{CdCl}_2$  is the activation of the Nrf2 pathway (Limonciel and Jennings, 2013; Wilmes *et al.*, 2011). In response to  $\text{CdCl}_2$  the

displacement of biological metals, like zinc, cells can activate the metal stress response via the metal-responsive transcription factor 1 (MTF1) and metallothionein (MT) (Jennings *et al.*, 2013).

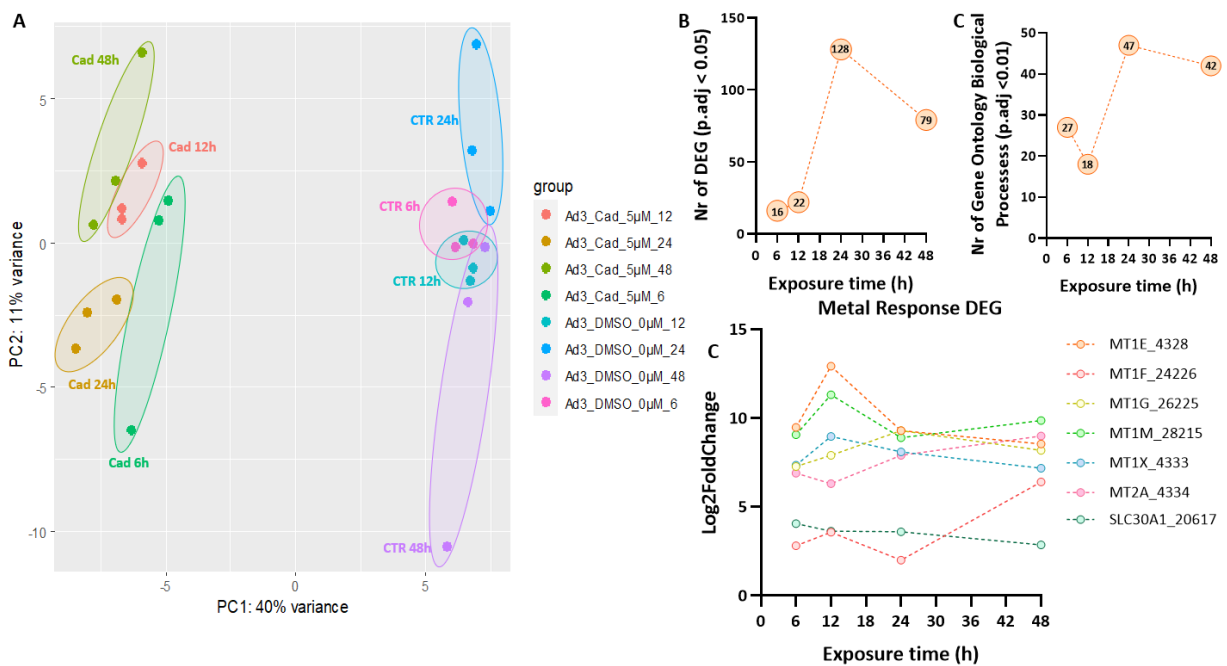


**Figure 5.2.: Cad exposure activates the metal stress response in BS**

(A) PCA of all control and Cad treated samples. Each dot represents a sample and each colour represents a control or treated group. (B) Number of DEG (p.adj < 0.05) per condition after DSeq2 analysis. (C) Number of gene ontology biological processes (p.adj < 0.01) per condition. (D) Metal stress response linked DEG log2fold change along exposure time to cad.

The PCA plot of control and samples treated with CdCl<sub>2</sub> showed a clear difference between groups (Fig. 5.2 A). There is a peak of detected DEG and biological processes at 24h of exposure to CdCl<sub>2</sub> (Fig. 5.2 B and C). Within the biological processes obtained in the analysis, the ones related to metal response and response to CdCl<sub>2</sub> exposure exhibited the highest p-adjusted value (Table 5.2). When plotting the log2FoldChange of genes linked to the metal response, (I) metallothionein 1E (MT1E\_4328), MT1M\_28215, MT1X\_4333 and MT1F\_24226 show the highest value after 12h of exposure; (II) MT1G\_26225 after 24h of exposure; (III) MT2A after the 48h of exposure; (IV) Zinc transporter 1 (SLC30A1\_20617) has log2FoldChange values quite stable along exposure times (Fig. 5.2 C). Furthermore, oxidative stress response starts to be detected at 24h exposure to CdCl<sub>2</sub> (Table 5.2).

**Table 5.1.: Potential disturbed BIOLOGICAL PROCESSES linked to metal response and oxidative stress (Gene ontology, p.adj value <0.01) linked to cad mechanism of action in BS after exposure.**

Time point (h)	Biological Process		Involved DEG	
	Name	p.adj	geneID	Count
6	Detoxification of inorganic compound	6.7E-16	MT1M, MT1G, MT1E, MT1X, MT2A, SLC30A1, MT1F	7
	Response to cadmium ion	2.7E-14	MT1M, MT1G, MT1E, MT1X, MT2A, SLC30A1, HMOX1, MT1F	8
	Cellular response to cadmium ion	1.1E-13	MT1M, MT1G, MT1E, MT1X, MT2A, HMOX1, MT1F	7
	Cellular transition metal ion homeostasis	1.1E-12	MT1M, MT1G, MT1E, MT1X, MT2A, SLC30A1, HMOX1, MT1F	8
	Transition metal ion homeostasis	3.8E-12	MT1M, MT1G, MT1E, MT1X, MT2A, SLC30A1, HMOX1, MT1F	8
	Response to metal ion	1.5E-10	MT1M, MT1G, MT1E, MT1X, MT2A, SLC30A1, HMOX1, MT1F, HOMER1	9
12	Detoxification of inorganic compound	9.4E-15	MT1G, MT1M, MT1E, MT2A, MT1X, SLC30A1, MT1F	7
	Response to cadmium ion	6.1E-13	MT1G, MT1M, MT1E, HMOX1, MT2A, MT1X, SLC30A1, MT1F	8
	Cellular response to cadmium ion	1.5E-12	MT1G, MT1M, MT1E, HMOX1, MT2A, MT1X, MT1F	7
	Cellular transition metal ion homeostasis	2.4E-11	MT1G, MT1M, MT1E, HMOX1, MT2A, MT1X, SLC30A1, MT1F	8
	Transition metal ion homeostasis	8.5E-11	MT1G, MT1M, MT1E, HMOX1, MT2A, MT1X, SLC30A1, MT1F	8
24	Cellular response to cadmium ion	4.1E-09	MT1M, MT1G, MT1E, MT2A, MT1X, HMOX1, MT1F, MAPK3, AKT1	9
	Detoxification of inorganic compound	6.4E-09	MT1M, MT1G, MT1E, MT2A, MT1X, SLC30A1, MT1F	7
	Response to cadmium ion	6.4E-09	MT1M, MT1G, MT1E, MT2A, MT1X, HMOX1, SLC30A1, MT1F, MAPK3, AKT1	10
	Response to metal ion	6.8E-04	MT1M, MT1G, MT1E, MT2A, MT1X, HMOX1, SLC30A1, NQO1, MT1F, MAPK3, AKT1, TFAP2A	12
	Response to oxidative stress	1.0E-03	HMOX1, NQO1, MAPK3, HSPA1B, PRDX2, HSPB1, GPX4, GCLM, FYN, AKT1, DAPK1, MT-ND6, RHOB	13
48	Detoxification of inorganic compound	4.0E-10	MT1G, MT1M, MT1E, MT2A, MT1X, SLC30A1, MT1F	7
	Cellular response to cadmium ion	2.0E-09	MT1G, MT1M, MT1E, MT2A, HMOX1, MT1X, MT1F, SOD1	8
	Response to cadmium ion	2.9E-09	MT1G, MT1M, MT1E, MT2A, HMOX1, MT1X, SLC30A1, MT1F, SOD1	9
	Cellular response to inorganic substance	6.1E-08	MT1G, MT1M, MT1E, MT2A, HMOX1, MT1X, MT1F, NQO1, CALR, HSPA5, SOD1, PRKAA1	12
	Cellular transition metal ion homeostasis	2.5E-07	MT1G, MT1M, MT1E, MT2A, HMOX1, MT1X, SLC30A1, MT1F, SOD1	9
	Response to metal ion	8.6E-07	MT1G, MT1M, MT1E, MT2A, HMOX1, MT1X, SLC30A1, MT1F, NQO1, CALR, HSPA5, SOD1, PRKAA1	13
	Transition metal ion homeostasis	8.6E-07	MT1G, MT1M, MT1E, MT2A, HMOX1, MT1X, SLC30A1, MT1F, SOD1	9
	Response to oxidative stress	5.2E-05	HMOX1, HSPA1B, DHRS2, NQO1, GCLM, HSPB1, SGK2, TPM1, SOD1, SCARA3, GNAO1, PRKAA1	12

## 5.4 Results Outline

The results presented in this chapter showed strong development-dependent changes in the expression of genes specific for brain cells. They also showed that BS react to CdCl<sub>2</sub> by mounting the metal response, suggesting this pathway is functional in BS. The further analyses of all these data, together with the data collected for the other 4 compounds (rotenone, antimycin, tunicamycin and arsenic), will lead to a better understanding of the ability of BS to respond to various classes of chemicals, and the developmental-dependence of these responses will be established.



---

## Chapter 6: Activation of human microglia is deleterious for oligodendrocytes in a complex human iPSC-derived 3D model

---

*The following results are presented in the form of an article, that is in preparation.*

## 6.1. Introduction

Microglia is one of the key players in neuroinflammation, a process involved in many neurodegenerative diseases. *In vitro* human central nervous system models containing functional microglia have been difficult to build for the obvious difficulty to obtain primary human microglia, and also because microglia lose their identity when isolated from others brain cells. Therefore, a complete *in vitro* human model able to mimic strong cell-to-cell interactions between the various brain cell types and to reproduce the cascade of neuroinflammatory reactions when subjected to an immune challenge is lacking. Here we show that such an *in vitro* system can be produced.

## 6.2. Contribution

I participated on the development of the protocol to add microglia progenitors to BS. I was involved in the experimental design and supervised the master student Kelvin Ramirez-Cuevas for the execution of the experiments. I performed the immunocytochemistry quantification. I contributed to the first draft of the manuscript and the development of the figures.

## 6.3. Summary of the results

We found that human iPSC-derived microglia progenitors (pMicroglia) introduced in our previously described BrainSphere model (BS) extend ramifications, suggesting their maturation and the acquisition of microglia-like cells (MLCs) surveilling phenotype. MLCs lost their ramifications after exposure to LPS + IFNg. Furthermore, mRNA levels for inflammatory markers increased, and markers for oligodendrocytes decreased in the BrainSpheres containing MLCs ( $\mu$ BS), whereas none of these changes was observed in BrainSpheres devoid of microglia. Our results suggest that pMicroglia become functional MLCs when in contact with brain parenchymal cell types, and that MLCs activation has deleterious effects on oligodendrocytes. This new *in vitro* human complex 3D system recapitulates neuroinflammatory reactions by allowing interactions between microglia, macroglia and neurons. We anticipate our new  $\mu$ BS model to become a powerful tool to study neuroinflammation associated to brain diseases and to improve the *in vitro* detection of the neurotoxicity of environmental chemical compounds and drugs in development.

*The manuscript in preparation is found is the following pages.*

## Activation of human microglia is deleterious for oligodendrocytes in a complex human iPSC-derived 3D model

Carolina Nunes<sup>1,2</sup>, Kelvin Ramirez-Cuevas<sup>1,2</sup>, Cathy Browne<sup>3,4</sup>, Denise Tavel<sup>1</sup>, Sally Cowley<sup>3,4</sup>,  
David Pamies<sup>1,2</sup> and Marie- Gabrielle Zurich<sup>1,2</sup>

1. Department of Biomedical Sciences, University of Lausanne, Rue du Bugnon 7, 1005 Lausanne, Switzerland
2. Swiss Centre for Applied Human Toxicology (SCAHT), University of Basel Missionsstrasse 64, 4055 Basel, Switzerland
3. Sir William Dunn School of Pathology, University of Oxford, South Parks Road, Oxford OX1 3RE, UK
4. Oxford Parkinson's Disease Centre, University of Oxford, South Parks Road, Oxford OX1 3QX, UK

### Abstract

Microglia is one of the key players in neuroinflammation, a process involved in many neurodegenerative diseases. *In vitro* human central nervous system models containing functional microglia have been difficult to build for the obvious difficulty to obtain primary human microglia, and also because microglia lose their identity when isolated from others brain cells. Therefore, a complete *in vitro* human model able to mimic strong cell-to-cell interactions between the various brain cell types and to reproduce the cascade of neuroinflammatory reactions when subjected to an immune challenge is lacking. Here we show that such an *in vitro* system can be produced. We found that human iPSC-derived microglia progenitors (pMicroglia) introduced in our previously described BrainSphere model (BS) extend ramifications, suggesting their maturation and the acquisition of microglia-like cells (MLCs) surveilling phenotype. MLCs lost their ramifications after exposure to LPS + IFN $\gamma$ . Furthermore, mRNA levels for inflammatory markers increased, and markers for oligodendrocytes decreased in the BrainSpheres containing MLCs ( $\mu$ BS), whereas none of these changes was observed in BrainSpheres devoid of microglia. Our results suggest that pMicroglia become functional MLCs when in contact with brain parenchymal cell types, and that MLCs activation has deleterious effects on oligodendrocytes. This new *in vitro* human complex 3D system recapitulates neuroinflammatory reactions by allowing interactions between microglia, macroglia and neurons. We anticipate our new  $\mu$ BS model to become a powerful tool to study neuroinflammation associated to brain diseases and to improve the *in vitro* detection of the neurotoxicity of environmental chemical compounds and drugs in development.

## List of abbreviations

B3T:	Tubulin beta-3 chain
BS:	BrainSpheres
BS+:	BrainSpheres grown in differentiation medium plus IL34 and GM-CSF
CNS:	Central nervous system.
CSF1:	Colony Stimulating Factor 1
DCX:	Doublecortin
DPBS:	Dulbecco's phosphate-buffered saline
FKBP5:	FK506-binding protein 5
GFAP:	Glial fibrillary acidic protein
GM-CSF:	Granulocyte-macrophage colony-stimulating factor
IFN $\gamma$ :	Interferon gamma
IL34:	Interleukin 34
IPSC:	Induced pluripotent stem cell.
LPS:	Lipopolysaccharide
MBP:	Myelin basic protein
MCT4:	Monocarboxylate transporter 4
MLC:	Microglia-like cell
MOG:	Myelin Oligodendrocyte Glycoprotein
NEFH:	Neurofilament, heavy polypeptide
NEM:	N-Ethylmaleimide
OLIG2:	Oligodendrocyte Transcription Factor 2
PLP1:	Proteolipid Protein 1
PSMB8:	Proteasome subunit beta type-8
PTX3:	Pentraxin 3
S100 $\beta$ :	S100 calcium-binding protein B
SYP:	Synaptophysin
VIM:	Vimentin
$\mu$ BS:	BrainSpheres containing microglia

## 1. Introduction

Microglia are brain-resident macrophages and the main immune cells in the brain (Graeber, 2010; Mrdjen *et al.*, 2018). They were discovered a century ago (Pérez-Cerdá *et al.*, 2015) and over the years many functions have been attributed to them (e.g., axonal guidance, synaptic formation and plasticity, homeostasis, immune response) (Colonna and Butovsky, 2017). They communicate with other brain cell types via fractalkine signalling, secrete soluble factors and extracellular vesicles (Szepesi *et al.*, 2018). Microglia constitute the primary defence line against the presence of pathogens but are also involved in injuries, neurodegenerative diseases and response to environmental compounds and drugs. Microglia release reactive oxygen products and inflammatory molecules in order to repair damage or eliminate pathogens. For that reason, microglia constantly monitor parenchyma tissue, patrolling and inspecting the brain by extending and retracting their processes looking for any element that interferes with homeostasis (Nimmerjahn *et al.*, 2005). However, under chronic inflammatory response, microglia can lead to progressive brain damage (Bachiller *et al.*, 2018). Microglia have shown to be involved in many neurodegenerative diseases such as Alzheimer's disease, Parkinson's disease, frontotemporal dementia, amyotrophic lateral sclerosis or prion disease (Bachiller *et al.*, 2018; Fakhoury, 2017; Geloso *et al.*, 2017; Hansen *et al.*, 2018; Haukedal and Freude, 2019; Ho, 2019). They also have been involved in the deleterious response to environmental chemicals (Monnet-Tschudi *et al.*, 1996, 1995; Purisai *et al.*, 2007; Sandström von Tobel *et al.*, 2014; Von Tobel *et al.*, 2014). A better understanding of their behaviour is crucial to produce efficient treatments against multiple brain conditions.

The majority of microglia studies have been produced in rodents due to the evident difficulties in obtaining human tissue, allowing relatively little research to determine interspecies similarities and differences. In addition, and despite a core set of important genes conserved, several authors have reported numerous differences between mice and human microglia (Lenz and Nelson, 2018; LR and MR, 2014; Mestas and Hughes, 2004; Smith and Dragunow, 2014; Thion *et al.*, 2018). Over the years various microglia *in vitro* models have been developed such as primary dissociated cell cultures, cell lines and stem cell-derived microglia (Carson *et al.*, 2008; Timmerman *et al.*, 2018). Human induced pluripotent stem cells (iPSC)-derived microglia retained a lot of attention due to their potential to become an unlimited resource of human cells and an incredible tool for disease modeling, drug testing and transplantation (Haenseler and Rajendran, 2019; Speicher *et al.*, 2019). However, many of the microglia functions are directly related to interactions with other cell types (e.g., neurons, astrocytes, oligodendrocytes, other immune cells) so monocultures make microglia lose their

unique identity (Haenseler and Rajendran, 2019). An example of strong interactions between the main brain cell types is the 3D primary rat aggregating brain cell cultures, containing neurons, astrocytes, oligodendrocytes and microglial cells, that allowed to apprehend the role of microglia in demyelination, to very successfully detect neurotoxicity, and to observe the activation of microglia in response to environmental chemicals for the first time *in vitro* (Defaux *et al.*, 2011, 2010; F *et al.*, 1995; Forsby *et al.*, 2009; Zurich *et al.*, 2013b). We aim now at generating a similar human model.

Recently, the development of stem cells with new culture technologies enabled the establishment of more complex systems that better mimic human brain physiology and better recapitulate human diseases. Microglia are absent from the majority of these co-culture models since they do not originate from the same precursors than the brain parenchyma cells, and to date, only one report showed their presence in cerebral organoids (Lancaster and Knoblich, 2014; Nayernia *et al.*, 2013; Ormel *et al.*, 2018; Pamies *et al.*, 2017a; Pamies and Hartung, 2017; Paşca *et al.*, 2015; Song *et al.*, 2019). Some groups have introduced microglia from various sources in these 3D cultures, but only few have been able to introduce iPSC-derived microglia into a 3D organotypic culture (Abreu *et al.*, 2018; Abud *et al.*, 2017; Muffat *et al.*, 2018; Ormel *et al.*, 2018; Song *et al.*, 2019). We recently developed a human iPSC-derived 3D brain model (called BrainSpheres (BS)) that is very reproducible in shape, size and content (Pamies *et al.*, 2017a). The model is composed of differentiated mature neurons and glial cells (astrocytes, oligodendrocytes) that reproduce the topology and connectivity of neuronal-glia interactions, mimicking the central nervous system. High axonal myelination is observed (approximately 40%) and functional spontaneous electrical activity is recorded (Pamies *et al.*, 2017a). BrainSpheres constitute a novel tool to study neurotoxicity and is promising for different medical applications. One of the multiple advantages of this model is to fit in high throughput analyses, making it a powerful tool for drug screening (Abreu *et al.*, 2018; Leite *et al.*, 2019a; Plummer *et al.*, 2019b; Zander *et al.*, 2017; Zhong *et al.*, 2020b). We have previously successfully incorporated human immortalized SV40 primary microglia (39) in BS, however these co-cultures can be used only during a very short period of time (1 week) before microglia overcome the whole system (Abreu *et al.*, 2018).

In the present study, we aim at generating a human *in vitro* complex system able to produce a neuroinflammatory response upon challenge. To achieve this goal, we incorporated iPSC-derived microglia progenitors into BrainSpheres (Haenseler *et al.*, 2017). We observed microglia activation after a classical inflammatory stimulus. In addition, we show results indicating that astrocyte activation and oligodendrocytes damage may appear only in presence

of microglia after exposure to an inflammatory stimulus. We believe that human microglia-BS co-cultures ( $\mu$ BS) constitute a novel model to study neuroinflammation, opening many possibilities such as patient specific studies and personalized medicine.

## **2. Methods**

### **2.1. NPCs expansion**

Neural progenitors cells (NPCs) Ad3G2 were differentiated from human induced pluripotent stem cell (hiPSC) line SBAAd3 (StemBANCC project) following the Gibco® PSC Neural Induction Medium protocol (ThermoFisher, MAN0008031). SBAAd3 hiPSC were cultured on Matrigel® (Corning) in the mTeSR™1 (StemCell Technology) feeder-free medium. Medium was replaced every day and cells were passaged every 4-5 days using Versene® according to the suppliers' protocol (ThermoFisher). Ad3G2 NPCs were cultured on Geltrex (ThermoFisher) in Neural Expansion Medium (NEM), consisting on Neurobasal® Medium (Gibco, A1647701), Advanced™ DMEM/F-12 Medium (Gibco, 12634) and Neural Induction Supplement (Gibco A1647701). The medium was replaced every 2-3 days. NPCs were passaged every 7 days using StemPro® Accutase® according to the suppliers' protocol (Thermo Fisher Scientific) or used to generate BS. Cells were cultured at 37 °C and 5% CO<sub>2</sub>.

### **2.2. BS generation and maintenance**

BS generation was based on previously described protocol (Pamies *et al.*, 2017a) with some modifications. At 90% confluence and between passages 10-15, Ad3G2 NPCs were dissociated using StemPro® Accutase® Cell Dissociation Reagent (Gibco A11105-01). After counting the cells with a Countess™ instrument (Invitrogen),  $2 \times 10^6$  cells in 2mL of NEM per well were plated in six well plates (Corning). Cells were placed in an incubator at 37 °C and 5% CO<sub>2</sub> under constant gyratory shaking (86rpm). After 24 hours, 1ml of Neuronal Differentiation Medium (NDM) was added to each well. NDM consists of Neurobasal® Electro Medium (Gibco), 2% of B27 Electro (Gibco), 0.01  $\mu$ g/mL BDNF (Peprotech), 0.01  $\mu$ g/mL GDNF (Peprotech) and 1% Penicillin-Streptomycin 10,000 U/mL (Gibco). After another 24 hours and every 2-3 days 3/4 media was replaced with fresh NDM.

### **2.3. $\mu$ BS generation**

BrainSpheres containing microglia ( $\mu$ BS) (Fig. 1A), were generated using microglia progenitors (pMicroglia) AH016-3 R-IP (RFP positive) derived from hiPSCs (cell line) and Ad3G2 NPCs. pMicroglia were prepared as previously described and shipped from UK to Switzerland

the day before the generation of  $\mu$ BS (Haenseler *et al.*, 2017). To generate  $\mu$ BS, a single cell suspension was prepared containing Ad3G2 NPCs ( $1 \times 10^6$  cell/mL) and AH016-3 R-IP pMicroglia ( $2.5 \times 10^5$  cells/mL) in NEM supplemented with Interleukin 34 (IL34) (Peprotech, 200-34) and Granulocyte-macrophage colony-stimulating factor (GM-CSF) (Peprotech, 300-03), at a concentration of 100 ng/mL and 10 ng/mL respectively. The pMicroglia:NPC cell suspension was then distributed in six-well plates (Corning) in a final volume of 2 mL per well and kept at 37 °C and at 5% CO<sub>2</sub> under constant gyratory shaking (86 rpm). After 24 hours, 1mL of NDM supplemented with IL34 (100 ng/mL) and GM-CSF (10 ng/mL) was added to each well. After another 24 hours and every 2-3 days 3/4 media was replaced with fresh NDM supplemented with IL34 (100 ng/mL) and GM-CSF (10 ng/mL). Due to the incorporation of IL34 and GM-CSF to the medium, BS were also generated and differentiated with  $\mu$ BS media (+BS) in parallel, as control condition.

#### **2.4. Treatment**

BS, BS+ and  $\mu$ BS were exposed at 2 and 4 weeks of development to lipopolysaccharide (LPS) at 100 ng/ml and interferon gamma (IFN $\gamma$ ) at 100 ng/ml for 6, 12 and 24 hours.

#### **2.5. Real-Time Quantitative PCR (RT-qPCR)**

Total RNA was extracted using the RNeasy kit (Qiagen) on a QIAcube (QIAGEN) according to the manufacturer's instructions and yield was determined by spectrophotometry (NanoDrop, ND-1000). Reverse transcription was performed on 0.5-1  $\mu$ g total mRNA using the High Capacity cDNA Reverse Transcription kit (Thermo Fischer Scientific). Semi-quantitative real time PCR (RT-qPCR) was performed with SYBR Green<sup>®</sup> (Thermofisher) or TaqMan<sup>®</sup> (Thermofisher) technology. Sequences of RT-qPCR SYBR Green<sup>®</sup> primers are listed in Table 1 and references for RT-qPCR TaqMan<sup>®</sup> probes in Table 2. RLP13A and Beta actin (Act $\beta$ ) were used as internal control gene for SYBR Green and Taqman detection, respectively, and the  $\Delta\Delta$ Ct method was used to calculate relative mRNA expression (Livak and Schmittgen, 2001). RT-qPCR was performed in a ViiA 7 Real-Time PCR System where cycles above 40 were set to be undetermined.

#### **2.6. Immunohistochemistry**

Spheres collected for immunocytochemistry were washed in Phosphate buffered saline (PBS) and fixed with 4% paraformaldehyde/PBS. After 1 hour, spheres were put in PBS and kept at 4 °C until further processing.

For all mount immunocytochemistry, about 10 spheres per condition were incubated in blocking solution (PBS with 10% Normal Goat Serum (NGS) (Thermofisher) and 4% 1X TritonX) for 2 hours at 4 °C. Spheres were incubated at 4 °C for 48 hours with a combination of primary antibodies (Table 3) in a concentration 1:200 with the primary antibody solution (PBS with 10% NGS and 1% 1X TritonX). Spheres were washed in PBS for 5 minutes three times and incubated 1 hour at room temperature (RT) protected from the light with the correspondent secondary IgG labeled with fluorophores Alexa 488 and 594 antibodies (Table 3) diluted 1:200 in the secondary antibody solution (PBS with 10% NGS). Spheres were washed in PBS for 5 minutes three times and incubated 30min at RT protected from the light with the nuclear staining Hoechst (1:10,000 in PBS). Finally, spheres were mounted on glass slides and coverslips with ProLong™ Gold antifade reagent (Thermo Fisher Scientific). Images were acquired using a Zeiss LSM 900 and analyzed using ImageJ® Fiji.

**Table 1: Sequences of qPCR primers used with SYBR green® and cDNA input**

Gene name	Sequence (3'-5')	cDNA (ng/well)
NEFH	F' TTCTGGAAGCGAGAAAGGAA R' CAGGACCTGCTCAATGTCAA	1
DCX	F' TCAGGACCACAGGCAATAAA R' AGACCGGGGTTGTCAAAAA	1
TNF $\alpha$	F' GAGGCCAAGCCCTGGTATG R' CGGGCCGATTGATCTCAGC	10
IL1 $\beta$	F' TTCGACACATGGGATAACGAGG R' TTTTGTGCTGTGAGTCCCGGAG	1
IL6	F' CCTGAACCTTCCAAAGATGGC R' TCACCAGGCAAGTCTCCTCA	1
SYP	F' TGACGAGGAGTAGTCCCAA R' CGAGGTCGAGTTCGAGTACC	1
MCT4	F' CCATGCTCTACGGGACAGG R' GCTTGCTGAAGTAGCGGTT	1
FKBP5	F' CTCCTAAAATCCCTCGAATGC R' CCCTCTCCTTCCGTTTGGTT	1
PTX3	F' AGGCTTGAGTCTTTTAGTGCC R' ATGGATTCTCTTTGTGCCATAG	1
Vimentin	F' ATTCCACTTTCGTTCAAGG R' CTTCAGAGAGAGGAAGCCGA	1
S100 $\beta$	F' ATGTCTGAGCTGGAGAAGGC R' TTCAAAGAACTCGTGGCAGG	1
MBP	F' ACCTCGTTTCCAAACCACAG R' GGAAGTGAATGAGCCGGTTA	10
B3T	F' AGTCGCCCACGTAGTTGC R' CGCCAGTATGAGGGAGAT	1
RLP13A	F' CATAGGAAGCTGGGAGCAAG R' GCCCTCAATCAGTCTTCTG	1
PSMB8	F' CACGCTCGCCTTCAAGTTC R' AGGCACTAATGTAGGACCCAG	1
Olig2	F' TGGCTTCAAGTCATCCTCGTC R' ATGGCGATGTTGAGGTCGTG	1

**Table 2: References for TaqMan® assays and cDNA input**

Gene name	Assay ID (Thermofisher)	cDNA (ng/well)
NFKB1	Hs00765730_m1	1
NFKB2	Hs01028901_g1	1
STAT1	Hs01013996_m1	1
STAT3	Hs00374280_m1	1
IL10	Hs00961622_m1	5
IBA1	Hs00610419_g1	20
PLP1	Hs00166914_m1	5
RLP13A	Hs01926559_g1	1
GFAP	Hs00909233_m1	20

For sectioned samples immunocytochemistry, fixed spheres were first embedded in agarose (Agarose 3.5%) and sectioned at a thickness of 40  $\mu$ m using a Vibratome™ (LEICA). Slices underwent permeabilization for 90 minutes in PBS with 0.5% TritonX followed by a blocking step of 1 hour in PBS with 2% BSA and 0.5% Triton X at RT. Primary antibodies, diluted 1:1000, were added overnight with constant shaking at 4 °C. Slices were washed three times with PBS for 5 minutes and incubated 1 hour at RT protected from the light with the correspondent secondary IgG labelled with fluorophores Alexa 488 and 594 antibodies diluted at 1:1000 in the same solution used for the blocking step. Slices were washed three times with PBS for 5 minutes and incubated 15 minutes at RT protected from the light with the nuclear staining Hoechst (1:10,000 in PBS). Finally, spheres were mounted on glass slides and coverslips with ProLong™ Gold antifade reagent (Thermo Fisher Scientific). Images were acquired using a Nikon 90i and analyzed using ImageJ® Fiji.

**Table 3: List of primary and secondary antibodies used for Immunohistochemistry**

Type	Name	Species	Reference
Primary	SYP	Mouse	Sigma Cat# SAB4200544
	S100 $\beta$ b	Rabbit	Abcam Cat# ab52642
	GFAP	Rabbit	Sigma Cat# G9269
	B3T	Mouse	Sigma Cat# T8660
	O4	Mouse	Sigma Cat# MAB1326
Secondary	Alexa® 594 against Rabbit	Goat	ThermoFisher Cat#A11037
	Alexa® 488 against Mouse	Donkey	ThermoFisher Cat#A21202

## 2.7. Statistical analyses

GraphPad Prism (Version 8, Graph Pad) was used for statistical testing.

For RT-qPCR: T-tests were used to assess difference between two groups. Comparison between three or more groups were made using a one-way analysis of variance (ANOVA) followed by Tukey's post-hoc analysis (adjusted with Bonferroni). A p-value lower than 0.05 was

considered significant. Comparisons are presented in figures as \*  $p < 0.05$ , \*\*  $p < 0.01$ , \*\*\*  $p < 0.001$ , \*\*\*\*  $p < 0.0001$ , or n.s. (not significant). Data are shown as mean  $\pm$  SEM if not indicated otherwise.

For Immunohistochemistry: Comparison between three or more groups were made using a one-way analysis of variance (ANOVA) followed by Tukey's post-hoc analysis (adjusted with Bonferroni). A p-value lower than 0.05 was considered significant. Comparisons are presented in figures as \*  $p < 0.05$ , \*\*  $p < 0.01$ , \*\*\*  $p < 0.001$ , \*\*\*\*  $p < 0.0001$ , or ns (not significant). Data are shown as mean  $\pm$  SEM if not indicated otherwise.

### 3. Results

#### 3.1. iPSC-derived microglia progenitors show ramifications after inclusion in BS

The quality of the iPSC-derived precursors of microglia (pMicroglia), labelled with RFP, was checked by immunohistochemistry. Most of the RFP-positive pMicroglia were also positive for IBA1, showing they belong to the macrophage/microglia lineage (Fig. 1 B, last line).

pMicroglia were then introduced into the BrainSpheres (BS) by mixing them with the NPCs at the start of BS formation. Different ratios between pMicroglia and NPCs were tested to select the best one (data not shown). Confocal microscopy (Fig. 1 B, 2 first lines) and RT-qPCR (Fig. 1 D) show that pMicroglia were successfully incorporated into BrainSpheres.

pMicroglia acquired ramifications (Fig. 2A) in BS, suggesting their differentiation in microglia-like cells that survived up to 4 weeks in presence of IL34 and GM-CSF in the medium, both ligands for CSF1 receptor and playing an important role in macrophage-microglia proliferation and differentiation (Lee *et al.*, 1994; Mathews *et al.*, 2019; Wei *et al.*, 2010). We first tested the potential impact of the presence of microglia-like cells on the development of neurons, astrocytes and oligodendrocytes in BS by measuring cell type-specific gene expression. However, the activation of CSF1 receptor also plays other functions in the CNS such as promotion of neurite outgrowth, enhancement of adult neocortical neuron's survival, and regulation of neural progenitor cell maintenance and maturation (Michaelson *et al.*, 1996; Nandi *et al.*, 2012; Wang *et al.*, 1999). Therefore, we compared three groups in order to rule out effects only due to the presence of growth factors, and not to the microglia: BS in normal differentiation medium (BS), BS in medium supplemented with the growth factors IL34 and GM-CSF (BS+), and BS containing microglia in medium supplemented with growth factors ( $\mu$ BS+), after 2 and 4 weeks in culture.

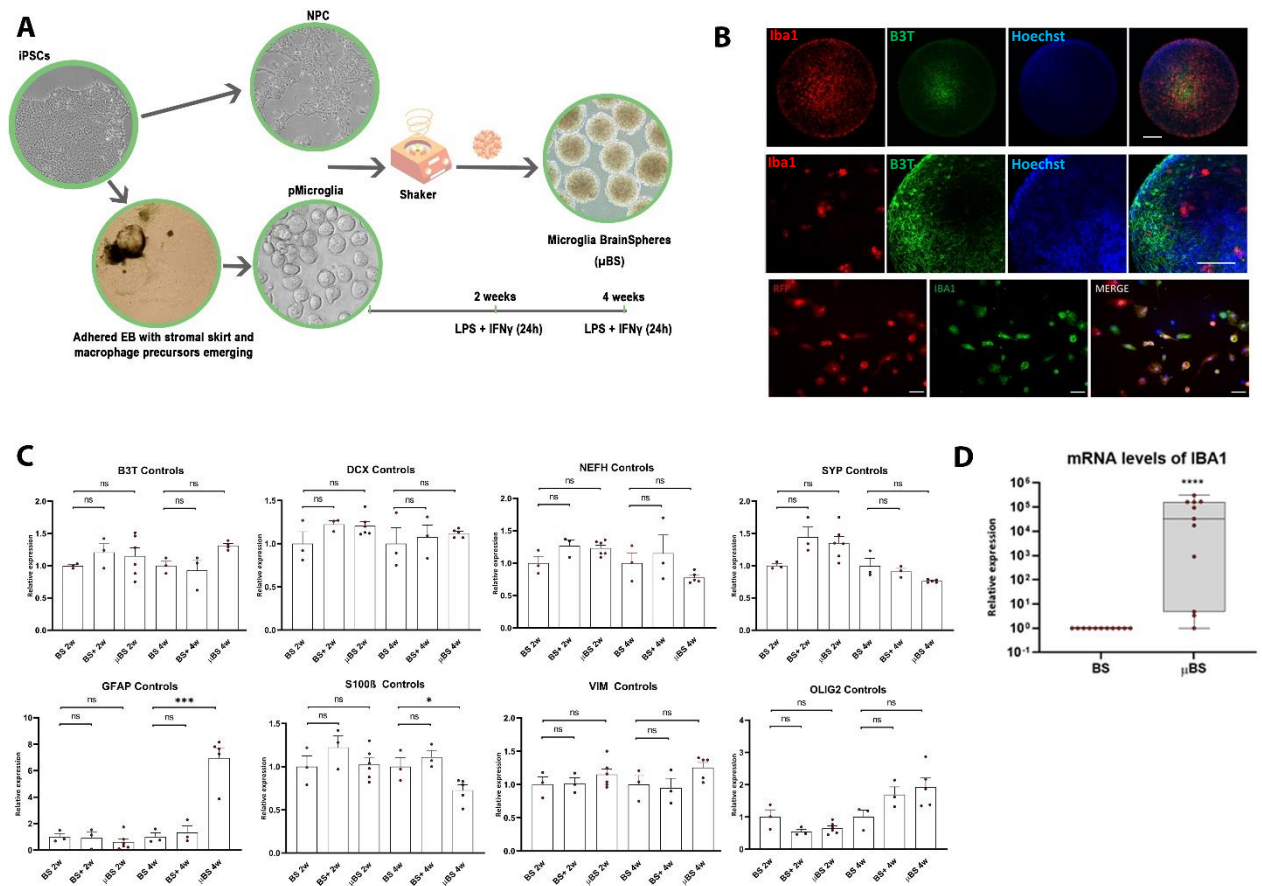


**Figure 2. Microglia progenitors successfully integrated in BS**

(A) Schematic description of the 3D culturing process. (B) Representative immunostaining images of different markers for neurons (B3T) and microglia (Iba1) of 2 weeks 3D  $\mu$ BS and RFP and Iba1 in 2D pMicroglia (last line). Scale bar = 50 $\mu$ m. (n = 3). (C) Gene expression of neuronal (B3T, DCX, NEFH, SYP), oligodendrocyte marker (OLIG2) and astrocytic (S100 $\beta$ , GFAP and VIM) markers in BS, BS+ and  $\mu$ BS after 2 and 4 weeks in culture. Each bar represents the mean ( $\pm$ SD) of 3 (BS and BS+) and 5 ( $\mu$ BS) samples. (D) Gene expression of the microglia marker Iba1 in BS and  $\mu$ BS after 2 in culture. Each bar represents the mean ( $\pm$ SD) of 11 samples collected in 3 different experiments.

The presence of microglia-like cells in the BS did not induce statistically significant change in the mRNA expression of neuronal markers (B3T, DCX, NEFH, SYP), and oligodendrocyte marker (OLIG2) (Figure 1C). The astrocyte markers GFAP and S100 $\beta$  were downregulated in  $\mu$ BS as compared to BS, whereas Vimentin mRNA remained unchanged. The strong reduction in GFAP mRNA level was also found in BS+, indicating this effect is due to IL34 and GM-CSF. However, we could not observe any morphological changes in GFAP immunohistochemistry (not shown). In the case of S100 $\beta$ , we observed a decrease only in  $\mu$ BS, indicating that this change may be due to the microglia incorporation and not to the addition of growth factors.

### 3.2. Inflammatory stimulus activates microglia-like cells in BrainSpheres

In order to determine whether microglia-like cells in BS can be activated by an immune challenge, BS and  $\mu$ BS were exposed to LPS and IFN $\gamma$ , then their morphology and the expression of inflammatory related genes were studied. Under physiological conditions, microglial cells present highly ramified and long processes with a small soma, which allow them exert their surveillance function (Colonna and Butovsky, 2017). The activation of microglia is characterized by a change from ramified to amoeboid morphology, by the production of certain cytokines, and by the increased expression of complement receptors and histocompatibility complex molecules (Graeber *et al.*, 2011). Immunohistochemistry showed that both red fluorescent protein (RFP) and IBA1 marker staining were able to identify microglia-like cells into the BS (Figure 2A). Ramified microglia-like cells were observed in control  $\mu$ BS after both 2 weeks and 4 weeks in culture. After exposure to LPS and IFN $\gamma$ , microglia-like cells (MLCs) reversed to amoeboid morphology, suggesting that MLCs are activable (Figure 2A).

Gene expression levels of transcription factors involved in neuroinflammation (NFkB1, NFkB2, STAT1, STAT3), pro-inflammatory (TNF $\alpha$ , IL1 $\beta$ , IL6) cytokine, anti-inflammatory cytokine (IL10), and microglia marker (IBA1) were quantified (Figure 2B). After exposure to LPS and IFN $\gamma$ , a significant increase in TNF $\alpha$ , IL1 $\beta$ , IL6 and NFkB2 mRNA was observed at the two developmental stages (2w and 4w) only in the presence of MLC ( $\mu$ BS black vs white columns), while no change was observed in BS (Figure 2B). For NFkB1, the increase was significant only when cells were exposed after 4 weeks in culture, and for IL-10 mRNA, the increase was observed only after 2 weeks in culture. LPS and IFN $\gamma$  also induced an increase in STAT1 and STAT3 mRNA levels in  $\mu$ BS (Figure 2B), however the same effect was observed in BS.

These results show a clear difference in the inflammatory response in  $\mu$ BS compared to BS, although they do not allow to distinguish which cell type is responsible for the diverse gene upregulation observed.

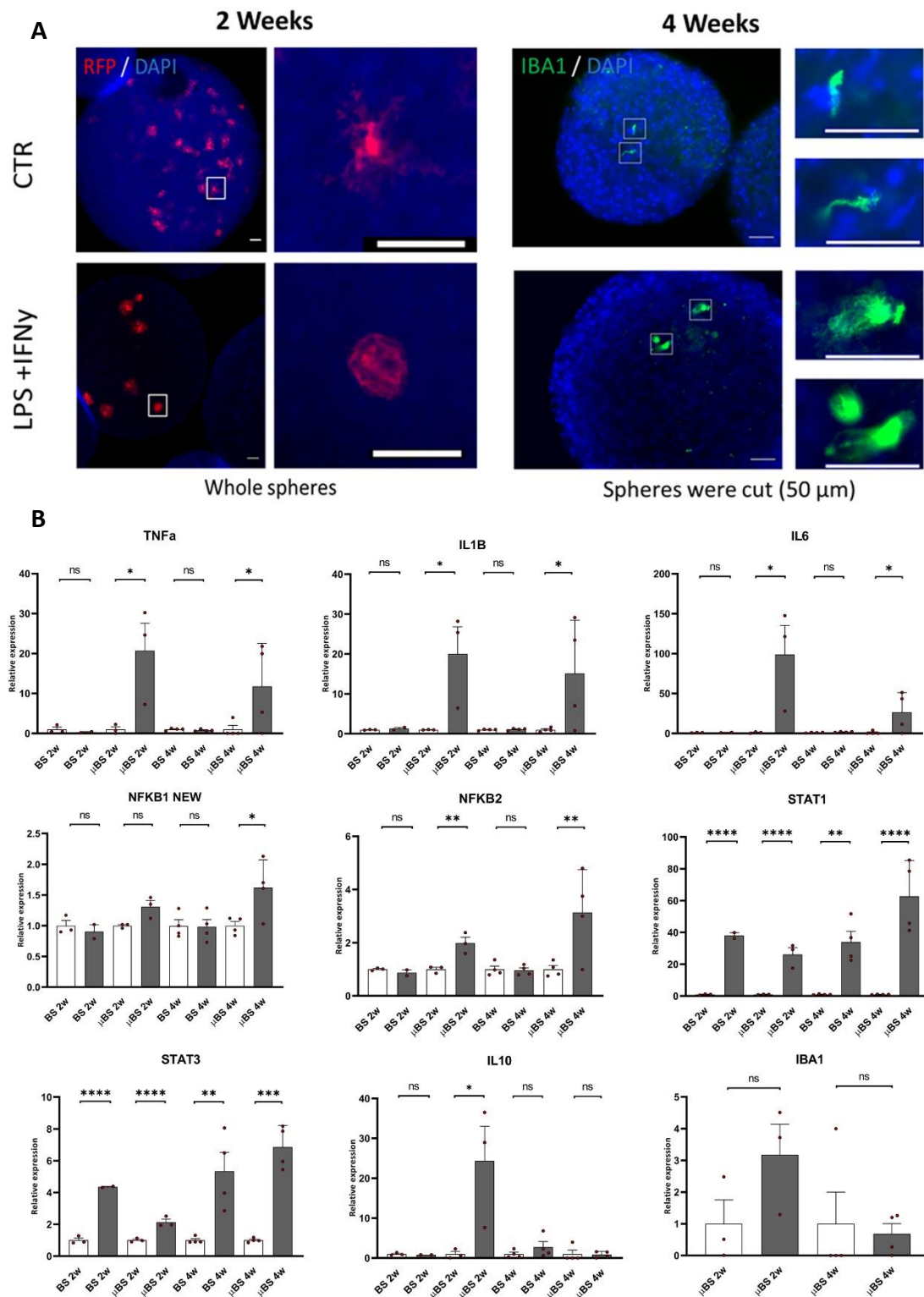


**Figure 2. Inflammatory stimulus activates microglia-like cells in BrainSpheres**

(A) Representative immunostaining images of the microglia marker Iba1 and RFP fluorescence of  $\mu$ BS after 2 and 4 weeks in culture control or exposed to LPS + IFN $\gamma$  for 24h. Scale bar = 50 $\mu$ m. (B) Gene expression of different neuroinflammation markers in BS, BS+ and  $\mu$ BS after 2 and 4 weeks in culture. Each bar represents the mean ( $\pm$ SD) of 3 - 4 samples.

### 3.3. LPS and IFN $\gamma$ induce astrocyte activation and subsequent oligodendrocytes damage in human BrainSpheres only in presence of microglia-like cells

The interplay between microglia and astrocyte activation, as well as the detrimental effects of activated microglia and astrocytes on other brain cells types have been described, therefore we looked for these effects in our new *in vitro* model, in order to evaluate its ability to develop a complete neuroinflammatory response (Jha *et al.*, 2018; Vainchtein and Molofsky, 2020).

First, we assessed the effects of the treatment on the astrocytes. After 24h of exposure to LPS and IFN $\gamma$ , vimentin mRNA level stayed unchanged in all groups (Fig. 3B), S100 $\beta$  was significantly upregulated in  $\mu$ BS only at 2 weeks of differentiation. The strongest effect was observed on GFAP mRNA level in  $\mu$ BS at 4 weeks, suggesting astrocyte activation. Immunostaining did not allow to show any change at the protein level for GFAP or S100 $\beta$  (Fig. 3A and 3C) in such a short exposure time. FK506-binding protein 5 (FKBP5) and proteasome subunit beta type-8 (PSMB8) have been shown by Liddelov *et al.* to be upregulated in the astrocytes activated in the deleterious way (A1 phenotype), and pentraxin 3 (PTX3) to be upregulated in the alternate astrocyte activation (A2 phenotype) (Liddelov *et al.*, 2017). Here, we observed an upregulation of FKBP5 only in presence of microglia and only at week 4 of culture, the upregulation of PSMB8 also in BS (Fig. 3 B), and no change in PTX3 mRNA level. These results may indicate the activation of astrocyte towards the deleterious phenotype.

Activation of astrocytes and microglia are known to produce deleterious effects on neurons and oligodendrocytes. We therefore assessed the status of these two brain cell types after exposure to LPS and IFN $\gamma$ . mRNA and protein levels of BIII-Tubulin (B3T) and synaptophysin (SYP) were not affected by the treatment (Fig. 3 A and B), whereas immunostaining for O4, a marker of oligodendrocytes, was strongly decreased only in  $\mu$ BS, at 4 weeks (Fig. 3 A). OLIG2 mRNA level decreased in  $\mu$ BS at 4 weeks, but not significantly. However, OLIG2 was strongly decreased after one week of repeated exposure (not shown). Gene expression for myelin markers, myelin basic protein (MBP), Proteolipid Protein 1 (PLP1) and myelin oligodendrocyte glycoprotein (MOG), remained unchanged, suggesting that oligodendrocytes are affected in this short exposure time, but not the myelin sheet (Fig. 3B).

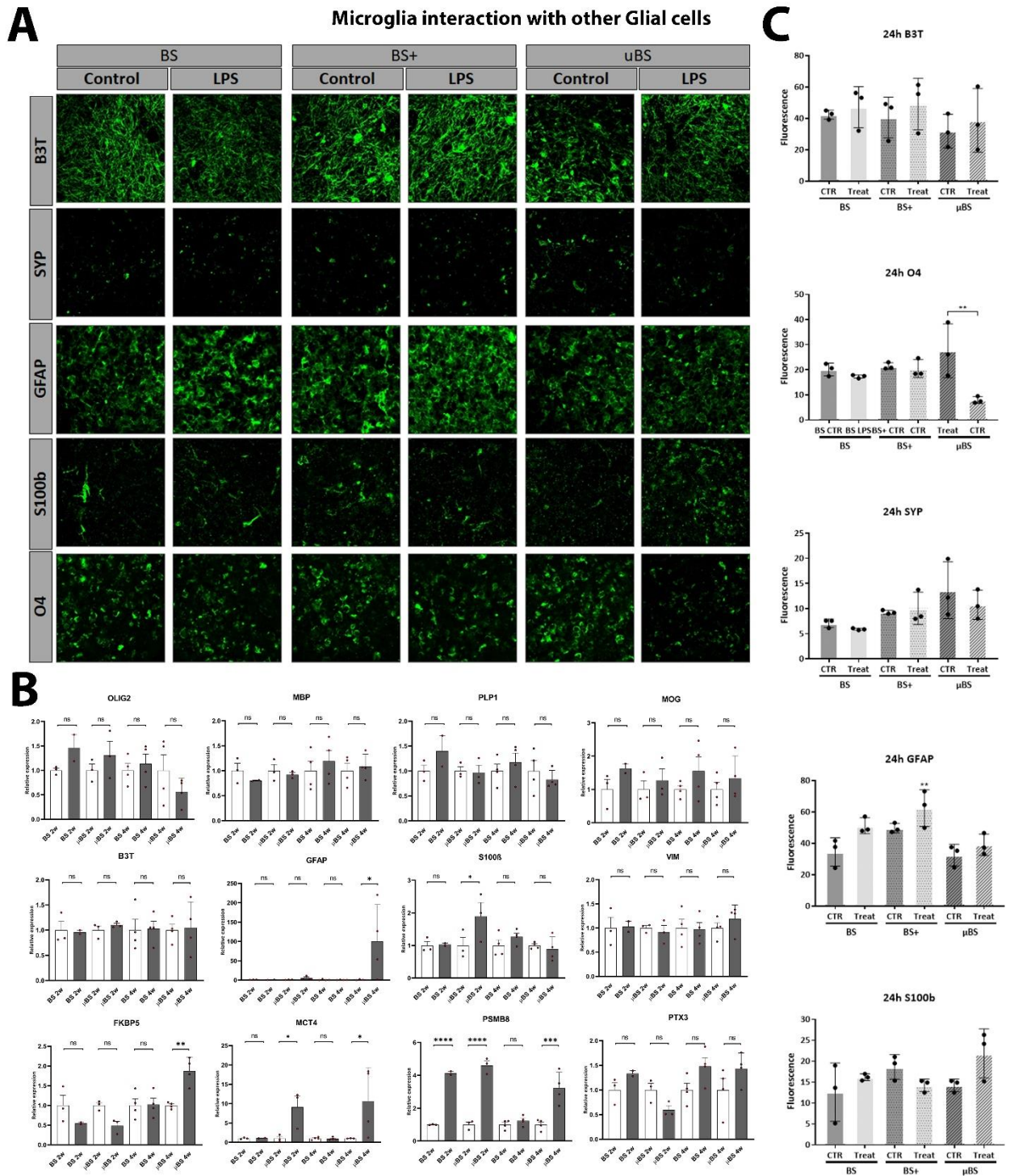


**Figure 3. Upon activation, MLC may lead to deleterious effects on oligodendrocytes.**

(A) Representative immunostaining images of B3T (neurons), SYP (synapses), GFAP and S100β (astrocytes) and O4 (oligodendrocytes) markers in BS, BS+ and μBS after 4 weeks in culture control or exposed to LPS + IFNγ (LPS) for 24h. Scale bar = 50μm. (B) Gene expression of different neuronal- (B3T), astrocytic- (GFAP, S100β, VIM, FKBP5, MCT4, PSMB8 and PTX3), oligodendrocytic- (Olig2) and myelin (MBP, PLP1 and MOG) markers in BS, BS+ and μBS after 2 and 4 weeks in culture. Each bar represents the mean (±SD) of 3 - 4 samples. (C) ImageJ quantifications of 3 pictures per condition in A.

#### 4. Discussion

BrainSpheres constitute a novel tool for neurotoxicity investigations, to study neurological diseases and also brain injury (Pamies *et al.*, 2018c, 2017b; Plummer *et al.*, 2019a; Zander *et al.*, 2017; Zhong *et al.*, 2020a). However, microglia, the key cell type to trigger and sustain neuroinflammation, is not present in the model since they do not differentiate from the same lineage than the brain parenchymal cells forming the BS. We previously incorporated the SV40 immortalized human microglia into BS, however, their constant proliferation does not reflect the *in vivo* situation (Abreu *et al.*, 2018). For this reason, here we attempted to improve the BS model by the incorporation of microglia derived from hiPSCs, to generate a more physiologically relevant model.

In this protocol, the formation of the spheres starts with a single cell suspension of NPC and microglia progenitors (pMicroglia) maintained under gyratory shaking to generate BrainSpheres containing microglia ( $\mu$ BS). The ratio of pMicroglia:NPCs should be chosen to reach a proportion of microglia-like cells (MLCs) in the spheres comparable to the *in vivo* situation. The ratio 1:4 gave visually the most satisfying results among the ones we tried (data not shown). However, the quantification of the precise proportion of MLCs in  $\mu$ BS is absolutely required and will be performed in the future. After two weeks in culture inside the spheres, microglia progenitors exhibited a ramified morphology, suggesting their differentiation in surveillant microglia cells due to the favourable environment formed by neurons, astrocytes and oligodendrocytes present in the BS.

After an immune challenge consisting of LPS and IFN $\gamma$ , MLCs in  $\mu$ BS lost their ramifications, suggesting their activation (Figure 2A). Supporting this fact, the levels NF $\kappa$ B2 and pro-inflammatory cytokines increased only in the spheres containing microglia like cells (Figure 2B). MLCs therefore proved to be functional in  $\mu$ BS as they respond to the classical LPS and IFN $\gamma$  stimulus. These results are in line with those reported by Cowley's lab (47) which provided us with pMicroglia. In their study, microglia progenitors as well as co-culture of neurons and MLCs also showed higher levels of TNF $\alpha$  and IL6 after LPS and IFN $\gamma$  exposure, and this increase was higher in co-cultures than in neurons alone. We also report higher levels of IL1 $\beta$ , an observation that was not reported by Haenseler.

During neuroinflammation, activated microglia induce deleterious astrocytes reactivity (A1) (Liddelow *et al.*, 2017). A1 astrocytes gain neurotoxic functions, killing neurons and oligodendrocytes. Interestingly, we found that astrocytic markers (GFAP and S100 $\beta$ ) and A1 marker (FKBP5) increased in  $\mu$ BS after immune challenge, suggesting astrocyte activation towards A1 phenotype, while the expression of these markers did not change in BS (Figure 2B).

The lack of microglia in BS seem to prevent this mechanism from occurring. Furthermore, monocarboxylate transporter 4 (MCT4) expression is upregulated after LPS + IFN $\gamma$  also in BS only. This increase may be attributed to astrocytes and/or microglial cells, since both cell types express this transporter and upregulate it when they are activated (Pierre and Pellerin, 2005). These results are in line with the reported MCT4 increase in macrophages after LPS + IFN $\gamma$  exposure associated to increased glycolysis and lactate production sustaining the inflammatory response in immune cells and they consolidate the fact that  $\mu$ BS can replicate a complete neuroinflammatory response (Tan *et al.*, 2015).

We investigated the impact of the neuroinflammatory cascade on neurons and oligodendrocytes in  $\mu$ BS. While neurons were not altered by both single and repeated exposure to LPS and IFN $\gamma$  (Figure 3A and 3B) according to the markers we used, oligodendrocytes appeared to be already affected after 24h exposure (Figure 3A), as seen by the decreased signal observed in preliminary immunostaining for O4 after challenge compared to control (Figure 3). Interestingly, Liddelow *et al.* reported that A1 reactive astrocytes killed mature oligodendrocytes and inhibited oligodendrocyte precursor cell proliferation and differentiation (Liddelow *et al.*, 2017). Our results suggest that during neuroinflammation in  $\mu$ BS, astrocytes are activated and impact oligodendrocytes. We did not see effects on neurons in  $\mu$ BS after single and repeated challenge, whereas Liddelow *et al.* reported the killing of neurons exposed to reactive astrocytes. A one-week exposure to LPS and IFN $\gamma$  may have been too short to impact the neurons, or we investigated too few markers to detect deleterious effects on neurons. Alternatively, it may be due to inter-species differences, since Liddelow *et al.* worked on rodent cells whereas in the present study we used human cells.

In this study, we have developed a protocol to generate a 3D *in vitro* system able to mimic a complete neuroinflammatory response. We now must improve the stability of the Microglia-BrainSphere model and characterize it in depth. Indeed, the survival of the microglia-like cells was not optimal, since their number decreased with time in culture, and we couldn't perform experiments after 4 weeks in culture. Different approaches are possible, such as the adjunction of other factors to increase the survival of MLCs. A good candidate is the transforming growth factor beta (TGF- $\beta$ ) which was found to be of importance for microglia function (Qin *et al.*, 2018). One difficulty of this protocol is that a large proportion of microglia progenitors was not incorporated in the spheroids at the start of the culture. Therefore, different plates could be used to generate the spheroids, such as the ones proposed by SunBioscience ("SUN bioscience SA," n.d.), which are standardized culture platforms limiting adhesion to the wells. This may increase the number of pMicroglia incorporated in the

BrainSpheres. Alternatively, we are currently testing the invasion of already formed BS whose cells express elevated levels of fractalkine mRNA (fig.3 ), a cytokine attracting microglia and important for microglia functions (Paolicelli *et al.*, 2014). This would be a more physiological solution since microglia progenitors invade the developing human brain at around four weeks of development. Finally, extensive characterization of  $\mu$ BS in terms proportion of microglia-like cells present in the spheres and functionality of these cells, including release of cytokines and phagocytosis capability, is required in order to delimitate the application domain of this new cell culture model.

## 5. Conclusions

Our results suggest that the presence of microglia is necessary for the activation of astrocytes, and therefore confirm the work of Liddelow *et al.* (56), emphasizing the importance of the new cell culture model we are developing. Adding microglia in the BrainSphere model allows to generate a human *in vitro* model able to reproduce different steps of neuroinflammation. Improvements of this model will permit more accurate *in vitro* studies of the human neuroinflammatory response and a better detection of neurotoxicity.

## Funding

This work was funded by the Swiss Centre for Applied Human Toxicology (SCAHT).

## Authors' contributions

CN was involved in study design, performed most of the experiments and immunostaining and analyzed the data. KRC performed part of the experiments and analyzed the samples. DT performed qRT-PCR analyses. SC provided the iPSC-derived microglia. DP and MG were involved in study design, supervised the experiments and wrote the manuscript. All authors contributed to improve the manuscript and approved the final version.

## Acknowledgements

We are grateful to MSCA-ITN in3 #721975 and to the Swiss Centre for Applied Human Toxicology (SCAHT) for funding this study.

## 6. References

- Abreu, C.M., Gama, L., Krasemann, S., Chesnut, M., Odwin-Dacosta, S., Hogberg, H.T., Hartung, T., Pamies, D., 2018. Microglia Increase Inflammatory Responses in iPSC-Derived Human BrainSpheres. *Front. Microbiol.* 0, 2766. <https://doi.org/10.3389/FMICB.2018.02766>
- Abud, E.M., Ramirez, R.N., Martinez, E.S., Healy, L.M., Nguyen, C.H.H., Newman, S.A., Yeromin, A. V., Scarfone, V.M., Marsh, S.E., Fimbres, C., Caraway, C.A., Fote, G.M., Madany, A.M., Agrawal, A., Kaye, R., Gylys, K.H., Cahalan, M.D., Cummings, B.J., Antel, J.P., Mortazavi, A., Carson, M.J., Poon, W.W., Blurton-Jones, M., 2017. iPSC-Derived Human Microglia-like

- Cells to Study Neurological Diseases. *Neuron* 94, 278-293.e9. <https://doi.org/10.1016/J.NEURON.2017.03.042>
- Bachiller, S., Jiménez-Ferrer, I., Paulus, A., Yang, Y., Swanberg, M., Deierborg, T., Boza-Serrano, A., 2018. Microglia in Neurological Diseases: A Road Map to Brain-Disease Dependent-Inflammatory Response. *Front. Cell. Neurosci.* 0, 488. <https://doi.org/10.3389/FNCEL.2018.00488>
- Carson, M.J., Crane, J., Xie, A.X., 2008. Modeling CNS microglia: the quest to identify predictive models. *Drug Discov. Today Dis. Model.* 5, 19–25. <https://doi.org/10.1016/J.DDMOD.2008.07.006>
- Colonna, M., Butovsky, O., 2017. Microglia Function in the Central Nervous System During Health and Neurodegeneration. <https://doi.org/10.1146/annurev-immunol-051116-052358> 35, 441–468. <https://doi.org/10.1146/ANNUREV-IMMUNOL-051116-052358>
- Defaux, A., Zurich, M.G., Honegger, P., Monnet-Tschudi, F., 2011. Minocycline promotes remyelination in aggregating rat brain cell cultures after interferon- $\gamma$  plus lipopolysaccharide-induced demyelination. *Neuroscience* 187, 84–92. <https://doi.org/10.1016/J.NEUROSCIENCE.2011.04.053>
- Defaux, A., Zurich, M.G., Honegger, P., Monnet-Tschudi, F., 2010. Inflammatory responses in aggregating rat brain cell cultures subjected to different demyelinating conditions. *Brain Res.* 1353, 213–224. <https://doi.org/10.1016/J.BRAINRES.2010.07.016>
- F, M.-T., MG, Z., BM, R., P, H., 1995. Effects of trimethyltin (TMT) on glial and neuronal cells in aggregate cultures: dependence on the developmental stage. *Neurotoxicology* 16, 97–104.
- Fakhoury, M., 2017. Microglia and astrocytes in Alzheimer’s disease: implications for therapy. *Curr. Neuropharmacol.* 15. <https://doi.org/10.2174/1570159X15666170720095240>
- Forsby, A., Bal-Price, A.K., Camins, A., Coecke, S., Fabre, N., Gustafsson, H., Honegger, P., Kinsner-Ovaskainen, A., Pallas, M., Rimbau, V., Rodríguez-Farré, E., Suñol, C., Vericat, J.A., Zurich, M.G., 2009. Neuronal *in vitro* models for the estimation of acute systemic toxicity. *Toxicol. Vitr.* 23, 1564–1569. <https://doi.org/10.1016/J.TIV.2009.07.017>
- Geloso, M.C., Corvino, V., Marchese, E., Serrano, A., Michetti, F., D’Ambrosi, N., 2017. The Dual Role of Microglia in ALS: Mechanisms and Therapeutic Approaches. *Front. Aging Neurosci.* 0, 242. <https://doi.org/10.3389/FNAGI.2017.00242>
- Graeber, M.B., 2010. Changing face of microglia. *Science (80-. )*. 330, 783–788. <https://doi.org/10.1126/SCIENCE.1190929>
- Graeber, M.B., Li, W., Rodriguez, M.L., 2011. Role of microglia in CNS inflammation. *FEBS Lett.* 585, 3798–3805. <https://doi.org/10.1016/J.FEBSLET.2011.08.033>
- Haenseler, W., Rajendran, L., 2019. Concise Review: Modeling Neurodegenerative Diseases with Human Pluripotent Stem Cell-Derived Microglia. *Stem Cells* 37, 724–730. <https://doi.org/10.1002/STEM.2995>
- Haenseler, W., Sansom, S.N., Buchrieser, J., Newey, S.E., Moore, C.S., Nicholls, F.J., Chintawar, S., Schnell, C., Antel, J.P., Allen, N.D., Cader, M.Z., Wade-Martins, R., James, W.S., Cowley, S.A., 2017. A Highly Efficient Human Pluripotent Stem Cell Microglia Model Displays a Neuronal-Co-culture-Specific Expression Profile and Inflammatory Response. *Stem Cell Reports* 8, 1727–1742. <https://doi.org/10.1016/J.STEMCR.2017.05.017>
- Hansen, D. V., Hanson, J.E., Sheng, M., 2018. Microglia in Alzheimer’s disease. *J. Cell Biol.* 217, 459–472. <https://doi.org/10.1083/JCB.201709069>
- Haukedal, H., Freude, K., 2019. Implications of Microglia in Amyotrophic Lateral Sclerosis and Frontotemporal Dementia. *J. Mol. Biol.* 431, 1818–1829. <https://doi.org/10.1016/J.JMB.2019.02.004>
- Ho, M.S., 2019. Microglia in Parkinson’s Disease. *Adv. Exp. Med. Biol.* 1175, 335–353. [https://doi.org/10.1007/978-981-13-9913-8\\_13](https://doi.org/10.1007/978-981-13-9913-8_13)
- Jha, M.K., Jo, M., Kim, J.-H., Suk, K., 2018. Microglia-Astrocyte Crosstalk: An Intimate Molecular

- Conversation: <https://doi.org/10.1177/1073858418783959> 25, 227–240.  
<https://doi.org/10.1177/1073858418783959>
- Lancaster, M.A., Knoblich, J.A., 2014. Generation of cerebral organoids from human pluripotent stem cells. *Nat. Protoc.* 9, 2329–2340. <https://doi.org/10.1038/nprot.2014.158>
- Lee, S.C., Liu, W., Brosnan, C.F., Dickson, D.W., 1994. GM-CSF promotes proliferation of human fetal and adult microglia in primary cultures. *Glia* 12, 309–318. <https://doi.org/10.1002/GLIA.440120407>
- Leite, P.E.C., Pereira, M.R., Harris, G., Pamies, D., dos Santos, L.M.G., Granjeiro, J.M., Hogberg, H.T., Hartung, T., Smirnova, L., 2019. Suitability of 3D human brain spheroid models to distinguish toxic effects of gold and poly-lactic acid nanoparticles to assess biocompatibility for brain drug delivery. *Part. Fibre Toxicol.* 2019 161 16, 1–20. <https://doi.org/10.1186/S12989-019-0307-3>
- Lenz, K.M., Nelson, L.H., 2018. Microglia and Beyond: Innate Immune Cells As Regulators of Brain Development and Behavioral Function. *Front. Immunol.* 0, 698. <https://doi.org/10.3389/FIMMU.2018.00698>
- Liddelw, S.A., Guttenplan, K.A., Clarke, L.E., Bennett, F.C., Bohlen, C.J., Schirmer, L., Bennett, M.L., Münch, A.E., Chung, W.-S., Peterson, T.C., Wilton, D.K., Frouin, A., Napier, B.A., Panicker, N., Kumar, M., Buckwalter, M.S., Rowitch, D.H., Dawson, V.L., Dawson, T.M., Stevens, B., Barres, B.A., 2017. Neurotoxic reactive astrocytes are induced by activated microglia. *Nat.* 2017 5417638 541, 481–487. <https://doi.org/10.1038/nature21029>
- Livak, K.J., Schmittgen, T.D., 2001. Analysis of Relative Gene Expression Data Using Real-Time Quantitative PCR and the 2- $\Delta\Delta$ CT Method. *Methods* 25, 402–408. <https://doi.org/10.1006/METH.2001.1262>
- LR, W., MR, H., 2014. A concern on comparing “apples” and “oranges” when differences between microglia used in human and rodent studies go far, far beyond simply species: comment on Smith and Dragunow. *Trends Neurosci.* 37, 189–190. <https://doi.org/10.1016/J.TINS.2014.02.004>
- Mathews, S., Branch Woods, A., Katano, I., Makarov, E., Thomas, M.B., Gendelman, H.E., Poluektova, L.Y., Ito, M., Gorantla, S., 2019. Human Interleukin-34 facilitates microglia-like cell differentiation and persistent HIV-1 infection in humanized mice. *Mol. Neurodegener.* 2019 141 14, 1–15. <https://doi.org/10.1186/S13024-019-0311-Y>
- Mestas, J., Hughes, C.C.W., 2004. Of Mice and Not Men: Differences between Mouse and Human Immunology. *J. Immunol.* 172, 2731–2738. <https://doi.org/10.4049/JIMMUNOL.172.5.2731>
- Michaelson, M.D., Bieri, P.L., Mehler, M.F., Xu, H., Arezzo, J.C., Pollard, J.W., Kessler, J.A., 1996. CSF-1 deficiency in mice results in abnormal brain development. *Development* 122, 2661–2672. <https://doi.org/10.1242/DEV.122.9.2661>
- Monnet-Tschudi, F., Zurich, M.G., Honegger, P., 1996. Comparison of the developmental effects of two mercury compounds on glial cells and neurons in aggregate cultures of rat telencephalon. *Brain Res.* 741, 52–59. [https://doi.org/10.1016/S0006-8993\(96\)00895-5](https://doi.org/10.1016/S0006-8993(96)00895-5)
- Monnet-Tschudi, F., Zurich, M.G., Pithon, E., van Melle, G., Honegger, P., 1995. Microglial responsiveness as a sensitive marker for trimethyltin (TMT) neurotoxicity. *Brain Res.* 690, 8–14. [https://doi.org/10.1016/0006-8993\(95\)00509-O](https://doi.org/10.1016/0006-8993(95)00509-O)
- Mrdjen, D., Pavlovic, A., Hartmann, F.J., Schreiner, B., Utz, S.G., Leung, B.P., Lelios, I., Heppner, F.L., Kipnis, J., Merkler, D., Greter, M., Becher, B., 2018. High-Dimensional Single-Cell Mapping of Central Nervous System Immune Cells Reveals Distinct Myeloid Subsets in Health, Aging, and Disease. *Immunity* 48, 380–395.e6. <https://doi.org/10.1016/J.IMMUNI.2018.01.011>
- Muffat, J., Li, Y., Omer, A., Durbin, A., Bosch, I., Bakiasi, G., Richards, E., Meyer, A., Gehrke, L., Jaenisch, R., 2018. Human induced pluripotent stem cell-derived glial cells and neural

- progenitors display divergent responses to Zika and dengue infections. *Proc. Natl. Acad. Sci.* 115, 7117–7122. <https://doi.org/10.1073/PNAS.1719266115>
- Nandi, S., Gokhan, S., Dai, X.M., Wei, S., Enikolopov, G., Lin, H., Mehler, M.F., Richard Stanley, E., 2012. The CSF-1 receptor ligands IL-34 and CSF-1 exhibit distinct developmental brain expression patterns and regulate neural progenitor cell maintenance and maturation. *Dev. Biol.* 367, 100–113. <https://doi.org/10.1016/J.YDBIO.2012.03.026>
- Nayernia, Z., Turchi, L., Cosset, E., Peterson, H., Dutoit, V., Dietrich, P.Y., Tirefort, D., Chneiweiss, H., Lobrinus, J.A., Krause, K.H., Virolle, T., Preynat-Seauve, O., 2013. The relationship between brain tumor cell invasion of engineered neural tissues and *in vivo* features of glioblastoma. *Biomaterials* 34, 8279–8290. <https://doi.org/10.1016/J.BIOMATERIALS.2013.07.006>
- Nimmerjahn, A., Kirchhoff, F., Helmchen, F., 2005. Neuroscience: Resting microglial cells are highly dynamic surveillants of brain parenchyma *in vivo*. *Science* (80- ). 308, 1314–1318. <https://doi.org/10.1126/SCIENCE.1110647>
- Ormel, P.R., Vieira de Sá, R., van Bodegraven, E.J., Karst, H., Harschnitz, O., Sneeboer, M.A.M., Johansen, L.E., van Dijk, R.E., Scheefhals, N., Berdenis van Berlekom, A., Ribes Martínez, E., Kling, S., MacGillavry, H.D., van den Berg, L.H., Kahn, R.S., Hol, E.M., de Witte, L.D., Pasterkamp, R.J., 2018. Microglia innately develop within cerebral organoids. *Nat. Commun.* 2018 91 9, 1–14. <https://doi.org/10.1038/s41467-018-06684-2>
- Pamies, D., Barrera, P., Block, K., Makri, G., Kumar, A., Wiersma, D., Smirnova, L., Zhang, C., Bressler, J., Christian, K.M., Harris, G., Ming, G., Berlinicke, C.J., Kyro, K., Song, H., Pardo, C.A., Hartung, T., Hogberg, H.T., 2017a. A Human Brain Microphysiological System Derived from Induced Pluripotent Stem Cells to Study Neurological Diseases and Toxicity. *ALTEX* 34, 362. <https://doi.org/10.14573/ALTEX.1609122>
- Pamies, D., Barreras, P., Block, K., Makri, G., Kumar, A., Wiersma, D., Smirnova, L., Zhang, C., Bressler, J., Christian, K.M., Harris, G., Ming, G.L., Berlinicke, C.J., Kyro, K., Song, H., Pardo, C.A., Hartung, T., Hogberg, H.T., 2017b. A human brain microphysiological system derived from induced pluripotent stem cells to study neurological diseases and toxicity. *ALTEX* 34, 362–376. <https://doi.org/10.14573/altex.1609122>
- Pamies, D., Block, K., Lau, P., Gribaldo, L., Pardo, C.A., Barreras, P., Smirnova, L., Wiersma, D., Zhao, L., Harris, G., Hartung, T., Hogberg, H.T., 2018. Rotenone exerts developmental neurotoxicity in a human brain spheroid model. *Toxicol. Appl. Pharmacol.* 354, 101–114. <https://doi.org/10.1016/J.TAAP.2018.02.003>
- Pamies, D., Hartung, T., 2017. 21st Century Cell Culture for 21st Century Toxicology HHS Public Access. *Chem Res Toxicol* 30, 43–52. <https://doi.org/10.1021/acs.chemrestox.6b00269>
- Paolicelli, R.C., Bisht, K., Tremblay, M.-È., 2014. Fractalkine regulation of microglial physiology and consequences on the brain and behavior. *Front. Cell. Neurosci.* 0, 129. <https://doi.org/10.3389/FNCEL.2014.00129>
- Paşca, A.M., Sloan, S.A., Clarke, L.E., Tian, Y., Makinson, C.D., Huber, N., Kim, C.H., Park, J.-Y., O'Rourke, N.A., Nguyen, K.D., Smith, S.J., Huguenard, J.R., Geschwind, D.H., Barres, B.A., Paşca, S.P., 2015. Functional cortical neurons and astrocytes from human pluripotent stem cells in 3D culture. *Nat. Methods* 12, 671–678. <https://doi.org/10.1038/nmeth.3415>
- Pérez-Cerdá, F., Sánchez-Gómez, M.V., Matute, C., 2015. Pío del Río Hortega and the discovery of the oligodendrocytes. *Front. Neuroanat.* 0, 92. <https://doi.org/10.3389/FNANA.2015.00092>
- Pierre, K., Pellerin, L., 2005. Monocarboxylate transporters in the central nervous system: distribution, regulation and function. *J. Neurochem.* 94, 1–14. <https://doi.org/10.1111/J.1471-4159.2005.03168.X>
- Plummer, S., Wallace, S., Ball, G., Lloyd, R., Schiapparelli, P., Quiñones-Hinojosa, A., Hartung, T., Pamies, D., 2019a. A Human iPSC-derived 3D platform using primary brain cancer cells to

- study drug development and personalized medicine. *Sci. Reports* 2019 9, 1–11. <https://doi.org/10.1038/s41598-018-38130-0>
- Plummer, S., Wallace, S., Ball, G., Lloyd, R., Schiapparelli, P., Quiñones-Hinojosa, A., Hartung, T., Pamies, D., 2019b. A Human iPSC-derived 3D platform using primary brain cancer cells to study drug development and personalized medicine. *Sci. Rep.* 9, 1–11. <https://doi.org/10.1038/s41598-018-38130-0>
- Purisai, M.G., McCormack, A.L., Cumine, S., Li, J., Isla, M.Z., Di Monte, D.A., 2007. Microglial activation as a priming event leading to paraquat-induced dopaminergic cell degeneration. *Neurobiol. Dis.* 25, 392–400. <https://doi.org/10.1016/J.NBD.2006.10.008>
- Qin, Y., Garrison, B.S., Ma, W., Wang, R., Jiang, A., Li, J., Mistry, M., Bronson, R.T., Santoro, D., Franco, C., Robinton, D.A., Stevens, B., Rossi, D.J., Lu, C., Springer, T.A., 2018. A Milieu Molecule for TGF- $\beta$  Required for Microglia Function in the Nervous System. *Cell* 174, 156–171.e16. <https://doi.org/10.1016/J.CELL.2018.05.027>
- Sandström von Tobel, J., Zoia, D., Althaus, J., Antinori, P., Mermoud, J., Pak, H.S., Scherl, A., Monnet-Tschudi, F., 2014. Immediate and delayed effects of subchronic Paraquat exposure during an early differentiation stage in 3D-rat brain cell cultures. *Toxicol. Lett.* 230, 188–197. <https://doi.org/10.1016/j.toxlet.2014.02.001>
- Smith, A.M., Dragunow, M., 2014. The human side of microglia. *Trends Neurosci.* 37, 125–135. <https://doi.org/10.1016/J.TINS.2013.12.001>
- Song, L., Yuan, X., Jones, Z., Vied, C., Miao, Y., Marzano, M., Hua, T., Sang, Q.-X.A., Guan, J., Ma, T., Zhou, Y., Li, Y., 2019. Functionalization of Brain Region-specific Spheroids with Isogenic Microglia-like Cells. *Sci. Reports* 2019 9, 1–18. <https://doi.org/10.1038/s41598-019-47444-6>
- Speicher, A.M., Wiendl, H., Meuth, S.G., Pawlowski, M., 2019. Generating microglia from human pluripotent stem cells: novel *in vitro* models for the study of neurodegeneration. *Mol. Neurodegener.* 2019 14, 1–16. <https://doi.org/10.1186/S13024-019-0347-Z>
- Szepesi, Z., Manouchehrian, O., Bachiller, S., Deierborg, T., 2018. Bidirectional Microglia–Neuron Communication in Health and Disease. *Front. Cell. Neurosci.* 0, 323. <https://doi.org/10.3389/FNCEL.2018.00323>
- Tan, Z., Xie, N., Banerjee, S., Cui, H., Fu, M., Thannickal, V.J., Liu, G., 2015. The Monocarboxylate Transporter 4 Is Required for Glycolytic Reprogramming and Inflammatory Response in Macrophages \*. *J. Biol. Chem.* 290, 46–55. <https://doi.org/10.1074/JBC.M114.603589>
- Thion, M.S., Low, D., Silvin, A., Chen, J., Grisel, P., Schulte-Schrepping, J., Blecher, R., Ulas, T., Squarzonni, P., Hoefel, G., Culpier, F., Siopi, E., David, F.S., Scholz, C., Shihui, F., Lum, J., Amoyo, A.A., Larbi, A., Poidinger, M., Buttgerit, A., Lledo, P.M., Greter, M., Chan, J.K.Y., Amit, I., Beyer, M., Schultze, J.L., Schlitzer, A., Pettersson, S., Ginhoux, F., Garel, S., 2018. Microbiome Influences Prenatal and Adult Microglia in a Sex-Specific Manner. *Cell* 172, 500–516.e16. <https://doi.org/10.1016/J.CELL.2017.11.042>
- Timmerman, R., Burm, S.M., Bajramovic, J.J., 2018. An Overview of *in vitro* Methods to Study Microglia. *Front. Cell. Neurosci.* 0, 242. <https://doi.org/10.3389/FNCEL.2018.00242>
- Vainchtein, I.D., Molofsky, A. V., 2020. Astrocytes and Microglia: In Sickness and in Health. *Trends Neurosci.* 43, 144–154. <https://doi.org/10.1016/J.TINS.2020.01.003>
- Von Tobel, J.S., Antinori, P., Zurich, M.G., Rosset, R., Aschner, M., Glück, F., Scherl, A., Monnet-Tschudi, F., 2014. Repeated exposure to Ochratoxin A generates a neuroinflammatory response, characterized by neurodegenerative M1 microglial phenotype. *Neurotoxicology* 44, 61–70. <https://doi.org/10.1016/J.NEURO.2014.04.005>
- Wang, Y.-Q., Berezovska, O., Fedoroff, S., 1999. Expression of Colony Stimulating Factor-1 Receptor (CSF-1R) by CNS Neurons in Mice. *J. Neurosci. Res* 57, 616–632. [https://doi.org/10.1002/\(SICI\)1097-4547\(19990901\)57:5](https://doi.org/10.1002/(SICI)1097-4547(19990901)57:5)
- Wei, S., Nandi, S., Chitu, V., Yeung, Y.-G., Yu, W., Huang, M., Williams, L.T., Lin, H., Stanley, E.R.,

2010. Functional overlap but differential expression of CSF-1 and IL-34 in their CSF-1 receptor-mediated regulation of myeloid cells. *J. Leukoc. Biol.* 88, 495–505. <https://doi.org/10.1189/JLB.1209822>
- Zander, N.E., Piehler, T., Hogberg, H., Pamies, D., 2017. Explosive Blast Loading on Human 3D Aggregate Minibrains. *Cell. Mol. Neurobiol.* 2017 377 37, 1331–1334. <https://doi.org/10.1007/S10571-017-0463-7>
- Zhong, X., Harris, G., Smirnova, L., Zufferey, V., Sá, R. de C. da S. e., Baldino Russo, F., Baleeiro Beltrao Braga, P.C., Chesnut, M., Zurich, M.G., Hogberg, H.T., Hartung, T., Pamies, D., 2020a. Antidepressant Paroxetine Exerts Developmental Neurotoxicity in an iPSC-Derived 3D Human Brain Model. *Front. Cell. Neurosci.* 14, 1–11. <https://doi.org/10.3389/fncel.2020.00025>
- Zhong, X., Harris, G., Smirnova, L., Zufferey, V., Sá, R. de C. da S. e., Baldino Russo, F., Baleeiro Beltrao Braga, P.C., Chesnut, M., Zurich, M.-G., Hogberg, H.T., Hartung, T., Pamies, D., 2020b. Antidepressant Paroxetine Exerts Developmental Neurotoxicity in an iPSC-Derived 3D Human Brain Model. *Front. Cell. Neurosci.* 0, 25. <https://doi.org/10.3389/FNCEL.2020.00025>
- Zurich, M.-G., Stanzel, S., Kopp-Schneider, A., Prieto, P., Honegger, P., 2013. Evaluation of aggregating brain cell cultures for the detection of acute organ-specific toxicity. *Toxicol. Vitr.* 27, 1416–1424. <https://doi.org/10.1016/j.tiv.2012.06.018>

---

## Chapter 7: Participation on the development of AOP17 Binding to SH/selen-proteins can trigger neuroinflammation leading to neurodegeneration

---

*This described KER is present on annex 3 of this manuscript.*

*The final AOP can be found at: <https://aopwiki.org/wiki/index.php/Aop:17>*

## 7.1. Abstract

This AOP describes the cascade of events initiated by binding to selenoproteins causing a depletion of glutathione (GSH), one of the most important anti-oxidants in the brain. This will lead to oxidative stress which is deleterious to neurons. Neuroinflammation, characterized by microglial and astrocyte reactivity, will be triggered in response to neuronal damage. When neuroinflammation induces a 'neurodegenerative phenotype' associated with the production of pro-inflammatory cytokines and the expression of specific microglial markers, it can lead to neurodegeneration, the adverse outcome. Neurodegeneration will amplify the inflammatory response and lead to a self-sustained neuroinflammation that exacerbates the neurodegenerative process. Such a self-sustained neuroinflammation-neurodegenerative loop is involved in neurodegenerative diseases such as Alzheimer's and Parkinson's diseases.

This AOP is relevant for neurotoxicity and developmental neurotoxicity testing following low dose and long-term exposure and for delayed adverse outcome, according to the Landrigan *et al.* (2005) hypothesis of early origins of neurodegenerative disease in later life. It is part of a broader effort initiated by JRC/Seurat to describe several AOPs relevant for neurotoxicity, that will be published in « Critical Reviews in Toxicology ». Currently, the only related endpoint for regulatory purposes is measurement of rodent brain glial fibrillary acidic protein (GFAP), whose increase is a marker of astrocyte reactivity; this is required by the US EPA for fuel additives but is optional for other chemical hazard evaluations.

## 7.2. Contribution

During the development of AOP17 I contributed for the bibliography search and description of the key event relationship (KER) "Stress leads to cell injury/death" between the key event "Oxidative Stress" and the key event "Cell injury/death".

---

## Chapter 8: Discussion

---

*“The brain is a world consisting of a number of unexplored continents and great stretches of unknown territory.”*  
Santiago Ramon y Cajal

Humans are continuously exposed to chemicals through skin contact, inhalation and ingestion. The contact with the chemicals can be through the surrounding environment, diet, household products and occupational activities (Fryer *et al.*, 2006). From all the chemicals that we are exposed to, such as pesticides, glues, solvents, metals, several are known to induce CNS related effects. In 2014, a literature review identified 214 neurotoxicants (Grandjean and Landrigan, 2014). Exposure to neurotoxicants is not so rare, from this 214 roughly half are identified as high production chemicals and others are largely consumed, like alcohol (Trantham-Davidson and Chandler, 2015; Wang *et al.*, 2018).

The understanding of the potential harmful effects of chemicals in the CNS can be used for the establishment of more reliable safe exposure limits. With these exposure limits better regulation can be put in place to protect individuals of potential detriment effects caused by chemicals.

Currently, chemical safety evaluation is carried out mainly employing whole animal tests. With the encouragement of regulatory authorities, hiPSC-derived models are increasingly used for *in vitro* neurotoxicity testing (Tukker *et al.*, 2018). These hiPSC-derived neural cultures bring the advantages of avoiding interspecies translation, being more ethically sound and the potential of being less costly than animal experimentation.

In 2017, Pamies *et al.* developed the protocol to obtain a 3D hiPSC-derived brain model called BrainSpheres (BS) (Pamies *et al.*, 2017a). This protocol drives the differentiation of neuroprogenitor cells (NPC) into neurons, astrocytes and oligodendrocyte and allows strong cell-to-cell interactions, exemplified by the presence of compact myelin and spontaneous electrical activity. From evaluation of the developmental neurotoxicity (DNT) of the drug paroxetine to the study of the process of SARS-CoV infection in the brain, BS model has been used in different field of research (Bullen *et al.*, 2020; Zhong *et al.*, 2020a).

With the goal of using BS for neurotoxicity testing, its ability to respond to various classes of chemicals and to replicate human response needs to be evaluated. The work presented in this dissertation described the efforts made to characterize which biological processes are present and can be affected upon chemical exposure in BS plus the work done on adding microglia-like cells to be able to access neuroinflammation. In the last 4 years, (i) BS model was successfully established in our lab from a new cell line; (ii) Toxicodynamics and toxicokinetics were established after acute and repeated exposure of BS to several drugs and environmental compounds; (iii) The ability of BS to respond to chemicals by the main known toxicology pathways was determined and (iv) Attempts were made to improve the performance of the BS model by adding microglia.

### 8.1. Successful establishment of BrainSpheres using a new hiPSC line

The model BS was developed at the Center for Alternatives to Animal Testing of Johns Hopkins University, Baltimore, USA. There, BS were established using NPC derived from the hiPSC line CCD-1079Sk (ATCC® CRL2097™) using a protocol passing through the stages of embryonic bodies and neural tube-like rosettes (Wen *et al.*, 2014). For the establishment of the BS protocol in our lab, two protocols were tested for the preparation of NPCs, namely the dual inhibition of SMAD signalling (Stuart M. Chambers *et al.*, 2009) and a protocol by Gibco using a defined PSC Neural Induction medium (Technologies, 2015), to produce NPCs from the SBAD3 hiPSC obtained from StemBANCC (Morrison, 2018). The cells obtained with the dual inhibition of SMAD signalling protocol could not be kept for more than 4 passages and, very importantly, could not be frozen and thawed, preventing us from preparing a bank of cells. Since the Ad3G2 NPCs obtained with the 7-day Gibco protocol were stable, as observed by flow cytometry analyses (Suppl. Table 5), able to proliferate for at least 14 passages, to be frozen and thawed, they were chosen to be used for the preparation of BS.

Even using a different hiPSC line and a different technique to produce NPCs than in the original publication, the BS model was successfully established. Characterization by RT-qPCR and immunohistochemistry showed that BS derived from the Ad3G2 NPCs present very similar developmental-dependent gene and protein expression than reported in the original publication (Fig. 1 chapter 3 and (Pamies *et al.*, 2017a). In detail, BS presented a decreasing gene expression of stem cell and proliferation markers (Nestin, Sox2, NANOG and Ki67) and increasing expression of neuronal markers (MAP2, GRIN1, ACHE, TH and GRIN1), astrocytic and oligodendrocytic markers (S100 $\beta$ , GFAP, Vimentin and Olig2) over weeks in culture. Immunocytochemistry with NF200 and GFAP showed comparable staining patterns indicating the development of cell neuronal and astrocytic cell processes from week 2 to 8 in culture. Staining with the oligodendrocytic marker, showed the presence of positive O4 cells at all time-points. Comparing our results with the ones obtained by Pamies *et al.* 2017, there are clear similarities in gene and protein expression between the BS produced in the two labs indicate that BS with the same cell composition can be derived from NPCs produced with different techniques and from a different donor.

A further characterization of the model was performed by TempO-Seq analysis on NPCs and BS collected after each week in culture. As a targeted gene expression technique, TempO-Seq was performed with the EU-ToxRisk v2.1 panel (Limonciel *et al.*, 2018; Mav *et al.*, 2018). This panel of 3565 probes was designed to assess the expression of valuable genes for characterization of diseases, toxicity processes and several cell types. Regarding neural cells,

within the 3565 probes, there are genes related to neurons (GRIN1, MAP2, NEFL, BDNF, ACHE), astrocytes (S100B and GFAP), and oligodendrocytes (Olig1 and Olig2). The probe list also presents the pre-synaptic protein coding gene SYP. After preliminary analysis, results showed that cells keep differentiating along the 8 weeks in culture with the biggest change happening between week 1 and 2 in culture (Fig 5.1). Further analysis must be done to better delineate the expression dynamics of neural genes along weeks in culture, as well as the development-dependent expression of the toxicity pathways.

## **8.2. Establishment of an exposure window to assess effects on cell types and their interactions**

The human brain is a complex structure composed of highly specialized cells, i.e., astrocytes, microglia, neurons and oligodendrocytes (Purves *et al.*, 2004; Stiles and Jernigan, 2010). This cellular composition and the cell-cell interactions are essential to maintain brain homeostasis and functions (Purves *et al.*, 2004). In consequence, the disturbance of the cellular composition or of the cell-cell communications by xenobiotics can lead to neurotoxicity (Cerbai *et al.*, 2012; Pistollato *et al.*, 2020; Sandström *et al.*, 2017). Neurotoxicology (NT) is the study of adverse effects on nervous system resultant from an exposure to a chemical.

The development of the brain consists of a long sequence of complex processes that gives rise to a complex structure composed of highly specialized cells (Edwards, 2015; Fritsche *et al.*, 2018; Stiles and Jernigan, 2010). Trying to reproduce this complex processes and structure *in vitro* in a reasonable time window is a challenge. Development neurotoxicology can be studied in *in vitro* models starting from stem cells and that reproduce development steps. The assessment of effects of chemical exposure with the same *in vitro* models to predict NT must be made with caution. The work presented in this manuscript had the goal of assess chemical action mechanisms that could help predict NT. Due to the difficulty of deriving an *in vitro* model reflecting all the complexity of the adult brain, we focused on effects on a particular neural cell type and on cell-cell interactions with BS. To do so, it is of utmost necessity to have as much cell types as possible at exposure time, even if not completely differentiated.

Gene expression assessed with RT-qPCR shows that after 6 weeks in culture, Ad3G2 BS present significant expression of neuronal- (MAP2), astrocytic- (S100 $\beta$  and GFAP) and oligodendrocytic- (Olig2) markers. It was also possible to detect expression of specific markers of dopaminergic, glutamatergic and cholinergic neurons (TH, GRIN1 and ACHE) indicating their presence after 6 weeks in culture. Immunocytochemistry on BS after 6 weeks in culture shows

positive cells for markers of neurons (NF200), astrocytes (S100 $\beta$ ) and oligodendrocytes (O4) with differentiated pattern. Compared with earlier time points, there is an increased amount of positive staining for the pre-synaptic protein SYP after 6 weeks in culture indicating higher chances of presence of functional synapses. TempO-Seq data showed a reduced level of difference in comparison to NPC towards the end of time in culture indicating that cells are still differentiating but at a slower pace. Altogether, these results show the presence neurons, astrocytes and oligodendrocytes after 6 weeks in culture. Expression of the myelin protein encoding gene MBP and positive staining for SYP on 6 weeks old BS indicate cell-cell interaction. Starting the exposures at this time allow us to go for acute, repeated and repeated plus a wash-out period exposure keeping the protocol described 8 weeks in culture.

### **8.3. Exposure concentration and their epidemiological relevance**

In 2007 the US National Research Council (NRC) proposed a paradigm shift in toxicology for the 21st century (Tox 21) (NRC, 2007). In the report “Toxicity Testing in the 21st Century: A Vision and a Strategy” the NRC proposes a re-orientation from empirical, animal-based testing to a mechanistic understanding of chemical-induced biological perturbations in toxicity pathways and networks, for predictive toxicology (Hartung *et al.*, 2017; Roper and Tanguay, 2020).

One of the aims of this doctoral thesis was to evaluate to which extent the BS could allow the detection of the diverse mechanisms of toxicity triggered by chemicals. Since the goal was to evaluate organ-specific effects, it was important to use concentrations that (i) avoid over cytotoxicity but still produce effects on the system and (ii) are epidemiologic relevant.

For VPA, AMI, Pb, PQ and DOXO, viability was assessed by MTT assay after exposure of BS to a wide range of concentrations. Concentration-dependent curves for cytotoxicity were established after 48h and 7d exposures, as well as after 7 days of exposure followed by one week of washout period (7dW) depending on the chemical. Except for VPA, it was possible to obtain concentration-dependent curves. BS shown differential sensitivity to all these chemicals, as seen by the comparison of the IC<sub>50</sub> after a 7-day exposure (AMI = 1.8  $\mu$ M; PQ = 7.7  $\mu$ M; Pb = 11  $\mu$ M; DOXO = 113 nM), that may be explained by BS differential dependency on the affected biological processes by each chemical, or by the toxicokinetics characteristics of each chemical. Indeed, the later would affect the available concentration of chemical that interacts with the different targets and therefore would have an impact on the cytotoxicity (Ankley *et al.*, 2010; Escher *et al.*, 2005). Concentration-dependent curves of AMI and PQ were established for acute and repeated exposure, in both cases, BS showed more sensitivity to a repeated exposure.

Distribution kinetics quantification of AMI in the BS system showed an accumulation of AMI after the 7d repeated exposure in the cell fraction explaining the higher sensitivity detected after the repeated exposure. Future distribution kinetics on BS exposed to PQ should also help to understand the difference in the cytotoxicity observed after acute and repeated exposure.

Concentrations used for the investigation of neuro-specific effects were chosen in order to assure that BS were exposed to at least one concentration <IC<sub>20</sub> for cytotoxicity after repeated exposure of 1 week.

Plasma concentrations found in literature were used to assess the epidemiological relevance of the concentrations used in the experiments. AMI, VPA and DOXO concentrations used were relevant, according to the literature. Indeed, in patients undergoing long term treatment, AMI can reach 0.5-1.2  $\mu\text{M}$  in plasma (Lafuente-Lafuente *et al.*, 2009), whereas patients undergoing daily treatment of VPA till 3000 mg/day present an average 300  $\mu\text{M}$  in plasma (Haroutiunian *et al.*, 2009). Finally, it was detected 51.7 nM to 6.9  $\mu\text{M}$  of DOXO in plasma of patients with breast cancer (Barpe *et al.*, 2010). On the other hand, the concentrations used for PQ and Pb in this study, are higher than the quantified amount in plasma and cerebrospinal fluid (CSF). Quantifications of Pb in plasma of 110 workers in a Pb smelter showed a range of 0.0015 and 0.13  $\mu\text{M}$  (Bergdahl *et al.*, 1997). The lead content of cerebrospinal fluid (CSF) of 12 patients was between 0.06 – 0.2  $\mu\text{M}$  (Conradi *et al.*, 1976). Paraquat poisoning patients survived with PQ plasma levels less than 0.39  $\mu\text{M}$  after 24h to 0.023  $\mu\text{M}$  after 15 days after ingestion (Scherrmann *et al.*, 1987). In a 14-months-old poisoned boy, it was possible to detect 0.02  $\mu\text{M}$  PQ in the CSF 90 days after the acute exposure (Houzé *et al.*, 1990). To better assess the relevance of the concentrations of chemical used *in vitro*, not only quantification of each chemical in the CSF and quantification of their passage through the BBB are needed, but also, the *in vitro* distribution toxicokinetics is of highest importance.

#### **8.4. BS can be used to assess chemical effect on different biological processes**

Understanding which pathways are disturbed by a chemical provides a mechanistic insight on how a chemical can affect an organ upon exposure and potentially help uncover its molecular initiating event (MIE) (Jennings, 2015b; Jennings *et al.*, 2013). Recent toxicogenomic data shows that xenobiotics can induce several stress pathways, such as oxidative stress pathway, endoplasmic reticulum stress pathway, UPR and metal response, as an attempt to restore homeostasis (Limonciel *et al.*, 2018; Singh *et al.*, 2021; Wellens *et al.*, 2021). In order to gain insight into the ability of BS to react to diverse classes of chemicals, these cultures were exposed to model chemicals known to trigger stress pathways.

From a list of chemicals known to activate particular biological processes upon exposure, cadmium was used as a known activator of the oxidative stress and the metal response pathway (Singh *et al.*, 2021). TempO-Seq analysis showed an upregulation of different metallothionein (MTs), MT1M, MT1G, MT1F, MT1E, MT1X and MT2A in cadmium-exposed BS. Metallothionein's are known to be regulated by metal response elements (Juárez-Rebollar *et al.*, 2017). Although their expression changed with time, these genes kept being significantly upregulated from 6 to 48h after exposure. In general, metal response genes were so strongly differently expressed that their associated gene ontology biological processes presented very low P-adjusted values at all the assessed time-points. Differently, the biological process "response to oxidative stress" only presented a sufficiently low P-adjusted value after 24h. Also, the exposure to Pb significantly affected genes related to oxidative stress, such as NQO1 and HMOX1. On BS exposed to PQ, besides oxidative stress, was detected effects on endoplasmic reticulum (ER) stress related genes linked to two different unfolded protein responses (UPR) biological processes (PERK and ATF6 mediated UPR). Effects of PQ exposure on ER stress and UPR were already described in human lung epithelial cells (Chinta *et al.*, 2008; Omura *et al.*, 2013).

Besides oxidative stress effects, the chemical used along this work produced effect on other biological processes. One of the known secondary effects of a long term treatment with AMI is the development of liver steatosis due to disturbed lipid metabolism (Anthérieu *et al.*, 2011; Wandrer *et al.*, 2020). After analysis, AMI exposure in BS gave rise to several DEG associated with lipid metabolism. To our knowledge, this is the first time that AMI lipid disturbance is demonstrated in brain cells. As previously described in rat cardiomyocytes, DOXO produced differentially expression of genes involved in DNA damage biological processes (L'Ecuyer *et al.*, 2006). Even if no direct inhibitory effect on HDAC was detected after VPA exposure, TempO-Seq analysis identified several differentially expressed histones.

Even if further analysis needs to be done to completely characterize each pathway found disturbed in BS after exposures, the results obtained indicate that BS can be used to assess effects of chemicals on diverse pathways. More work must be done to fully understand the expression dynamics of the interest genes of each pathway along development and along exposure. Additional characterization will come from the analysis of the TempO-seq data obtained after exposure of BS to rotenone to study mitochondria complex I, to Antimycin A for the mitochondria complex III, to Tunicamycin for the UPR and finally to Arsenic to completely assess Nrf2 mediated response.

## 8.5. Distribution kinetics, an important player in neurotoxicity assessment

With reliable quantitative *in vitro* to *in vivo* extrapolations (QIVIVE) in mind, understanding the link between nominal concentration (i.e., concentration added to the *in vitro* system), free concentration for uptake in the medium and concentration of the chemical accumulated in the cells is extremely important to establish in an *in vitro* exposure (Groothuis *et al.*, 2015; Kramer *et al.*, 2015; Proença *et al.*, 2021). In BS model, that means quantifying the available chemical before and after exposure in the medium, in the cell and plastic fraction. Determination of these different concentrations allow the establishment of concentration-effect relationships.

Although is not clear if AMI goes through the human BBB, small quantities can be found in the brain (Adams *et al.*, 1985). Patients undergoing continuous treatment with AMI describe several secondary effects such as tremor, ataxia and peripheral neuropathy that can be traced back to the CNS (Jafari-Fesharaki and Scheinman, 1998; Pathmanathan and Cleary, 2021; Pomponio *et al.*, 2015). Distribution kinetics of AMI in the BS showed that cells accumulated AMI along repeated exposure and released it at a low rate during the washout period. Considering that the CNS is not completely protected with a BBB structure (Miyata, 2015), even if AMI does not cross the BBB, and knowing that studies in bovine cells shows that it does not damage it either (Fabulas-da Costa *et al.*, 2013), it could reach the CNS. Here we showed that brain cells have the potential to accumulate AMI. Even if a small amount of AMI arrives to the CNS, if the treatment is long enough, it could reach a concentration that can produce detrimental effects on cells. It would be interesting to further investigate the effects of AMI on the brain cells metabolism by metabolomic approaches.

Used as treatment of epilepsy, bipolar disorders, and migraine, VPA is inefficiently delivered to the brain and clinical effects require high doses (Baltes *et al.*, 2007). This inefficiency is in part explained by the carrier-mediated exchange of VPA across the BBB with efflux transport being much more efficient than influx transport (Gibbs *et al.*, 2004). For bipolar disorder and seizures, the recommended VPA therapeutic range is 50–125 mg/L (0.3–0.8 mM) (Leo and Narendran, 1999; Methaneethorn, 2017). CNS toxicity in humans starts to be detected when VPA exceed 175–200 mg/L (1–1.2 mM) and coma from at least 850 mg/L (1.5 mM) in blood (Methaneethorn, 2018; Sztajnkrzyer, 2002). Distribution kinetics showed that BS did not efficiently take up VPA and did not accumulate it. This absence of accumulation may be due to a higher efflux than influx transport, as previously observed at the level of the BBB in rats (Kakee *et al.*, 2002). Cytotoxicity was only detectable after washout-out period for the highest VPA concentrations used. TempO-Seq analysis showed less DEG after repeated exposure than after

acute 48h exposure. Even if few effects were detected, repeated exposure caused the upregulation of oxidative stress markers and decreased expression of neuronal markers after repeated exposure. Knowing that CNS effects are correlated to very high VPA concentrations in the blood and that VPA seems not to be efficiently uptaken by the cells, the concentration used here were potentially too low to fully evaluate effects of VPA on BS.

The results obtained from AMI and VPA exposures emphasize the need to integrate the toxicokinetics of the chemicals and its physicochemical characteristics to the toxicodynamics data, in order to correctly evaluate the toxic effects of these chemicals *in vitro*.

## 8.6. TempO-Seq data analysis as a screening tool

Toxicogenomics combines transcript, protein and metabolite profiling with conventional toxicology to investigate changes in the interaction between genes caused by chemical exposure. (Waters and Fostel, 2004). As a more efficient way to characterise molecular events, toxicogenomics can be used to assess affected pathways helping predict chemical toxicity (Alexander-Dann *et al.*, 2018; Jennings *et al.*, 2013). The targeted gene expression technique TempO-Seq presents itself as a new, cost-effective and high throughput technique for toxicogenomic studies.

In the “in3” project, TempO-Seq for 3565 probes was used to assess the mechanistic toxicological response of different organ/structure representative models to diverse chemicals. In the case of this thesis, TempO-Seq was used to characterize the mechanism of action in different organ/structure representative models exposed to PQ and the response of BS to different chemicals. Along the different chapters, DeSeq2 package thresholds and over-representation analysis tools (e.g., ConsensusPathDB or biological processes from Gene Ontology) used were adapted to the type of study. For the comparison of PQ response in different models, there was the need to filter samples and probes, fix thresholds on differentially expressed genes (DEG) for P-adjusted values ( $<0.05$ ) and FDR ( $>|0.58|$ ) and the standard thresholds on ConsensusPathDB to be able to reliably compare data coming from different models maintaining high quality standard. For BS exposed to VPA, AMI, DOXO, Pb and CdCl<sub>2</sub>, the only threshold fixed was for P-adjusted value ( $<0.05$ ) for the DEG and for gene ontology over-representation analysis (P-adjusted value  $<0.01$  or  $<0.05$ ) to extract the most likely affected biological processes upon exposure.

Over-representation analysis of BS samples exposed to PQ using ConsensusPathDB and Gene Ontology showed some differences. Both strategies are able to detect general effects on neural cells, oxidative stress and lipids, but the number of pathways or biological processes

associated to these big groups clearly changes between ConsensusPathDB and Gene Ontology. The detected differences probably rise from the fact that each strategy used different databases leading to differences on gene-pathway association. To have a better overview of disruptions caused by chemical exposure, both approaches could be taken in consideration for all studies.

Differences between data analysis strategies reinforce the need to see this type of results as a screening that should be further confirmed by other gene and protein expression techniques. Having the opportunity to perform the different analysis myself showed me the influence of using different probe selection, statistical thresholds, and over-representation strategies on the final results. Acquired data should be interpreted in the light of the used workflow and confirmed before drawing any conclusion.

## 8.7. Microglia

Microglia is one of the key players in neuroinflammation, a process associated with damage in the CNS (Von Tobel *et al.*, 2014; Zurich *et al.*, 2002). Microglia are the brain-resident macrophages and the main immune cells in the brain. They constitute the primary defence line against the presence of pathogens but are also involved in injuries, neurodegenerative diseases and response to environmental compounds and drugs (Graeber, 2010; Mrdjen *et al.*, 2018). Their activation has been proposed as an indicator of neurotoxicity (Monnet-Tschudi *et al.*, 2007, 1995).

In development, immature macrophages migrate from the blood islands in the yolk sac to the primitive brain at around embryonic age 8 in mammalian embryo (Greter and Merad, 2013). In the brain these immature macrophages differentiate into microglia. Due to the interest on assess neuroinflammation upon chemical exposure, several attempts have been made to add microglia to BS. In this thesis, hiPSC-derived microglia progenitors were added to single-cell NPC and BS protocol was followed giving rise to BS with microglia-like cells ( $\mu$ BS). Upon exposure with LPS + IFN $\gamma$ , microglia-like cells presented signs of reactivity and potential caused detrimental effects on oligodendrocytes.

Even if it was possible to establish  $\mu$ BS with positive cells for the microglia/macrophage-specific Iba1 with surveillance phenotype, the model shows low reproducibility. The number of positive Iba1 cells was quite variable between spheres and experiments, so more replicates were considered per experiment. Due to loss of Iba1 positive cells after 4 weeks in culture, spheres were exposed after 2 and 4 weeks of development.

To obtain a reasonable number of integrated Iba1 positive cells in  $\mu$ BS, high yield of microglia progenitors is needed. There was a high number of microglia progenitors not

integrated in the spheres. To avoid this loss and increase the number of integrated progenitors in the spheres, we intend to test plates that induce aggregation developed and produced by Matthias Lutolf *et al.* (Girgin *et al.*, 2021). In order to have a model completely derived from the same hiPSC, a collaboration with the lab of Rosa Chiara Paolicelli is in place to derive the microglia progenitors from the same cell line used to derive the BS.

## 8.8. Concluding remarks and perspectives

Proper brain function depends critically on a wide range of highly regulated processes (p. ex. calcium homeostasis, neurotransmitter release and electrical activity) (Edwards, 2015). Due to the diversity of cell types and complexity of the biological processes involved, the human brain is very vulnerable to toxic insults and difficult to model *in vitro*. Today, a broad range of *in vitro* models are available to study the potential effects of chemicals on brain function (see chapter 1.4).

The work presented in this doctoral thesis adds precious information on the hiPSC-derived 3D model BS and therefore constitutes a contribution to the development of the *in vitro* models for a more human based and mechanistic neurotoxicity testing approach. The work developed in the different chapters demonstrates that BS were successfully established from a new NPC cell line giving rise to different types of neurons, astrocytes and oligodendrocytes strongly interacting in the 3D structure (Fig.: 8.1). In addition, the ability of keeping the model for a reasonable amount of time in culture allows the assessment of effects of acute and repeated exposures at different differentiation stages. Acquired data through different techniques showed that the main stress pathways can be activated upon chemicals exposure in BS, suggesting that most chemicals hazardous to brain could be detected with BS. The distinct cell types, cell-cell interactions and present biological processes grant a vast chemical targets to be assessed for neurotoxicity assessment. This work also shows the feasibility of determining distribution kinetics for chemicals in BS and how it can be used to help design more epidemiological-representative experiments. Therefore, BS could be a valuable asset for the extrapolation of very important kinetic values that will contribute to the development of reliable QIVIVE models.

However, even if BS can be used to assess many different parameters important for the prediction of neurotoxicity in humans, it has limitations. Due to the long and complex development time of a human brain together with its intricate structure, it is not viable to say that BS could completely model the human brain response to chemical exposure. Many different parameters have to be taken in consideration besides cell-cell interactions, cell type and

biological processes effects to properly model brain exposure and response to chemicals. In one side, BS do not fully represent the brain microenvironment, at least microglia cells and BBB representants are missing (Fig.: 8.1). Being neuroinflammation activation an important indicator or neurotoxicity and important for brain development and homeostasis, all the possible applications of BS would profit from having microglia integrated in the model. The amount of available chemical to interact with brain cells is highly dependent on the BBB permeability. On its turn, BBB permeability and behaviour can be altered by the exposure. Adding an exterior layer of BBB-like cells to BS could be highly valuable to understand the chemical biokinetics in the brain, predict the real amount of chemical that arrives to neuronal cells and its effects. From a structural point, BS also do not represent the structure of the brain since no particular organization is detected. On the other side, human exposure is a complex process that involves different absorption, distribution, metabolism and excretion (ADME) patterns between chemicals and individuals. As BS can be used to model the direct effects of the chemical in certain neural cells and pathways, additional *in vitro* (e.g., liver, BBB, etc) and *in silico* (e.g., PBK) models representing other structures/organs and ADME should be taken in account to aim predict the human neurotoxicity of a compound.

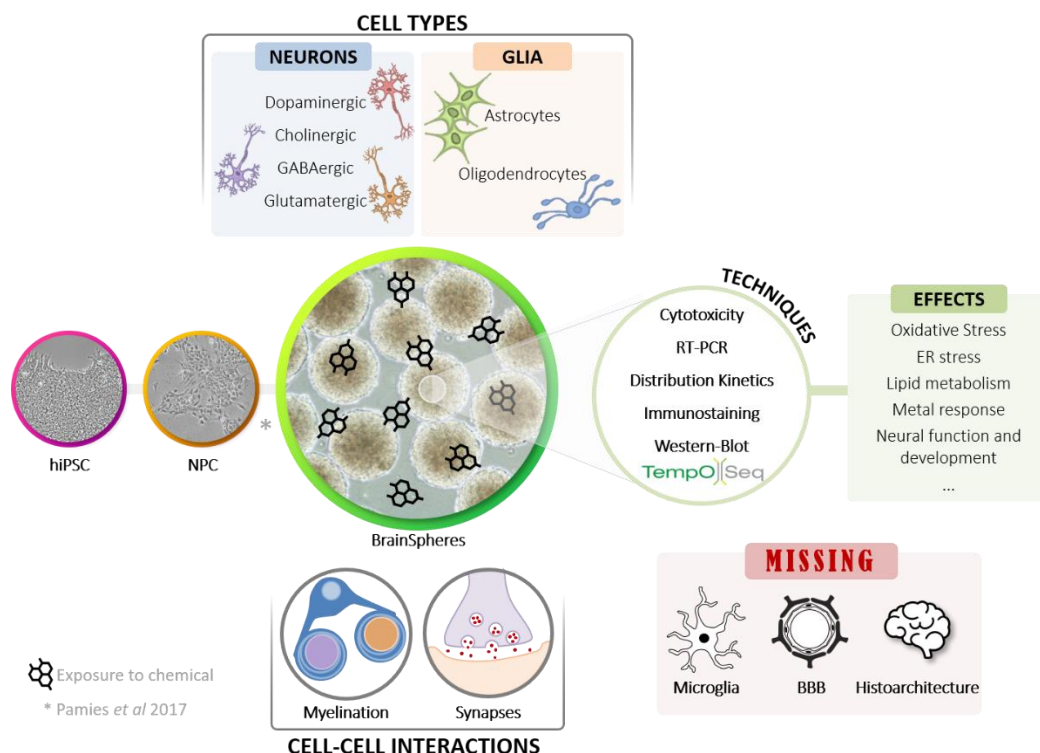


**Figure 8.1.: BrainSpheres (BS) indicates presence of different cell types, cell-cell interactions and biological processes**

Schematic description of BS protocol together with the detected cell types and cell-cell interactions. Upon exposure with different chemicals, it was possible to detect effects in different biological processes through different techniques. To fully represent the brain cell types and microenvironment, at least microglia-like cells, BBB representants and structure are missing.

As it stands now, BS is still a very expensive model to produce and far from the required high throughput level to be used in risk management decisions. Actions should be taken in the direction of adapting the protocol for smaller plates that would allow more replicate wells per experiment using the same resources. In case of success all the *in vitro* assays performed in BS would have to be adapted to the new format.

The AOP framework defines the links between a MIE and a final pathology or AO. During the last few years, I was personally involved in the complex but needed process of describing AOP 17 “Binding to SH/selen-proteins can trigger neuroinflammation leading to neurodegeneration”. One important step, after having an accepted AOP, is adding mechanism knowledge in order to have a quantitative AOP (qAOP). The quantification of an AOP will allow to define the threshold underlining the transition of upstream KE to downstream KE (Conolly *et al.*, 2017; LaLone *et al.*, 2017). The work presented in this dissertation showed that BS was able to replicate some of the known toxic mechanism for the 6 studied chemicals. The ability to reproduce the known mechanism of action of some chemicals, indicates that BS could be a good model to help develop qAOP linked to the brain. Currently, there is a collaboration between our lab and Prof. Mark Cronin’s lab to establish quantifications for some of the KE involved on the AOP13 “Chronic binding of antagonist to N-methyl-D-aspartate receptors (NMDARs) during brain development induces impairment of learning and memory abilities” on BS.

Finally, I believe that BS characterisation and amelioration should continue to be a priority. Keeping characterizing the possible uses of BS, such as to study neurological diseases, would allow to take the maximum advantage of this model. Further improvements, like efficiently adding microglia and BBB representative cells, would allow to increase the number of biological processes possible to study in BS. While keep going with the characterization, like myelination with electron microscopy or metabolomics and synapses with MEA chips, could help increase the range of end points possible to study in BS.

---

# References

---

- Abreu, C.M., Gama, L., Krasemann, S., Chesnut, M., Odwin-Dacosta, S., Hogberg, H.T., Hartung, T., Pamies, D., 2018. Microglia Increase Inflammatory Responses in iPSC-Derived Human BrainSpheres. *Front. Microbiol.* 0, 2766. <https://doi.org/10.3389/FMICB.2018.02766>
- Adams, P.C., Holt, D.W., Storey, G.C.A., Morley, A.R., Callaghan, J., Campbell, R.W., 1985. Amiodarone and its desethyl metabolite: Tissue distribution and morphologic changes during long-term therapy. *Circulation* 72, 1064–1075. <https://doi.org/10.1161/01.CIR.72.5.1064>
- Alexander-Dann, B., Pruteanu, L.L., Oerton, E., Sharma, N., Berindan-Neagoe, I., Módos, D., Bender, A., 2018. Developments in toxicogenomics: Understanding and predicting compound-induced toxicity from gene expression data. *Mol. Omi.* 14, 218–236. <https://doi.org/10.1039/c8mo00042e>
- Andryszak, P., Wilkość, M., Żurawski, B., Izdebski, P., 2018. Verbal memory in breast cancer patients treated with chemotherapy with doxorubicin and cyclophosphamide. *Eur. J. Cancer Care (Engl.)* 27, e12749. <https://doi.org/10.1111/ECC.12749>
- Ankley, G.T., Bennett, R.S., Erickson, R.J., Hoff, D.J., Hornung, M.W., Johnson, R.D., Mount, D.R., Nichols, J.W., Russom, C.L., Schmieder, P.K., Serrano, J.A., Tietge, J.E., Villeneuve, D.L., 2010. Adverse outcome pathways: A conceptual framework to support ecotoxicology research and risk assessment. *Environ. Toxicol. Chem.* 29, 730–741. <https://doi.org/10.1002/etc.34>
- Anthérieu, S., Rogue, A., Fromenty, B., Guillouzo, A., Robin, M.A., 2011. Induction of vesicular steatosis by amiodarone and tetracycline is associated with up-regulation of lipogenic genes in heparg cells. *Hepatology* 53, 1895–1905. <https://doi.org/10.1002/hep.24290>
- Aotani, E., Hamano, T., Gemma, A., Takeuchi, M., Takebayashi, T., Kobayashi, K., 2016. Identification of adverse events that have a negative impact on quality of life in a clinical trial comparing docetaxel versus S-1 with cisplatin in lung cancer. *Int. J. Clin. Oncol.* 2016 215 21, 836–842. <https://doi.org/10.1007/S10147-016-0960-6>
- Bailey, M.D., 2007. *Magic and superstition in Europe : a concise history from antiquity to the present.* Rowman & Littlefield Pub.
- Bal-Price, A., Pistollato, F., Sachana, M., Bopp, S.K., Munn, S., Worth, A., 2018. Strategies to improve the regulatory assessment of developmental neurotoxicity (DNT) using in vitro methods. *Toxicol. Appl. Pharmacol.* 354, 7–18. <https://doi.org/10.1016/j.taap.2018.02.008>
- Bal-Price, C., Coecke, S., Costa, L., Crofton, K.M., Fritsche, E., Goldberg, A., Grandjean, P., Lein, P.J., Li, A., Lucchini, R., Mundy, W.R., Padilla, S., Persico, A.M., M Seiler, A.E., Kreysa, J., 2012. Conference Report: Advancing the Science of Developmental Neurotoxicity (DNT): Testing for Better Safety Evaluation.
- Baltes, S., Fedrowitz, M., Tortós, C.L., Potschka, H., Löscher, W., 2007. Valproic acid is not a substrate for P-glycoprotein or multidrug resistance proteins 1 and 2 in a number of *in vitro* and *in vivo* transport assays. *J. Pharmacol. Exp. Ther.* 320, 331–343. <https://doi.org/10.1124/jpet.106.102491>
- Barpe, D.R., Rosa, D.D., Froehlich, P.E., 2010. Pharmacokinetic evaluation of doxorubicin plasma levels in normal and overweight patients with breast cancer and simulation of dose adjustment by different indexes of body mass. *Eur. J. Pharm. Sci.* 41, 458–463. <https://doi.org/10.1016/j.ejps.2010.07.015>
- Bergdahl, I., Schütz, A., Gerhardsson, L., Jensen, A., 1997. Lead concentrations in human plasma , urine and whole blood Author ( s ): Ingvar A Bergdahl , Andrejs Schütz , Lars Gerhardsson , Anker Jensen and Staffan Skerfving Source : Scandinavian Journal of Work , Environment

- & Health , October 1997 , Vol . 23 , P 23, 359–363.
- Bernson, V., Clausen, J., Ekwall, B., HOLME, J., HOGBERG, J., Niemi, M., Walum, E., 1986. Trends in Scandinavian cell toxicology. *ATLA-ALTERNATIVES TO Lab. Anim.* 13, 162–179.
- Boon, R., Kumar, M., Tricot, T., Elia, I., Ordovas, L., Jacobs, F., One, J., De Smedt, J., Eelen, G., Bird, M., Roelandt, P., Doglioni, G., Vriens, K., Rossi, M., Vazquez, M.A., Vanwelden, T., Chesnais, F., El Taghdouini, A., Najimi, M., Sokal, E., Cassiman, D., Snoeys, J., Monshouwer, M., Hu, W.S., Lange, C., Carmeliet, P., Fendt, S.M., Verfaillie, C.M., 2020. Amino acid levels determine metabolism and CYP450 function of hepatocytes and hepatoma cell lines. *Nat. Commun.* 11, 1–16. <https://doi.org/10.1038/s41467-020-15058-6>
- Box, G.E.P., Draper, N.R., 1987. Empirical model-building and response surfaces 669.
- Bullen, C.K., Hogberg, H.T., Bahadirli-Talbott, A., Bishai, W.R., Hartung, T., Keuthan, C., Looney, M.M., Pekosz, A., Romero, J.C., Sillé, F.C.M., Um, P., Smirnova, L., 2020. Infectability of human BrainSphere neurons suggests neurotropism of SARS-CoV-2. *ALTEX - Altern. to Anim. Exp.* 37, 665–671. <https://doi.org/10.14573/ALTEX.2006111>
- Cerbai, F., Lana, D., Nosi, D., Petkova-Kirova, P., Zecchi, S., Brothers, H.M., Wenk, G.L., Giovannini, M.G., 2012. The Neuron-Astrocyte-Microglia Triad in Normal Brain Ageing and in a Model of Neuroinflammation in the Rat Hippocampus. *PLoS One* 7. <https://doi.org/10.1371/journal.pone.0045250>
- Chambers, S.M., Fasano, C.A., Papapetrou, E.P., Tomishima, M., Sadelain, M., Studer, L., 2009. Highly efficient neural conversion of human ES and iPS cells by dual inhibition of SMAD signaling. *Nat. Biotechnol.* 27, 275–280. <https://doi.org/10.1038/nbt.1529>
- Chambers, S.M., Fasano, C.A., Papapetrou, E.P., Tomishima, M., Sadelain, M., Studer, L., Author, N.B., 2009. Highly efficient neural conversion of human ES and iPS cells by dual inhibition of SMAD signaling HHS Public Access Author manuscript. *Nat Biotechnol* 27, 275–280. <https://doi.org/10.1038/nbt.1529>
- Chandrasekaran, V., Carta, G., Pereira, C., Gupta, R., Murphy, C., Feifel, E., Kern, G., Lechner, J., Cavallo, A.L., Gupta, S., Caiment, F., Kleinjans, J.C.S., Gstraunthaler, G., 2021. Generation and characterization of iPSC - derived renal proximal tubule - like cells with extended stability. *Sci. Rep.* 1–17. <https://doi.org/10.1038/s41598-021-89550-4>
- Chinta, S.J., Rane, A., Poksay, K.S., Bredesen, D.E., Andersen, J.K., Rao, R. V., 2008. Coupling endoplasmic reticulum stress to the cell death program in dopaminergic cells: Effect of paraquat. *NeuroMolecular Med.* 10, 333–342. <https://doi.org/10.1007/s12017-008-8047-9>
- Chinta, S.J., Woods, G., Demaria, M., Rane, A., Zou, Y., McQuade, A., Rajagopalan, S., Limbad, C., Madden, D.T., Campisi, J., Andersen, J.K., 2018. Cellular Senescence Is Induced by the Environmental Neurotoxin Paraquat and Contributes to Neuropathology Linked to Parkinson’s Disease. *Cell Rep.* 22, 930–940. <https://doi.org/10.1016/J.CELREP.2017.12.092>
- Coecke, S., Balls, M., Bowe, G., Davis, J., Gstraunthaler, G., Hartung, T., Hay, R., Merten, O.-W., Price, A., Schechtman, L., Stacey, G., Stokes, W., Second ECVAM Task Force on Good Cell Culture Practice, 2005. Guidance on good cell culture practice. a report of the second ECVAM task force on good cell culture practice. *Altern. Lab. Anim.* 33, 261–87.
- Congress Office of Technology, 1990. Neurotoxicity: Identifying and Controlling Poisons of the Nervous System.
- Conolly, R.B., Ankley, G.T., Cheng, W., Mayo, M.L., Miller, D.H., Perkins, E.J., Villeneuve, D.L., Watanabe, K.H., 2017. Quantitative Adverse Outcome Pathways and Their Application to Predictive Toxicology. *Environ. Sci. Technol.* 51, 4661–4672. <https://doi.org/10.1021/ACS.EST.6B06230>
- Conradi, S., Ronnevi, L.O., Vesterberg, O., 1976. Abnormal tissue distribution of lead in amyotrophic lateral sclerosis. *J. Neurol. Sci.* 29, 259–265. [https://doi.org/10.1016/0022-510X\(76\)90175-1](https://doi.org/10.1016/0022-510X(76)90175-1)

- Diederich, M., Chateavieux, S., Morceau, F., Dicato, M., 2010. Molecular and therapeutic potential and toxicity of valproic acid. *J. Biomed. Biotechnol.* 2010. <https://doi.org/10.1155/2010/479364>
- Dinis-Oliveira, R.J., Duarte, J.A., Sánchez-Navarro, A., Remião, F., Bastos, M.L., Carvalho, F., 2008. Paraquat Poisonings: Mechanisms of Lung Toxicity, Clinical Features, and Treatment. *Crit. Rev. Toxicol.* 38, 13–71. <https://doi.org/10.1080/10408440701669959>
- Draize, J.H., Woodard, G., Calvery, H.O., 1944. METHODS FOR THE STUDY OF IRRITATION AND TOXICITY OF SUBSTANCES APPLIED TOPICALLY TO THE SKIN AND MUCOUS MEMBRANES. *J. Pharmacol. Exp. Ther.* 82.
- Du, J., Zhang, A., Li, J., Liu, X., Wu, S., Wang, B., Wang, Y., Jia, H., 2021. Doxorubicin-Induced Cognitive Impairment: The Mechanistic Insights. *Front. Oncol.* 0, 1461. <https://doi.org/10.3389/FONC.2021.673340>
- EC, 2013. COMMUNICATION FROM THE COMMISSION TO THE EUROPEAN PARLIAMENT AND THE COUNCIL on the animal testing and marketing ban and on the state of play in relation to alternative methods in the field of cosmetics.
- Edwards, D.H., 2015. *Neuroscience*. Third Edition. Edited by Dale Purves , , George J Augustine , , David Fitzpatrick , , William C Hall , , Anthony-Samuel LaMantia , , James O McNamara , and , S Mark Williams. Sunderland (Massachusetts): Sinauer Associates. \$86.95. xix + 773 p + G-1–G-16 + SR-1–SR-6 + I-1–I-15; ill.; index. ISBN: 0–87893–725–0. [CD-ROM included.] 2004. . <https://doi.org/10.1086/504005> 81, 86–87. <https://doi.org/10.1086/504005>
- Ekwall, B., 1983. Screening of Toxic Compounds in Mammalian Cell Cultures. *Ann. N. Y. Acad. Sci.* 407, 64–77. <https://doi.org/10.1111/j.1749-6632.1983.tb47814.x>
- Ekwall, B., 1980. Screening of toxic compounds in tissue culture. *Toxicology* 17, 127–142. [https://doi.org/10.1016/0300-483X\(80\)90085-2](https://doi.org/10.1016/0300-483X(80)90085-2)
- Ekwall, B., Johansson, A., 1980. Preliminary studies on the validity of *in vitro* measurement of drug toxicity using HeLa cells I. Comparative *in vitro* cytotoxicity of 27 drugs. *Toxicol. Lett.* 5, 299–307. [https://doi.org/10.1016/0378-4274\(80\)90031-4](https://doi.org/10.1016/0378-4274(80)90031-4)
- Escher, B., Hermens, J., Schwarzenbach, R., 2005. Internal Exposure: Linking Bioavailability to Effects. International Workshop, 27 August 2004, Monte Verità, Switzerland. *Environ. Sci. Pollut. Res.* 12, 57–60. <https://doi.org/10.1065/espr2005.01.004>
- Eskes, C., Honegger, P., Juillerat-Jeanneret, L., Monnet-Tschudi, F., 2002. Microglial reaction induced by noncytotoxic methylmercury treatment leads to neuroprotection via interactions with astrocytes and IL-6 release. *Glia* 37, 43–52. <https://doi.org/10.1002/glia.10019>
- Eskes, C., Juillerat-Jeanneret, L., Leuba, G., Honegger, P., Monnet-Tschudi, F., 2003. Involvement of microglia-neuron interactions in the tumor necrosis factor- $\alpha$  release, microglial activation, and neurodegeneration induced by trimethyltin. *J. Neurosci. Res.* 71, 583–590. <https://doi.org/10.1002/jnr.10508>
- EUR-Lex, 2010. Directive 2010/63/EU of the European parliament and of the Council of 22 September 2010 on the protection of animals used for scientific purposes. *Off. J. Eur. Union* 1–61.
- Fabulas-da Costa, A., Aijjou, R., Hachani, J., Landry, C., Cecchelli, R., Culot, M., 2013. *In vitro* blood-brain barrier model adapted to repeated-dose toxicological screening. *Toxicol. Vitro* 27, 1944–1953. <https://doi.org/10.1016/j.tiv.2013.06.026>
- Forsby, A., Bal-Price, A.K., Camins, A., Coecke, S., Fabre, N., Gustafsson, H., Honegger, P., Kinsner-Ovaskainen, A., Pallas, M., Rimbau, V., Rodríguez-Farré, E., Suñol, C., Vericat, J.A., Zurich, M.G., 2009. Neuronal *in vitro* models for the estimation of acute systemic toxicity. *Toxicol. Vitro* 23, 1564–1569. <https://doi.org/10.1016/J.TIV.2009.07.017>
- Fransen, L.F.H., Leonard, M.O., 2021. CD34+ derived macrophage and dendritic cells display differential responses to paraquat. *Toxicol. Vitro* 75, 105198.

<https://doi.org/10.1016/J.TIV.2021.105198>

- Fritsche, E., Alm, H., Baumann, J., Geerts, L., Håkansson, H., Witters, H., 2015. Literature review on *in vitro* and alternative Developmental Neurotoxicity. DOI 10.2903/sp.efsa.2015.EN-778 1–186. <https://doi.org/10.2903/sp.efsa.2015.EN-778>
- Fritsche, E., Barenys, M., Klose, J., Masjosthusmann, S., Nimtz, L., Schmuck, M., Wuttke, S., Tigges, J., 2018. Development of the Concept for Stem Cell-Based Developmental Neurotoxicity Evaluation. *Toxicol. Sci.* 165, 14–20. <https://doi.org/10.1093/toxsci/kfy175>
- Fryer, M., Collins, C.D., Ferrier, H., Colvile, R.N., Nieuwenhuijsen, M.J., 2006. Human exposure modelling for chemical risk assessment: A review of current approaches and research and policy implications. *Environ. Sci. Policy* 9, 261–274. <https://doi.org/10.1016/j.envsci.2005.11.011>
- Gabriel, E., Ramani, A., Karow, U., Gottardo, M., Natarajan, K., Gooi, L.M., Goranci-Buzhala, G., Krut, O., Peters, F., Nikolic, M., Kuivanen, S., Korhonen, E., Smura, T., Vapalahti, O., Papantonis, A., Schmidt-Chanasit, J., Riparbelli, M., Callaini, G., Krönke, M., Utermöhlen, O., Gopalakrishnan, J., 2017. Recent Zika Virus Isolates Induce Premature Differentiation of Neural Progenitors in Human Brain Organoids. *Cell Stem Cell* 20, 397–406.e5. <https://doi.org/10.1016/j.stem.2016.12.005>
- Gallo, M.A., 2013. History and Scope of Toxicology, in: Casarett and Doull's Toxicology: The Basic Science of Poisons. McGraw-Hill Education / Medical.
- Gąssowska-Dobrowolska, M., Cieślik, M., Czapski, G.A., Jęśko, H., Frontczak-Baniewicz, M., Gewartowska, M., Dominiak, A., Polowy, R., Filipkowski, R.K., Babiec, L., Adamczyk, A., 2020. Prenatal Exposure to Valproic Acid Affects Microglia and Synaptic Ultrastructure in a Brain-Region-Specific Manner in Young-Adult Male Rats: Relevance to Autism Spectrum Disorders. *Int. J. Mol. Sci.* 2020, Vol. 21, Page 3576 21, 3576. <https://doi.org/10.3390/IJMS21103576>
- Gholami, S., Mazidi, Z., Pahlavan, S., Moslem, F., Hosseini, M., Taei, A., Hesarak, M., Barekat, M., Aghdami, N., Baharvand, H., 2021. A Novel Insight Into Endothelial And Cardiac Cells Phenotype In Systemic Sclerosis Using Patient-Specific Induced Pluripotent Stem Cell. *Cell J.* 23. <https://doi.org/10.22074/cellj.2021.7244>.This
- Gibbs, J.P., Adeyeye, M.C., Yang, Z., Shen, D.D., 2004. Valproic acid uptake by bovine brain microvessel endothelial cells: Role of active efflux transport. *Epilepsy Res.* 58, 53–66. <https://doi.org/10.1016/j.eplepsyres.2003.12.008>
- Gillis, B.S., Arbieva, Z., Gavin, I.M., 2012. Analysis of lead toxicity in human cells. *BMC Genomics* 13, 1. <https://doi.org/10.1186/1471-2164-13-344>
- Girgin, M.U., Broguiere, N., Mattolini, L., Lutolf, M.P., 2021. Gastruloids generated without exogenous Wnt activation develop anterior neural tissues. *Stem Cell Reports* 16, 1143–1155. <https://doi.org/10.1016/j.stemcr.2021.03.017>
- Graeber, M.B., 2010. Changing face of microglia. *Science* (80-. ). 330, 783–788. <https://doi.org/10.1126/SCIENCE.1190929>
- Grandjean, P., Landrigan, P.J., 2014. Neurobehavioural effects of developmental toxicity. *Lancet Neurol.* 13, 330–338. [https://doi.org/10.1016/S1474-4422\(13\)70278-3](https://doi.org/10.1016/S1474-4422(13)70278-3)
- Green, P.S., Leeuwenburgh, C., 2002. Mitochondrial dysfunction is an early indicator of doxorubicin-induced apoptosis. *Biochim. Biophys. Acta - Mol. Basis Dis.* 1588, 94–101. [https://doi.org/10.1016/S0925-4439\(02\)00144-8](https://doi.org/10.1016/S0925-4439(02)00144-8)
- Greim, H., 2020. Aims and Mission of Regulatory Toxicology. *Regul. Toxicol.* 1–21. [https://doi.org/10.1007/978-3-642-36206-4\\_25-2](https://doi.org/10.1007/978-3-642-36206-4_25-2)
- Greim, H., Snyder, R., 2018. Introduction to the Discipline of Toxicology. *Toxicol. Risk Assess.* 1–19. <https://doi.org/10.1002/9781119135944.CH1>
- Greter, M., Merad, M., 2013. Regulation of microglia development and homeostasis. *Glia* 61, 121–127. <https://doi.org/10.1002/glia.22408>

- Groothuis, F.A., Heringa, M.B., Nicol, B., Hermens, J.L.M., Blaauboer, B.J., Kramer, N.I., 2015. Dose metric considerations in *in vitro* assays to improve quantitative *in vitro-in vivo* dose extrapolations. *Toxicology* 332, 30–40. <https://doi.org/10.1016/j.tox.2013.08.012>
- Haroutiunian, S., Rabinovich, B., Adam, M., Hoffman, A., Ratz, Y., 2009. Valproic acid plasma concentration decreases in a dose-independent manner following administration of meropenem: A retrospective study. *J. Clin. Pharmacol.* 49, 1363–1369. <https://doi.org/10.1177/0091270009334377>
- Hartung, T., FitzGerald, R.E., Jennings, P., Mirams, G.R., Peitsch, M.C., Rostami-Hodjegan, A., Shah, I., Wilks, M.F., Sturla, S.J., 2017. Systems Toxicology: Real World Applications and Opportunities. *Chem. Res. Toxicol.* 30, 870–882. <https://doi.org/10.1021/acs.chemrestox.7b00003>
- Hayes, A.N., Gilbert, S.G., 2009. Historical milestones and discoveries that shaped the toxicology sciences. pp. 1–35. [https://doi.org/10.1007/978-3-7643-8336-7\\_1](https://doi.org/10.1007/978-3-7643-8336-7_1)
- Hernandez-Aya, L.F., Gonzalez-Angulo, A.M., 2013. Adjuvant Systemic Therapies in Breast Cancer. *Surg. Clin. North Am.* 93, 473–491. <https://doi.org/10.1016/J.SUC.2012.12.002>
- Houzé, P., Baud, F.J., Mouy, R., Bismuth, C., Bourdon, R., Scherrmann, J.M., 1990. Toxicokinetics of Paraquat in Humans. *Hum. Exp. Toxicol.* 9, 5–12. <https://doi.org/10.1177/096032719000900103>
- Ismael, M.A., Elyamine, A.M., Moussa, M.G., Cai, M., Zhao, X., Hu, C., 2019. Cadmium in plants: uptake, toxicity and its interactions with selenium fertilizers. *Metallomics* 11, 255–277. <https://doi.org/10.1039/C8MT00247A>
- Jafari-Fesharaki, M., Scheinman, M.M., 1998. Adverse effects of amiodarone. *PACE - Pacing Clin. Electrophysiol.* 21, 108–120. <https://doi.org/10.1111/j.1540-8159.1998.tb01068.x>
- Jennings, P., 2015a. “The future of *in vitro* toxicology.” *Toxicol. Vitro.* 29, 1217–1221. <https://doi.org/10.1016/j.tiv.2014.08.011>
- Jennings, P., 2015b. The future of *in vitro* toxicology. *Toxicol. Vitro.* 29, 1217–1221. <https://doi.org/10.1016/j.tiv.2014.08.011>
- Jennings, P., Limonciel, A., Felice, L., Leonard, M.O., 2013. An overview of transcriptional regulation in response to toxicological insult. *Arch. Toxicol.* 87, 49–72. <https://doi.org/10.1007/s00204-012-0919-y>
- JJ, F., AG, P., R, T.-V., J, X., 2019. Systematic review and meta-analyses of lead (Pb) concentrations in environmental media (soil, dust, water, food, and air) reported in the United States from 1996 to 2016. *Sci. Total Environ.* 694. <https://doi.org/10.1016/J.SCITOTENV.2019.07.295>
- John, T., Lomeli, N., Bota, D.A., 2017. Systemic cisplatin exposure during infancy and adolescence causes impaired cognitive function in adulthood. *Behav. Brain Res.* 319, 200–206. <https://doi.org/10.1016/J.BBR.2016.11.013>
- Juárez-Rebollar, D., Rios, C., Nava-Ruiz, C., Méndez-Armenta, M., 2017. Metallothionein in Brain Disorders. *Oxid. Med. Cell. Longev.* 2017. <https://doi.org/10.1155/2017/5828056>
- Takee, A., Takanaga, H., Hosoya, K.I., Sugiyama, Y., Terasaki, T., 2002. *In vivo* evidence for brain-to-blood efflux transport of valproic acid across the blood-brain barrier. *Microvasc. Res.* 63, 233–238. <https://doi.org/10.1006/mvre.2001.2378>
- Kramer, N.I., Di Consiglio, E., Blaauboer, B.J., Testai, E., 2015. Biokinetics in repeated-dosing *in vitro* drug toxicity studies. *Toxicol. Vitro.* 30, 217–224. <https://doi.org/10.1016/j.tiv.2015.09.005>
- L’Ecuyer, T., Sanjeev, S., Thomas, R., Novak, R., Das, L., Campbell, W., Vander Heide, R., 2006. DNA damage is an early event in doxorubicin-induced cardiac myocyte death. *Am. J. Physiol. - Hear. Circ. Physiol.* 291, 1273–1280. <https://doi.org/10.1152/ajpheart.00738.2005>
- Lafuente-Lafuente, C., Alvarez, J.-C., Leenhardt, A., Mouly, S., Extramiana, F., Caulin, C., Funck-Brentano, C., Bergmann, J.-F., 2009. Amiodarone concentrations in plasma and fat tissue

- during chronic treatment and related toxicity. *Br. J. Clin. Pharmacol.* 67, 511–519. <https://doi.org/10.1111/j.1365-2125.2009.03381.x>
- LaLone, C.A., Ankley, G.T., Belanger, S.E., Embry, M.R., Hodges, G., Knapen, D., Munn, S., Perkins, E.J., Rudd, M.A., Villeneuve, D.L., Whelan, M., Willett, C., Zhang, X., Hecker, M., 2017. Advancing the adverse outcome pathway framework—An international horizon scanning approach. *Environ. Toxicol. Chem.* 36, 1411–1421. <https://doi.org/10.1002/etc.3805>
- Lancaster, M.A., Knoblich, J.A., 2014. Generation of cerebral organoids from human pluripotent stem cells. *Nat. Protoc.* 9, 2329–2340. <https://doi.org/10.1038/nprot.2014.158>
- Leeuwen, C. van, Vermeire, T., 2007. Risk assessment of chemicals: an introduction.
- Leist, M., Hartung, T., 2013. Inflammatory findings on species extrapolations: humans are definitely no 70-kg mice. *Arch. Toxicol.* 87, 563–567. <https://doi.org/10.1007/s00204-013-1038-0>
- Leite, P.E.C., Pereira, M.R., Harris, G., Pamies, D., Dos Santos, L.M.G., Granjeiro, J.M., Hogberg, H.T., Hartung, T., Smirnova, L., 2019. Suitability of 3D human brain spheroid models to distinguish toxic effects of gold and poly-lactic acid nanoparticles to assess biocompatibility for brain drug delivery. *Part. Fibre Toxicol.* 16, 1–20. <https://doi.org/10.1186/s12989-019-0307-3>
- Leo, R.J., Narendran, R., 1999. Anticonvulsant Use in the Treatment of Bipolar Disorder: A Primer for Primary Care Physicians. *Prim. Care Companion J. Clin. Psychiatry* 1, 74–84. <https://doi.org/10.4088/pcc.v01n0304>
- Limonciel, A., Ates, G., Carta, G., Wilmes, A., Watzele, M., Shepard, P.J., VanSteenhouse, H.C., Seligmann, B., Yeakley, J.M., van de Water, B., Vinken, M., Jennings, P., 2018. Comparison of base-line and chemical-induced transcriptomic responses in HepaRG and RPTEC/TERT1 cells using TempO-Seq. *Arch. Toxicol.* 2018 928 92, 2517–2531. <https://doi.org/10.1007/S00204-018-2256-2>
- Limonciel, A., Jennings, P., 2013. A review of the evidence that ochratoxin A is an Nrf2 inhibitor: Implications for nephrotoxicity and renal carcinogenicity. *Toxins (Basel)*. 6, 371–379. <https://doi.org/10.3390/toxins6010371>
- Liu, S., Yin, N., Faiola, F., 2017. Prospects and Frontiers of Stem Cell Toxicology. *Stem Cells Dev.* 26, 1528–1539. <https://doi.org/10.1089/scd.2017.0150>
- Lo Giudice, M., Mihalik, B., Turi, Z., Dinnyés, A., Kobolák, J., 2019. Calcilytic NPS 2143 Reduces Amyloid Secretion and Increases sA $\beta$ PP $\alpha$  Release from PSEN1 Mutant iPSC-Derived Neurons. *J. Alzheimer's Dis.* 72, 885–899. <https://doi.org/10.3233/JAD-190602>
- Masjosthusmann, S., Barenys, M., El-gamal, M., Geerts, L., Gorreja, A., Kühne, B., Marchetti, N., Tigges, J., Witters, H., Fritsche, E., 2018. Literature review and appraisal on alternative neurotoxicity testing methods. DOI:10.2903/sp.efsa.2018.EN-1410. <https://doi.org/10.2903/sp.efsa.2018.EN-1410>
- Mav, D., Shah, R.R., Howard, B.E., Auerbach, S.S., Bushel, P.R., Collins, J.B., Gerhold, D.L., Judson, R.S., Karmaus, A.L., Maull, E.A., Mendrick, D.L., Merrick, B.A., Sipes, N.S., Svoboda, D., Paules, R.S., 2018. A hybrid gene selection approach to create the S1500+ targeted gene sets for use in high-throughput transcriptomics. *PLoS One* 13, e0191105. <https://doi.org/10.1371/JOURNAL.PONE.0191105>
- Mayor, A., 2003. Greek fire, poison arrows, and scorpion bombs: biological and chemical warfare in the ancient world. Overlook Duckworth.
- Methaneethorn, J., 2018. A systematic review of population pharmacokinetics of valproic acid. *Br. J. Clin. Pharmacol.* 84, 816–834. <https://doi.org/10.1111/bcp.13510>
- Methaneethorn, J., 2017. Population Pharmacokinetics of Valproic Acid in Patients with Mania: Implication for Individualized Dosing Regimens. *Clin. Ther.* 39, 1171–1181. <https://doi.org/10.1016/j.clinthera.2017.04.005>
- Mitra, P., Sharma, S., Purohit, P., Sharma, P., 2017. Clinical and molecular aspects of lead toxicity:

- An update. <https://doi.org/10.1080/10408363.2017.1408562> 54, 506–528.  
<https://doi.org/10.1080/10408363.2017.1408562>
- Miyata, S., 2015. New aspects in fenestrated capillary and tissue dynamics in the sensory circumventricular organs of adult brains. *Front. Neurosci.* 9, 1–15.  
<https://doi.org/10.3389/fnins.2015.00390>
- Modafferi, S., Zhong, X., Kleensang, A., Murata, Y., Fagiani, F., Pamies, D., Hogberg, H.T., Calabrese, V., Lachman, H., Hartung, T., Smirnova, L., 2021. Gene–Environment Interactions in Developmental Neurotoxicity: a Case Study of Synergy between Chlorpyrifos and CHD8 Knockout in Human BrainSpheres. *Environ. Health Perspect.* 129.  
<https://doi.org/10.1289/EHP8580>
- Monnet-Tschudi, F., Zurich, M.G., Honegger, P., 2007. Neurotoxicant-induced inflammatory response in three-dimensional brain cell cultures. *Hum. Exp. Toxicol.* 26, 339–346.  
<https://doi.org/10.1177/0960327107074589>
- Monnet-Tschudi, F., Zurich, M.G., Pithon, E., van Melle, G., Honegger, P., 1995. Microglial responsiveness as a sensitive marker for trimethyltin (TMT) neurotoxicity. *Brain Res.* 690, 8–14. [https://doi.org/10.1016/0006-8993\(95\)00509-0](https://doi.org/10.1016/0006-8993(95)00509-0)
- Morris-Schaffer, K., McCoy, M.J., 2020. A Review of the LD50 and Its Current Role in Hazard Communication. *ACS Chem. Heal. Saf.* 28, 25–33.  
<https://doi.org/10.1021/ACS.CHAS.0C00096>
- Morrison, M., 2018. Making Cells Worthwhile: Calculations of Value in a European Consortium for Induced Pluripotent Stem Cell Banking. <https://doi.org/10.1080/09505431.2018.1538331> 28, 46–69.  
<https://doi.org/10.1080/09505431.2018.1538331>
- Mrdjen, D., Pavlovic, A., Hartmann, F.J., Schreiner, B., Utz, S.G., Leung, B.P., Lelios, I., Heppner, F.L., Kipnis, J., Merkler, D., Greter, M., Becher, B., 2018. High-Dimensional Single-Cell Mapping of Central Nervous System Immune Cells Reveals Distinct Myeloid Subsets in Health, Aging, and Disease. *Immunity* 48, 380–395.e6.  
<https://doi.org/10.1016/J.IMMUNI.2018.01.011>
- Murphy, C., Feifel, E., Jennings, P., Gstraunthaler, G., Wilmes, A., 2019. A Protocol for One-Step Differentiation of Human Induced Pluripotent Stem Cells into Mature Podocytes, in: Mandenius, C.-F., Ross, J.A. (Eds.), *Cell-Based Assays Using iPSCs for Drug Development and Testing*. Springer New York, New York, NY, pp. 93–99. [https://doi.org/10.1007/978-1-4939-9477-9\\_8](https://doi.org/10.1007/978-1-4939-9477-9_8)
- National Research Council, 2007. *Toxicity Testing in the 21st Century: A Vision and a Strategy* [WWW Document]. Natl. Acad. Press. Washington, DC. URL [https://books.google.ch/books?hl=pt-PT&lr=&id=3AWfAAQBAJ&oi=fnd&pg=PT21&dq=Toxicity+Testing+in+the+21st+Century:+A+Vision+and+a+Strategy&ots=UwnqSFwazc&sig=KCxUqgElnoh\\_RuE2YHTzTTuNRMU&redir\\_esc=y#v=onepage&q=Toxicity Testing in the 21st Century%3A A Vis](https://books.google.ch/books?hl=pt-PT&lr=&id=3AWfAAQBAJ&oi=fnd&pg=PT21&dq=Toxicity+Testing+in+the+21st+Century:+A+Vision+and+a+Strategy&ots=UwnqSFwazc&sig=KCxUqgElnoh_RuE2YHTzTTuNRMU&redir_esc=y#v=onepage&q=Toxicity+Testing+in+the+21st+Century%3A+A+Vis) (accessed 4.30.21).
- Needleman, H., 2004. Lead Poisoning. *Annu. Rev. Med.* 55, 209–222.  
<https://doi.org/10.1146/annurev.med.55.091902.103653>
- NRC, 2007. *Toxicity Testing in the 21st Century*. National Academies Press, Washington, D.C.  
<https://doi.org/10.17226/11970>
- Nunes, C., Zurich, M.-G., 2020. *Neurotoxicology and Disease Modelling*. Springer, Cham, pp. 229–246. [https://doi.org/10.1007/978-3-030-43939-2\\_12](https://doi.org/10.1007/978-3-030-43939-2_12)
- Omura, T., Asari, M., Yamamoto, J., Oka, K., Hoshina, C., Maseda, C., Awaya, T., Tasaki, Y., Shiono, H., Yonezawa, A., Masuda, S., Matsubara, K., Shimizu, K., 2013. Sodium tauroursodeoxycholate prevents paraquat-induced cell death by suppressing endoplasmic reticulum stress responses in human lung epithelial A549 cells. *Biochem. Biophys. Res.*

- Commun. 432, 689–694. <https://doi.org/10.1016/j.bbrc.2013.01.131>
- Oredsson, S., Coecke, S., van der Valk, J., Vinken, M., 2019. What is understood by “animal-free research”? *Toxicol. Vitr.* 57, 143–144. <https://doi.org/10.1016/j.tiv.2019.03.001>
- Pamies, D., Bal-Price, A., Chesné, C., Coecke, S., Dinnyes, A., Eskes, C., Grillari, R., Gstraunthaler, G., Hartung, T., Jennings, P., Leist, M., Martin, U., Passier, R., Schwamborn, J.C., Stacey, G.N., Ellinger-Ziegelbauer, H., Daneshian, M., 2018a. Advanced Good Cell Culture Practice for human primary, stem cell-derived and organoid models as well as microphysiological systems. *ALTEX* 35, 353–378. <https://doi.org/10.14573/altex.1710081>
- Pamies, D., Barrera, P., Block, K., Makri, G., Kumar, A., Wiersma, D., Smirnova, L., Zhang, C., Bressler, J., Christian, K.M., Harris, G., Ming, G., Berlinicke, C.J., Kyro, K., Song, H., Pardo, C.A., Hartung, T., Hogberg, H.T., 2017a. A Human Brain Microphysiological System Derived from Induced Pluripotent Stem Cells to Study Neurological Diseases and Toxicity. *ALTEX* 34, 362. <https://doi.org/10.14573/ALTEX.1609122>
- Pamies, D., Barreras, P., Block, K., Makri, G., Kumar, A., Wiersma, D., Smirnova, L., Zhang, C., Bressler, J., Christian, K.M., Harris, G., Ming, G.L., Berlinicke, C.J., Kyro, K., Song, H., Pardo, C.A., Hartung, T., Hogberg, H.T., 2017b. A human brain microphysiological system derived from induced pluripotent stem cells to study neurological diseases and toxicity. *ALTEX* 34, 362–376. <https://doi.org/10.14573/altex.1609122>
- Pamies, D., Block, K., Lau, P., Gribaldo, L., Pardo, C.A., Barreras, P., Smirnova, L., Wiersma, D., Zhao, L., Harris, G., Hartung, T., Hogberg, H.T., 2018b. Rotenone exerts developmental neurotoxicity in a human brain spheroid model. *Toxicol. Appl. Pharmacol.* 354, 101–114. <https://doi.org/10.1016/J.TAAP.2018.02.003>
- Pappas, A.A., Massoll, N.A., Cannon, D.J., 1999. Toxicology: Past, present, and future. *Ann. Clin. Lab. Sci.* 29, 253–262. <https://doi.org/10.1080/089583799196907>
- Parasuraman, S., 2011. Toxicological screening. *J. Pharmacol. Pharmacother.* 2, 74. <https://doi.org/10.4103/0976-500X.81895>
- Pathmanathan, A., Cleary, L., 2021. Amiodarone-Associated Neurotoxicity. *Am. J. Ther.* 28, e165–e166. <https://doi.org/10.1097/MJT.0000000000001035>
- Petry, T., Knowles, R., Meads, R., 2006. An analysis of the proposed REACH regulation. *Regul. Toxicol. Pharmacol.* 44, 24–32. <https://doi.org/10.1016/J.YRTPH.2005.07.007>
- Pistollato, F., Bremer-Hoffmann, S., Healy, L., Young, L., Stacey, G., 2012. Standardization of pluripotent stem cell cultures for toxicity testing. *Expert Opin. Drug Metab. Toxicol.* 8, 239–257. <https://doi.org/10.1517/17425255.2012.639763>
- Pistollato, F., de Gyves, E.M., Carpi, D., Bopp, S.K., Nunes, C., Worth, A., Bal-Price, A., 2020. Assessment of developmental neurotoxicity induced by chemical mixtures using an adverse outcome pathway concept. *Environ. Heal.* 2020 191 19, 1–26. <https://doi.org/10.1186/S12940-020-00578-X>
- Pistollato, F., Madia, F., Corvi, R., Munn, S., Grignard, E., Paini, A., Worth, A., Bal-Price, A., Prieto, P., Casati, S., Berggren, E., Bopp, S., Zuang, V., 2021. Current EU regulatory requirements for the assessment of chemicals and cosmetic products: challenges and opportunities for introducing new approach methodologies. *Arch. Toxicol.* 95, 1867–1897. <https://doi.org/10.1007/S00204-021-03034-Y>
- Plummer, S., Wallace, S., Ball, G., Lloyd, R., Schiapparelli, P., Quiñones-Hinojosa, A., Hartung, T., Pamies, D., 2019. A Human iPSC-derived 3D platform using primary brain cancer cells to study drug development and personalized medicine. *Sci. Rep.* 9, 1–11. <https://doi.org/10.1038/s41598-018-38130-0>
- Pomponio, G., Zurich, M.G., Schultz, L., Weiss, D.G., Romanelli, L., Gramowski-Voss, A., Di Consiglio, E., Testai, E., 2015. Amiodarone biokinetics, the formation of its major oxidative metabolite and neurotoxicity after acute and repeated exposure of brain cell cultures. *Toxicol. Vitr.* <https://doi.org/10.1016/j.tiv.2015.01.012>

- Proença, S., Escher, B.I., Fischer, F.C., Fisher, C., Grégoire, S., Hewitt, N.J., Nicol, B., Paini, A., Kramer, N.I., 2021. Effective exposure of chemicals in *in vitro* cell systems: A review of chemical distribution models. *Toxicol. Vitro*. 73. <https://doi.org/10.1016/j.tiv.2021.105133>
- Purves, D., Augustine, G.J., Fitzpatrick, D., Hall, W.C., LaMantia, A.-S., McNamara, J.O., Williams, S.M. (Eds.), 2004. *Neuroscience*, 3rd ed., Neuroscience, 3rd ed. Sinauer Associates, Sunderland, MA, US.
- Ramalho, M., Fontes, F., Ruano, L., Pereira, S., Lunet, N., 2017. Cognitive impairment in the first year after breast cancer diagnosis: A prospective cohort study. *The Breast* 32, 173–178. <https://doi.org/10.1016/J.BREAST.2017.01.018>
- Rehman, W., Arfons, L.M., Lazarus, H.M., 2011. The rise, fall and subsequent triumph of thalidomide: lessons learned in drug development. *Ther. Adv. Hematol.* 2, 291–308. <https://doi.org/10.1177/2040620711413165>
- Roper, C., Tanguay, R.L., 2020. Tox21 and adverse outcome pathways. *An Introd. to Interdiscip. Toxicol.* 559–568. <https://doi.org/10.1016/b978-0-12-813602-7.00040-5>
- Russell, W.M.S., Burch, R.L., 1959. *The principles of humane experimental technique*. Princ. Hum. Exp. Tech.
- Sandström, J., Eggermann, E., Charvet, I., Roux, A., Toni, N., Greggio, C., Broyer, A., Monnet-Tschudi, F., Stoppini, L., 2017. Development and characterization of a human embryonic stem cell-derived 3D neural tissue model for neurotoxicity testing. *Toxicol. Vitro*. 38, 124–135. <https://doi.org/10.1016/J.TIV.2016.10.001>
- Scherrmann, J.M., Houze, P., Bismuth, C., Bourdon, R., 1987. Prognostic Value of Plasma and Urine Paraquat Concentration. *Hum. Exp. Toxicol.* 6, 91–93. <https://doi.org/10.1177/096032718700600116>
- Schmidt, B.Z., Lehmann, M., Gutbier, S., Nembo, E., Noel, S., Smirnova, L., Forsby, A., Hescheler, J., Avci, H.X., Hartung, T., Leist, M., Kobolák, J., Dinnyés, A., 2017. *In vitro* acute and developmental neurotoxicity screening: an overview of cellular platforms and high-throughput technical possibilities. *Arch. Toxicol.* 91, 1–33. <https://doi.org/10.1007/s00204-016-1805-9>
- Sewell, F., Aggarwal, M., Bachler, G., Broadmeadow, A., Gellatly, N., Moore, E., Robinson, S., Rooseboom, M., Stevens, A., Terry, C., Burden, N., 2017. The current status of exposure-driven approaches for chemical safety assessment: A cross-sector perspective. *Toxicology* 389, 109–117. <https://doi.org/10.1016/j.tox.2017.07.018>
- Shimizu, K., Matsubara, K., Ohtaki, K., Fujimaru, S., Saito, O., Shiono, H., 2003. Paraquat induces long-lasting dopamine overflow through the excitotoxic pathway in the striatum of freely moving rats. *Brain Res.* 976, 243–252. [https://doi.org/10.1016/S0006-8993\(03\)02750-1](https://doi.org/10.1016/S0006-8993(03)02750-1)
- Sierra, A., Paolicelli, R.C., Kettenmann, H., 2019. Cien Años de Microglía: Milestones in a Century of Microglial Research. *Trends Neurosci.* 42, 778–792. <https://doi.org/10.1016/j.tins.2019.09.004>
- Singh, P., Chandrasekaran, V., Hardy, B., Wilmes, A., Jennings, P., Exner, T.E., 2021. Temporal transcriptomic alterations of cadmium exposed human iPSC-derived renal proximal tubule-like cells. *Toxicol. Vitro*. 73.
- Stiles, J., Jernigan, T.L., 2010. The Basics of Brain Development. *Neuropsychol. Rev.* 2010 204 20, 327–348. <https://doi.org/10.1007/S11065-010-9148-4>
- Sumner, J., 2000. *The natural history of medicinal plants*. Timber Press, Portland.
- Sztajnkrzyca, M.D., 2002. Valproic Acid Toxicity: Overview and Management. <https://doi.org/10.1081/CLT-120014645> 40, 789–801. <https://doi.org/10.1081/CLT-120014645>
- Takahashi, K., Tanabe, K., Ohnuki, M., Narita, M., Ichisaka, T., Tomoda, K., Yamanaka, S., 2007. Induction of Pluripotent Stem Cells from Adult Human Fibroblasts by Defined Factors. *Cell* 131, 861–872. <https://doi.org/10.1016/J.CELL.2007.11.019>

- Technologies, L., 2015. Induction of Neural Stem Cells from Human Pluripotent Stem Cells Using PSC Neural Induction Medium (MAN0008031 Rev A.0).
- Tiffany-Castiglioni, E., 1993. Cell culture models for lead toxicity in neuronal and glial cells. *Neurotoxicology* 14, 513–36.
- Trantham-Davidson, H., Chandler, L.J., 2015. Alcohol-induced alterations in dopamine modulation of prefrontal activity. *Alcohol* 49, 773–779. <https://doi.org/10.1016/j.alcohol.2015.09.001>
- Trevar, J.W., 1927. PROCEEDINGS THE ROYAL B OF SOCIETY B IOLOGIC! SCIENCES The Error of Determination of Toxicity References. <https://doi.org/10.1098/rspb.1927.0030>
- Tukker, A.M., Wijnolts, F.M.J., de Groot, A., Westerink, R.H.S., 2018. Human iPSC-derived neuronal models for *in vitro* neurotoxicity assessment. *Neurotoxicology* 67, 215–225. <https://doi.org/10.1016/j.neuro.2018.06.007>
- Tunali, S., Cimen, E.S., Yanardag, R., 2020. The effects of chard on brain damage in valproic acid-induced toxicity. *J. Food Biochem.* 44, e13382. <https://doi.org/10.1111/JFBC.13382>
- Veronesi, B., 1992. *In vitro* screening batteries for neurotoxicants. *Neurotoxicology* 13, 185–95.
- Von Tobel, J.S., Antinori, P., Zurich, M.G., Rosset, R., Aschner, M., Glück, F., Scherl, A., Monnet-Tschudi, F., 2014. Repeated exposure to Ochratoxin A generates a neuroinflammatory response, characterized by neurodegenerative M1 microglial phenotype. *Neurotoxicology* 44, 61–70. <https://doi.org/10.1016/J.NEURO.2014.04.005>
- Wandrer, F., Frangež, Ž., Liebig, S., John, K., Vondran, F., Wedemeyer, H., Veltmann, C., Pfeffer, T.J., Shibolet, O., Schulze-Osthoff, K., Simon, H.U., Bantel, H., 2020. Autophagy alleviates amiodarone-induced hepatotoxicity. *Arch. Toxicol.* 94, 3527–3539. <https://doi.org/10.1007/s00204-020-02837-9>
- Wang, Y., Wang, X., Li, H., Xu, M., Frank, J., Luo, J., 2018. Binge ethanol exposure induces endoplasmic reticulum stress in the brain of adult mice. *Toxicol. Appl. Pharmacol.* 356, 172–181. <https://doi.org/10.1016/j.taap.2018.08.006>
- Waters, M.D., Fostel, J.M., 2004. Toxicogenomics and systems toxicology: Aims and prospects. *Nat. Rev. Genet.* 5, 936–948. <https://doi.org/10.1038/nrg1493>
- Wellens, S., Dehouck, L., Chandrasekaran, V., Singh, P., Loiola, R.A., Sevin, E., Exner, T., Jennings, P., Gosselet, F., Culot, M., 2021. Evaluation of a human iPSC-derived BBB model for repeated dose toxicity testing with cyclosporine A as model compound. *Toxicol. Vitro.* 73, 105112. <https://doi.org/10.1016/j.tiv.2021.105112>
- Wen, Z., Nguyen, H.N., Guo, Z., Lalli, M.A., Wang, X., Su, Y., Kim, N.S., Yoon, K.J., Shin, J., Zhang, C., Makri, G., Nauen, D., Yu, H., Guzman, E., Chiang, C.H., Yoritomo, N., Kaibuchi, K., Zou, J., Christian, K.M., Cheng, L., Ross, C.A., Margolis, R.L., Chen, G., Kosik, K.S., Song, H., Ming, G.L., 2014. Synaptic dysregulation in a human iPS cell model of mental disorders. *Nature* 515, 414–418. <https://doi.org/10.1038/nature13716>
- Williams, E.S., Panko, J., Paustenbach, D.J., 2009. The European Union’s REACH regulation: a review of its history and requirements. <https://doi.org/10.1080/10408440903036056> 39, 553–575. <https://doi.org/10.1080/10408440903036056>
- Wilmes, A., Crean, D., Aydin, S., Pfaller, W., Jennings, P., Leonard, M.O., 2011. Identification and dissection of the Nrf2 mediated oxidative stress pathway in human renal proximal tubule toxicity. *Toxicol. Vitro.* 25, 613–622. <https://doi.org/10.1016/j.tiv.2010.12.009>
- Wittwehr, C., Blomstedt, P., Gosling, J.P., Peltola, T., Raffael, B., Richarz, A.N., Sienkiewicz, M., Whaley, P., Worth, A., Whelan, M., 2020. Artificial Intelligence for chemical risk assessment. *Comput. Toxicol.* 13, 100114. <https://doi.org/10.1016/J.COMTOX.2019.100114>
- Wu, W., Yao, H., Dwivedi, I., Negraes, P.D., Zhao, H.W., Wang, J., Trujillo, C.A., Muotri, A.R., Haddad, G.G., 2020. Methadone Suppresses Neuronal Function and Maturation in Human Cortical Organoids. *Front. Neurosci.* 0, 1175. <https://doi.org/10.3389/FNINS.2020.593248>

- Zhong, X., Harris, G., Smirnova, L., Zufferey, V., Sá, R. de C. da S. e., Baldino Russo, F., Baleeiro Beltrao Braga, P.C., Chesnut, M., Zurich, M.G., Hogberg, H.T., Hartung, T., Pamies, D., 2020a. Antidepressant Paroxetine Exerts Developmental Neurotoxicity in an iPSC-Derived 3D Human Brain Model. *Front. Cell. Neurosci.* 14, 1–11. <https://doi.org/10.3389/fncel.2020.00025>
- Zhong, X., Harris, G., Smirnova, L., Zufferey, V., Sá, R. de C. da S. e., Baldino Russo, F., Baleeiro Beltrao Braga, P.C., Chesnut, M., Zurich, M.-G., Hogberg, H.T., Hartung, T., Pamies, D., 2020b. Antidepressant Paroxetine Exerts Developmental Neurotoxicity in an iPSC-Derived 3D Human Brain Model. *Front. Cell. Neurosci.* 0, 25. <https://doi.org/10.3389/FNCEL.2020.00025>
- Zurich, M.-G., Stanzel, S., Kopp-Schneider, A., Prieto, P., Honegger, P., 2013. Evaluation of aggregating brain cell cultures for the detection of acute organ-specific toxicity. *Toxicol. Vitr.* 27, 1416–1424. <https://doi.org/10.1016/J.TIV.2012.06.018>
- Zurich, M.G., Eskes, C., Honegger, P., Bérode, M., Monnet-Tschudi, F., 2002. Maturation-dependent neurotoxicity of lead acetate *in vitro*: Implication of glial reactions. *J. Neurosci. Res.* 70, 108–116. <https://doi.org/10.1002/jnr.10367>
- Zurich, M.G., Honegger, P., Schilter, B., Costa, L.G., Monnet-Tschudi, F., 2000. Use of aggregating brain cell cultures to study developmental effects of organophosphorus insecticides. *Neurotoxicology* 21, 599–605.
- Zurich, M.G., Monnet-Tschudi, F., Bérode, M., Honegger, P., 1998. Lead acetate toxicity *in vitro*: Dependence on the cell composition of the cultures. *Toxicol. Vitr.* 12, 191–196. [https://doi.org/10.1016/S0887-2333\(97\)00089-1](https://doi.org/10.1016/S0887-2333(97)00089-1)

# Supplementary data

**Supplementary Table 1.: Potential disturbed BP (Gene ontology, p.adj value <0.01) after treatment with 10 µM Pb.**

Time Point	Biological Process		Involved DEG	
	Name	p.ad	Names	Count
48h	Protein localization to endoplasmic reticulum	4.71E-06	PPP1R15A, RPL28, RPL3, RPS5, UBA52, RPLP0, RPL27, RPL26	8
	Co-translational protein targeting to membrane	6.37E-06	RPL28, RPL3, RPS5, UBA52, RPLP0, RPL27, RPL26	7
	Establishment of protein localization to endoplasmic reticulum	1.01E-05	RPL28, RPL3, RPS5, UBA52, RPLP0, RPL27, RPL26	7
	Nuclear transcribed mRNA catabolic process nonsense mediated decay	1.22E-05	RPL28, RPL3, RPS5, UBA52, RPLP0, RPL27, RPL26	7
	Translational initiation	1.33E-05	PPP1R15A, RPL28, RPL3, RPS5, UBA52, RPLP0, RPL27, RPL26	8
	Ribosome biogenesis	1.89E-05	WDR3, NOP56, RPL3, RPS5, NSA2, RPLP0, RPL27, RPS27L, RPL26	9
	Protein targeting to membrane	0.000162	RPL28, RPL3, RPS5, UBA52, RPLP0, RPL27, RPL26	7
	Viral gene expression	0.000162	RPL28, RPL3, RPS5, UBA52, RPLP0, RPL27, RPL26	7
	Nuclear transcribed mRNA catabolic process	0.000229	RPL28, RPL3, RPS5, UBA52, RPLP0, RPL27, RPL26	7
	Ribonucleoprotein complex biogenesis	0.000248	WDR3, NOP56, RPL3, RPS5, NSA2, RPLP0, RPL27, RPS27L, RPL26	9
	Establishment of protein localization to membrane	0.000314	BCL2, RPL28, RPL3, RPS5, UBA52, RPLP0, RPL27, RPL26	8
	RNA catabolic process	0.001483	RPL28, RPL3, PSMA4, RPS5, UBA52, RPLP0, RPL27, RPL26	8
	Ribosome assembly	0.002558	RPL3, RPS5, RPLP0, RPS27L	4
	Post embryonic development	0.009417	BCL2, IGF2R, GNAS, PSEN1	4
168h	Response to nutrient	1.29E-05	NQO1, MDM2, HMOX1, AHCY	4

**Supplementary table 2.: Potential disturbed stress, apoptosis and neural BP (Gene ontology, p.adj value <0.01) after treatment with 25 nM DOXO for 7d.**

	Biological Process name	p.adj	Involved DEG
Stress and apoptosis	Response to oxidative stress	1.3E-07	36
	Regulation of apoptotic signalling pathway	1.3E-07	34
	Intrinsic apoptotic signalling pathway	2.6E-09	31
	Neuron apoptotic process	2.2E-08	27
	Cellular response to chemical stress	7.0E-05	25
	Extrinsic apoptotic signalling pathway	2.4E-07	24
	Signal transduction by p53 class mediator	9.1E-05	21
	Negative regulation of apoptotic signalling pathway	1.3E-04	19
	Negative regulation of neuron apoptotic process	2.2E-06	18
	Regulation of intrinsic apoptotic signalling pathway	8.8E-06	18
	Response to endoplasmic reticulum stress	3.4E-03	18
	Apoptotic mitochondrial changes	4.6E-06	16
	Positive regulation of apoptotic signalling pathway	2.5E-04	16
	Regulation of signal transduction by p53 class mediator	8.6E-04	15
	Regulation of extrinsic apoptotic signalling pathway	1.9E-03	13
	Regulation of DNA templated transcription in response to stress	1.1E-03	12
	Intrinsic apoptotic signalling pathway by p53 class mediator	1.0E-04	11
	Negative regulation of intrinsic apoptotic signalling pathway	6.5E-04	11
DNA damage response signal transduction by p53 class mediator	1.2E-03	11	
Epithelial cell apoptotic process	1.6E-03	11	

	Signal transduction in response to DNA damage	4.9E-03	11
	Extrinsic apoptotic signalling pathway via death domain receptors	9.7E-04	10
	Negative regulation of extrinsic apoptotic signalling pathway	3.1E-03	10
	Positive regulation of neuron apoptotic process	3.3E-04	9
	Cell death in response to oxidative stress	5.7E-03	9
	Intrinsic apoptotic signalling pathway in response to DNA damage	8.8E-03	9
	Positive regulation of intrinsic apoptotic signalling pathway	2.1E-03	8
	Intrinsic apoptotic signalling pathway in response to endoplasmic reticulum stress	2.2E-03	8
	G1 DNA damage checkpoint	2.4E-03	8
	Regulation of oxidative stress induced cell death	5.7E-03	8
	Regulation of response to endoplasmic reticulum stress	9.4E-03	8
	Positive regulation of transcription from RNA polymerase ii promoter in response to stress	3.4E-04	7
	Intrinsic apoptotic signalling pathway in response to oxidative stress	1.4E-03	7
	Regulation of extrinsic apoptotic signalling pathway in absence of ligand	2.0E-03	7
	Regulation of oxidative stress induced intrinsic apoptotic signalling pathway	8.9E-04	6
	Protein insertion into mitochondrial membrane involved in apoptotic signalling pathway	7.4E-04	5
	Regulation of intrinsic apoptotic signalling pathway by p53 class mediator	8.3E-03	5
	Positive regulation of transcription from RNA polymerase ii promoter in response to ER stress	1.8E-03	4
	Response to nitrosative stress	1.8E-03	4
	Negative regulation of oxidative stress induced intrinsic apoptotic signalling pathway	9.5E-03	4
Neural	Neuron death	2.5E-13	41
	Synapse organization	2.6E-06	31
	Regulation of trans synaptic signalling	6.3E-05	29
	Neuron projection guidance	1.1E-07	28
	Neuron apoptotic process	2.2E-08	27
	Positive regulation of neuron differentiation	7.7E-05	26
	Regulation of axonogenesis	2.6E-09	25
	Negative regulation of neuron differentiation	7.8E-07	23
	Negative regulation of neuron death	1.1E-06	22
	Glial cell differentiation	1.6E-06	22
	Positive regulation of neuron death	2.0E-11	21
	Positive regulation of neuron projection development	2.5E-04	21
	Negative regulation of neuron apoptotic process	2.2E-06	18
	Neuron projection extension	9.9E-06	18
	Post synapse organization	9.9E-06	18
	Axon extension	8.4E-07	17
	Central nervous system neuron differentiation	9.7E-05	17
	Negative regulation of neuron projection development	4.8E-05	16
	Neuron migration	7.4E-05	16
	Regulation of synapse structure or activity	2.9E-03	16
	Synapse assembly	7.5E-04	15
	Positive regulation of axonogenesis	2.4E-06	14
	Positive regulation of synaptic transmission	1.0E-03	14
	Central nervous system neuron development	4.6E-06	13
	Regulation of synaptic plasticity	7.0E-03	13
	Long term synaptic potentiation	2.3E-04	11
	Regulation of post synapse organization	8.7E-04	11
	Glial cell development	2.1E-03	11
	Neuron projection organization	1.2E-03	10
	Positive regulation of axon extension	5.3E-05	9
	Neuron recognition	9.0E-05	9
	Positive regulation of neuron apoptotic process	3.3E-04	9
	Astrocyte differentiation	2.2E-03	9
	Forebrain generation of neurons	2.2E-03	8
	Negative regulation of axonogenesis	3.3E-03	8
	Forebrain neuron differentiation	2.8E-03	7
	Post synapse assembly	1.6E-03	6
	Postsynaptic membrane organization	4.7E-03	6
	Regulation of long-term synaptic potentiation	8.3E-03	6
	Axonal fasciculation	2.8E-03	5
	Commissural neuron axon guidance	2.3E-03	4
Radial glial cell differentiation	2.3E-03	4	

**Supplementary table 3.: Potential disturbed neural function, oxidative stress and ER stress BP (Gene ontology, p.adj value <0.01) after treatment with PQ along concentrations and time points.**

GO Biological Processes		48h	168h		
Group	Name	5	1	2.5	5
Neural function	Amyloid Fibril Formation		1		
	Autonomic Nervous System Development				1
	Axon Extension				1
	Axonal Transport Of Mitochondrion	1	1		1
	Commissural Neuron Axon Guidance	1			
	Glial Cell Development				1
	Negative Regulation Of Amyloid Beta Clearance	1	1	1	
	Negative Regulation Of Neural Precursor Cell Proliferation				1
	Negative Regulation Of Neuron Apoptotic Process	1			1
	Negative Regulation Of Neuron Death	1			1
	Neural Precursor Cell Proliferation				1
	Neuron Apoptotic Process	1	1		1
	Neuron Death	1	1		1
	Positive Regulation Of Axon Extension	1	1		1
	Positive Regulation Of Axonogenesis	1	1		
	Positive Regulation Of Neuroblast Proliferation				1
	Positive Regulation Of Neuron Death		1		
	Positive Regulation Of Neuron Projection Development	1	1		
	Regulation Of Amyloid Beta Clearance		1	1	
	Regulation Of Axonogenesis	1	1		
Regulation Of Neural Precursor Cell Proliferation				1	
Synapse Organization	1				
Synaptic Transmission Glutamatergic	1				
Oxidative Stress	Regulation Of Transcription From Rna Polymerase Ii Promoter In Response To Oxidative Stress	1			
	Negative Regulation Of Oxidative Stress Induced Intrinsic Apoptotic Signaling Pathway	1			
	Cell Redox Homeostasis	1			
	Cellular Detoxification	1			
	Cellular Response To Oxygen Levels A	1			
	Cellular Response To Oxygen Levels B	1			
	Cellular Response To Oxygen Radical	1			
	Detoxification	1			
	Reactive Oxygen Species Metabolic Process	1			
	Regulation Of Reactive Oxygen Species Metabolic Process	1			
	Response To Oxygen Radical	1			
Response To Reactive Oxygen Species	1				
ER Stress	Atf6 Mediated Unfolded Protein Response				1
	Cellular Response To Topologically Incorrect Protein				1
	Chaperone Cofactor Dependent Protein Refolding				1
	De Novo Protein Folding				1
	Negative Regulation Of Endoplasmic Reticulum Unfolded Protein Response				1
	Perk Mediated Unfolded Protein Response	1	1	1	1
	Regulation Of Endoplasmic Reticulum Unfolded Protein Response		1		
	Regulation Of Perk Mediated Unfolded Protein Response				1
	Er Overload Response		1		1
	Intrinsic Apoptotic Signaling Pathway In Response To Endoplasmic Reticulum Stress		1	1	1
	Positive Regulation Of Endoplasmic Reticulum Stress Induced Intrinsic Apoptotic Signaling Pathway		1		
	Positive Regulation Of Response To Endoplasmic Reticulum Stress		1		
	Positive Regulation Of Transcription From Rna Polymerase Ii Promoter In Response To Endoplasmic Reticulum Stress		1		1
	Regulation Of Response To Endoplasmic Reticulum Stress		1		
Response To Endoplasmic Reticulum Stress		1		1	
<b>TOTAL</b>		<b>26</b>	<b>25</b>	<b>13</b>	<b>39</b>

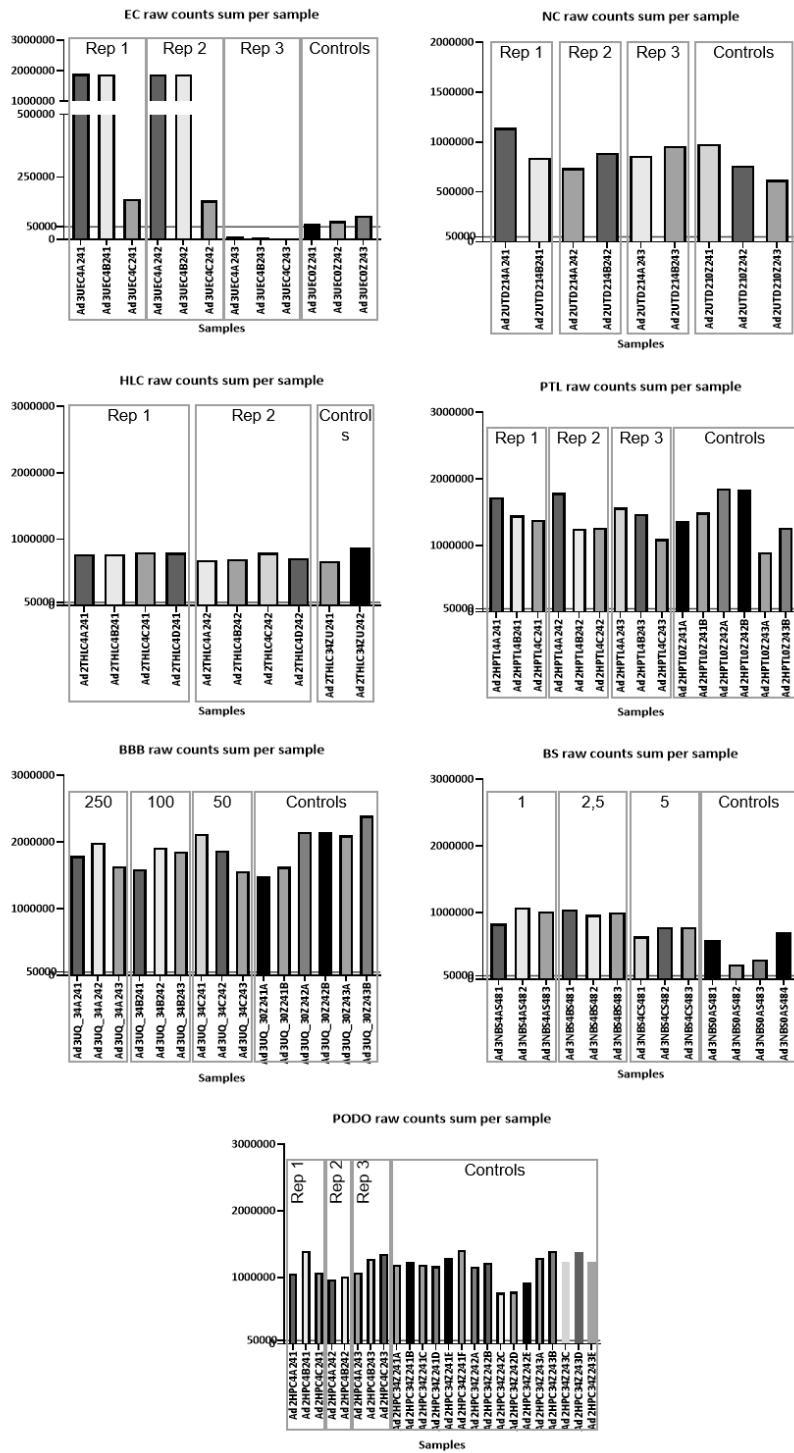
**Supplementary table 4.: Potential activated BP (Gene ontology, p.adj value <0.01) linked to neuronal function in BS after 56d in culture.**

Group	Biological Process		DEG involved
	Name	p.adj	
Axonogenesis	Regulation of axonogenesis	1.5E-15	41
	Positive regulation of axonogenesis	3.9E-12	25
	Axon extension	2.6E-08	24
	Negative regulation of axonogenesis	5.4E-06	15
	Positive regulation of axon extension	1.4E-06	13
	Negative regulation of axon extension	7.3E-04	9
	Regulation of axon guidance	1.0E-03	9
	Central nervous system projection neuron axonogenesis	1.5E-04	8
	Central nervous system neuron axonogenesis	1.3E-03	8
	Axonal fasciculation	5.9E-04	7
	Negative regulation of axon guidance	8.0E-03	6
Dendrite development	Dendrite development	5.0E-05	28
	Dendrite morphogenesis	2.4E-04	19
	Regulation of dendrite development	7.5E-03	16
	Dendritic spine morphogenesis	8.4E-03	9
Glial Cells	Glial cell differentiation	6.5E-07	30
	Glial cell development	1.8E-04	17
	Astrocyte differentiation	1.8E-03	12
Neuron function	Positive regulation of neuron differentiation	8.9E-08	44
	Positive regulation of neuron projection development	1.4E-08	39
	Neuron projection guidance	6.6E-07	35
	Negative regulation of neuron differentiation	3.2E-08	33
	Neuron projection extension	1.0E-08	29
	Negative regulation of neuron projection development	4.8E-06	23
	Central nervous system neuron differentiation	8.9E-05	23
	Neuron migration	1.0E-04	21
	Central nervous system neuron development	4.9E-08	19
	Neuron projection organization	1.3E-03	13
	Neuron recognition	5.9E-04	10
	Neuron projection regeneration	2.2E-03	10
Regulation of neuron migration	4.5E-03	8	
Synapsis	Synapse organization	7.6E-09	49
	Regulation of trans synaptic signalling	6.8E-08	49
	Regulation of synapse structure or activity	2.9E-06	30
	Post synapse organization	2.4E-05	23
	Synapse assembly	5.4E-05	23
	Regulation of synaptic plasticity	1.1E-04	23
	Neurotransmitter transport	9.4E-03	23
	Vesicle mediated transport in synapse	1.5E-03	22
	Positive regulation of synaptic transmission	1.5E-04	21
	Glutamate receptor signalling pathway	1.7E-06	19
	Synaptic transmission glutamatergic	5.0E-05	17
	Regulation of postsynaptic membrane potential	1.7E-03	17
	Regulation of neurotransmitter receptor activity	2.5E-06	16
	Regulation of synaptic vesicle cycle	1.1E-03	15
	Synaptic vesicle exocytosis	4.4E-03	14
	Regulation of glutamate receptor signalling pathway	5.5E-05	13
	Regulation of post synapse organization	4.2E-03	13
	Regulation of synapse assembly	6.2E-03	13
	Chemical synaptic transmission postsynaptic	7.3E-03	13
	Regulation of NMDA receptor activity	5.4E-06	11
	Regulation of synaptic vesicle exocytosis	4.7E-03	11
	Long term synaptic potentiation	9.1E-03	11
	Synaptic vesicle localization	7.3E-03	9
Ionotropic glutamate receptor signalling pathway	1.9E-04	8	
Regulation of long term neuronal synaptic plasticity	1.2E-03	7	
Synapse maturation	1.2E-03	7	
Postsynaptic signal transduction	8.1E-03	7	

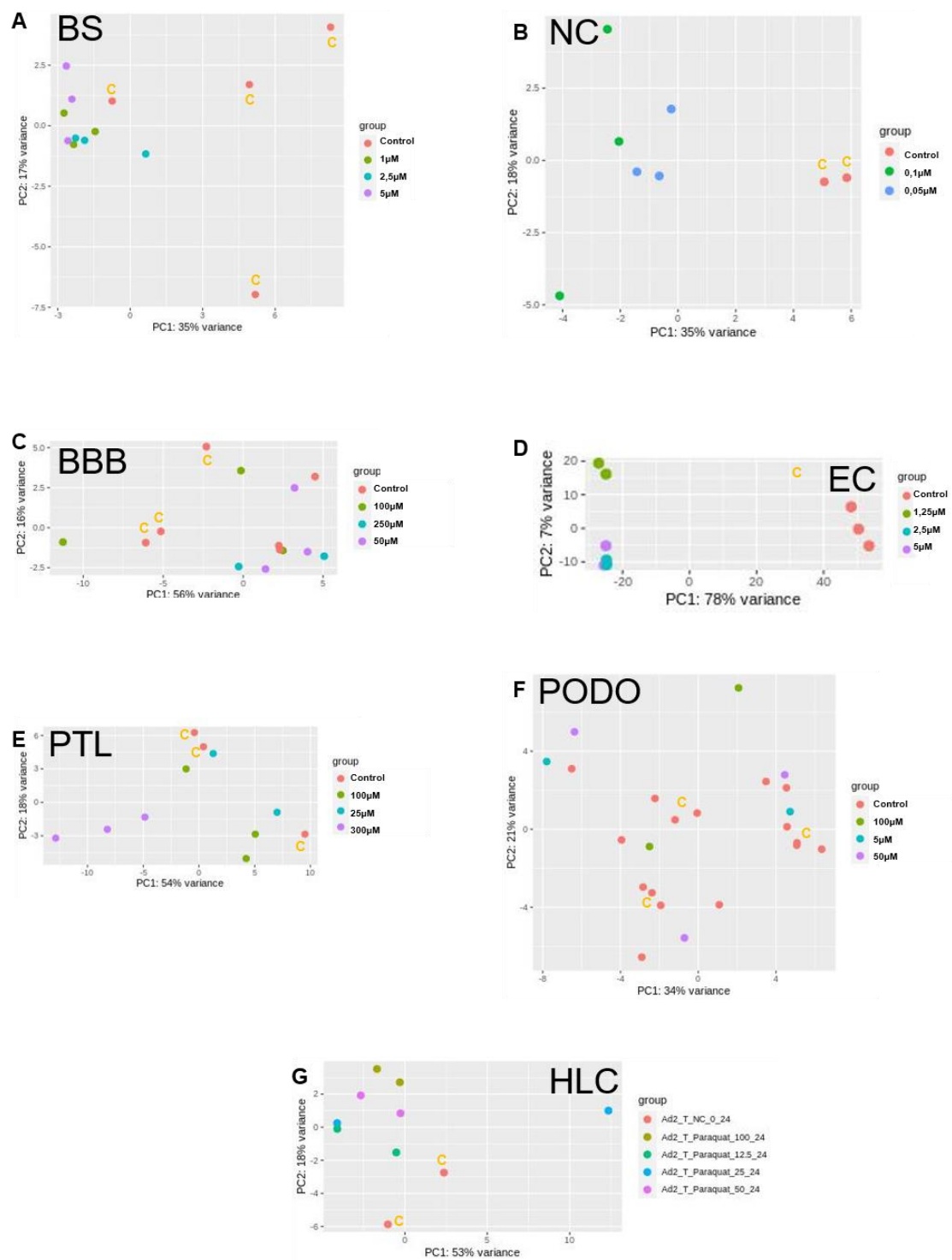
**Supplementary table 5.: Flow cytometry analysis of Ad3G2 cells after passage 4 and 14 in culture for neural crest, neural, neuroepithelial and pluripotent markers.**

<b>Ad3G2</b>		<b>Total ( % )</b>		<b>Expected results ( % )</b>
<b>Antibodies</b>		<b>Passage 4</b>	<b>Passage 14</b>	
<b>CD271</b>	<b>Neural Crest</b>	4.7	6.3	≤10%
<b>CD56</b>	<b>Neural</b>	98	97.3	≥90%
<b>CD57</b>	<b>Neuroepithelial</b>	99.8	99	≥90%
<b>SSEA4</b>	<b>Pluripotency</b>	0.03	0	≤2%

# Annex 1.: Chapter 2 Supplementary Data



Supplementary Figure 1.: TempO-Seq raw read counts per sample for each hiPSC-derived model



**Supplementary Figure 2.** PCA of all samples per model after filtering. (A) BS (B) NC (C) BBB (D) EC (E) PTL (F) PODO (G) HLC.

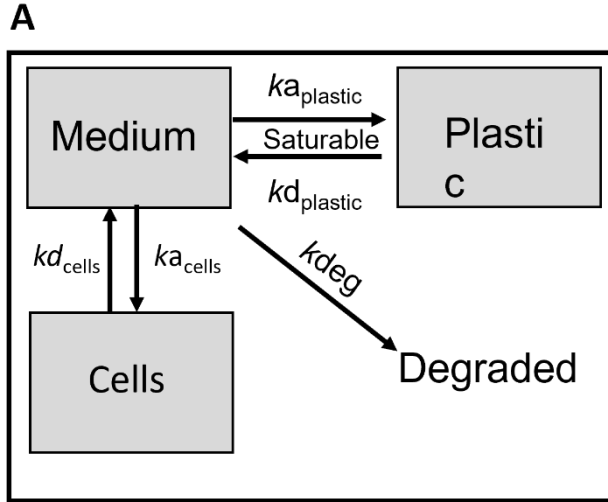
Shared Genes	LFC per model per condition ( $\mu\text{M}$ )																	
	BS			NC		BBB			PTL			PODO			HLC			
	1	2,5	5	0,05	0,1	50	100	250	25	100	300	5	50	100	12,5	25	50	100
MAFF_27478		x		1,88	2,31	0,02	0,72	0,78	0,39	1,64	2,82	-0,43	0,51	1,11	0,24	1,52	1,26	1,68
PPP1R15A_14098	0,49	0,50	0,85	1,03	1,86		x		0,28	1,27	2,32	0,19	0,22	0,81	0,38	1,12	0,98	1,28
VEGFA_28053	0,60	0,79	0,90	0,93	1,06		x		0,13	1,21	2,14	0,05	0,37	0,74			x	
ATF4_500		x		0,60	0,70	0,31	0,47	0,93	-0,04	0,27	1,48		x		0,25	0,42	0,30	1,04
GDF15_18329		x		1,58	1,93	0,29	0,91	1,89	1,09	3,18	6,75		x		0,97	0,84	1,27	1,67

Shared Genes	LFC per model per condition ( $\mu\text{M}$ )					
	PODO			PTL		
	5	50	100	25	100	300
CD55_28297	0,49	1,01	1,51	0,51	1,09	1,27
CHKA_14315	0,26	0,44	0,69	0,06	0,43	0,75
DUSP1_24234	0,20	0,36	0,99	0,29	0,70	2,33
ENO2_13140	0,82	0,67	0,96	0,18	0,80	0,95
HSPA1B_3136	-0,35	-0,12	-0,82	0,59	0,42	1,28
MAFF_27478	-0,43	0,51	1,11	0,39	1,64	2,82
MAFG_20735	0,47	0,42	1,20	0,28	1,20	2,06
PPP1R15A_14098	0,19	0,22	0,81	0,28	1,27	2,32
VEGFA_28053	0,05	0,37	0,74	0,13	1,21	2,14

Shared Genes	LFC per model per condition ( $\mu\text{M}$ )				
	BS			NC	
	1	2,5	5	0,05	0,1
CBX4_16907	0,72	0,67	0,56	0,66	1,05
EIF1_2074	0,28	0,28	0,63	0,53	0,88
PPP1R15A_14098	0,49	0,50	0,85	1,03	1,86
SLC3A2_20164	0,60	0,56	0,74	1,48	2,17
TUBA1B_7399	-1,34	-0,97	-1,40	-0,40	-0,84
VEGFA_28053	0,60	0,79	0,90	0,93	1,06

**Supplementary Figure 3.:** List of the DEGs shared by at least 4 models or by modelled organ (brain and kidney). Log2 fold changes (LFC) of genes presented in Table 3.

# Annex 2.: Chapter 3 Supplementary Data



**B**

$$\frac{dA_{plastic}}{dt} = -Kd_{plastic} \times A_{plastic} + Ka_{plastic} \times (N_{max} - A_{plastic}) \times A_{medium}$$

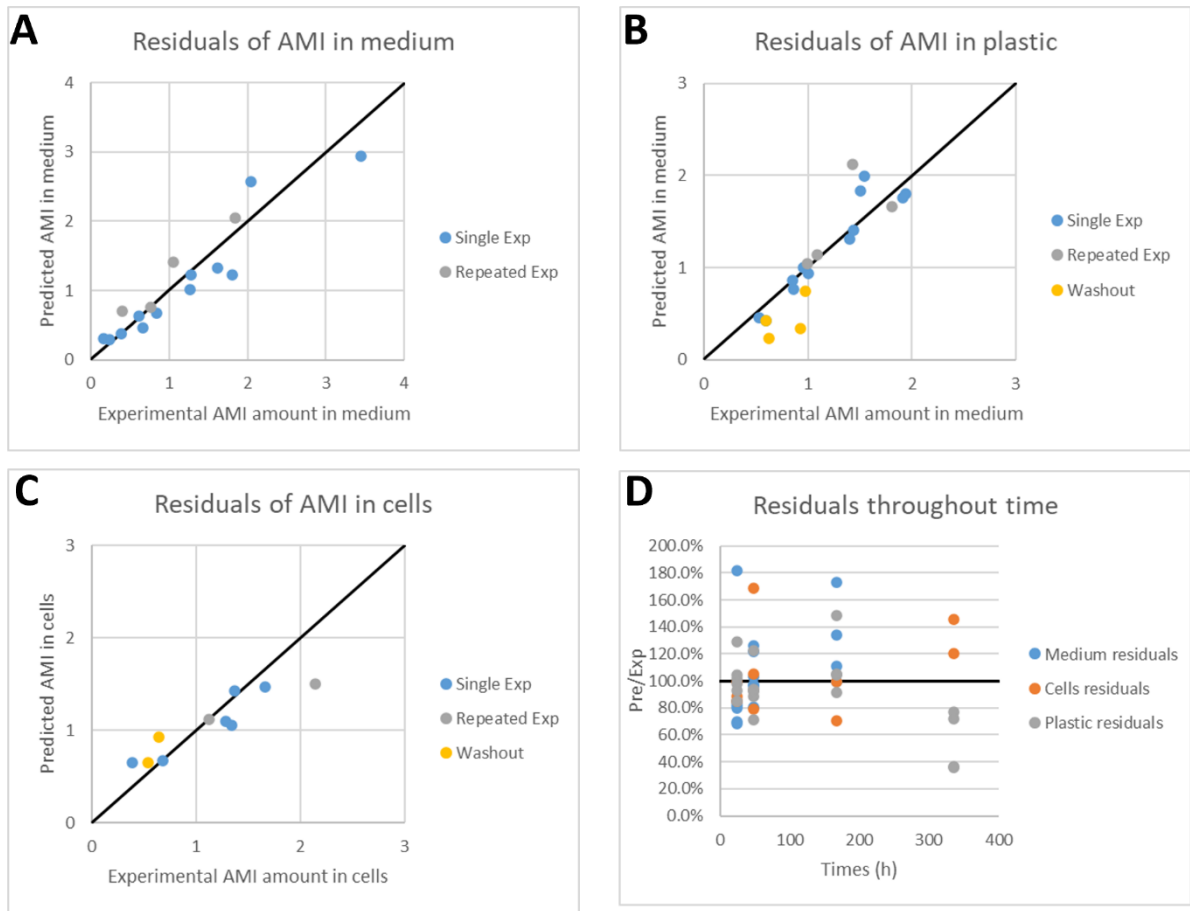
$$\frac{dA_{cells}}{dt} = -Kd_{cells} \times A_{cells} + Ka_{cells} \times A_{medium}$$

**C**

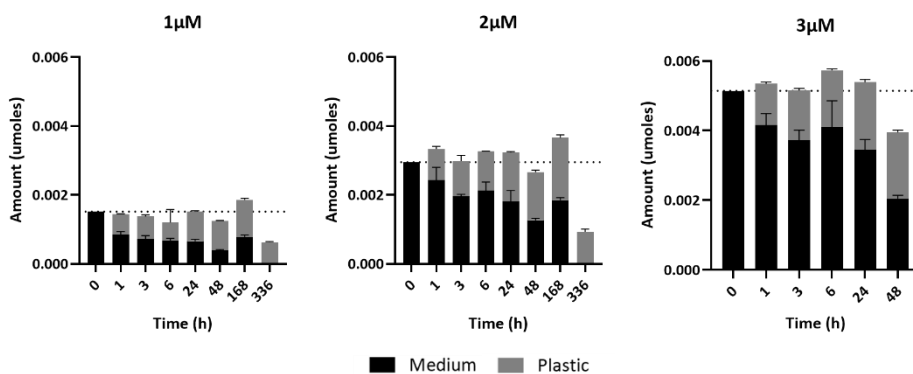
Fit parameter	Value
$ka_{plastic}$ (nmoles <sup>-1</sup> ×h <sup>-1</sup> )	0.434
$kd_{plastic}$ (nmoles <sup>-1</sup> ×h <sup>-1</sup> )	0.138
$N_{max}$ (nmoles)	2.278
$k_{deg}$ (nmoles <sup>-1</sup> ×h <sup>-1</sup> )	0.0096
$ka_{cells}$ (nmoles <sup>-1</sup> ×h <sup>-1</sup> )	0.368
$kd_{cells}$ (nmoles <sup>-1</sup> ×h <sup>-1</sup> )	0.248

**Suppl. Figure 1. Compartmental model developed to simulate the distribution of AMI in the BS in vitro system after repeated exposure.** (A) Conceptual representation of the compartments and mass transfer in the model. (B) Differential equations used to simulate the mass transfer of amiodarone between medium, plastic and cells and respective parameters and constants:  $A_{plastic}$  = amount in plastic (nmoles),  $A_{medium}$  = amount in medium (nmoles),  $k_{deg}$ =rate constant of irreversible loss process (nmoles<sup>-1</sup> × h<sup>-1</sup>),  $ka_{plastic}$  = rate constant of sorption to plastic (nmoles<sup>-1</sup>×h<sup>-1</sup>) and  $kd_{plastic}$  = rate constant of

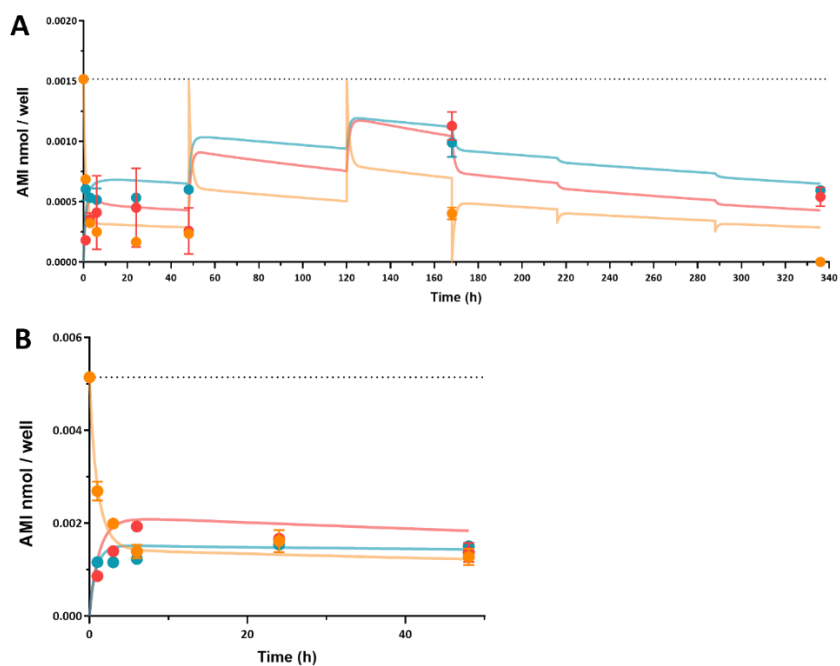
desorption from plastic ( $\text{nmoles}^{-1} \times \text{h}^{-1}$ ). (C) Fit parameters used in biokinetic in silico model for AMI exposure in BS cultures and respective no -cells controls. These parameters were fit by minimization of RMSE using FGS algorithm implemented through optim function in R.



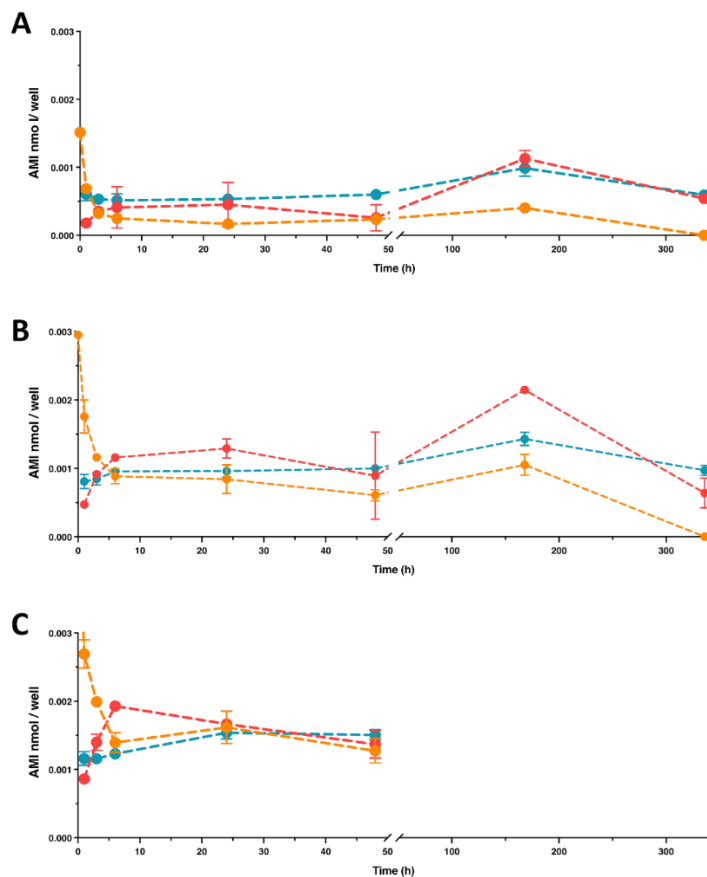
**Suppl. Figure 2. Plots of residuals from kinetic model predictions of AMI amount in the different compartments.** Residuals from predictions of AMI in (A) Medium, (B) Plastic and (C) Cells. (D) Residuals of the three compartments throughout time D).



**Suppl. Figure 3. AMI distribution kinetic in absence of cells.** (A) Relative distribution of AMI in the different compartments without cells: medium (black bars) and plastic binding (grey bars) after acute (1 - 48 h) and repeated treatment (168 h = 7d and 336 h = 7dW). Results are reported as mean  $\pm$  SD of three replicates.



**Suppl. Figure 4. AMI distribution kinetic: in vitro experimental values and in silico prediction simulation.** Kinetic profile of AMI experimentally measured in cell lysates (red circles), in medium (orange circles) and in plastic bound fraction (blue circles) of BS exposed to (A) 1  $\mu$ M and (B) 3  $\mu$ M. Each value is the mean ( $\pm$ SD) of 3 replicates. Predicted curves are superimposed on experimentally measured values, cells (red line), medium (orange line), plastic binding (blue line). Dotted line represents the quantification of AMI in the medium at time = 0.



**Suppl. Figure 5. AMI distribution kinetic.** Kinetic profile of AMI experimentally measured in cell lysates (red), in medium (Orange) and in plastic binding samples (blue) of BS exposed to AMI (A) 1  $\mu$ M and (B) 2  $\mu$ M and (C) 3  $\mu$ M. Each value is the mean ( $\pm$ SD) of 3 replicates.

**Suppl. Table 1: Sequences of qPCR primers used with SYBR green® and cDNA input**

Gene name	Sequence (5'-3')	cDNA (ng/well)
Nestin	F' GGGAGTTCTCAGCCTCCAG R' GGAGAAACAGGGCCTACAGA	1
RLP13A	F' CATAGGAAGCTGGGAGCAAG R' GCCCTCCAATCAGTCTTCTG	1
Sox2	F' CCATGCAGGTTGACACCGTTG R' TCGGCAGACTGATTCAAATAATACAG	1
Ki67	F' GCCTGCTCGACCCTACAGA R' GCTTGTCAACTGCGGTTGC	1
TH	F' GGTGGATTTTGGCTTCAAAC R' CTGTGGCCTTTGAGGAGAAG	1
SYP	F' TGACGAGGAGTAGTCCCAA R' CGAGGTCGAGTTCGAGTACC	1
MAP2	F' GGGTCTACTGCCATCACTCC R' GATGGCGACCTTCTTCTCAC	1
GRIN1	F' GGTATACAGTGGCAGCATCG R' CAGGGACCAAGAACGTGAC	1
ACHE	F' TACGAGCCCTCATCCTTAC R' CCTTCGTGCCTGTGGTAGAT	1
Vimentin	F' ATTCCAATTTGCGTTCAAGG R' CTTCAGAGAGAGGAAGCCGA	1
S100 $\beta$	F' ATGTCTGAGCTGGAGAAGGC R' TTCAAAGAACTCGTGGCAGG	1
MBP	F' ACCTCGTTTCAAACCACAG R' GGAAGTGAATGAGCCGGTTA	10
B3T	F' AGTCGCCACGTAGTTGC R' CGCCAGTATGAGGGAGAT	1
GABBR1	F' CTCCTGGAAGCCTCCTGTCT R' CATGCTGAATCCTGCCAATA	1
PSMB8	F' CACGCTCGCCTTCAAGTTC R' AGGCACTAATGTAGGACCCAG	1
Olig2	F' TGGCTTCAAGTCATCCTCGTC R' ATGGCGATGTTGAGGTCGTG	1

**Suppl. Table 2: References for TaqMan® assays and cDNA input**

Gene name	Assay ID (Thermofisher)	cDNA (ng/well)
SLC27A4	Hs00192700_m1	1
PPARGC1	Hs00173304_m1	1
FASN	Hs001005622_m1	1
GDPD3	Hs00225626_m1	5
LPL	Hs00174325_m1	5
PLIN1	Hs00160173_m1	5
PLIN2	Hs00605340_m1	10
PLIN3	Hs00998416_m1	1
PLIN4	Hs00287411_m1	10

PLIN5	Hs00965990_m1	5
RLP13A	Hs01926559_g1	1
GFAP	Hs00909233_m1	20

**Suppl. Table 3: List of primary and secondary antibodies used for Immunohistochemistry**

Type	Name	Species	Reference
Primary	NF200	Rabbit	Sigma Cat# N4142
	SYP	Mouse	Sigma Cat# SAB4200544
	S100 $\beta$ a	Rabbit	Agilent Cat# Z0311
	S100 $\beta$ b	Rabbit	Abcam Cat# ab52642
	GFAP	Rabbit	Sigma Cat# G9269
	B3T	Mouse	Sigma Cat# T8660
	O4	Mouse	Sigma Cat# MAB1326
Secondary	Alexa <sup>®</sup> 594 against Rabbit	Goat	ThermoFisher Cat#A11037
	Alexa <sup>®</sup> 488 against Mouse	Donkey	ThermoFisher Cat#A21202

---

# Annex 3.: AOP17 KER: Oxidative Stress leads to Cell injury/death

---

**Upstream event:** Oxidative Stress

**Downstream event:** Cell injury/death

## 7.3.1. Key Event Relationship Description

Oxidative stress (OS) as a concept in redox biology and medicine has been formulated in 1985 (Sies, 2015). OS is intimately linked to cellular energy balance and comes from the imbalance between the generation and detoxification of reactive oxygen and nitrogen species (ROS/RNS) or from a decay of the antioxidant protective ability. OS is characterized by the reduced capacity of endogenous systems to fight against the oxidative attack directed towards target biomolecules (Pisoschi and Pop, 2015; Wang and Michaelis, 2010). Glutathione, the most important redox buffer in cells (antioxidant), cycles between reduced glutathione (GSH) and oxidized glutathione disulfide (GSSG), and serves as a vital sink for control of ROS levels in cells (Reynolds *et al.*, 2007). Several case-control studies have reported the link between lower concentrations of GSH, higher levels of GSSG and the development of diseases (Rossignol and Frye, 2014). OS can cause cellular damage and subsequent cell death because the ROS oxidize vital cellular components such as lipids, proteins, and nucleic acids (Gilgun-Sherki *et al.*, 2001; Wang and Michaelis, 2010).

The central nervous system is especially vulnerable to free radical damage since it has a high oxygen consumption rate, an abundant lipid content and reduced levels of antioxidant enzymes (Coyle and Puttfarcken, 1993; Markesbery, 1997). It has been shown that the developing brain is particularly vulnerable to neurotoxicants and OS due to differentiation processes, changes in morphology, lack of physiological barriers and less intrinsic capacity to cope with cellular stress (Grandjean and Landrigan, 2014; J. Sandström *et al.*, 2017). OS has been linked to brain aging, neurodegenerative diseases, and other related adverse conditions. There is evidence that free radicals play a role in cerebral ischemia-reperfusion, head injury, Parkinson's disease, amyotrophic lateral sclerosis, Down's syndrome, and Alzheimer's disease due to cellular damage (Gilgun-Sherki *et al.*, 2001; Markesbery, 1997; Wang and Michaelis, 2010). OS has also been linked to neurodevelopmental diseases and deficits like autism spectrum disorder and postnatal motor coordination deficits (Bhandari and Kuhad, 2015; Rossignol and Frye, 2014; Wells *et al.*, 2009).

### 7.3.4. Evidence Supporting this KER

#### 7.3.4.1. Biological Plausibility

A noteworthy insight, early on, was the perception that oxidation-reduction (redox) reactions in living cells are utilized in fundamental processes of redox regulation, collectively termed 'redox signalling' and 'redox control' (Sies, 2015).

Free radical-induced damage in OS has been confirmed as a contributor to the pathogenesis and patho-physiology of many chronic diseases, such as Alzheimer, atherosclerosis, Parkinson, but also in traumatic brain injury, sepsis, stroke, myocardial infraction, inflammatory diseases, cataracts and cancer (Bar-Or *et al.*, 2015; Pisoschi and Pop, 2015). It has been assessed that oxidative stress is correlated with over 100 diseases, either as source or outcome (Pisoschi and Pop, 2015).

Therefore, the fact that ROS over-production can kill neurons is well accepted (Brown and Bal-Price, 2003; Taetzsch and Block, 2013). This ROS over-production can occur in the neurons themselves or can also have a glial origin (Yuste *et al.*, 2015).

#### 7.3.4.2. Empirical support for linkage

##### Mercury

Oxidative stress has been implicated in the pathogenesis of methylmercury (MeHg) neurotoxicity. Studies of mature neurons suggest that the mitochondrion may be a major source of MeHg-induced reactive oxygen species and a critical mediator of MeHg-induced neuronal death, likely by activation of apoptotic pathways. (Polunas *et al.*, 2011)

(Lu *et al.*, 2011) - MeHg in the mouse cerebrum (*in vivo*) and in cultured Neuro-2a cells (*in vitro*).

- *In vivo* - 50µg/kg/day MeHg for 7 consecutive weeks - increased levels of lipid peroxidation in the plasma and cerebral cortex. Decreased GSH level and increase the expressions of caspase-3, -7, and -9, accompanied by Bcl-2 down-regulation and up-regulation of Bax, Bak, and p53.
- *In vitro* – 3 and 5 µM MeHg - reduced cell viability, increased oxidative stress damage, and induced several features of mitochondria-dependent apoptotic signals, including increased sub-G1 hypodiploids, mitochondrial dysfunctions, and the activation of PARP, and caspase cascades.

- These MeHg-induced apoptotic-related signals could be remarkably reversed by antioxidant NAC.

(Sarafian *et al.*, 1994) - Hypothalamic mouse neural cell line GT1-7 without and with expression construct for the anti-apoptotic proto-oncogene, bcl-2.

- 3h exposure, 10  $\mu$ M MeHg - increased formation of reactive ROS, and decreased levels of GSH, associated with 20% cell death. Cells transfected with an expression construct bcl-2, displayed attenuated ROS induction and negligible cell death.
- 24h exposure, 5  $\mu$ M MeHg - killed 56% of control cells, but only 19% of bcl-2-transfected cells.
- By using diethyl maleate to deplete cells of GSH, we demonstrate that the differential sensitivity to MeHg was not due solely to intrinsically different GSH levels. The data suggest that MeHg-mediated cell killing correlates more closely with ROS generation than with GSH levels and that bcl-2 protects MeHg-treated cells by suppressing ROS generation.

(Castoldi *et al.*, 2000) - *In vitro* exposure of primary cultures of rat CGCs to MeHg resulted in a time- and concentration-dependent cell death.

- 1 hr exposure, 5–10  $\mu$ M MeHg - impairment of mitochondrial activity, de-energization of mitochondria and plasma membrane lysis, resulting in necrotic cell death.
- 1hr exposure, 0.5–1  $\mu$ M MeHg - did not compromise cell viability, mitochondrial membrane potential and function at early time points.
- 1hr exposure, 1  $\mu$ M MeHg - only a small population of neurons (+20%) dies by necrosis. The surviving neurons show network damage, but maintain membrane integrity, mitochondrial membrane potential and function at early time points. Later, however, the cells progressively display the morphological signs of apoptosis.
- 18hr exposure, 0.5–1  $\mu$ M MeHg – cells progressively underwent apoptosis reaching the 100% cell death
- insulin-like growth factor-I partially rescued CGCs from MeHg-triggered apoptosis.

(Kaur *et al.*, 2006) - primary cell cultures of cerebellar neurons and astrocytes from 7-day-old NMRI mice. 5 mM MeHg for 30 min.

- Twenty-one days post-astrocyte isolation - 250mM N-acetyl cysteine (NAC) or 3mM diethyl maleate (DEM) added to the wells 12 h prior to MeHg exposure
- 7 days post-neurons isolation - 200mM of NAC or 1.8mM of DEM added to the wells 12 h prior to MeHg exposure
- The intracellular GSH content was modified by pretreatment with NAC or DEM for 12 h.
- Treatment with 5 mM Me Hg for 30 min led to significant ( $p < 0.05$ ) increase in ROS and reduction ( $p < 0.001$ ) in GSH content.
- Depletion of intracellular GSH by DEM further increased the generation of MeHg-induced ROS in both cell cultures.
- NAC supplementation increased intracellular GSH and provided protection against MeHg-induced oxidative stress in both cell cultures.

(Franco *et al.*, 2007) – Mitochondrial enriched fractions from adult (2 months old) Swiss Albino male mice.

- MeHg and HgCl<sub>2</sub> (10–100  $\mu$ M) significantly decreased mitochondrial viability; this phenomenon was positively correlated to mercurial-induced glutathione oxidation.
- Both mercurials induced a significant reduction of GSH in a dose-dependent manner.
- Correlation analyses showed significant positive correlations between mitochondrial viability and glutathione content for MeHg (Pearson coefficient) 0.933;  $P < 0.01$ ) and or HgCl<sub>2</sub> (Pearson coefficient) 0.854;  $P < 0.01$ ).
- Quercetin (100–300  $\mu$ M) prevented mercurial-induced disruption of mitochondrial viability. Moreover, quercetin, which did not display any chelating effect on MeHg or HgCl<sub>2</sub>, prevented mercurial-induced glutathione oxidation.

(Polunas *et al.*, 2011) - Murine embryonal carcinoma (EC) cells, which differentiate into neurons following exposure to retinoic acid.

- 4h exposure, 1.5 mM MeHg - earlier and significantly higher levels of ROS production and more extensive mitochondrial depolarization in neurons than in undifferentiated EC cells. cyclosporin A (CsA) completely inhibited mitochondrial depolarization by MeHg in EC cells but only delayed this response in the neurons. In contrast, CsA significantly inhibited MeHg-induced neuronal ROS production. Cyt c release was also more extensive in neurons, with less protection afforded by CsA.

(Sandström *et al.*, 2016) - *in vitro* 3D human neural tissues from neural progenitor cells derived from human embryonic stem cells. Single MeHg exposure at day 42 of 3D culturing (week 6) and material was collected 72 h after.

- 1-10  $\mu\text{M}$  - LDH activity increased, confirming induced cell death.
- 5 and 10  $\mu\text{M}$  - increased HMOX1 gene expression as indirect marker of oxidative stress.

#### Acrylamide

(Allam *et al.*, 2011) - sixty albino *Rattus norvegicus*, 45 virgin females and 15 mature males. This study examined its effects on the development of external features in cubs.

- prenatal intoxicated group - newborns from mothers treated with ACR from day 7 (GD 7) of gestation till birth
- perinatal intoxicated group - newborns from mothers treated with ACR from GD7 of gestation till D28 after birth
- ACR administered either prenatally or perinatally has been shown to induce significant retardation in the newborns' body weights development, increase of thiobarbituric acid-reactive substances (TBARS) and oxidative stress (significant reductions in glutathione reduced, total thiols, superoxide dismutase and peroxidase activities) in the developing cerebellum. ACR treatment delayed the proliferation in the granular layer and delayed both cell migration and differentiation. Purkinje cell loss was also seen in acrylamide-treated animals. Ultrastructural studies of Purkinje cells in the perinatal group showed microvacuolations and cell loss.

(Lakshmi *et al.*, 2012) - Wistar male albino rats, four groups (n = 6 per group)

- II – (Acrylamide) ACR - 30 mg/kg ACR for 30 days: increase in the lipid peroxidative (LPO), protein carbonyl, hydroxyl radical and hydroperoxide levels with subsequent decrease in the activities of enzymic antioxidants and level of GSH. Cortex showed condensed nuclei along with damaged cells. Decrease in the expression of Bcl2 along with simultaneous increase in the expressions of Bax and Bad as compared to control.
- II rats – ACR + Fish oil - 0.5 ml/kg b.w. fish oil orally 10 min before ACR induction with 30 mg/kg for 30 days – reversed significantly all the OS markers.

#### 4.3.4.3. Uncertainties and Inconsistencies

Mercury-induced upregulation of GSH level and GR activity as an adaptive mechanism following lactational exposure to methylmercury (10 mg/L in drinking water) associated with motor deficit, suggesting neuronal impairment (Franco *et al.*, 2006).

### 7.3.5. Quantitative Understanding of the Linkage

**Table 8.1: Quantitative understanding**

Reference	Chemical Concentration	OS	Cell injury/death
(Sarafian <i>et al.</i> , 1994)	MeHg 0 $\mu$ M	ROS – $\pm$ 100% DCF Fluorescence GSH – $\pm$ 150% MCB Fluorescence	$\pm$ 90% Viability
	MeHg 5 $\mu$ M	ROS – $\pm$ 150% DCF Fluorescence GSH – $\pm$ 100% MCB Fluorescence	$\pm$ 80% Viability
	MeHg 10 $\mu$ M	ROS – $\pm$ 200% DCF Fluorescence GSH – $\pm$ 70% MCB Fluorescence	$\pm$ 70% Viability
(Lu <i>et al.</i> , 2011)	MeHg 0 $\mu$ M	(2h) ROS – $\pm$ 100% DCF Fluorescence (24h) 100% intracellular GSH levels	100% Cell viability
	MeHg 3 $\mu$ M	(2h) ROS – $\pm$ 160 DCF Fluorescence (24h) $\pm$ 60% intracellular GSH levels	$\pm$ 50% Cell viability
	MeHg 5 $\mu$ M	(2h) ROS – $\pm$ 230 DCF Fluorescence (24h) $\pm$ 30% intracellular GSH levels	$\pm$ 10% Cell viability
	MeHg 3 $\mu$ M + NAC 1mM	(2h) ROS – $\pm$ 70 DCF Fluorescence (24h) $\pm$ 90% intracellular GSH levels	$\pm$ 90% Cell viability
	MeHg 5 $\mu$ M + NAC 1mM	(2h) ROS% – $\pm$ 70 DCF Fluorescence (24h) $\pm$ 90% intracellular GSH levels	$\pm$ 90% Cell viability
(Kaur <i>et al.</i> , 2006)	0 mM MeHg	Neurons - GSH – 100v MCB Fluorescence ROS – 100% CMH2DCFDA Fluorescence Astrocytes - GSH – 100v MCB Fluorescence ROS – 100% CMH2DCFDA Fluorescence	(Neurons) 100% Cell viability (Astrocytes) 100% Cell viability
	5 mM MeHg	Neurons - GSH – $\pm$ 50v MCB Fluorescence ROS – $\pm$ 400% CMH2DCFDA Fluorescence Astrocytes - GSH – $\pm$ 70% MCB Fluorescence ROS – $\pm$ 120% CMH2DCFDA Fluorescence	(Neurons) $\pm$ 60% Cell viability (Astrocytes) $\pm$ 75% Cell viability
	5 mM MeHg + NAC	Neurons - GSH – $\pm$ 80% MCB Fluorescence ROS – $\pm$ 200% CMH2DCFDA Fluorescence Astrocytes - GSH – $\pm$ 80% MCB Fluorescence ROS – $\pm$ 90% CMH2DCFDA Fluorescence	(Neurons) $\pm$ 90% Cell viability (Astrocytes) $\pm$ 90% Cell viability
	5 mM MeHg + DEM	Neurons - GSH – $\pm$ 50% MCB Fluorescence ROS – $\pm$ 470% CMH2DCFDA Fluorescence Astrocytes - GSH – $\pm$ 70% MCB Fluorescence ROS – $\pm$ 120% CMH2DCFDA Fluorescence	(Neurons) $\pm$ 55% Cell viability (Astrocytes) $\pm$ 65% Cell viability
	NAC	Neurons - GSH – $\pm$ 110% MCB Fluorescence ROS – $\pm$ 100% CMH2DCFDA Fluorescence Astrocytes - GSH – $\pm$ 100% MCB Fluorescence ROS – $\pm$ 60% CMH2DCFDA Fluorescence	(Neurons) $\pm$ 110% Cell viability (Astrocytes) $\pm$ 110% Cell viability
	DEM	Neurons - GSH – $\pm$ 60% MCB Fluorescence ROS – $\pm$ 250% CMH2DCFDA Fluorescence Astrocytes - GSH – $\pm$ 80% MCB Fluorescence ROS – $\pm$ 110% CMH2DCFDA Fluorescence	(Neurons) $\pm$ 80% Cell viability (Astrocytes) $\pm$ 85% Cell viability
(Franco <i>et al.</i> , 2007)	0 $\mu$ M MeHg	100% GSH	100% mitochondrial viability
	30 $\mu$ M MeHg	$\pm$ 70% GSH	$\pm$ 70% mitochondrial viability
	0 $\mu$ M HgCl <sub>2</sub>	100% GSH	100% mitochondrial viability
	30 $\mu$ M HgCl <sub>2</sub>	$\pm$ 65% GSH	$\pm$ 65% mitochondrial viability
(Lakshmi <i>et al.</i> , 2012)	Control	GSH – 0.5 $\mu$ moles/mg of protein	$\pm$ 6 Damaged cells/Field
	Acrylamid	GSH – 0.2 $\mu$ moles/mg of protein	$\pm$ 20 Damaged cells/Field
	Acrylamid + Fish Oil	GSH – 0.4 $\mu$ moles/mg of protein	$\pm$ 11 Damaged cells/Field
	Fish Oil	GSH – 0.5 $\mu$ moles/mg of protein	$\pm$ 5 Damaged cells/Field

### 7.3.6. Domain of Applicability

Rat, Mouse: (Castoldi *et al.*, 2000; Franco *et al.*, 2007; Kaur *et al.*, 2006; Lu *et al.*, 2011; Polunas *et al.*, 2011; Sarafian *et al.*, 1994)

(Richetti *et al.*, 2011) - Adult and healthy zebrafish of both sexes (12 animals and housed in 3 L) mercury chloride final concentration of 20 mg/L. Mercury chloride promoted a significant decrease in acetylcholinesterase activity and the antioxidant competence was also decreased.

(Berntssen *et al.*, 2003) - Atlantic salmon (*Salmo salar* L.) were supplemented with mercuric chloride (0, 10, or 100 mg Hg per kg) or methylmercury chloride (0, 5, or 10 mg Hg per kg) for 4 months.

#### Methylmercury chloride

- accumulated significantly in the brain of fish fed 5 or 10 mg/kg
- No mortality or growth reduction
- 5mg/kg - 2-fold increase in the antioxidant enzyme super oxide dismutase (SOD) in the brain
- 10 mg/kg - 7-fold increase of lipid peroxidative products (thiobarbituric acid reactive substances, TBARS) and a subsequently 1.5-fold decrease in anti oxidant enzyme activity (SOD and glutathione peroxidase, GSH-Px). Fish also had pathological damage (vacuolation and necrosis), significantly reduced neural enzyme activity (5-fold reduced monoamine oxidase, MAO, activity), and reduced overall post-feeding activity behaviour.

#### Mercuric chloride

- accumulated significantly in the brain only at 100 mg/kg
- No mortality or growth reduction
- 100 mg/kg - significant reduced neural MAO activity and pathological changes (astrocyte proliferation) in the brain, however, neural SOD and GSH-Px enzyme activity, lipid peroxidative products (TBARS), and post feeding behaviour did not differ from controls.

### 7.3. References

- Allam, a, El-Ghareeb, a a, Abdul-Hamid, M., Baikry, a, Sabri, M.I., 2011. Prenatal and perinatal acrylamide disrupts the development of cerebellum in rat: Biochemical and morphological studies. *Toxicol. Ind. Health* 27, 291–306. <https://doi.org/10.1177/0748233710386412>
- Bar-Or, D., Bar-Or, R., Rael, L.T., Brody, E.N., 2015. Oxidative stress in severe acute illness. *Redox Biol.* 4, 340–345. <https://doi.org/10.1016/j.redox.2015.01.006>
- Berntssen, M.H.G., Aatland, A., Handy, R.D., 2003. Chronic dietary mercury exposure causes oxidative stress, brain lesions, and altered behaviour in Atlantic salmon (*Salmo salar*) parr.

- Aquat. Toxicol. 65, 55–72. [https://doi.org/10.1016/S0166-445X\(03\)00104-8](https://doi.org/10.1016/S0166-445X(03)00104-8)
- Bhandari, R., Kuhad, A., 2015. Neuropsychopharmacotherapeutic efficacy of curcumin in experimental paradigm of autism spectrum disorders. *Life Sci.* 141, 156–169. <https://doi.org/10.1016/j.lfs.2015.09.012>
- Castoldi, A.F., Barni, S., Turin, I., Gandini, C., Manzo, L., 2000. Early acute necrosis, delayed apoptosis and cytoskeletal breakdown in cultured cerebellar granule neurons exposed to methylmercury. *J. Neurosci. Res.* 59, 775–787. [https://doi.org/10.1002/\(SICI\)1097-4547\(20000315\)59:6<775::AID-JNR10>3.0.CO;2-T](https://doi.org/10.1002/(SICI)1097-4547(20000315)59:6<775::AID-JNR10>3.0.CO;2-T)
- Coyle, J., Puttfarcken, P., 1993. Glutamate Toxicity. *Science* (80-. ). 262, 689–95.
- Franco, J.L., Braga, H.C., Stringari, J., Missau, F.C., Posser, T., Mendes, B.G., Leal, R.B., Santos, A.R.S., Dafre, A.L., Pizzolatti, M.G., Farina, M., 2007. Mercurial-induced hydrogen peroxide generation in mouse brain mitochondria: Protective effects of quercetin. *Chem. Res. Toxicol.* 20, 1919–1926. <https://doi.org/10.1021/tx7002323>
- Gilgun-Sherki, Y., Melamed, E., Offen, D., 2001. Oxidative stress induced-neurodegenerative diseases: The need for antioxidants that penetrate the blood brain barrier. *Neuropharmacology* 40, 959–975. [https://doi.org/10.1016/S0028-3908\(01\)00019-3](https://doi.org/10.1016/S0028-3908(01)00019-3)
- Grandjean, P., Landrigan, P.J., 2014. Neurobehavioural effects of developmental toxicity. *Lancet Neurol.* 13, 330–338. [https://doi.org/10.1016/S1474-4422\(13\)70278-3](https://doi.org/10.1016/S1474-4422(13)70278-3)
- Kaur, P., Aschner, M., Syversen, T., 2006. Glutathione modulation influences methyl mercury induced neurotoxicity in primary cell cultures of neurons and astrocytes. *Neurotoxicology* 27, 492–500. <https://doi.org/10.1016/j.neuro.2006.01.010>
- Lakshmi, D., Gopinath, K., Jayanthi, G., Anjum, S., Prakash, D., Sudhandiran, G., 2012. Ameliorating effect of fish oil on acrylamide induced oxidative stress and neuronal apoptosis in cerebral cortex. *Neurochem. Res.* 37, 1859–1867. <https://doi.org/10.1007/s11064-012-0794-1>
- Lu, T.H., Hsieh, S.Y., Yen, C.C., Wu, H.C., Chen, K.L., Hung, D.Z., Chen, C.H., Wu, C.C., Su, Y.C., Chen, Y.W., Liu, S.H., Huang, C.F., 2011. Involvement of oxidative stress-mediated ERK1/2 and p38 activation regulated mitochondria-dependent apoptotic signals in methylmercury-induced neuronal cell injury. *Toxicol. Lett.* 204, 71–80. <https://doi.org/10.1016/j.toxlet.2011.04.013>
- Markesbery, W.R., 1997. Oxidative stress hypothesis in Alzheimer’s disease. *Free Radic. Biol. Med.* 23, 134–147. [https://doi.org/10.1016/S0891-5849\(96\)00629-6](https://doi.org/10.1016/S0891-5849(96)00629-6)
- Pisoschi, A.M., Pop, A., 2015. The role of antioxidants in the chemistry of oxidative stress: A review. *Eur. J. Med. Chem.* 97, 55–74. <https://doi.org/10.1016/j.ejmech.2015.04.040>
- Polunas, M., Halladay, A., Tjalkens, R.B., Philbert, M.A., Lowndes, H., Reuhl, K., 2011. Role of oxidative stress and the mitochondrial permeability transition in methylmercury cytotoxicity. *Neurotoxicology* 32, 526–534. <https://doi.org/10.1016/j.neuro.2011.07.006>
- Reynolds, A., Laurie, C., Lee Mosley, R., Gendelman, H.E., 2007. Oxidative Stress and the Pathogenesis of Neurodegenerative Disorders. *Int. Rev. Neurobiol.* 82, 297–325. [https://doi.org/10.1016/S0074-7742\(07\)82016-2](https://doi.org/10.1016/S0074-7742(07)82016-2)
- Richetti, S.K., Rosemberg, D.B., Ventura-Lima, J., Monserrat, J.M., Bogo, M.R., Bonan, C.D., 2011. Acetylcholinesterase activity and antioxidant capacity of zebrafish brain is altered by heavy metal exposure. *Neurotoxicology* 32, 116–122. <https://doi.org/10.1016/j.neuro.2010.11.001>
- Rosignol, D.A., Frye, R.E., 2014. Evidence linking oxidative stress, mitochondrial dysfunction, and inflammation in the brain of individuals with autism. *Front. Physiol.* 5 APR, 1–15. <https://doi.org/10.3389/fphys.2014.00150>
- Sandström, J., Broyer, A., Zoia, D., Schilt, C., Greggio, C., Fournier, M., Do, K.Q., Monnet-Tschudi, F., 2017. Potential mechanisms of development-dependent adverse effects of the herbicide paraquat in 3D rat brain cell cultures. *Neurotoxicology* 60, 116–124.

- <https://doi.org/10.1016/j.neuro.2017.04.010>
- Sandström, J., Eggermann, E., Charvet, I., Roux, A., Toni, N., Greggio, C., Broyer, A., Monnettschudi, F., Stoppini, L., 2016. Toxicology *in Vitro* Development and characterization of a human embryonic stem cell-derived 3D neural tissue model for neurotoxicity testing. *Tiv.* <https://doi.org/10.1016/j.tiv.2016.10.001>
- Sarafian, T.A., Vartavarian, L., Kane, D.J., Bredenden, D.E., Verity, M.A., 1994. Bcl-2 Expression Decreases Methyl Mercury-Induced Free-Radical Generation and Cell Killing in a Neural Cell Line. *Toxicol. Lett.* 74, 149–155.
- Sies, H., 2015. Oxidative stress: A concept in redox biology and medicine. *Redox Biol.* 4, 180–183. <https://doi.org/10.1016/j.redox.2015.01.002>
- Wang, X., Michaelis, E.K., 2010. Selective neuronal vulnerability to oxidative stress in the brain. *Front. Aging Neurosci.* 2, 1–13. <https://doi.org/10.3389/fnagi.2010.00012>
- Wells, P.G., McCallum, G.P., Chen, C.S., Henderson, J.T., Lee, C.J.J., Perstin, J., Preston, T.J., Wiley, M.J., Wong, A.W., 2009. Oxidative stress in developmental origins of disease: Teratogenesis, neurodevelopmental deficits, and cancer. *Toxicol. Sci.* 108, 4–18. <https://doi.org/10.1093/toxsci/kfn263>